NOTICE

AVIS

UNIVERSITY OF ALBERTA

SCALED EXPERIMENTS OF FLOW NEAR, AND INSIDE, A

HORIZONTAL WELL IN STEAMFLOODING

BY

QUANG THE DOAN

A THESIS

SUBMITTED TO THE FACULTY OF GRADUATE STUDIES AND RESEARCH

IN PARTIAL FULFILLMENT OF THE REQUIREMENTS FOR THE DEGREE

OF MASTER OF SCIENCE

IN

PETROLEUM ENGINEERING

DEPARTMENT OF MINING, METALLURGICAL AND PETROLEUM

ENGINEERING

EDMONTON, ALBERTA

SPRING, 1991

Canada

UNIVERSITY OF ALBERTA

RELEASE FORM

NAME OF AUTHOR: Quang The Doan
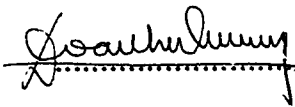
TITLE OF THESIS: Scaled Experiments of Flow Near, and Inside, a Horizontal Well in Steamflooding

DEGREE FOR WHICH THESIS WAS PRESENTED : MASTER OF SCIENCE

YEAR THE DEGREE WAS GRANTED : SPRING, 1991

Permission is hereby granted to the UNIVERSITY OF ALBERTA LIBRARY to reproduce single copies of this thesis and to lend or sell such copies for private, scholarly or scientific research purposes only.

The author reserves other publication rights, and neither the thesis nor extensive extracts from it may be printed or otherwise reproduced without the author's written permission.

(SIGNED) ....

PERMANENT ADDRESS:
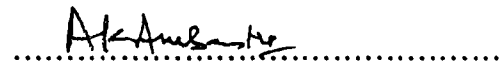
10244 - 89 Street

Edmonton, Alberta

Canada   T5H 1R1

DATED :   April 15 1991

UNIVERSITY OF ALBERTA

FACULTY OF GRADUATE STUDIES AND RESEARCH
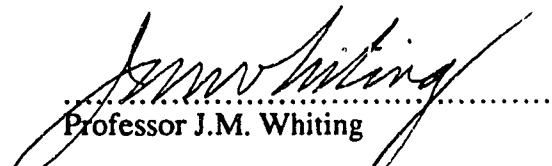
The undersigned certify that they have read and recommend to the Faculty of Graduate Studies and Research, for acceptance, a thesis entitled SCALED EXPERIMENTS OF FLOW NEAR, AND INSIDE A HORIZONTAL WELL IN STEAMFLOODING submitted by QUANG THE DOAN in partial fulfillment of the requirements for the degree of MASTER OF SCIENCE in PETROLEUM ENGINEERING.

Professor S.M. Farouq Ali (Supervisor)

Professor A.K. Ambastha

Professor R.G. Bentsen

Professor W.S. Tortike

Professor J.M. Whiting

Professor J.D. Scott (External Examiner)

DATED : Dec 18, 70

Công Cha Như Núi Thái Sơn,
Nghĩa Mẹ Như Nước Trong Nguồn Chảy Ra,
Một Lòng Thờ Mẹ Kính Cha,
Cho Tròn Chữ Hiếu Mới Là Đạo Con.

Ca Dao Tục Ngữ Việt Nam

ABSTRACT

Mathematical equations were formulated to model flow in the vicinity of, and inside, a horizontal wellbore. Inspectional analysis was next used to isolate and identify scaling groups from the dimensionless form of these equations. Two different sets of scaling criteria were developed: one for the flow process in the reservoir, and the other for flow inside the horizontal well. The scaling criteria were then used to design and construct linear, high-pressure scaled physical models, as well as to determine the operating conditions for a series of steam injection experiments, which were carried out in the physical models.

The experiments were intended to determine primarily the effects of wellbore geometry and well completion on the performance of various steam injection recovery processes. Apparatus was set up to inject continuously superheated steam at a constant steam injection pressure into a model reservoir of tightly packed and compressed Ottawa silica sand, and saturated with water and FAXAM-100 oil. A variety of horizontal well designs and perforated casings, along with different combinations of injector and producer, were tested. Their performance, based upon various oil recovery performance indicators, was compared to determine the relative merits and potential effectiveness of variable- and constant-diameter horizontal wells — both with and without casing, vertical producers, and horizontal injectors.

Based on the experimental results, it is concluded that first, variable diameter horizontal wells can reduce the axial well pressure gradients, provide a higher fluid production rate, recover more oil, and achieve higher thermal efficiency than their constant-diameter counterparts. Second, perforated casing can reduce the overall recovery performance (i.e. lower fluid production rate, oil recovery, and thermal efficiency) of a horizontal producer by impeding the flow of reservoir fluids into the well.

ACKNOWLEDGEMENTS

TABLE OF CONTENTS

LIST OF TABLES

LIST OF FIGURES

xiv

LIST OF PLATES

NOMENCLATURE

a	length scaling factor, dimensionless
a_w	fraction of peripheral area of horizontal well open to inflow, dimensionless
A	area between reservoir and overburden, associated with res. volume V_b, m^2
$\bar{A}$	average area of horizontal well, m^2
C	specific heat, kJ/kg-°C
C_{ij}	concentration of component j in phase i, mass fraction
g	constant for acceleration due to gravity, 9.80665 m/s^2
h_i	enthalpy of phase i (i=oleic, aqueous, and vapour), kJ/kg
H	thickness of reservoir, m
J	mechanical equivalence of heat energy, dimensionless
k	absolute permeability of porous medium, m^2
k_{ri}	relative permeability of phase i (i=oleic, aqueous, and vapour), dimensionless
k_h	thermal conductivity, kW/m-°C
L	length of reservoir, m
p_i	pressure of phase i (i=oleic, aqueous, and vapour), Pa
P_c	capillary pressure, Pa
Δp	pressure drop across horizontal well, Pa
q_i	fluid rate per unit volume (inj. +ve, prod. -ve) of phase i, kg/s-m^3
q_h	heat rate per unit volume (injection +ve, production -ve), kJ/s-m^3
q_l	heat loss rate per unit volume, kJ/s-m^3
r, z	cylindrical coordinates (r is positive upward), m, m
r_w	horizontal wellbore radius, m
S_i	saturation of phase i (i=oleic, aqueous, and vapour), fraction
T	temperature, °C
U	internal energy, kJ/kg
U_i	internal energy of phase i (i=oleic, aqueous, and vapour), kJ/kg
v	velocity of the fluids flowing inside the horizontal well, m/s
V_b	bulk volume of the reservoir, m^3
W	work energy done by/or the fluids flowing inside the well, kJ/s-kg
W_{ij}	mass injection rate of component j in phase i, kg/s

Superscript :

* = at standard conditions

Subscript :

g = vapour phase

m = mixture of oil and steam condensate

o = oleic phase

p = across horizontal well

r = reservoir

s = steam additive

w = horizontal well

ga = conc. of steam additive in vapour phase

go = (capillary pressure) between gas and oil

gw = conc. of water component in vapour phase

oa = conc. of steam additive in oleic phase

ob = overburden

oo = conc. of oil component in oleic phase

ow = (capillary pressure) between oil and water

rg = relative (permeability) for vapour phase

ro = relative (permeability) for oleic phase

rw = relative (permeability) for aqueous phase

w, avg = average wellbore radius

ww = conc. of water component in aqueous phase

in = at the inlet of the horizontal well

inj = injection

out = at the outlet of the horizontal well

$prod$ = production

D = dimensionless

F = field prototype

H = horizontal well

M = model

R = reference quantity

Greek Symbol :

α	thermal diffusivity ($\alpha = k_h/\rho C$), m^2/s
θ	cylindrical coordinate, degree
μ_i	viscosity of phase i (i=oleic, aqueous, vapour), mPa· s
ρ	density, kg/m^3
ρ_i	density of phase i (i=oleic, aqueous, and vapour), kg/m^3
ϕ	porosity, fraction
Φ	potential, Pa

1. INTRODUCTION

Horizontal wells are increasingly being drilled and used in the recovery of petroleum fluids. Within the last 15 years, there have been many studies published examining the recovery performance of, and the advantages offered by, horizontal wells over conventional vertical wells in different light oil/gas recovery applications as well as in thermal recovery processes. It has been shown that, in general, horizontal wells have a higher productivity index, and better recovery than vertical wells in reservoirs experiencing gas/water coning problems. For thermal recovery applications, horizontal wells have been demonstrated to be capable of accelerating oil recovery and increasing steam sweep efficiency. However, an overwhelming majority of these studies do not deal with the flow behaviour in the vicinity of, and inside, a horizontal wellbore. In most cases, they treat the flow inside the horizontal well as a constant-rate flow process, or assume that there is no pressure drop along the length of the horizontal wellbore.

This study is an attempt to contribute to an understanding of the flow behaviour in the vicinity of, and inside, a horizontal well. Specifically, it examines experimentally the production/recovery performance of different types of horizontal wells, both cased and open, in a variety of steam injection experiments. To do this, mathematical equations, along with their initial and boundary conditions are formulated, first, to describe the above two flow processes, and second, to serve as the basis for obtaining the scaling criteria. Inspectional analysis is used to render the equations dimensionless, and then isolate and identify the scaling groups. An attempt was made to satisfy and use as many of the scaling requirements as possible in the design, construction, and operation of a linear, high-pressure physical model. The recovery performance of different types, and combinations of vertical and horizontal wells was then compared to evaluate the effects of near wellbore, and inside, wellbore conditions on the flow behaviour.

2. OBJECTIVES

The broad objectives of this study are to determine experimentally the effects of wellbore geometry and well completion on the recovery performance of a horizontal producer in different steam injection recovery processes. A scaled linear physical model is to be designed, constructed, and used to carry out the experiments for this purpose.

Scaling criteria are to be developed for the physical model, considering separately the two flow processes involved in the overall problem. The first process consists of the flow of reservoir fluids in the porous medium, and the second process consists of the flow of these fluids into, and inside, a horizontal wellbore. The scaling criteria are to be derived using a suitable scaling method, and have to be flexible enough to permit the actual design and construction of a physical model. Particular emphasis is placed on finding a suitable approach to scale down the size of a prototype horizontal well for laboratory experiments.

The objectives of the steam injection experiments are as follows:

1) To select suitable scaling groups to scale down the size of the prototype horizontal well, and the prototype reservoir dimensions.

2) To fabricate the physical model, along with the different types of horizontal well and casing.

3) To assemble the different apparatus for a series of steam injection experiments.

4) To design and carry out a series of steam injection experiments, and to analyze the results.

5) To draw conclusions, from the experimental results, regarding the flow behaviour in the vicinity of, and inside a horizontal wellbore — especially with respect to the effects of wellbore internal geometry and well completion on oil recovery.

3. LITERATURE REVIEW

Horizontal wells are being used ever more widely for primary and enhanced recovery of petroleum fluids. In view of the favourable response of the various existing pilots, more horizontal wells are being drilled to augment the productive capacity of existing reservoirs and/or to develop new reservoirs. This trend of increasing prominence of horizontal wells will continue as innovations in drilling and completion technologies boost their performance potential and reduce the costs. Yet, experimental and theoretical modelling of horizontal wells is still rather inadequate. The available models have moderate success in predicting well performance. Efforts are currently underway to gain a better understanding of horizontal-well mechanics.

3.1 History of Horizontal Drainholes and Horizontal Wells

The idea of extending reservoir to well contact area by drilling wells horizontally into a reservoir is not new. It has long been recognized that a horizontal borehole, due to its length, would be able to effectively drain a much larger area of a reservoir than a vertical borehole under most conditions. Accordingly, as early as 1919, attempts were made to drill horizontal holes from a main vertical bore. Special drilling equipment like the flexible non-rotating drillpipe and turbine bit were designed in the 1940's to allow the drilling of horizontal tributary holes or drainholes from a vertical borehole. They were field-tested and found to be successful in reviving production from a California well that had not produced for 17 years prior to the drilling of the drainholes [1].

Hyland [2] provided accounts of several drainhole drilling projects which included both the drilling of short horizontal drainholes into oil-bearing deposits from subsurface chambers or mines, and the directional drilling of lateral drainholes from a conventional wellbore. Mechanical unreliability of early lateral drilling equipment, coupled with the development of fracturing techniques and the lack of economic incentives led to the abandonment of these projects and prolonged skepticism by the oil industry of the potentials of horizontal and lateral drainhole drilling. In the last 15 years, interest in horizontal drainholes/wells has been revived and sustained mainly by innovations in lateral drilling technology and the need to recover oil and gas more efficiently, as well as by the success of many of the existing horizontal well pilots.

3.2 Drilling and Completion of Horizontal Wells

3.2.1 Drilling of Horizontal Wells

In general, there are four types of horizontal well: regular, short-radius, ultra-short radius, and drainholes. Horizontal drainholes are generally drilled from existing vertical wellbores, and are in many instances quite short — 30 m to 150 m. A single drainhole or multiple drainholes can be drilled from a vertical wellbore. The main purpose of horizontal drainholes is to extend the reservoir contact

area around the vicinity of a vertical hole, and thus allow more fluids to be drained toward the hole. Horizontal wells, on the other hand, are normally new wells and can be long (> 300 m). They are drilled from the surface using directional drilling technology. As drilling technology progresses, horizontal wells will start to supplant horizontal drainholes in oil-field applications. Today, horizontal wells can be drilled from either underground access chambers or surface locations (on land, offshore platforms) — depending mainly on the physical characteristics of an oil deposit.

3.2.1.1 Drilling from Underground Access

For many shallow and easily accessible oil deposits, it is possible to drill long horizontal wells from subsurface excavated chambers. This is true especially for many oil sand deposits in the Athabasca region. For the SATAC (Shaft-And-Tunnel Access Concept) method, a subsurface access chamber is first created by sinking a vertical shaft from the surface to the oil-bearing deposit and constructing a network of tunnels in either the reservoir itself, or in formations directly above and/or below the oil-bearing zone. The shaft and tunnels must provide safe access for men and machinery during the initial construction and drilling stage, as well as subsequent recovery operation periods. Modified equipment like slanted drilling rigs are next used to drill horizontal wells from the tunnels into the reservoir. The wells are then completed for production [3] . Haston et al. [4] described the implementation of the above method for the AOSTRA Underground Test Facility (UTF) outside Fort McMurray.

Subsurface chambers can also be excavated in the oil-bearing horizon around an existing vertical hole. In this case, the chamber size can be quite small — often just large enough for the deployment of an erectible whipstock which allows the tubing-conveyed drillhead to make a 90°, tight-radius (one foot) turn. The drillhead consists of circular nozzles capable of delivering water jets of 1000 hp to the formation face. Holes of 4-6 inches diameter, 100-200 ft length can be drilled by this ultra-short radius horizontal drilling technique. Pendleton and Ramesh [5] , Dickinson and Dickinson [6] described this method of drilling short horizontal wells and a specialized logging tool for these holes. These short horizontal holes are most suited to improve steam injection response for California heavy-oil fields which usually require very small vertical well spacing to be effective.

3.2.1.2 Drilling from Surface

Long horizontal wells (> 300 m) can be drilled from the surface to reach deep and inaccessible oil/gas deposits. They are classified into three different categories according to the radius of curvature of the axis of the wells as they change direction from vertical to horizontal. The categories are: short-radius (radius of curvature, r=20-40 ft/6-12 m), medium-radius (r=300-500 ft/100-150 m), and long-radius (r> 600 ft/180 m). Friction between the drillpipe and the hole as the drillpipe passes around the curved section is greater for a short radius of curvature than for a long radius of curvature. A direct

consequence of this is that a smaller force is applied to advance the bit through the reservoir. As a result, short-radius horizontal wells (typical length: 600-1500 ft/180-450 m) are much shorter than long-radius wells which can reach lengths of 3000-4500 ft/900-1500 m.

A general feature of these three drilling methods is the use of a downhole mud motor and flexible, curved drillpipe to achieve deviation of the drill bit from the original vertical. Detailed descriptions of the tools and techniques employed to drill short-, medium-, and long-radius horizontal wells are contained in several papers [7-11]. As pointed out in these papers, one of the most important lateral drilling innovations was the introduction of Measurement-While-Drilling (MWD) tools. These tools are normally placed some distance behind the mud motor to transmit data of the drill bit progress to the surface. Appropriate adjustments can then be made to steer the drill bit to the desired azimuth of a selected horizontal plane. Efforts are being made to locate MWD tools nearer to the drill bit so that a precise well trajectory can be achieved, and intersections with fractures in the oil-bearing zone can be used to advantages.

It is pointed out [12] that substantial economic and reservoir performance advantages could be realized by drilling long horizontal wells from offshore platforms. In this case, the extra cost of drilling horizontal wells is small because offshore wells are very often already highly deviated. On the other hand, horizontal wells are believed — because of their extended reservoir contact — to be much more productive than conventional offshore wells, under appropriate conditions.

3.2.2 Completion of Horizontal Wells

Early horizontal drainholes and wells were completed as open holes with either a slotted or pre-drilled liner. This type of completion is the simplest, least expensive, and hence most commonly used. However, it is also most susceptible to the production of sand and unwanted fluids. As a result, wells completed this way often require workovers or recompletions to remain productive [13]. Gravel packs can be used to protect holes or liners from sand production, but they cannot protect these holes or liners from unwanted fluid invasion. Spreux, Georges, and Lessi [14] illustrated various completion techniques for horizontal holes with, and without a liner. Packers can be used to isolate parts of the horizontal section of a well from inflow fluids. Dickinson, Anderson, Dickinson, and Dystra [15] reported a two-stage laboratory process capable of providing 100% fill of gravel and some consolidation of horizontal boreholes.

Casing and cementing a horizontal well may reduce sand or fines plugging and production of unwanted fluids, it is necessary to case and cement it. Production tubing can then be run in, casing perforated, and the well put into production. This type of completion can be very expensive, but it is flexible, especially when it comes to recompletion or stimulation efforts to improve well productivity. A major problem for cased completion of horizontal wells is the quality of the cementing

job, especially for the horizontal section of the well. Mud cuttings and solid particles in the cement slurry will settle and deposit at the bottom of the hole. Water, on the other hand, will migrate to the top of the hole. This causes several problems: presence of flow passages above the horizontal well, uneven cement bond around the wellbore, and the well being eccentric. This last problem could result in unequal standoff distance for perforation guns, which could lead to serious damage to the casing. Zaleski, Jr., and Spatz [16], Lessi and Spreux [17], Cooper and Troncoso [18] discussed techniques and tools to overcome these problems and successfully cement horizontal wells. Weirich, Zaleski, Jr., and Mulcahy [19] described a hydraulically balanced perforation gun for use in horizontal wells.

Soliman, Hunt, and El Rabaa [20], and Economides and Nolte [21] examined the problem of fracturing horizontal wells, including the orientation of holes and fractures, fracture height, number of fractures, and effect of fracture conductivity on well performance. Dorel [13] detailed the efforts to drill and complete two onshore horizontal wells in France (Lacq 90 and Lacq 91) and one long horizontal well offshore of Italy (Rospo Mare 6D). Wilkirson, Smith, Stagg, and Walters [22] described the drilling and completion of three horizontal wells at Prudhoe Bay, Alaska. The authors noted that the total cost and drilling time were reduced drastically as the operator became more familiar with the technology. MacDonald [23] reported the drilling and completion of Esso Resources Canada Ltd. Cold Lake Horizontal well Pilot No. 2. Sheikholeslami, Schlottman, Siedel, and Button [24] comprehensively illustrated the drilling and completion of horizontal wells to increase production from the highly-fractured Austin Chalk field in Texas. Reiley et al. [25] described the cementing of liners in horizontal and high-angle wells at Prudhoe Bay, Alaska while Ashton, Liput, Lemons, and Summerlin [26] provided an account of how single-screen liners were packed successfully with gravel for offshore California horizontal and highly-deviated holes.

3.3 Application of Horizontal Wells for Light Oil/Gas Recovery

3.3.1 Advantages of Horizontal Wells/Drainholes

The most important advantages horizontal wells can offer over conventional vertical wells include: higher productivity index, better control of coning problems, and higher probability of intersecting systems of vertical and horizontal fractures in a reservoir. These are discussed briefly below.

3.3.1.1 Increase in Productivity Index

Horizontal wells can improve the fluid production rate and efficiency of a recovery process by providing a bigger and more effective contact area between the well and the reservoir. Conventional vertical wells normally have only a small part of their total length open for flow of reservoir fluids. As the fluids flow radially from different regions toward the vertical production well, the area for flow decreases, the flow velocity increases, and the pressure gradient rises rapidly. Most of the pressure

drop occurs in the near wellbore region. Horizontal wells, provide a much larger area for the inflow of reservoir fluids. As a consequence, the pressure drop is decreased — resulting in higher rates of drainage or production. Fluid velocity is also much lower — resulting in a more even, uniform flow distribution and less oil trapped behind. The effects are similar to those resulting from the presence of vertical and horizontal fractures intersecting a vertical wellbore. However, quite often the fracture length is finite, fracture orientation is not known with great certainty, fracture conductivity is not infinite, and fractures may close with time.

Perrine [27] , using an electrolytic model, reported experimental data on well productivity increase due to drainholes whose maximum length was 100 ft. The following conclusions were reached: very large increases (10-fold) in productivity can be realized only for damaged wells, as the maximum increase in well productivity for undamaged wells with drainholes obtained was only 2 1/2 times the undamaged productivity; drainhole length of penetration had the most important effect on productivity gain, for it was found that there was a linear relationship between the productivity increase and well length; the number and pattern of drainholes had a lesser impact on productivity gain than the length of each drainhole, as it was found that additional length was more effective in improving productivity than increasing the number of drainholes — irrespective of the condition of damage. This study showed experimentally the potential of improving well productivity by extending well/reservoir contact area through the use of horizontal drainholes.

Borisov [28] , examined the idea of oil field production using horizontal and highly-deviated wells. In the case of oil flow toward an isolated horizontal well located in the center of a homogeneous and isotropic bed, an approximate equation was derived to calculate oil production rate based on the total flow resistance which consisted of two components: external resistance to inflow, and internal resistance due to flow inside the well. Analysis was carried out also to investigate the use of horizontal wells in reservoirs bounded by a gas cap and a water leg. An interesting conclusion was the flow of a unit of length of a selectively perforated vertical well was much higher than that of a unit of length of a horizontal well. In the absence of a discussion of near-wellbore pressure gradients, the above conclusion implies that horizontal wells are not as productive as vertical wells when the driving force is due to gas cap expansion or water influx. It is important to note that in all of the above analyses a single pressure was assumed for the horizontal well.

Giger, Reiss, and Jourdan [29] provided simple analytical formulae and numerical examples to evaluate the productivity and water coning of horizontal wells. For homogeneous and isotropic reservoirs, a formula comparing the productivity indices of conventional, fully penetrating vertical wells and horizontal wells of length L was given. For anisotropic reservoirs, it was shown from examples that when $k_v/k_h < 1$, vertical anisotropy is not favourable for horizontal well application, and

when $k_v/k_h > 1$ (due to the presence of vertical fractures) the productivity of horizontal wells is improved. A formula was also given to determine the critical production rate for horizontal wells to avoid coning. The authors concluded that in multiphase flow, horizontal wells offer two advantages over vertical wells: the same flow rate can be achieved with a smaller drawdown, and the distance between the producing horizon and the oil-water contact can be optimized.

Giger [30] pointed out that the productivity of a horizontal well is less sensitive to unfavourable heterogeneities in its vicinity than it is for a vertical well. This is because the open production interval of the well and its near-wellbore pressure distribution allow it to take advantage of high-permeability zones while also diminishing the negative impact of low-permeability horizontal variations. In addition, the author stated that the pressure drop in flow toward a horizontal well is the sum of two components: the first component takes into account the partial penetration of the drainage area, and the second component represents the pressure drop due to the convergence of fluid streamlines. Productivity of fractured horizontal wells was also considered.

Joshi [31] derived an equation to calculate the steady-state oil production rate for horizontal wells draining an elliptical drainage area. Influences of reservoir anisotropy, thickness, well drainage area, and eccentricity (well location other than the reservoir centre) on horizontal well productivity, along with gas and water coning tendencies of horizontal wells were also investigated. The following conclusions were reached: horizontal well productivity improvements depend upon reservoir thickness, well length and location, and reservoir anisotropy; and horizontal wells reduce gas and water coning tendencies. The comparison of vertical and horizontal well productivity index in this and previously mentioned references was based on one important assumption: the drainage area is box-shaped and is equal for both types of wells.

Karcher, Giger, and Combe [32] presented a review of previously derived equations to calculate horizontal well productivity. Also presented were results of a numerical model investigating the areal sweep efficiency of horizontal wells in regular pattern floods. It was observed that horizontal wells, when drilled along the lines of producers in a line-drive like pattern, resulted in areal sweep efficiencies close to 1. In this setup, the horizontal wells behaved like artificial fractures — oriented in the optimum direction for efficient oil displacement.

Plahn, Startzman, and Wattenberger [33] attempted to construct type curves based on numerical simulation results to predict horizontal well performance in solution-gas drive reservoirs. A fully-implicit, finite difference, black-oil simulator was used to generate production histories for various sets of fluid PVT properties and reservoir relative permeabilities. Type curves were then developed based on dimensionless time and cumulative production variables to correlate the numerically generated data. Some of the assumptions used in the type curve development included: the horizontal wells

produce at their maximum rate with constant bottomhole pressure, capillary pressure is ignored, and the reservoir initial pressure is at the bubble-point. An exact correlation was not obtained due to the numerous complex interactions between PVT properties, rock properties, well dimensions, and relative permeability characteristics.

Giger [34] developed equations for steady-state flow into horizontal wells and pressure distribution using the theory of complex functions. From these, criteria were given to enable a comparison of vertical and horizontal well performance in low-permeability reservoirs, as well as to evaluate the effect of permeability anisotropy and assess the economic advantage of horizontal wells. The criteria were based on two newly introduced concepts of equivalent vertical wellbore radius, and equivalent areal productivity. Calculated values of the replacement ratio (i.e. how many vertical wells will be needed to show performance comparable to one horizontal well draining the same area) and ratio of areal productivity (ratio of productivity of same drainage area developed in one case by vertical wells and in the other, by horizontal wells) led to the conclusion that horizontal wells are highly suited for thin reservoirs and reservoirs having good vertical permeability. A method to determine the optimum spacing of horizontal wells was also presented.

Sung and Ertekin [35] carried out numerical simulations to investigate and compare the production performance of horizontal wells and hydraulically stimulated vertical wells in low-permeability natural gas reservoirs. The main parameters studied were: reservoir thickness, permeability, isotropicity of the formation, and penetration lengths of the hydraulic fractures and horizontal boreholes. The authors concluded that for equal surface area the production from horizontal boreholes is greater than that from hydraulic fractures of similar penetration lengths. Invariably, in all cases (horizontal boreholes, vertical and horizontal fractures), gas production rates increased with increased penetration length. Reservoir thickness was found to be the most important factor in determining the performance potential of a horizontal borehole: the superiority of performance for horizontal boreholes became more apparent in thinner reservoirs, and tighter formations. It was also suggested that in the case of anisotropic reservoirs horizontal boreholes should be drilled perpendicular to the largest permeability direction.

The performance of horizontal wells in bottom-water drive reservoirs was studied by Ozkan and Raghavan [36] who developed analytical solutions to determine the pressure distribution in these reservoirs. In their development, the horizontal wellbore was treated as a line source subject to either an infinite conductivity or a uniform flux boundary condition. It was concluded that the influence of anisotropy on the productivity of horizontal wells is less significant than on the productivity of vertical wells.

Babu and Odeh [37] presented an equation to calculate the pseudo-steady state flow of a horizontal

well. Two parameters are needed for this equation: the first parameter accounts for the effect of permeability anisotropy, location of the horizontal well, and the relative dimensions of the drainage volume, while the second parameter considers the skin factor due to the restricted entry problem (i.e. well length compared to length of drainage volume). Based on numerous calculation examples, the following observations were made: a permeability decrease in each of the three directions will result in lower horizontal well productivity — the effect is especially more pronounced in all cases of partially penetrating horizontal wells (i.e. well length is less than drainage volume length); to achieve maximum productivity the horizontal well should be located at the centre of the drainage volume. Hence, it was concluded that the length of a horizontal well and its degree of penetration have the strongest influence on well productivity.

Mutalik, Godbole, and Joshi [38] computed reservoir pressure responses to determine the effect of drainage area shapes on the productivity of horizontal wells, as well as the beginning of pseudo-steady state for centered and off-centre horizontal wells and fully penetrating infinite-conductivity vertical fractures. Shape factors and corresponding equivalent skin factors for these cases were calculated from analytical pressure transient solutions. The following conclusions were reached: horizontal well pressure response asymptotically approaches that of fully penetrating, infinite-conductivity vertical fractures at very large values of dimensionless well length, which was defined to incorporate formation anisotropy; fully penetrating infinite-conductivity vertical fractures represent the limit on the productivity of horizontal wells; and off-centre horizontal wells are less efficient than centrally located wells for draining any given reservoir volume.

A parametric comparison of horizontal and vertical well performance was carried out by Mukherjee and Economides [39]. The authors also compared the performance of a fully completed horizontal well with that of a hydraulically fractured vertical well, and the performance of a hydraulically fractured horizontal well with that of a hydraulically fractured vertical well. Numerical examples revealed that in low-permeability formations the performance of horizontal wells depends mainly on the permeability anisotropy factor β ($\beta = \sqrt{k_h/k_v}$). When vertical permeability is low, infinite-conductivity vertical fractures outperformed horizontal wells. On the other hand, horizontal wells are very effective in naturally fissured formations because they can intersect a number of discrete natural fractures and cause a significant improvement in production. Furthermore, the authors introduced a new skin effect to describe the drop in the fluid flow rate resulting from the limited contact between horizontal wells and vertical fractures.

Joshi [40] described production forecasting methods for horizontal wells for different types of reservoirs: homogeneous, naturally fractured, bottom-water drive, and solution-gas drive. Again, horizontal well performance was compared with that of stimulated vertical wells. The production

forecasting methods were based on analytical solutions and correlations of numerical model results. The following conclusions were reached: horizontal well productivities are either comparable to or exceed those of commercially stimulated vertical wells, and horizontal wells are very effective in thin reservoirs or reservoirs with a high vertical permeability.

Van Dijkum [41] discussed the drilling of three short-radius horizontal wells in low-permeability formations in Kuwait, the performance of these wells compared to their vertical counterparts, and the simulation studies carried out to history match and predict future performance. The horizontal section of the wells varied from 65 to 120 m. No problems were encountered in drilling the wells. Analysis of the actual performance and that from simulation studies showed that oil production was enhanced by a factor of two to three. This enhancement was conditional on the assumptions that well location is optimal with respect to the oil-water contact, and well orientation is optimal with respect to the number of layers in a heterogeneous formation penetrated by the wellbore.

Chang, Tomutsa, and Tham [42] reported the incorporation of horizontal and slanted wellbore models into BOAST, with the aim of predicting potential production rates for such wells. A special feature of the horizontal wellbore model is that the productivity index for the wellbore within each penetrated grid block consists of three component productivity indices in the x-, y-, and z-directions. The model can be run under either pressure or rate constraints, and can be used to calculate the productivity index based on the length and location of the wellbore within a block. The model results were checked against analytical formulae of transient pressure behaviour in an infinite slab reservoir and published analytical type curves, with good agreement with both. It was concluded that the advantage of horizontal/slanted wells over vertical wells in production rates depends primarily on the length of the wellbore, slant angle, vertical and radial permeability, and well eccentricity. It was also noted that vertical permeability discontinuities have a smaller impact on the production rate of a slanted well than that of a horizontal well.

Bendakhlia and Aziz [43] developed dimensionless inflow performance relationships for horizontal wells in solution-gas drive reservoirs. The approach paralleled that used for vertical wells: numerical simulation was performed to generate sets of oil production rate versus pressure drawdown curves, and an empirical equation was then developed to correlate the curves generated. Two cases were considered: first, a base case with typical fluid, rock, and well properties was studied; then changes to fluid properties, reservoir properties, and well properties were introduced to investigate the effects of these variations. The IPR (Inflow Performance Ratio) curves exhibited a high initial oil productivity which declined rapidly with cumulative production. The authors attributed the high initial productivity to a large contact area between the horizontal well and the reservoir, and the rapid decline in productivity to the limited transmissibility and finite size of the reservoir.

Dikken [44] studied the pressure drop in horizontal wells and its effect on the production performance. He noted that the commonly used assumption of laminar flow in horizontal wells is not necessarily true for most practical situations, and proceeded to demonstrate this with calculated examples. A second-order differential equation linking single-phase turbulent well flow with stabilized reservoir flow was derived and solved numerically for various boundary conditions. The following conclusions were drawn: turbulent well flow in the horizontal section of a horizontal well may result in an appreciable reduction of drawdown at various positions away from the lifting end of the section, and that the total production will level off and become virtually constant when the well length exceeds a certain critical value. This study was the first to investigate the effect of the pressure gradient inside the well on well performance. The importance of this can certainly not be ignored keeping in mind that future horizontal wells, in view of innovations in lateral drilling technology, will tend to be much longer.

3.3.1.2 Suppression of Coning Problems

Horizontal wells could improve the recovery performance for reservoirs experiencing gas and/or water coning. A horizontal well, because of its extensively large contact area with the reservoir, can reduce significantly flow pressure gradients. This reduction means that a production rate comparable to that of a vertical well can be achieved at a lower pressure drawdown, or conversely, for a given pressure drawdown a horizontal well would provide a much higher fluid production rate than a vertical well. In short, a horizontal well has a much higher tolerance for "critical fluid production rate" or "critical pressure drawdown" than a vertical well does before the onset of the production of undesired fluids. This is important for reservoirs under active gas-cap expansion drive and/or bottom-water drive. It has often been the case that these reservoirs, when developed by vertical wells, have a highly restrictive critical flow rate and/or pressure drawdown which could make them economically unattractive. Recovery in these instances constitutes only a small portion of the initial hydrocarbon in place before water and/or gas breakthrough takes place.

Chaperon [45] presented a study to estimate the critical production rate of horizontal wells in anisotropic formations. The analysis, based on the assumption of steady-state or pseudo-steady state flow conditions, was identical to Muskat's approach: only static stable cones were considered. Only flow in the plane perpendicular to the horizontal well axis was examined. Static equilibrium and dynamic equilibrium requirements were used to derive a simple equation for calculating the critical fluid production rate per unit length of a horizontal well in isotropic and anisotropic reservoirs. The critical rate was then compared with that for a vertical well to estimate the possible gain in horizontal well rate. The critical cones usually came closer to the horizontal wells than to vertical wells. It was concluded that critical production rate per unit length of a horizontal well

is a function of the horizontal transmissibility of the oil layer, initial oil column thickness, and the distance between the well and the lateral boundary. Furthermore, the critical production rate for horizontal wells is not as sensitive to vertical permeability variation as that for vertical wells.

Karcher, Giger, and Combe [32] compared the critical rate for infinite horizontal wells calculated by Chaperon [45] with the rate calculated by a numerical model. The critical rate of the infinite horizontal well was between two to three times that of vertical wells, and that the oil recovery at the critical rate for horizontal wells more than tripled the recovery at breakthrough for vertical wells. When a horizontal well of finite length was used, it was seen that for a small drainhole length the increase in critical rate could be quite large. However, beyond an optimum drainhole length the increase became smaller. On the other hand, a longer drainhole length resulted in better recovery at the critical rate. Furthermore, it was concluded that production at supercritical rates could bring the same magnitude of improvements at breakthrough, but not afterwards. The final recovery was more or less the same for horizontal and vertical wells. This was the first work to examine the ridging and cresting effect of horizontal wells in bottom-water drive reservoirs.

Joshi [40] applied Chaperon's work to bottom-water drive reservoirs, and came to the conclusion that horizontal well critical rates were substantially higher than those for vertical wells, even in high-permeability reservoirs. It was also noted that there was a rapid decline in horizontal well rates. The explanation given was that the reservoir oil column thickness for a horizontal well – due to the higher production rate – declined more rapidly than that for a vertical well. Gains in critical rate for horizontal wells are dependent mainly upon well length, and drainage area dimensions. The author also proposed a modification to a conventional equation used to determine water cone height for vertical wells to enable calculations of water breakthrough time and water cut for horizontal wells.

Van Dijkum [41] reported numerical model results for the Al Huwaisah, Oman, reservoir which showed that, contrary to expectation, horizontal wells did not improve oil production significantly. It was believed that most probably the reservoir was produced still at supercritical flow rates, and hence the difference in performance between horizontal and vertical wells was indifferentiable.

Papatzacos, Herring, Martinsen, and Skjaeveland [46] derived a semi-analytical approach to calculate cone breakthrough time for horizontal wells. This approach was unlike previous approaches employed by Giger [30], Chaperon [45], Karcher et al. [32], which derived equations to calculate the critical rate for horizontal wells based on the assumption of steady-state flow conditions. In this analysis, the oil-water contact and gas-oil contact were treated as moving boundaries. Hence the position, shape, and size of the cones became functions of time. These moving boundaries, along with the standard Laplacian potential flow equation, were transformed, made dimensionless, reformulated into a standard boundary value problem, and solved numerically. Three different cases were studied: a

two-cone case with simultaneous gas and water coning, single-phase gas coning, and single-phase water coning. Different anisotropy ratios, water viscosities, and gas viscosities were used to determine their effects on cone breakthrough time. Results generated compared favourably with actual field test data for the Helder field in the North Sea.

3.3.2 Pressure Transient Analysis of Horizontal Wells

Goode and Thambynayagam [47] provided an analytical solution for the pressure response of a horizontal well produced at constant rate with no wellbore storage during pressure drawdown and buildup. For the pressure buildup case, two different boundary conditions were considered: infinite reservoir, and a reservoir of finite width. It was noted that there were four flow periods for horizontal wells: early times when the flow is radial, intermediate times when the flow is linear, late intermediate time when the flow reverts to radial, and late time when the flow is linear. Simplified equations permitting the determination of directional permeabilities, average pressures, and mechanical skin factors were developed for each of the flow periods, as were their durations. An important assumption in the analysis was the uniform-flux distribution over the horizontal well.

Daviau, Mouronval, Bourdarot, and Curutchet [48] studied the behaviour of a uniform-flux or infinite-conductivity horizontal well in an infinite or finite reservoir. They showed that there are two types of flow around a horizontal well: vertical radial flow in early periods when the effect of reservoir boundaries or of well ends has not been felt, and pseudo-radial flow at late times. Each of these two flow periods can be analyzed by conventional techniques. The initial vertical radial flow response may be influenced by wellbore storage. For this, time criteria were suggested to determine the onset and duration of each of the two flow periods.

Clonts and Ramey, Jr. [49] examined pressure behaviour of vertical wells with uniform-flux horizontal drainholes in an anisotropic reservoir of finite thickness. Dimensionless variables were introduced to enable the derivation of the analytical solution of the potential flow equation by source functions. It was stated that the analytical solution derived is not readily applicable except for some limiting cases, and thus it would be necessary to evaluate the solution numerically. The main finding by this analytical approach was that there are two possible types of transient pressure behaviour depending on the length of the drainhole relative to the height of the reservoir. If the drainhole is short, initial radial flow perpendicular to the drainhole axis is followed by a transition to a pseudo-radial flow period. In this respect, the observation is similar to that by Daviau et al. [48]. If the drainhole is long compared to the reservoir thickness, then the initial radial flow period ends quickly and flow is characterized by early-time flow followed by a transition to late-time pseudo-radial flow.

It was concluded also that the pressure transient response for multiple drainholes is identical to the single drainhole solution provided that the dimensionless variables are defined relative to the number

of drainholes. The analysis did not consider the effect of a skin factor on the surface of the drainhole and wellbore storage.

Rosa and de Souza Carvalho [50], also using instantaneous sources and Green's functions, developed a mathematical model to evaluate the transient pressure behaviour of an infinite-conductivity horizontal well. The main difference between this model and that used by Clonts and Ramey, Jr. [49] was that this model allows for the calculation of wellbore pressure. This was done by comparing the short- and long-time approximations for both the infinite-conductivity and uniform-flux cases to determine the point along the wellbore length where the two pressure responses are the same. This value is then used with the uniform-flux model to calculate wellbore pressure.

Ozkan, Raghavan, and Joshi [51] extended the solution proposed by Clonts and Ramey, Jr. [49] to generate pressure transient responses for horizontal wells, and presented these results in the form of pseudoskin factors and type curves. Derivative type curves using pressure-time predictions were given also. Their calculations revealed that horizontal well productivity depends primarily on its length, formation thickness, vertical and horizontal permeabilities, and well radius. It was concluded that the pressure response and pseudoskin factor of horizontal wells are insensitive to well location in the vertical plane of the reservoir.

Kuchuk, Goode, Wilkinson, and Thambynayagam [52] examined the pressure behaviour of horizontal wells in reservoirs with and without a gas cap or aquifer. The main features of this analysis were that the analytical solutions were presented in the Laplace transform domain, and average pressure along the length of a horizontal well was used instead of an equivalent pressure point. The following flow regimes were identified: first and second radial flow periods at early time, intermediate time linear flow period, intermediate time radial flow period, and steady-state flow period. Equations and existence criteria were given for each of the flow periods. Wellbore storage effect was included in the analysis. The authors noted that identification of the no-flow boundary would be almost impossible when wellbore storage and skin effects are dominant.

Kuchuk, Goode, Brice, Sherrard, and Thambynayagam [53] applied techniques developed for analyzing horizontal well pressure behaviour [52] to interpret an actual horizontal well test, and came to the following conclusions: the complex geometry associated with horizontal wells makes interpretation of well tests a difficult task, and thus determining well-reservoir system parameters from short-time pressure tests is not possible; combining drawdown and buildup tests with accurate downhole flow rate measurements is critical for proper interpretation. Solutions for the inflow performance of a horizontal well completed in a rectangular drainage volume were obtained from pressure transient analysis for pseudo-steady state flow. These showed that the inflow performance of a horizontal well is affected mainly by its length.

de Souza Carvalho and Rosa [54] extended their mathematical model [50] to study transient pressure behaviour of horizontal wells in naturally fractured reservoirs, which were modelled as double-porosity, double-permeability porous media with pseudo-steady state inter-porosity flow. Wellbore storage and skin effects were included by applying the Laplace transformation to the superposition theorem. The main conclusion reached by the study was that if wellbore storage effects are not dominant, then conventional and/or type curve matching techniques can be applied to estimate well and reservoir parameters.

Aguilera and Ng [55] identified the following flow periods for horizontal wells in anisotropic naturally fractured reservoirs: a first radial flow period at early times from the natural fractures into the well; a transition period due to flow from the matrix into the fractures; a second radial flow period which starts when pressures in the fractures and matrix reach an equilibrium; a linear flow period when the pressure transient reaches the vertical boundaries of the reservoir; a pseudo-radial flow period in a horizontal plane toward the horizontal wellbore; and a linear flow period when the pressure transient reaches the outer parallel boundaries. Recognition of these six flow periods can lead to the calculation of pressures, permeabilities in the x-, y-, z-directions, storativity, average distance between natural fractures, fracture porosity and aperture, skin, and pseudoskin due to vertical and horizontal partial penetration.

Odeh and Babu [56], utilizing their previous work on horizontal well productivity [37], derived equations for pressure drawdown and buildup flow behaviour for each of the four flow periods: early radial, early linear, late pseudo-radial, and late linear. These equations were derived using a closed drainage volume, with arbitrary anisotropy, location and length of the horizontal well. Incorporating assumptions of infinite or semi-infinite extension of reservoir boundaries could lead to the forced presence or absence of some flow periods and consequently erroneous interpretation of test data.

In summary, it can be seen that the study of pressure transient behaviour for horizontal wells — even though still in its early development stage — is progressing rapidly. The publications examined above have tried to present methods to analyze pressure behaviour of horizontal wells along the line of development for vertical wells. In general, these studies came to a common conclusion that pressure transient behaviour of horizontal wells is far different from that of vertical wells, and that insufficient well test time for horizontal wells will have a larger negative impact on the determination of reservoir and well parameters than would be the case for vertical wells. In addition, these studies still utilize infinite-conductivity or uniform-flux horizontal wells which simplify the solution methodology, but which also result in losses in the faithful description of the actual physical problem.

3.4 Application of Horizontal Wells in Enhanced Oil Recovery

Besides finding increased application in primary recovery of conventional light oil/gas reservoirs,

horizontal wells are also beginning to be utilized for enhanced recovery projects — especially in the thermal exploitation of heavy oils and oil sands.

3.4.1 Horizontal Wells in Thermal Recovery of Heavy Oils and Oil Sands

For countries like Canada, the United States, and Venezuela, which have large deposits of heavy oil and oil sands, horizontal wells offer a new way of recovering these resources efficiently and economically. In Canada, most of the heavy-oil and oil-sand reservoirs are located at medium depths (150-400 m below ground level) and are thus not suitable for high steam injectivity strategies, below parting pressures. Furthermore, a majority of these reservoirs in Saskatchewan and Alberta are quite thin (5-6 m pay) and in communication with contiguous bottom water zones. In these cases, the heat loss to the surrounding formations including the non-productive bottom water will be unacceptably high. In California, most of the heavy-oil reservoirs require very close well spacing (2-5 acres) for steam recovery processes to be efficient. Horizontal wells, due to their extended reach and ability to be located at the optimum horizon in the pay zone, offer means to improve the recovery efficiency in these types of reservoirs. Hence, it is not surprising to find pioneering pilot projects evaluating the applicability of horizontal wells to thermal recovery in Canada and the United States.

3.4.1.1 Steam-Assisted Gravity Drainage

Butler, McNab, and Lo [57] presented a study on steam-assisted gravity drainage of heavy oils to horizontal wells placed at the bottom of the oil-bearing formation. The study included theoretical analysis and scaled model experiments in visual and pressurized physical models. Briefly, steam-assisted gravity drainage involves the continuous injection of steam into a constant-pressure steam zone which expands slowly in different directions and mobilizes (by conductive heat transfer mechanism) the surrounding bitumen, which is then drained continuously by gravity downwards into a horizontal well at the base of the formation. It was pointed out by the authors that the main advantages of steam-assisted gravity drainage over conventional steam processes (steamflooding and cyclic steam stimulation) include a slower and more uniform displacement front which leads to a higher steam sweep efficiency, and improved flow mobility due to the unhindered flow of oil as oil and steam flow separately and in opposite directions. Equations were derived to predict the steady-state rate of oil drainage into a horizontal well, as well as the lateral position of the steam zone-oil interface as functions of time and height of the steam zone.

Experiments were carried out in scaled visual and pressurized physical models to validate theoretical analyses. Actual Cold Lake crude was used, and the porous pack materials were selected carefully to ensure dimensional similarity between prototype reservoir parameters and those of laboratory models. Steam pressure for the scaled pressurized model experiments was 3 MPa. Oil recovery was plotted against time, and results were compared with those predicted by theory. The agreement

was fairly good, although the observed production rates were less than those predicted. This was attributed to the smaller gravity head in the model — a result of the depletion of oil from the upper part of the model. The authors also pointed out that the predicted drainage rates would be somewhat optimistic because their analysis assumed that all of the gravity head available would be used to drain the oil downwards. This was believed to be not necessarily true, as some head will be needed to move oil sideways into the horizontal well.

Butler and Stephens [58] extended the above study to consider the effects of repeating well patterns on the oil drainage rate. Also, modifications were introduced into the original analysis to account for the fact that part of the available head is required to move the draining oil sideways to the horizontal well. The pattern investigated in this study consisted of a series of parallel horizontal wells, with a steam zone above each well. This geometry differed from that used previously [57] which represented a reservoir having infinite lateral boundaries. Equations were derived to approximate the time required for the steam zone to move horizontally to the no-flow plane located half-way between horizontal wells. Scaled model experiments were performed with the aim of validating the theoretical analysis. The experimental drainage rate fell off rapidly as the reservoir became depleted, and that the newly modified theory gave results in reas onable agreement with those from the experiments.

In these studies, the experiments were set up such that the steam zone grew predominantly in the horizontal direction. The analyses did not consider the movement of the steam zone in the vertical direction. This deficiency could certainly explain the discrepancy between experimental and theoretical results in initial production periods during which the steam zone grew mainly in the vertical rather than the lateral direction.

Butler, Stephens, and Weiss [59] attempted to rectify this deficiency in their work which considered both the vertical growth of the steam zone from the base to the top of the reservoir, as well as the rate of lateral growth as the steam zone rises slowly upwards. The analysis assumed that the steam zone was circular in shape, and that the horizontal well was the centre of this circle. Hence, the rate of rise of the steam zone was postulated to be the rate of increase of its radius. An equation was then derived to predict the height of the steam zone as a function of time. The authors pointed out that the result given by this equation would be optimistic since in its derivation the restriction to the growth of the steam zone by the top of the reservoir was not included.

The predictive ability of this equation was tested against results of scaled visual model experiments, which surprisingly showed a more rapid rise of the steam zone than predicted. This experimental finding was attributed to the observation that the steam zone, instead of being a single circle, was composed of many small steam fingers. This allowed faster penetration of steam into the surrounding heavy oil regions and, consequently, faster rise of the steam zone. Additional equations

were formulated to approximate the total drainage rate into a horizontal well from a rising steam zone and the effective thickness of a mobile oil layer. The new mathematical model presented in this study was rather simple in its formulation, yet sufficiently effective in its ability to predict field rates of vertical growth of the steam zone.

Laboratory studies of the steam-assisted gravity drainage process were carried out by Griffin and Trofimenkoff [60] to support Esso Resources Canada Ltd.'s horizontal well pilot in the Cold Lake area. Like previous studies [57-59] their experiments were of two different types: those conducted using a visual model and those using high-pressure models. The scaling criteria used to design the experiments were those reported by Butler et al. [57] . In the visual experiments, atmospheric pressure steam was injected into a horizontal injector located slightly above a horizontal producer. Fairly good agreement was achieved between theoretically predicted values [57-59] and experimental data with respect to oil production rate and horizontal growth rate of the steam zone. The experiments also revealed that there was little steam override at the top of the reservoir. This observation differed considerably from theoretical predictions.

In the high-pressure model runs, high-pressure steam (1.4–2.7 MPa) was injected into a vertical injector located above a horizontal producer. As was the case with the visual model runs, Cold Lake crude was used. In these runs, the experimental production rates were substantially higher than the calculated values. Most of the extra production was believed to have come from the end regions of the steam zone; this was confirmed by isotherm contour mapping of the steam zone. As expected, increases in steam injection pressure and temperature did lead to increased oil production rates and reduced oil-steam ratios. In conclusion, the authors stated that the results from scaled model experiments agreed well with previously developed theories.

Butler [61] presented an approach for predicting the bitumen drainage rate from around a spreading steam zone above a horizontal well. In this approach, the steam zone interface is treated as a number of segments. The oil drainage rate for each of the segments is calculated for successive time steps and the rates are then used to calculate the displacement of the whole interface. The change in accumulated heat penetration between the steam zone and the surrounding bitumen is estimated using an approximate differential equation. The following conclusions were reached: the new approach predicts drainage rates of the same order as those obtained from earlier methods, thermal efficiency for unconfined wells is highly dependent upon the degree of override of the steam zone, and that the effect of well confinement is to greatly increase the thermal efficiency by reducing steam override (i.e. closer well spacing gives higher efficiency).

Joshi [62] extended the previous work on steam-assisted gravity drainage to include the effects of well completion, shale barriers, and limited entry on oil recovery. Two basic well configurations were

employed: horizontal injector and producer for one configuration, vertical injector and horizontal producer for the other. Two different geometries of shale barriers were used also: continuous and discontinuous. In all cases, fairly good agreement between the theoretically predicted and experimental results was achieved. In addition, it was seen that steam-assisted gravity drainage not only gives a high sweep efficiency but also good oil-steam ratios — indicating a high thermal efficiency for producing heavy oils.

It was also concluded that the combination of a vertical injector and a horizontal producer yielded higher and more rapid oil recovery than the horizontal injector and producer combination for reservoirs with shale barriers. The performance was comparable for homogeneous, isotropic reservoirs. The presence of shale barriers was deemed to have no significant influence on final oil recovery. It did result in lower oil-steam ratios, and lower instantaneous oil production rates. It was recommended that for a reservoir with shale barriers, a preferable location for a horizontal well was below a shale barrier discontinuity. Experimental data also indicated that limited steam entry caused by vertical fractures perpendicular to the horizontal well did not adversely affect the steam-assisted gravity drainage process. Rather, it provided an easier path for the vertical migration of steam and thus resulted in high initial oil production.

Butler [63] developed an approximate expression to predict the rate at which a steam zone will rise in a reservoir. The main assumption in the model development was that the zone rises at a constant rate which is determined mainly by the ability of steam to flow into the advancing steam fingers composing the steam zone. The predicted velocities are proportional to the reservoir permeability, and strongly dependent upon the oil viscosity and steam temperature. It was also shown that steam fingers of different sizes rise at the same rate, and that the width of the steam fingers is inversely proportional to the reservoir permeability. Curves were constructed to predict steam zone rise rates for the Athabasca bitumen and the Lloydminster crude at different steam temperatures. It was noted that by using reasonable assumed relative permeabilities the theory would predict steam zone rise velocities in fair agreement with previously reported values for a field experiment in Athabasca.

Edmunds, Haston, and Best [64] described the implementation of the steam-assisted gravity drainage process at the AOSTRA Underground Test Facility (UTF). The authors analyzed the growth rate of steam zones in terms of ceiling and slope drainage. It was pointed out that ceiling drainage occurs at the top of a rising steam zone while slope drainage occurs at the sides of the same zone as it spreads sideways. The effects of anisotropy, heterogeneities, solution gas, and capillary pressure on the steam zone growth rate were examined. The authors also reported the design and implementation of a testing program to evaluate steam-assisted gravity drainage in oil sands. This program consisted of the drilling and completion of three pairs of horizontal wells in the lower interval of the McMurray

pay. The horizontal spacing between the well pairs was 25 m, and the vertical spacing between each of the paired horizontal injector and horizontal producer was approximately 5 m. The completed section of each well was 60 meters long, and the wells were fitted with sand screens. According to the authors, the production results have been satisfactory to date, and the testing program will be successful in meeting all test objectives.

Chung and Butler [65] reported new experimental results on physical model studies of the steam-assisted gravity drainage process. The physical model used a preheated vertical steam injector perforated near the top of the pay zone, and a horizontal prod... at the base. For this, previously developed theories had been modified to account for the initial operating condition of communication between the vertical injector and horizontal producer. In addition, scaled experiments were performed to predict recovery performance for the AOSTRA UTF project. The use of a preheated vertical injector led to higher initial oil production rates. With respect to well spacing effects, the following two conclusions were stated: the rise rate of non-interfering steam chambers is independent of the well spacing, and the ultimate recovery is also independent of the well spacing, but closer well spacing gives a higher instantaneous rate of recovery. The authors also remarked that their extrapolated production from the scaled experiments approximately agreed with that predicted by a numerical reservoir simulator developed for the project.

Summarizing, the steam-assisted gravity drainage process – when used with horizontal wells – may constitute a promising means of recovering viscous oil from shallow deposits efficiently. It offers high oil production rates, improved steam sweep efficiency, as well as improved thermal efficiency. The studies listed above, both scaled model and numerical, all showed a cumulative recovery of more than 50% of initial oil in place and thus confirm the promising potential of this recovery process.

3.4.1.2 Conventional Steamflood and Cyclic Steam Stimulation

3.4.1.2.1 Scaled Physical Model Studies

Huygen and Black [66] conducted scaled model experiments to investigate the effectiveness of different horizontal and vertical well combinations in steamflooding Athabasca oil sand. They remarked that for accurate physical modelling of steaming through horizontal wells, both the heat flow (conduction and convection) and mass transport (due to gravity drainage and phase changes) must be scaled properly. Scaling criteria for the other parameters were obtained using the approaches derived by Pujol and Boberg [87]. Injected steam pressure was set at 2.1 MPa. Most of the well configurations tested recovered more than half of the original oil in place, and also achieved high oil-steam ratios. Performance of the floods depended significantly on the geometry and communication between the injector and the producer.

Comparing the various geometries, it was concluded that communication must be established be-

tween wells for the steamflood to be efficient; horizontal fractures were an effective means to develop injectivity for steamflooding; and steamflooding through a single horizontal well was a viable and productive strategy for mobilizing bitumen. The authors pointed out two deficiencies in their experiments: results were optimistic insofar as the model initial oil saturation was always higher than that in the field, and they were rather conservative with regard to lateral growth of the steam zone since the model horizontal permeability was lower (relative to its vertical permeability) than in the field. The study did not consider the effect of steam injection rate on the growth of the steam zone and bitumen production.

Coates [67] and Toma, Redford, and Livesey [68] , using a horizontal well physical simulator, reported studies conducted in support of Texaco Canada Resources Ltd.'s horizontal and deviated well project in the Athabasca region. Coates described the design and construction of the physical model as well as the operating procedure. No mention was made of any particular scaling approach used to determine the dimensions of the model and properties of the porous pack. Actual oil sand was used to pack the porous medium which was subjected to simulated overburden and confining pressure. Steam pressure was set at 4450 kPa. Allowance was made for solvent injection along with steam. Experimental data including steam injection temperature, pressure, flow rate, oil production rate, and characteristic temperatures of the pack during a test were recorded, and analyzed to calculate the performance of the process. One notable feature of this physical model was that it was designed for the cyclic steam stimulation method. Hence, it had only one single horizontal well which was used both for injecting steam and producing bitumen.

Toma, Redford, and Livesey [68] examined the results of 14 experiments carried out in the above physical model. Linear regression was used to correlate oil recovery with other parameters such as the heat injected, and axial pressure loss in the horizontal well. Of interest and importance was the finding that oil production during the drawdown stages was due mainly to the flashing of the oil and condensate in the steam zone, as well as the penetration of steam along the horizontal well axis. The gravity drainage mechanism, in this case, played only a minor role in the recovery of oil. It was concluded that increasing the axial pressure drop could increase the production from a horizontal well in cyclic operations. The regression model showed well pressure drop, heat ratio, and open area of the horizontal well to be the parameters having the greatest influence on oil recovery. Injection of solvents like naphtha also led to improved recovery.

Chang, Farouq Ali, and George [69] reported results of low-pressure, scaled-model experiments utilizing different combinations of vertical and horizontal wells for steamflooding heavy oil formations underlain by a bottom-water zone. The well combinations included: vertical injector – producer, horizontal injector – vertical producer, vertical injector – horizontal producer, and horizontal injector

– producer. The recovery performance of these four well combinations was determined experimentally for three different reservoir cases: homogeneous reservoirs having no bottom water, reservoirs having a thin bottom water zone (10% of pay thickness) and a thick bottom water zone (50% of pay thickness). The following conclusions were reached: the horizontal injector – horizontal producer combination recovered the most oil in all three reservoir situations, horizontal wells had better performance in thin bottom-water situations than in homogeneous reservoirs having no bottom water, and in thick bottom-water reservoirs a horizontal injector was more effective than a vertical injector in preventing steam from going into the water zone. In addition, solvent injection ahead of the steam improved the recovery performance in thin bottom-water cases only marginally .

3.4.1.2.2 Numerical Simulation Studies

Rial [70] numerically investigated the effectiveness of steamflooding with a horizontal steam injector located at the bottom of a heavy-oil reservoir. A three-dimensional numerical model accounting for three-phase flow, steam distillation, temperature-dependent relative permeabilities, gravity, viscous and capillary forces was developed. In this work, as also in other studies discussed below, the flow within the horizontal well was not accounted for. The input data for the model were representative of the Kern River field, California. The results revealed that a horizontal steam injector had a more consistent areal sweep than a conventional vertical steam injector, a horizontal wellbore was more efficient than a vertical wellbore for steamflooding with regard to temperature and residual oil phase distributions, and a horizontal wellbore swept more heat through the grid system and produced more energy than a conventional vertical wellbore. For the field under consideration, the study showed that when a horizontal wellbore was used for steam injection, 71% of the original oil in place (OOIP) was recovered after 15 years, while only 58% of the OOIP was recovered for a vertical wellbore for the same time period.

Jain and Khosla [71] used a commercial simulator to predict steamflooding recovery performance of Athabasca oil for three different combinations of horizontal and vertical wells: the first configuration had two 150 m-long parallel horizontal wells which were spaced 60 m apart, the second configuraton had a 300 m-long horizontal steam injector and a vertical producer in communication with it, and the third configuration had a 400-m long horizontal producer with two vertical injectors in communication with each other to create a heated plane over the horizontal well. In the last configuration, steam-assisted gravity drainage was modelled, while in the first two steamdrive effects were assumed. The results showed that the last well configuration of a horizontal producer with a heated plane between two vertical injectors above it, despite having a larger drainage area, yielded the highest daily oil production rate and cumulative oil recovery.

Huang and Hight [72] conducted numerical simulation studies to examine the effectiveness of horizon-

tal wells to reduce steam override in a mature steamflood, as well as to prevent steam override in new operations. A commercial three-dimensional, three-phase flow thermal simulator which included the effects of gravity, viscous, and capillary forces was used. Heat transfer was modelled by conduction and convection, and relative permeability curves used were temperature dependent. The model had the capability to simulate well completions in any direction. Reservoir properties used were typical of a California unconsolidated heavy-oil reservoir. Simulation results indicated that horizontal wells were effective in recovering oil in areas bypassed by overriding steam. For the 18.5-acre, inverted 13-spot pattern studied horizontal wells improved oil recovery and shortened project life, as well as reduced oil saturation in blind spots from 60% to 30%. In addition, incorporating horizontal wells at the start of a steamflood project with the same well pattern and spacing led to a 72% OOIP recovery efficiency in seven years, and resulted in a residual oil saturation of 26% in blind spot areas.

Hsueh [73] presented results of a numerical simulation study of the HAS Drive (Heated Annulus Steam Drive) process. In short, this in-situ process utilizes a horizontal, cased, unperforated pipe running between a vertical steam injector and a vertical producer. High-pressure, high-temperature steam is circulated through the pipe which heats the surrounding tar sand by conduction. In this sense, the heated annulus acts as a communication path for steam drive between the injection and production wells. The main recovery mechanism in the HASDrive process is believed to be gravity drainage, which is also assisted by a steam drive. The effects of grid block size, relative permeability, heat transfer coefficient, HAS pipe diameter, pattern width, and well configuration were investigated. The simulation results showed the process to be effective for improving areal sweep efficiency and preventing premature steam breakthrough. The major advantage of this process over the conventional practice of creating fractures between the steam injector and oil production wells is its ability to provide a well-controlled fluid communication path which can be kept open throughout the life of a project. In addition, it can also lead to high steam conformance and reduce heat loss through fractures.

Dietrich [74] described the Kern River horizontal-well steam pilot which involved the drilling and completion of eight horizontal wells of varying lengths from a common vertical shaft. The horizontal wells were arranged in a spoke-like fashion, 45° apart from each other, and used for production. Poor oil response in initial periods was believed to have been caused by the placement of the horizontal wells in a highly unfavourable reservoir environment of low vertical permeability and depleted oil saturation and pressure conditions at the pilot site. The termination of the pilot was followed by numerical studies which aimed to develop better operating strategies and to predict future potential. The main conclusion derived from the simulation studies was that horizontal wells can be efficient at reducing steam override.

Folefac and Archer [75] discussed the simulation of horizontal wells in thermal recovery processes for heavy oils. The objectives of the study were to evaluate the effectiveness of horizontal wells in improving the productivity and injectivity indices, the potentials of horizontal wells in increasing sweep efficiency at breakthrough by minimizing gravity override and gravity segregation, and the effectiveness of horizontal wells in controlling coning tendencies. Conformal mapping techniques were employed to transform complex flow geometries in horizontal wells into simpler geometries for which the flow rates and productivity indices can be calculated readily. An important assumption used in the representation of the horizontal well continuum by various discretizing methods was that the horizontal well has infinite conductivity, i.e. there is no pressure drop along the well. The authors concluded that the improvements in productivity by horizontal wells are strongly dependent on well length and the lateral extent of the reservoir. In addition, horiozontal wells can maintain a stable displacement front for flow processes dominated by gravity forces, and thus lead to improved sweep efficiency. Finally, it was shown that increasing the horizontal well length in reservoirs exhibiting coning tendencies will reduce cone height and increase the critical production rate.

Combe, Burger, Renard, and Valentin [76] numerically investigated the improvements in recovery performance of steam drive when horizontal wells are employed. The cases considered included a wide range of fluid and reservoir characteristics, different spatial distributions for vertical and horizontal wells, as well as different injection strategies. The results showed horizontal wells to be efficient for exploiting thin, marginal heavy oil reservoirs with low oil mobility. Studies were also carried out for layered reservoirs with tight streaks between layers, and reservoirs with initial mobile water saturation. It was predicted, for the first case, that a significant acceleration of oil production would be achieved if horizontal wells were drilled in various layers than would have been the case if all the wells were in one layer.

In conclusion, horizontal wells can improve recovery performance of conventional thermal recovery methods. Their most important contribution is to reduce steam override and gravity segregation — thus leading to better steam sweep efficiency. In addition, they offer high oil production rates, accelerated recovery, and improved oil-steam ratios.

3.4.2 Horizontal Wells in Non-Thermal EOR

Chen and Olynyk [77] carried out numerical simulation runs to examine the improvement in displacement and sweep efficiencies for miscible floods due to the use of horizontal injectors and producers. A two-dimensional, homogeneous reservoir mathematical model was used to simulate the areal sweep efficiencies in a five-spot (or staggered line-drive) quarter pattern. Four different cases were studied: conventional vertical injector and producer, horizontal injector and producer – both of various lengths, vertical injector and horizontal producer, vertical producer and horizontal injector. In the

latter two cases, the horizontal wellbore length was equal to the length of the side of the quarter pattern. Care was taken when designing the grid system for each of the four cases to ensure a common performance comparison basis. In addition, a wide range of mobility ratios between the displacing solvents and displaced oil was used.

The simulation runs led to the following conclusions: the use of horizontal injectors and producers can significantly improve the areal sweep efficiency in miscible floods; in addition, the largest improvement in areal sweep efficiency would be achieved for the most adverse mobility ratios; extended horizontal wellbore lengths could lead to large increases in well productivity index and overall productivity; and finally, the use of horizontal wells could decrease the velocity of the solvent flood front, and thus result in a more stable flood front due to a reduction in viscous fingering and less dilution of the solvent due to dispersive mixing.

Butler and Mokrys [78] discussed a new approach analogous to the steam-assisted gravity drainage method to recover heavy oils from formations unsuitable for steam recovery processes. In this approach, a hydrocarbon solvent vapour near its dew point (propane is recommended by the authors) is injected simultaneously with hot water into the top of a thin heavy oil reservoir. The solvent vapour forms a vapour zone between the injector and the horizontal producer located near the reservoir base. It then moves to the chamber boundaries and dilutes the surrounding heavy oil, which is drained downwards by gravity into the horizontal producer. As the diluted oil drains downwards it comes into contact with the hot water, which vapourizes the dissolved solvent out of the draining oil stream. The warm vapour then rises countercurrent to the draining diluted heavy oil, and increases its temperature as it interacts with hotter water near the top of the reservoir. Once it reaches the top, the solvent vapour moves to the edges of the vapour zone and propagates laterally.

In this mechanism, the solvent serves to dilute the viscous oil as well as to act as a heat carrier for even heat distribution around the vapour zone. Similarly, the hot water serves to heat the oil and reduce its viscosity, as well as to leach the dissolved solvent from the draining diluted oil for re-use at the top of the zone. In this process a large percentage of the injected solvent can be recovered and re-used.

Laboratory experimental results led the authors to conclude that the overall success of this new recovery process depends largely on the selection of a proper solvent, and the ability to raise reservoir temperature to a suitable range for the optimum recovery and recycling of solvent.

4. DEVELOPMENT OF SCALING CRITERIA

Physical models have been used extensively to study hydrodynamic phenomena. In general, the models can be classified into three groups: unscaled, partially scaled, and fully scaled. *Unscaled models* are easy and inexpensive to build and operate. They are used mainly to detect and observe flow phenomena. Because of their unscaled nature, these models cannot be used to predict accurately flow conditions quantitatively. *Partially scaled models* are more expensive and difficult to build and operate. In these models, some aspects of the flow process under investigation are scaled while the other aspects are not. Hence, some knowledge of the flow process is required. Partially scaled models can be used to provide certain quantitative predictions for the flow process, especially with respect to those aspects that are scaled. *Fully scaled models* are the most complex and difficult to build and operate. In this case, every aspect of the flow process under study is scaled. Complete knowledge of the most important mechanisms of the process is required. As a result, these models can be used confidently to predict the desired aspects of the flow process. In reality, it is almost always impossible to satisfy all of the scaling requirements, and/or to construct and employ fully scaled models. This is particularly true for models used to study fluid flow in porous media. Partially scaled and fully scaled models require the derivation of certain *scaling groups* and the use of these groups in their construction and operation.

4.1 Scaling Techniques

Scaling theory as it is applied to the design, construction, and operation of physical models is based upon the Principle of Similarity. The models are characterized by the same ratios of dimensions, forces, velocities, temperature differences and concentration differences as those occurring in the prototypes. The performance of these models is governed by the values of a number of parameters, which can be combined into different dimensionless similarity groups. There are two methods for deriving these scaling groups: dimensional analysis and inspectional analysis.

4.1.1 Dimensional Analysis

Dimensional analysis is based on the Buckingham π-Theorem. This method is used to derive the dimensionless similarity groups when the differential equations describing the flow process of interest are not known. It requires that all of the relevant variables for the process are known prior to the actual analysis. The variables are combined and arranged in a set of dimensionless groups ($\pi's$). The set is complete if all the groups in the set are independent of each other, and if every dimensionless group containing the same variables, and not belonging to the set, can be formed by combining groups belonging to the set. A general rule for dimensional analysis is that if there are n separate variables, and m primary quantities (mass, length, time, temperature, force, heat) then the set

will be complete when there are $n - m$ dimensionless groups. A complete treatment of dimensional analysis and its application to scaled models can be found in Langhaar's work [79].

4.1.2 Inspectional Analysis

Inspectional analysis is more systematic in its approach for obtaining the dimensionless groups, if the process under study can be described satisfactorily by means of differential equations. For this technique, differential equations relating the independent and dependent variables as well as the constraints of the flow process serve as the basis from which the set of dimensionless groups is obtained. This is done first by making the equations dimensionally homogeneous. Next, the dependent variables can be rendered dimensionless by dividing each equation by one of its coefficients. In almost all instances, the equations describing a flow process are partial differential equations, and as such relevant boundary and initial conditions need to be specified for the process to be completely described. These are handled in the same manner to obtain the dimensionless boundary and initial conditions.

Historically, dimensional analysis was used extensively for early scaled model studies of reservoir fluid flow. Only recently has inspectional analysis been used to determine the scaling groups for scaled model experiments.

Leverett, Lewis, and True [80] were among the first investigators to apply scaling laws to model study the flow of fluids in petroleum reservoirs. They used dimensional analysis to obtain the dimensionless groups governing the water drive process. Subsequently, other authors like Rapoport and Leas [81], and Croes and Schwarz [82] extended the above analysis, again using dimensional analysis, to examine various parameters involved in the displacement of light oil by cold water. Offeringa and van der Poel [83] used the same approach to carry out scaled model experiments on oil recovery by solvent injection.

Geertsma, Croes, and Schwarz [84] pointed out that in general the set of dimensionless similarity groups from dimensional analysis is bigger than that from inspectional analysis. However, the physical meaning of the similarity groups derived by dimensional analysis is generally less apparent than that of the groups derived by inspectional analysis. To illustrate these points, the authors derived the dimensionless similarity groups for three types of oil displacement: cold-water drive, hot-water drive, and solvent injection. In all three cases, dimensional analysis gave more groups than inspectional analysis, and the similarity groups derived by inspectional analysis were more flexible and useful with respect to the realization of a scaled physical model. Rojas and Farouq Ali [85-86] combined dimensional analysis and inspectional analysis to derive all of the scaling groups governing the carbon dioxide/brine immiscible flooding of heavy oils.

Work dealing specifically with scaling of steam injection processes has been carried out by a number

of researchers. Pujol and Boberg [87] examined the scaling accuracy of laboratory steamflooding models, especially with regard to the scaling of capillary pressure. They found that for highly viscous oils accurate scaling of capillary pressure was not crucial. This was because the ratio of capillary to viscous forces was so small that unscaled capillary pressures would have negligible effects on oil recovery. In the case of medium-viscosity oils ($\mu < 1000$ mPa.s), unscaled capillary pressure resulted in optimistic oil recovery. Oil recovery, for their study, depended mainly on the heat input per unit volume of reservoir sand. Injection rate was found to be a much less important parameter affecting oil recovery.

Stegemeier, Laumbach, and Volek [88] carried out scaled model studies for the Mt. Poso and Midway Sunset prototypes. The dimensionless similarity groups were obtained using inspectional analysis. The novel feature of this study was the use of vacuum models to carry out the experiments at pressures well below atmospheric pressure. The authors stated that the Clausius-Clapeyron relationship would be scaled properly when the experiments are conducted in subatmospheric and low-temperature conditions. Techniques were devised with regard to materials selected to represent the porous media and reservoir fluids to ensure dimensional similarity between the models and the prototypes. The results showed that the quantity of steam injected was the most important factor affecting the amount of oil recovered.

Farouq Ali and Redford [89] provided a thorough analysis of notable scaled laboratory thermal recovery studies. They examined the scaling groups derived for steam injection and in-situ combustion processes by various investigators. Kimber, Farouq Ali, and Puttagunta [90-92] presented an innovative and comprehensive analysis to obtain new scaling criteria for steam and steam-additive injection experiments. In these studies, both dimensional and inspectional analyses were used to obtain the set of similarity groups. The same conclusion as that of Geertsma et al. [84] was reached: the set of similarity groups derived by dimensional analysis was larger than that derived by inspectional analysis. The authors pointed out that it was difficult to satisfy all of the scaling criteria at the same time physically. Hence, some scaling groups had to be relaxed. Five different approaches were adopted, with each approach scaling a selected mechanism of the recovery process while relaxing the remaining mechanisms. High-pressure models were constructed and operated according to the five resulting sets of scaling criteria for the five approaches. Experimental data were then compared to determine the effects due to the relaxation of some of the scaling groups.

As a consequence of the above considerations, as well as due to the belief that at the present time there is a lack of knowledge regarding the variables relevant to the fluid flow processes in the vicinity of, and inside a horizontal wellbore, it was decided to use inspectional analysis to obtain the scaling criteria for the physical model of this study.

For the problem under investigation, it was of important that two different sets of scaling criteria be derived for the two different flow mechanisms involved in the overall process: flow of reservoir fluids in the porous medium, and flow of fluids inside the horizontal well itself. In each case, the governing partial differential equations, along with appropriate constraints, constitutive relationships, boundary and initial conditions were formulated first. These were then rewritten in terms of the dimensionless variables and their reference quantities, and the similarity groups were identified.

4.2 Flow of Reservoir Fluids in the Porous Medium

This flow process was treated as three-phase flow (oleic, aqueous, and vapour). Allowance was made for the injection of an additive along with steam. This steam-additive was assumed to exist only in the oleic and vapour phases. Diffusion and dispersion of the steam-additive between these phases were not considered in the analysis. Additional assumptions were needed, and these included: mass transfer took place solely due to convection; water condensed out of, or vapourized into steam; the porous medium was homogeneous and isotropic; rock compressibility and thermal expansion were negligible; the system was always in local thermodynamic equilibrium; kinetic, potential, and viscous energies were negligible compared to thermal energy; dispersive and diffusive heat losses were small compared to conductive heat flux. Also, Darcy's law was assumed valid for fluid flow, i.e. there were no appreciable inertial effects. Similarly, Fourier's law was assumed valid for heat flow due to conduction. Furthermore, it was assumed that the fluids under consideration behaved according to Newton's model for viscous fluids, and that their properties were functions of fluid pressures, temperatures, and concentrations. These assumptions altogether led to the following governing partial differential equations, which described the conservation of various physical quantities. Appendix A contains the derivation of these governing partial differential equations from first principles.

Mass balance for oil:

$$\frac{1}{r}\frac{\partial}{\partial r}\left[r\rho_o C_{oo}\frac{kk_{ro}}{\mu_o}\cdot\left(\frac{\partial p_o}{\partial r}+\rho_o g\frac{\partial(r sin\theta)}{\partial r}\right)\right]$$
$$+\frac{1}{r^2}\frac{\partial}{\partial \theta}\left[\rho_o C_{oo}\frac{kk_{ro}}{\mu_o}\cdot\left(\frac{\partial p_o}{\partial \theta}+\rho_o g\frac{\partial(r sin\theta)}{\partial \theta}\right)\right]$$
$$+\frac{\partial}{\partial z}\left[\rho_o C_{oo}\frac{kk_{ro}}{\mu_o}\cdot\frac{\partial p_o}{\partial z}\right]+q_o^* = \frac{\partial}{\partial t}\left(\phi S_o\rho_o C_{oo}\right) \quad . \tag{1}$$

Mass balance for water:

$$\frac{1}{r}\frac{\partial}{\partial r}\left[r\rho_w\frac{kk_{rw}}{\mu_w}\cdot\left(\frac{\partial p_w}{\partial r}+\rho_w g\frac{\partial(r sin\theta)}{\partial r}\right)\right]$$
$$+\frac{1}{r}\frac{\partial}{\partial r}\left[r\rho_g C_{gw}\frac{kk_{rg}}{\mu_g}\cdot\left(\frac{\partial p_g}{\partial r}+\rho_g g\frac{\partial(r sin\theta)}{\partial r}\right)\right]$$

$$+ \frac{1}{r^2} \frac{\partial}{\partial \theta} \left[\rho_w \frac{kk_{rw}}{\mu_w} \cdot \left(\frac{\partial p_w}{\partial \theta} + \rho_w g \frac{\partial (r sin\theta)}{\partial \theta} \right) \right]$$

$$+ \frac{1}{r^2} \frac{\partial}{\partial \theta} \left[\rho_g C_{gw} \frac{kk_{rg}}{\mu_g} \cdot \left(\frac{\partial p_g}{\partial \theta} + \rho_g g \frac{\partial (r sin\theta)}{\partial \theta} \right) \right]$$

$$+ \frac{\partial}{\partial z} \left[\rho_w \frac{kk_{rw}}{\mu_w} \cdot \frac{\partial p_w}{\partial z} \right] + \frac{\partial}{\partial z} \left[\rho_g C_{gw} \frac{kk_{rg}}{\mu_g} \cdot \frac{\partial p_g}{\partial z} \right]$$

$$+ q_w^* + q_g^* C_{gw}^* = \frac{\partial}{\partial t} \left(\phi S_w \rho_w + \phi S_g \rho_g C_{gw} \right) \quad . \tag{2}$$

Mass balance for the steam-additive:

$$\frac{1}{r} \frac{\partial}{\partial r} \left[r \rho_o C_{oa} \frac{kk_{ro}}{\mu_o} \cdot \left(\frac{\partial p_o}{\partial r} + \rho_o g \frac{\partial (r sin\theta)}{\partial r} \right) \right]$$

$$+ \frac{1}{r} \frac{\partial}{\partial r} \left[r \rho_g C_{ga} \frac{kk_{rg}}{\mu_g} \cdot \left(\frac{\partial p_g}{\partial r} + \rho_g g \frac{\partial (r sin\theta)}{\partial r} \right) \right]$$

$$+ \frac{1}{r^2} \frac{\partial}{\partial \theta} \left[\rho_o C_{oa} \frac{kk_{ro}}{\mu_o} \cdot \left(\frac{\partial p_o}{\partial \theta} + \rho_o g \frac{\partial (r sin\theta)}{\partial \theta} \right) \right]$$

$$+ \frac{1}{r^2} \frac{\partial}{\partial \theta} \left[\rho_g C_{ga} \frac{kk_{rg}}{\mu_g} \cdot \left(\frac{\partial p_g}{\partial \theta} + \rho_g g \frac{\partial (r sin\theta)}{\partial \theta} \right) \right]$$

$$+ \frac{\partial}{\partial z} \left[\rho_o C_{oa} \frac{kk_{ro}}{\mu_o} \cdot \frac{\partial p_w}{\partial z} \right] + \frac{\partial}{\partial z} \left[\rho_g C_{ga} \frac{kk_{rg}}{\mu_g} \cdot \frac{\partial p_g}{\partial z} \right]$$

$$+ q_o^* C_{oa}^* + q_g^* C_{ga}^* = \frac{\partial}{\partial t} \left(\phi S_o \rho_o C_{oa} + \phi S_g \rho_g C_{ga} \right) \quad . \tag{3}$$

Energy balance:

$$\frac{1}{r} \frac{\partial}{\partial r} (r k_{hr} \cdot \frac{\partial T}{\partial r}) + \frac{1}{r^2} \frac{\partial}{\partial \theta} (k_{hr} \cdot \frac{\partial T}{\partial \theta}) + \frac{\partial}{\partial z} (k_{hr} \cdot \frac{\partial T}{\partial z})$$

$$+ \frac{1}{r} \frac{\partial}{\partial r} \left[r \rho_o \frac{h_o kk_{ro}}{\mu_o} \cdot \left(\frac{\partial p_o}{\partial r} + \rho_o g \frac{\partial (r sin\theta)}{\partial r} \right) \right]$$

$$+ \frac{1}{r^2} \frac{\partial}{\partial \theta} \left[\rho_o \frac{h_o kk_{ro}}{\mu_o} \cdot \left(\frac{\partial p_o}{\partial \theta} + \rho_o g \frac{\partial (r sin\theta)}{\partial \theta} \right) \right] + \frac{\partial}{\partial z} \left[\rho_o \frac{h_o kk_{ro}}{\mu_o} \cdot \frac{\partial p_o}{\partial z} \right]$$

$$+ \frac{1}{r} \frac{\partial}{\partial r} \left[r \rho_w \frac{h_w kk_{rw}}{\mu_w} \cdot \left(\frac{\partial p_w}{\partial r} + \rho_w g \frac{\partial (r sin\theta)}{\partial r} \right) \right]$$

$$+ \frac{1}{r^2} \frac{\partial}{\partial \theta} \left[\rho_w \frac{h_w kk_{rw}}{\mu_w} \cdot \left(\frac{\partial p_w}{\partial \theta} + \rho_w g \frac{\partial (r sin\theta)}{\partial \theta} \right) \right] + \frac{\partial}{\partial z} \left[\rho_w \frac{h_w kk_{rw}}{\mu_w} \cdot \frac{\partial p_w}{\partial z} \right]$$

$$+ \frac{1}{r} \frac{\partial}{\partial r} \left[r \rho_g \frac{h_g kk_{rg}}{\mu_g} \cdot \left(\frac{\partial p_g}{\partial r} + \rho_g g \frac{\partial (r sin\theta)}{\partial r} \right) \right]$$

$$+ \frac{1}{r^2} \frac{\partial}{\partial \theta} \left[\rho_g \frac{h_g kk_{rg}}{\mu_g} \cdot \left(\frac{\partial p_g}{\partial \theta} + \rho_g g \frac{\partial (r sin\theta)}{\partial \theta} \right) \right] + \frac{\partial}{\partial z} \left[\rho_g \frac{h_g kk_{rg}}{\mu_g} \cdot \frac{\partial p_g}{\partial z} \right]$$

$$+ q_h^* - q_l^* = \frac{\partial}{\partial t} \left[(1 - \phi) \rho_r U_r + \phi S_o \rho_o U_o + \phi S_w \rho_w U_w + \phi S_g \rho_g U_g \right] \quad . \tag{4}$$

Table 1 shows a list of consultative relationships and constraints for the flow of reservoir fluids from the porous medium into the horizontal well. Appendix B contains the boundary and initial conditions chosen for this flow process.

Table 1: Constraints and Constitutive Relationships for Reservoir Flow.

a) Constitutive relationships:

$$\rho_o = \rho_o(p_o, T, C_{oa})$$

$$\rho_w = \rho_w(p_w, T)$$

$$\rho_g = \rho_g(p_g, T, C_{ga})$$

$$\mu_o = \mu_o(p_o, T, C_{oa})$$

$$\mu_w = \mu_w(p_w, T)$$

$$\mu_g = \mu_g(p_g, T, C_{ga})$$

$$k_{ro} = k_{ro}(S_o, S_w, k)$$

$$k_{rw} = k_{rw}(S_o, S_w, k)$$

$$k_{rg} = k_{rg}(S_o, S_w, k)$$

$$h_o = h_o(p_o, T, C_{oa})$$

$$h_w = h_w(p_w, T)$$

$$h_g = h_g(p_g, T, C_{gw})$$

$$h_r = h_r(T)$$

$$k_{hr} = k_{hr}(T)$$

$$k_{hob} = k_{hob}(T)$$

$$U_o = U_o(p_o, T, C_{oa})$$

$$U_w = U_w(p_w, T)$$

$$U_g = U_g(p_g, T, C_{gw})$$

b) Constraints:

$$S_o + S_w + S_g = 1$$

$$C_{oo} + C_{oa} = 1$$

$$C_{gw} + C_{ga} = 1$$

$$p_g = p_o + P_{cgo}(S_o, S_w)$$

$$p_w = p_o - P_{cow}(S_o, S_w)$$

c) Constants:

$$\dot{\phi} = const.$$

$$\rho_r = const.$$

$$g = const. \ (9.80665 m/s^2)$$

Each variable can be written in dimensionless form by dividing it by some characteristic reference quantity. For example, the general variable M can be rewritten as $M_D = M/M_R$, where M_D is the dimensionless form of the variable and M_R is some constant characteristic reference value. Substituting the above relationship for every variable in the governing partial differential equations, as well as the constraints, constitutive relationships, initial and boundary conditions allowed these to take the form as shown below for the mass balance of oil,

$$
\left[\frac{\rho_{oR}C_{ooR}kk_{roR}p_{oR}}{r_R^2\mu_{oR}}\right]\frac{1}{r_D}\frac{\partial}{\partial r_D}\left(\frac{r_D\rho_{oD}C_{ooD}kk_{roD}}{\mu_{oD}}\cdot\frac{\partial p_{oD}}{\partial r_D}\right)
$$

$$
+\left[\frac{\rho_{oR}^2C_{ooR}kk_{roR}g_R r_R sin\theta_R}{r_R^2\mu_{oR}}\right]\frac{1}{r_D}\frac{\partial}{\partial r_D}\left(\frac{r_D\rho_{oD}^2C_{ooD}kk_{roD}g_D}{\mu_{oD}}\cdot\frac{\partial(r_D sin\theta_D)}{\partial r_D}\right)
$$

$$
+\left[\frac{\rho_{oR}C_{ooR}kk_{roR}p_{oR}}{r_R^2\theta_R^2\mu_{oR}}\right]\frac{1}{r_D^2}\frac{\partial}{\partial\theta_D}\left(\frac{\rho_{oD}C_{ooD}kk_{roD}}{\mu_{oD}}\cdot\frac{\partial p_{oD}}{\partial\theta_D}\right)
$$

$$
+\left[\frac{\rho_{oR}^2C_{ooR}kk_{roR}g_R r_R sin\theta_R}{r_R\theta_R^2\mu_{oR}}\right]\frac{1}{r_D^2}\frac{\partial}{\partial\theta_D}\left(\frac{\rho_{oD}^2C_{ooD}kk_{roD}g_D}{\mu_{oD}}\cdot\frac{\partial(r_D sin\theta_D)}{\partial\theta_D}\right)
$$

$$
+\left[\frac{\rho_{oR}C_{ooR}kk_{roR}p_{oR}}{z_R^2\mu_{oR}}\right]\frac{\partial}{\partial z_D}\left(\frac{\rho_{oD}^2C_{ooD}kk_{roD}g_D}{\mu_{oD}}\cdot\frac{\partial p_{oD}}{\partial z_D}\right)
$$

$$
+q_{oR}^*q_{oD}^* = \left[\frac{\phi_R S_{oR}\rho_{oR}C_{ooR}}{t_R}\right]\frac{\partial}{\partial t_D}\left(\phi_D S_{oD}\rho_{oD}C_{ooD}\right). \tag{5}
$$

The reference quantities in the square brackets represent the coefficients of the terms in the equation. All coefficients have the same units. Dividing the entire equation by any of these coefficients yields the dimensionless form of the equation, with the similarity groups embedded in the dimensionless coefficients. For the mass balance of oil, the equation was divided by the first coefficient of the left-hand side, viz.

$$
\left[\frac{\rho_{oR}C_{ooR}kk_{roR}p_{oR}}{r_R^2\mu_{oR}r_D}\right] .
$$

This leads to the following equation:

$$
\frac{\partial}{\partial r_D}\left(\frac{r_D\rho_{oD}C_{ooD}kk_{roD}}{\mu_{oD}}\cdot\frac{\partial p_{oD}}{\partial r_D}\right)
$$

$$
+\left[\frac{\rho_{oR}g_R r_R sin\theta_R}{p_{oR}}\right]\frac{\partial}{\partial r_D}\left(\frac{r_D\rho_{oD}^2C_{ooD}kk_{roD}g_D}{\mu_{oD}}\cdot\frac{\partial(r_D sin\theta_D)}{\partial^\cdot_D}\right)
$$

$$
+\left[\frac{1}{\theta_R^2}\right]\frac{\partial}{\partial\theta_D}\left(\frac{\rho_{oD}C_{ooD}kk_{roD}}{\mu_{oD}}\cdot\frac{\partial p_{oD}}{\partial\theta_D}\right)
$$

$$
+\left[\frac{r_R^2\rho_{oR}g_R sin\theta_R}{\theta_R^2 p_{oR}}\right]\frac{1}{r_D}\frac{\partial}{\partial\theta_D}\left(\frac{\rho_{oD}^2C_{ooD}kk_{roD}g_D}{\mu_{oD}}\cdot\frac{\partial(r_D sin\theta_D)}{\partial\theta_D}\right)
$$

$$
+\left[\frac{r_R^2}{z_R^2}\right]r_D\frac{\partial}{\partial z_D}\left(\frac{\rho_{oD}^2C_{ooD}kk_{roD}g_D}{\mu_{oD}}\cdot\frac{\partial p_{oD}}{\partial z_D}\right)
$$

$$
+\left[\frac{q_{oR}^*r_R^2\mu_{oR}}{\rho_{oR}C_{ooR}kk_{roR}p_{oR}}\right]r_D q_{oD}^* = \left[\frac{\phi_R S_{oR}r_R^2\mu_{oR}}{kk_{roR}p_{oR}t_R}\right]r_D\frac{\partial}{\partial t_D}\left(\phi_D S_{oD}\rho_{oD}C_{ooD}\right). \tag{6}
$$

The dimensionless form of the other governing equations were obtained in a similar manner, and are listed in Appendix C. The set of dimensionless coefficients thus yielded may be replaced by any other set obtained from the products of the groups with any other group raised to any power. This allows for some simplification, and after some simplifying assumptions can lead to the final set of scaling criteria. Table 2 lists the set of scaling criteria for fluid flow from the reservoir to the horizontal well, while Table 3 indicates the physical meaning of these scaling criteria.

Table 2: Scaling Criteria for Reservoir Flow.

$$\frac{H}{2L}, \quad \frac{\rho_{oR} H g_R \sin\theta_R}{2p_{oR}}, \quad \frac{q^*_{oR} H^2 \mu_{oR}}{4\rho_{oR} kk_{roR} p_{oR}}, \quad \frac{\rho_{wR}}{\rho_{oR}}, \quad \frac{\rho_{gR}}{\rho_{oR}}, \quad \frac{p_{oR}}{p_{wR}}, \quad \frac{p_{oR}}{p_{gR}},$$

$$\frac{S_{wR}}{S_{oR}}, \quad \frac{S_{gR}}{S_{oR}}, \quad \frac{C^*_{gaR} q^*_{gR}}{C^*_{oaR} q^*_{oR}}, \quad \frac{k_{hrR} T_R \mu_{oR}}{\rho_{oR} kk_{roR} h_{oR} p_{oR}}, \quad \frac{\phi_R S_{oR} H^2 \mu_{oR}}{4kk_{roR} p_{oR} t_R}, \quad \frac{h_{wR}}{h_{oR}},$$

$$\frac{h_{gR}}{h_{oR}}, \quad \frac{q^*_{hR}}{q^*_{oR} h_{oR}}, \quad \frac{q^*_{hR}}{q^*_{lR}}, \quad \phi_R, \quad \frac{\rho_{rR} U_{rR}}{\rho_{oR} h_{oR}}, \quad \frac{U_{oR}}{h_{oR}}, \quad \frac{U_{wR}}{h_{oR}}, \quad \frac{U_{gR}}{h_{oR}}, \quad \frac{P_{cgoR}}{p_{oR}},$$

$$\frac{P_{cowR}}{p_{oR}}, \quad \frac{S_{oiR}}{S_{oR}}, \quad \frac{p_{oiR}}{p_{oR}}, \quad \frac{T_{iR}}{T_R}, \quad \frac{p_{oR} kk_{roR}}{\phi_R S_{oR} \mu_{oR} \alpha_{obR}}, \quad \frac{q^*_{lR} H^2}{4k_{hobR} T_{obR}}, \quad \frac{q^*_{oR}}{q^*_{wR}},$$

$$\frac{A^*_R k_{hobR} T_{obR}}{V_{bR} L q^*_{lR}}, \quad \frac{h^*_{winjR} q^*_{winjR}}{q^*_{hinjR}}, \quad \frac{h^*_{sinjR}}{h^*_{winjR}}, \quad \frac{q^*_{oprodR}}{C^*_{gwprodR} q^*_{gprodR}}, \quad \frac{k_{roR} \mu_{wR}}{k_{rwR} \mu_{oR}},$$

$$\frac{k_{roR} \mu_{gR}}{k_{rgR} \mu_{oR}}, \quad \frac{k_{rwR} \mu_{gR}}{k_{rgR} \mu_{wR}}, \quad \frac{W_{gwR} h_{gwinjR}}{W_{wR} h_{winjR}}, \quad \frac{W_{wR} \mu_{wR}}{\rho_{wR} kk_{rwR} H p_{wR}}$$

Table 3: Physical Meaning of the Scaling Criteria for Reservoir Flow.

ϕ_R	Porosity factor
$\dfrac{H}{2L}$	Geometrical factor
$\dfrac{\rho_{oR} H g_R \sin\theta_R}{2 p_{oR}}$	Ratio of gravitational force to pressure drawdown
$\dfrac{q^*_{oR} H^2 \mu_{oR}}{4 \rho_{oR} k k_{roR} P_{oR}}$	Ratio of viscous force to pressure drawdown
$\dfrac{\rho_{wR}}{\rho_{oR}}$	Ratio of aqueous and oleic phase densities
$\dfrac{\rho_{gR}}{\rho_{oR}}$	Ratio of vapour and oleic phase densities
$\dfrac{P_{oR}}{P_{wR}}$	Ratio of oleic and aqueous phase pressures
$\dfrac{P_{oR}}{P_{gR}}$	Ratio of oleic and vapour phase pressures
$\dfrac{S_{wR}}{S_{oR}}$	Ratio of aqueous and oleic phase saturations
$\dfrac{S_{gR}}{S_{oR}}$	Ratio of vapour and oleic phase saturations
$\dfrac{C^*_{gaR} q^*_{gR}}{C^*_{oaR} q^*_{oR}}$	Ratio of produced steam-additive in vapour and oleic phases
$\dfrac{k_{hrR} T_R \mu_{oR}}{\rho_{oR} k k_{roR} h_{oR} P_{oR}}$	Ratio of conductive heat to oleic phase convective heat
$\dfrac{\phi_R S_{oR} H^2 \mu_{oR}}{4 k k_{roR} P_{oR} t_R}$	Time scale factor

$$\frac{h_{wR}}{h_{oR}}$$ Ratio of aqueous and oleic phase enthalpies

$$\frac{h_{gR}}{h_{oR}}$$ Ratio of vapour and oleic phase enthalpies

$$\frac{\dot{q}_{hR}}{\dot{q}_{oR} h_{oR}}$$ Ratio of rate of heat inj./prod. to oleic phase enthalpy

$$\frac{\dot{q}_{hR}}{\dot{q}_{lR}}$$ Ratio of rate of heat inj./prod. to rate of heat loss

$$\frac{\rho_{rR} U_{rR}}{\rho_{oR} h_{oR}}$$ Ratio of reservoir rock energy to oleic phase enthalpy

$$\frac{U_{oR}}{h_{oR}}$$ Ratio of oleic phase internal energy and its enthalpy

$$\frac{U_{wR}}{h_{oR}}$$ Ratio of aqueous phase internal energy to oleic phase enthalpy

$$\frac{U_{gR}}{h_{oR}}$$ Ratio of vapour phase internal energy to oleic phase enthalpy

$$\frac{P_{cgoR}}{P_{oR}}$$ Ratio of gas-oil capillary pressure to oleic phase pressure

$$\frac{P_{cowR}}{P_{oR}}$$ Ratio of water-oil capillary pressure to oleic phase pressure

$$\frac{S_{oiR}}{S_{oR}}$$ Ratio of initial and instantaneous oleic phase saturation

$$\frac{P_{oiR}}{P_{oR}}$$ Ratio of initial and instantaneous oleic phase pressure

$$\frac{T_{iR}}{T_R}$$ Ratio of initial and instantaneous temperature

$$\frac{P_{oR} k k_{roR}}{\phi_R S_{oR} \mu_{oR} \alpha_{obR}}$$ Ratio of oleic phase prod. and thermal diffusion to overburden

$$\frac{q_{IR}^{*}H^2}{4k_{hobR}T_{obR}}$$ Ratio of heat loss to overburden thermal capacity

$$\frac{q_{oR}^{*}}{q_{wR}^{*}}$$ Ratio of oleic and vapour phase production rates

$$\frac{A_R^{*}k_{hobR}T_{obR}}{V_{bR}Lq_{IR}^{*}}$$ Ratio of overburden thermal conductivity to heat loss rate

$$\frac{h_{winjR}^{*}q_{winjR}^{*}}{q_{hinjR}^{*}}$$ Ratio of prod. aqueous phase enthalpy to heat injected

$$\frac{h_{sinjR}^{*}}{h_{winjR}^{*}}$$ Ratio of inj. steam-additive enthalpy and inj. aqueous enthalpy

$$\frac{q_{oprodR}^{*}}{C_{gwprodR}^{*}q_{gprodR}^{*}}$$ Ratio of prod. oleic phase and prod. steam-additive in vapour

$$\frac{k_{roR}\mu_{wR}}{k_{rwR}\mu_{oR}}$$ Mobility ratio between oleic and aqueous phases

$$\frac{k_{roR}\mu_{gR}}{k_{rgR}\mu_{oR}}$$ Mobility ratio between oleic and vapour phases

$$\frac{k_{rwR}\mu_{gR}}{k_{rgR}\mu_{wR}}$$ Mobility ratio between aqueous and vapour phases

$$\frac{W_{gwR}h_{gwinjR}}{W_{wR}h_{winjR}}$$ Ratio of inj. water enthalpy to inj. aqueous enthalpy

$$\frac{W_{wR}\mu_{wR}}{\rho_{wR}kk_{rwR}Hp_{wR}}$$ Ratio of aqueous injection rate and reservoir storage capacity

A brief look at the above set of scaling criteria shows that it is quite large, and therefore could be potentially difficult to use in the design and construction of a physical model, as well as the subsequent operation of the model in various experiments. However, it must be remembered that the flow process under investigation is complex in nature (steam-additive was included), and thus the set of scaling criteria for it would be necessarily large. In addition, many of the scaling groups would be automatically satisfied if the same porous medium and reservoir fluids are used in the model and the prototype — leading to a reduction in the number of criteria to be satisfied.

The Buckingham π-Theorem was invoked to check the number of scaling groups obtained by inspectional analysis. Altogether, there were 57 parameters used in the derivation of the governing partial differential equations, constitutive relationships, constraints, initial and boundary conditions. Given that six of these parameters were primary variables (mass, length, temperature, force, heat, and time), the theorem states that there should be 51 scaling groups for this particular flow process. Table 2 contains 38 groups. Here again dimensional analysis gives a larger set of scaling groups than inspectional analysis, as was observed in previous studies [84,90-92]. Based upon past experience, it is believed that the relevant groups are the ones derived by inspectional analysis.

4.3 Flow of Reservoir Fluids Within the Horizontal Well

It was assumed that the fluids flowing inside the horizontal well are incompressible and immiscible, and consist of heated bitumen and hot condensate. To simplify the derivation of the scaling criteria, the flow was treated as single-phase and steady-state, with the flowing fluid assumed to have a single density and viscosity (which could be approximated from the weight fractions of its two components, to be calculated from the produced water-oil ratio). Appendix D illustrates the derivation, from first principles, of the governing equations for the flow inside the horizontal well.

Mass balance of fluid flowing inside the horizontal well is as follows:

$$\frac{dv}{dz} + \frac{2v_{out}r_w}{r_{w,in}^2} \cdot \frac{dr_w}{dz} + \frac{2a_w r_{w,avg}kk_{rm}}{\mu_m r_{w,in}^2} \cdot \left[\frac{dp_m}{dr} + \rho_m g\frac{d}{dr}(rsin\theta)\right] = 0 \quad . \tag{7}$$

In the derivation of the above equation, it is assumed that the volume of inflow into the horizontal well is a function of the potential gradient between the reservoir and the horizontal well, and that this inflow has an average density of ρ_m , and an effective permeability of kk_{rm} .

The symbol a_w signifies that only a fraction of the periphery of the horizontal well was open to the inflow of fluids from the reservoir. Mainly, this is because only the regions of the reservoir located above the horizontal well are swept by the rising steam fingers. Areas at the sides of, and under the horizontal well are not contacted by the steam fingers until much later.

To describe the momentum balance of the flow inside the horizontal well, an equation was taken from Table 3.4-3 of Bird, Stewart, and Lightfoot [93] . It describes the momentum balance for the

flow of a Newtonian fluid of a constant density and viscosity inside a horizontal conduit. For the problem under investigation, the flow inside the horizontal well is axial, and the geometry of the horizontal well is symmetrical. Thus, v_θ and v_r are equal to zero, and the original equation is simplified to the form listed below, viz.

$$\rho_m v\frac{dv}{dz} = -\frac{dp_p}{dz} + \mu_m\left[\frac{1}{r_w}\frac{d}{dr_w}(r_w\frac{dv}{dr_w}) + \frac{d^2v}{dz^2}\right] \quad . \tag{8}$$

The mass balance equation was then combined with the momentum balance equation to produce an expression, which relates the velocity gradient of the fluid stream flowing from one end of the horizontal well to the other with other variables such as the axial pressure gradients, potential drawdown, and fluid viscosity. This combined mass and momentum balance equation is as follows:

$$-\frac{2a_w r_{w,avg}kk_{rm}}{r_{w,in}^2\mu_m}\cdot\frac{dp_m}{dr} - \frac{2a_w\rho_m gkk_{rm}r_{w,avg}}{r_{w,in}^2\mu_m}\cdot\frac{d}{dr}(rsin\theta) - \frac{2v_{out}r_w}{r_{w,in}^2}\cdot\frac{dr_w}{dz}$$
$$+\frac{1}{\rho_m v}\cdot\frac{dp_p}{dz} - \frac{\mu_m}{\rho_m v}\cdot\frac{1}{r_w}\cdot\frac{d}{dr_w}(r_w\frac{dv}{dr_w}) - \frac{\mu_m}{\rho_m v}\cdot\frac{d^2v}{dz^2} = 0 \quad . \tag{9}$$

Energy balance for fluid flow inside the horizontal well.

To describe the energy conservation of the flow inside the horizontal well, it was assumed that the convective heat transfer due to the movement of the heated bitumen and hot condensate from one end of the well to the other end, as well as from the reservoir into the horizontal well, is much greater than the conductive heat transfer taking place between the fluids and the walls of the well. This led to the following expression:

$$\frac{r_{w,in}^2}{r_{w,avg}^2}\cdot\frac{d}{dz}(\frac{vU}{J}) + \frac{2v_{out}U_{out}r_w}{Jr_{w,avg}^2}\cdot\frac{dr_w}{dz}$$
$$+\frac{2a_w kk_{rm}U_m}{\mu_m r_{w,avg}}\cdot\left[\frac{dp_m}{dr} + \rho_m g\frac{d}{dr}(rsin\theta)\right] - W = C_H\frac{dT}{dt} \quad . \tag{10}$$

The initial and boundary conditions for this flow include:

$$T(r,z,t=0) = 0 \quad ,$$

and for the no-fluid entering condition at the inlet of the horizontal well,

$$v(r_w,z=0(inlet),t) = 0 \quad .$$

The boundary condition at the outlet of the horizontal well is,

$$v(r_w, z = L(outlet), t) = \frac{q^*}{\pi r_{w,out}^2} \quad .$$

As in the development of the scaling criteria for the flow of fluids from the reservoir to the horizontal well, the above equations along h the initial and boundary conditions were also reduced to dimensionless form to permit the deter- ination of the dimensionless s. arity groups. Therefore, the dimensionless mass and momentum balance for in. side the horizontal well is:

$$
-\left[\frac{2a_{wR}k_R k_{rmR} r_{w,avgR} p_{mR}}{\mu_{mR} r_{w,inR}^2 T_R}\right]\left(\frac{a_{wD}k_D k_{rmD} r_{w,avgD}}{\mu_{mD} r_{w,inD}^2}\right) \cdot \frac{dp_{mD}}{dr_D}
$$
$$
-\left[\frac{2a_{wR}k_R k_{rmR} r_{w,avgR} \rho_{mR} g_R \sin\theta_R}{\mu_{mR} r_{w,inR}^2}\right]\left(\frac{a_{wD}\rho_{mD} g_D k_D k_{rmD} r_{w,avgD}}{r_{w,inD}^2 \mu_{mD}}\right) \cdot \frac{d}{dr_D}(r_D \sin\theta_D)
$$
$$
-\left[\frac{2v_{outR} r_{wR}^2}{r_{w,inR}^2 z_R}\right]\left(\frac{v_{outD} r_{wD}}{r_{w,inD}^2}\right) \cdot \frac{dr_{wD}}{dz_D} + \left[\frac{p_{pR}}{\rho_{mR} v_R z_R}\right]\left(\frac{1}{\rho_{mD} v_D}\right) \cdot \frac{dp_{pD}}{dz_D}
$$
$$
-\left[\frac{\mu_{mR}}{\rho_{mR} r_{wR}^2}\right]\left(\frac{\mu_{mD}}{\rho_{mD} v_D r_{wD}}\right) \cdot \frac{d}{dr_{wD}}\left(r_{wD}\frac{dv_D}{dr_{wD}}\right) - \left[\frac{\mu_{mR}}{\rho_{mR} z_R^2}\right]\left(\frac{\mu_{mD}}{\rho_{mD} v_D}\right) \cdot \frac{d^2 v_D}{dz_D^2} = 0 \quad . \quad (11)
$$

Dividing the above equation by the reference coefficient of the first term,

$$
-\left[\frac{2a_{wR}k_R k_{rmR} r_{w,avgR} p_{mR}}{\mu_{mR} r_{w,inR}^2 T_R}\right]
$$

leads to the following equation:

$$
\left(\frac{a_{wD}k_D k_{rmD} r_{w,avgD}}{\mu_{mD} r_{w,inD}^2}\right) \cdot \frac{dp_{mD}}{dr_D}
$$
$$
+\left[\frac{\rho_{mR} g_R T_R \sin\theta_R}{p_{mR}}\right]\left(\frac{a_{wD}\rho_{mD} g_D k_D k_{rmD} r_{w,avgD}}{r_{w,inD}^2 \mu_{mD}}\right) \cdot \frac{d}{dr_D}(r_D \sin\theta_D)
$$
$$
+\left[\frac{v_{outR} r_{wR}^2 \mu_{mR} T_R}{a_{wR} k_R k_{rmR} p_{mR} z_R T_{w,avgR}}\right]\left(\frac{v_{outD} r_{wD}}{r_{w,inD}^2}\right) \cdot \frac{dr_{wD}}{dz_D}
$$
$$
-\left[\frac{p_{pR}\mu_{mR} r_{w,inR}^2 T_R}{2\rho_{mR} v_R z_R a_{wR} k_R k_{rmR} p_{mR} r_{w,avgR}}\right]\left(\frac{1}{\rho_{mD} v_D}\right) \cdot \frac{dp_{pD}}{dz_D}
$$
$$
+\left[\frac{r_{w,inR}^2}{r_{wR}^2}\frac{\mu_{mR}^2 T_R}{2\rho_{mR} a_{wR} r_{w,avgR} k_R k_{rmR} p_{mR}}\right]\left(\frac{\mu_{mD}}{\rho_{mD} v_D r_{wD}}\right) \cdot \frac{d}{dr_{wD}}\left(r_{wD}\frac{dv_D}{dr_{wD}}\right)
$$
$$
+\left[\frac{r_{w,inR}^2}{z_R^2}\frac{\mu_{mR}^2 T_R}{2\rho_{mR} a_{wR} r_{w,avgR} k_R k_{rmR} p_{mR}}\right]\left(\frac{\mu_{mD}}{\rho_{mD} v_D}\right) \cdot \frac{d^2 v_D}{dz_D^2} = 0 \quad . \quad (12)
$$

Similarly, the dimensionless energy balance for fluid flow inside the horizontal well assumes the following form:

$$
\left[\frac{r_{w,inR}^2 v_R U_R}{r_{w,avgR}^2 J_R z_R}\right]\left(\frac{r_{w,inD}^2}{r_{w,avgD}^2}\right) \cdot \frac{d}{dz_D}\left(\frac{v_D U_D}{J_D}\right) + \left[\frac{2v_{outR} U_{outR} r_{wR}^2}{J_R z_R r_{w,avgR}^2}\right]\left(\frac{v_{outD} U_{outD} r_{wD}}{J_D r_{w,avgD}^2}\right) \cdot \frac{dr_{wD}}{dz_D}
$$

$$+ \left[\frac{2a_{wR}k_R k_{rmR}P_{mR}U_{mR}}{\mu_{mR}r_R r_{w,avgR}}\right]\left(\frac{a_{wD}k_D k_{rmD}U_{mD}}{\mu_{mD}r_{w,avgD}}\right) \cdot \frac{dp_{mD}}{dr_D}$$

$$+ \left[\frac{2a_{wR}k_R k_{rmR}U_{mR}\rho_{mR}g_R \sin\theta_R}{\mu_{mR}r_{w,avgR}}\right]\left(\frac{a_{wD}k_D k_{rmD}U_{mD}\rho_{mD}g_D}{\mu_{mD}r_{w,avgD}}\right) \cdot \frac{d}{dr_D}(r_D \sin\theta_D)$$

$$- W_R W_D = \left[\frac{C_{HR}T_R}{t_R}\right]C_{HD} \cdot \frac{dT_D}{dt_D} \quad . \tag{13}$$

As in the case of the mass and momentum balance equation, dividing the above energy conservation equation of flow inside the horizontal well by the coefficient,

$$\left[\frac{r_{w,inR}^2 v_R U_R}{r_{w,avgR}^2 J_R z_R}\right]$$

results in the following expression:

$$\left(\frac{r_{w,inD}^2}{r_{w,avgD}^2}\right) \cdot \frac{d}{dz_D}\left(\frac{v_D U_D}{J_D}\right) + \left[\frac{2v_{outR}U_{outR}r_{wR}^2}{v_R r_{w,inR}^2 U_R}\right]\left(\frac{v_{outD}U_{outD}r_{wD}}{J_D r_{w,avgD}^2}\right) \cdot \frac{dr_{wD}}{dz_D}$$

$$+ \left[\frac{2a_{wR}k_R k_{rmR}U_{mR}P_{mR}J_R z_R r_{w,avgR}}{\mu_{mR}r_{w,inR}^2 v_R U_R}\right]\left(\frac{a_{wD}k_D k_{rmD}U_{mD}}{\mu_{mD}r_{w,avgD}}\right) \cdot \frac{dp_{mD}}{dr_D}$$

$$+ \left[\frac{2a_{wR}k_R k_{rmR}U_{mR}\rho_{mR}r_{w,avgR}g_R \sin\theta_R J_R z_R}{\mu_{mR}r_{w,inR}^2 v_R U_R}\right]\left(\frac{a_{wD}k_D k_{rmD}U_{mD}\rho_{mD}g_D}{\mu_{mD}r_{w,avgD}}\right) \cdot \frac{d}{dr_D}(r_D \sin\theta_D)$$

$$- \left[\frac{W_R r_{w,avgR}^2 J_R z_R}{v_R r_{w,inR}^2 U_R}\right]W_D = \left[\frac{r_{w,avgR}^2 C_{HR}T_R J_R z_R}{r_{w,inR}^2 v_R U_R t_R}\right]C_{HD} \cdot \frac{dT_D}{dt_D} \quad . \qquad . \tag{14}$$

Table 4 contains the set of scaling criteria for the flow inside the horizontal well. These criteria are a result of invoking simplifying assumptions which allow for some manipulation of the set of dimensionless similarity groups. Table 5 gives their physical meanings.

Table 4: Scaling Criteria for Flow Inside the Horizontal Well.

$$\frac{r_{w,inlet}}{r_{w,outlet}}, \quad \frac{L}{r_{w,outlet}}, \quad \frac{\rho_{mR}Hg_R\sin\theta_R}{2p_{mR}}, \quad \frac{2v_{outR}U_{outR}}{W_RJ_RL}, \quad \frac{W_Rt_R}{C_{HR}T_R},$$

$$\frac{J_RU_{mR}\Delta p_R}{\rho_{mR}U_Rv_R^2}, \quad \frac{r_{w,outlet}^2\Delta p_R}{L\mu_{mR}v_R}, \quad \frac{3\mu_{mR}r_{w,inlet}^2v_RU_R}{8\pi kk_{mR}p_{mR}J_RLU_{mR}}$$

Table 5: Physical Meaning of Scaling Criteria for Inside-Well Flow.

$$\frac{r_{w,inlet}}{r_{w,outlet}}$$ Geometrical factor for horizontal well

$$\frac{L}{r_{w,outlet}}$$ Geometrical factor for horizontal well

$$\frac{\rho_{mR} H g_R \sin\theta_R}{2 p_{mR}}$$ Ratio of gravitational force to pressure drawdown

$$\frac{2 v_{outR} U_{outR}}{W_R J_R L}$$ Ratio of total energy at outlet to total work done

$$\frac{W_R t_R}{C_{HR} T_R}$$ Ratio of work done to the energy of the fluid inside the well

$$\frac{J_R U_{mR} \Delta p_R}{\rho_{mR} U_R v_R^2}$$ Ratio of energy loss to energy of fluid stream

$$\frac{r_{w,outlet}^2 \Delta p_R}{L \mu_{mR} v_R}$$ Ratio of pressure drop across well and fluid flow velocity

$$\frac{3 \mu_{mR} r_{w,inlet}^2 v_R U_R}{8\pi k k_{mR} p_{mR} J_R L U_{mR}}$$ Ratio of energy of inside-well flow to energy of inflow

According to the Buckingham π-Theorem, there should be at most 15 scaling groups for flow inside the horizontal well — given that there were 21 parameters in the formulation of the equations and 6 primary parameters. The set of scaling criteria derived by inspectional analysis contains 8 groups. The derivation of the scaling criteria for both the flow of reservoir fluids into the horizontal well, as well as the flow of these fluids within the well is quite general: both pressure drive and gravity drainage effects are included. In many practical situations, either one of these two recovery mechanisms could predominate, and thus there would be a need to consider both. In the following sections, consideration was given to the derivation of the scaling criteria for processes dominated solely by either steam drive or thermally-aided gravity drainage mechanism. It must be remembered that the sets of scaling criteria for either one of these two processes should be subsets of the original sets of scaling criteria (contained in Table 2 for the inflow process and Table 4 for the inside well flow process), since these were derived with both pressure drive effects and gravity drive effects taken into consideration.

4.4 Steam Drive Process

In a steam-drive process, the pressure gradients existing between the injection and production wells provide the driving force necessary to move the steam zone and mobilized oil bank forward toward the producer. Gravity plays a minor role — except promoting steam override and low sweep in the lower parts of the oil-bearing formation. To better represent these effects the following modification was introduced to the previously formulated equations: terms denoting the contribution to total flow by gravity were removed from the equations describing the inflow of reservoir fluids from the porous medium into the horizontal well, and inside well flow. For example, the mass balance equation for oil for reservoir flow now looks as follows:

$$\frac{1}{r}\frac{\partial}{\partial r}\left[r\rho_o C_{oo}\frac{kk_{ro}}{\mu_o}\cdot\frac{\partial p_o}{\partial r}\right] + \frac{1}{r^2}\frac{\partial}{\partial \theta}\left[\rho_o C_{oo}\frac{kk_{ro}}{\mu_o}\cdot\frac{\partial p_o}{\partial \theta}\right]$$
$$+ \frac{\partial}{\partial z}\left[\rho_o C_{oo}\frac{kk_{ro}}{\mu_o}\cdot\frac{\partial p_o}{\partial z}\right] + q_o^* = \frac{\partial}{\partial t}\left(\phi S_o \rho_o C_{oo}\right) \quad . \quad (15)$$

The mass balance equations for water and steam-additive, along with the energy balance equation were modified similarly. The result of these modifications was a smaller initial basis for the derivation of the final set of scaling criteria. The previous procedure for reducing the equations, along with the constraints, constitutive relationships, initial and boundary conditions in dimensionless form, and isolating the dimensionless similarity groups from the coefficients of different terms was used, leading to the set of scaling criteria for reservoir flow for the steam drive process (Table 6).

Equations describing the flow inside the horizontal well underwent a similar modification. For

example, the combined mass and momentum balance equation for inside well flow now looks as follows:

$$-\frac{2a_w r_{w,avg} k k_{rm}}{r_{w,in}^2 \mu_m} \cdot \frac{dp_m}{dr} - \frac{2v_{out} r_w}{r_{w,in}^2} \cdot \frac{dr_w}{dz} + \frac{1}{\rho_m v} \cdot \frac{dp_p}{dz}$$

$$-\frac{\mu_m}{\rho_m v} \cdot \frac{1}{r_w} \cdot \frac{d}{dr_w}(r_w \frac{dv}{dr_w}) - \frac{\mu_m}{\rho_m v} \cdot \frac{d^2 v}{dz^2} = 0 \quad . \quad (16)$$

In this case, it was assumed that the volume of inflow from the reservoir into the horizontal well was a function of the pressure gradients between them, and not a function of the potential gradients. The final set of scaling criteria for inside well flow for steam drive process is also listed in Table 6.

4.5 Thermally-Aided Gravity Drainage Process

In this case, the expansion of the steam zone as well as the movement of mobilized bitumen are caused by gravitational force. Accordingly, terms describing the contribution to total flow by pressure driving forces were removed. For example, the mass balance equation for oil for reservoir flow now becomes:

$$\frac{1}{r}\frac{\partial}{\partial r}\left[r\rho_o C_{oo}\frac{k k_{ro}}{\mu_o} \cdot \rho_o g \frac{\partial}{\partial r}(r \sin\theta)\right] + \frac{1}{r^2}\frac{\partial}{\partial \theta}\left[\rho_o C_{oo}\frac{k k_{ro}}{\mu_o} \cdot \rho_o g \frac{\partial}{\partial \theta}(r \sin\theta)\right]$$

$$+ \frac{\partial}{\partial z}\left[\rho_o C_{oo}\frac{k k_{ro}}{\mu_o} \cdot \frac{\partial p_o}{\partial z}\right] + q_o^* = \frac{\partial}{\partial t}\left(\phi S_o \rho_o C_{oo}\right) \quad . \quad (17)$$

As in the case of the pressure drive process, the modification to the governing equations led to a different set of scaling criteria for reservoir flow, which is contained in Table 7.

Correspondingly, the equations governing flow inside the horizontal well underwent similar changes. The equation describing the mass and momentum conservation now appears as follows:

$$-\frac{2a_w \rho_m g k k_{rm} r_{w,avg}}{r_{w,in}^2 \mu_m} \cdot \frac{d}{dr}(r \sin\theta) - \frac{2v_{out} r_w}{r_{w,in}^2} \cdot \frac{dr_w}{dz} + \frac{1}{\rho_m v} \cdot \frac{dp_p}{dz}$$

$$-\frac{\mu_m}{\rho_m v} \cdot \frac{1}{r_w} \cdot \frac{d}{dr_w}(r_w \frac{dv}{dr_w}) - \frac{\mu_m}{\rho_m v} \cdot \frac{d^2 v}{dz^2} = 0 \quad . \quad (18)$$

The set of scaling criteria for this flow for the thermally-aided gravity drainage process is also listed in Table 7.

In either case, the final sets of scaling criteria were smaller than those shown in Table 2 (for reservoir flow) and Table 4 (for inside well flow). This was expected since both of the cases considered were subsets of the original sets of scaling criteria.

Table 6: Scaling Criteria for Steam Drive Process.

a) Reservoir Flow:

$$\frac{H}{2L}, \quad \frac{\overset{\bullet}{q}_{oR}H^2\mu_{oR}}{4\rho_{oR}kk_{roR}p_{oR}}, \quad \frac{\rho_{wR}}{\rho_{oR}}, \quad \frac{\rho_{gR}}{\rho_{oR}}, \quad \frac{p_{oR}}{p_{wR}}, \quad \frac{p_{oR}}{p_{gR}}, \quad \frac{W_{wR}\mu_{wR}}{\rho_{wR}kk_{rwR}Hp_{wR}}$$

$$\frac{S_{wR}}{S_{oR}}, \quad \frac{S_{gR}}{S_{oR}}, \quad \frac{\overset{\bullet}{C}_{gaR}\overset{\bullet}{q}_{gR}}{\overset{\bullet}{C}_{oaR}\overset{\bullet}{q}_{oR}}, \quad \frac{k_{hrR}T_R\mu_{oR}}{\rho_{oR}kk_{roR}h_{oR}p_{oR}}, \quad \frac{\phi_R S_{oR}H^2\mu_{oR}}{4kk_{roR}p_{oR}\overset{\bullet}{t}_R}, \quad \frac{h_{wR}}{h_{oR}},$$

$$\frac{h_{gR}}{h_{oR}}, \quad \frac{\overset{\bullet}{q}_{hR}}{\overset{\bullet}{q}_{oR}h_{oR}}, \quad \frac{\overset{\bullet}{q}_{hR}}{\overset{\bullet}{q}_{lR}}, \quad \phi_R, \quad \frac{\rho_{rR}U_{rR}}{\rho_{oR}h_{oR}}, \quad \frac{U_{oR}}{h_{oR}}, \quad \frac{U_{wR}}{h_{oR}}, \quad \frac{U_{gR}}{h_{oR}}, \quad \frac{P_{cgoR}}{p_{oR}},$$

$$\frac{P_{cowR}}{p_{oR}}, \quad \frac{S_{oiR}}{S_{oR}}, \quad \frac{p_{oiR}}{p_{oR}}, \quad \frac{T_{iR}}{T_R}, \quad \frac{p_{oR}kk_{roR}}{\phi_R S_{oR}\mu_{oR}\alpha_{obR}}, \quad \frac{\overset{\bullet}{q}_{lR}H^2}{4k_{hobR}T_{obR}}, \quad \frac{\overset{\bullet}{q}_{oR}}{\overset{\bullet}{q}_{wR}},$$

$$\frac{\overset{\bullet}{A}_R k_{hobR}T_{obR}}{V_{bR}L\overset{\bullet}{q}_{lR}}, \quad \frac{\overset{\bullet}{h}_{winjR}\overset{\bullet}{q}_{winjR}}{\overset{\bullet}{q}_{hinjR}}, \quad \frac{\overset{\bullet}{h}_{sinjR}}{\overset{\bullet}{h}_{winjR}}, \quad \frac{\overset{\bullet}{q}_{oprodR}}{\overset{\bullet}{C}_{gwprodR}\overset{\bullet}{q}_{gprodR}}, \quad \frac{k_{roR}\mu_{wR}}{k_{rwR}\mu_{oR}},$$

$$\frac{k_{roR}\mu_{gR}}{k_{rgR}\mu_{oR}}, \quad \frac{k_{rwR}\mu_{gR}}{k_{rgR}\mu_{wR}}, \quad \frac{W_{gwR}h_{gwinjR}}{W_{wR}h_{winjR}}$$

b) Inside-Well Flow:

$$\frac{L}{r_{w,outlet}}, \quad \frac{2v_{outR}U_{outR}}{W_R J_R L}, \quad \frac{J_R U_{mR}\Delta p_R}{\rho_{mR}U_R v_R^2}$$

$$\frac{W_R t_R}{C_{HR}T_R}, \quad \frac{r_{w,outlet}^2\Delta p_R}{L\mu_{mR}v_R}, \quad \frac{3\mu_{mR}r_{w,inlet}^2 v_R U_R}{8\pi kk_{mR}p_{mR}J_R LU_{mR}}$$

Table 7: Scaling Criteria for Thermally-Aided Gravity Drainage Process.

a) Reservoir Flow:

$$\frac{Hp_{oR}}{2L^2\rho_{oR}g_R\sin\theta_R}, \quad \frac{q^*_{oR}H^2\mu_{oR}}{2\rho^2_{oR}kk_{roR}g_R\sin\theta_R}, \quad \frac{\rho_{wR}}{\rho_{oR}}, \quad \frac{\rho_{gR}}{\rho_{oR}}, \quad \frac{C^*_{gaR}q^*_{gR}}{C^*_{oaR}q^*_{oR}},$$

$$\frac{S_{wR}}{S_{oR}}, \quad \frac{S_{gR}}{S_{oR}}, \quad \frac{h_{wR}}{h_{oR}}, \quad \frac{k_{hrR}T_R\mu_{oR}}{\rho^2_{oR}kk_{roR}h_{oR}g_R\sin\theta_R}, \quad \frac{\phi_RS_{oR}H^2\mu_{oR}}{2\rho_{oR}kk_{roR}g_R\sin\theta_Rt_R},$$

$$\frac{h_{gR}}{h_{oR}}, \quad \frac{q^*_{hR}}{q^*_{oR}h_{oR}}, \quad \frac{q^*_{hR}}{q^*_{iR}}, \quad \phi_R, \quad \frac{\rho_{rR}U_{rR}}{\rho_{oR}h_{oR}}, \quad \frac{U_{oR}}{h_{oR}}, \quad \frac{U_{wR}}{h_{oR}}, \quad \frac{U_{gR}}{h_{oR}}, \quad \frac{P_{cgoR}}{P_{oR}},$$

$$\frac{P_{cowR}}{P_{oR}}, \quad \frac{S_{oiR}}{S_{oR}}, \quad \frac{p_{oiR}}{p_{oR}}, \quad \frac{T_{iR}}{T_R}, \quad \frac{P_{oR}kk_{roR}}{\phi_RS_{oR}\mu_{oR}\alpha_{obR}}, \quad \frac{q^*_{iR}H^2}{4k_{hobR}T_{obR}}, \quad \frac{q^*_{oR}}{q^*_{wR}},$$

$$\frac{A^*_Rk_{hobR}T_{obR}}{V_{bR}Lq^*_{iR}}, \quad \frac{h^*_{winjR}q^*_{winjR}}{q^*_{hinjR}}, \quad \frac{h^*_{sinjR}}{h^*_{winjR}}, \quad \frac{q^*_{oprodR}}{C^*_{gwprodR}q^*_{gprodR}}, \quad \frac{k_{roR}\mu_{wR}}{k_{rwR}\mu_{oR}},$$

$$\frac{k_{roR}\mu_{gR}}{k_{rgR}\mu_{oR}}, \quad \frac{k_{rwR}\mu_{gR}}{k_{rgR}\mu_{wR}}, \quad \frac{W_{gwR}h_{gwinjR}}{W_{wR}h_{winjR}}, \quad \frac{W_{wR}\mu_{wR}}{\rho_{wR}kk_{rwR}Hp_{wR}}$$

b) Inside-Well Flow:

$$\frac{L}{r_{w,outlet}}, \quad \frac{2v_{outR}U_{outR}}{W_RJ_RL}, \quad \frac{W_Rt_R}{C_{HR}T_R}, \quad \frac{r^2_{w,outlet}\Delta p_R}{L\mu_{mR}v_R},$$

$$\frac{J_RU_{mR}\Delta p_R}{\rho_{mR}U_Rv^2_R}, \quad \frac{3\mu_{mR}r^2_{w,inlet}v_RU_R}{8\pi kk_{mmR}\rho_{mR}Hg_R\sin\theta_RJ_RLU_{mR}}$$

5. EXPERIMENTAL STRATEGY

The primary objective of this investigation was to study the flow behaviour of fluids in the vicinity of, and inside, a horizontal wellbore. In addition, the effects of well geometry and completion on oil recovery performance were examined.

5.1 Experimental Strategy

To satisfy the stated objectives, the following strategy was followed: develop the scaling criteria for a physical model, design and construct the model, and use the model for a series of steam injection experiments. The experiments were to be set up and carried out to determine oil recovery performance for a constant diameter horizontal well — with and without two different types of perforated casing, and for a variable diameter horizontal well — again with and without two different types of perforated casing. Preliminary experiments were conducted also to investigate the oil recovery performance with a vertical producer in communication with a vertical steam injector, and a horizontal steam injector in conjunction with a horizontal producer. The aim of these preliminary runs was to establish a wide range of recovery performance for different types and combinations of wells.

During the design and construction of the scaled, linear physical model a series of high-pressure steam injection experiments were performed in a *partially scaled model*. These runs served to test different apparatus and their capabilities at various operating conditions, as well as to refine the experimental procedure for subsequent experiments in the scaled model. The results of these runs, despite being only partially scaled, would provide some insight into the possible effects due to changes in the operating conditions.

5.2 Design and Construction of the Linear Physical Model

5.2.1 Design of the Linear Physical Model

To perform a series of steam injection experiments in a scaled physical model, a number of steps must be followed. These include:

    1) Identification of the prototype.

    2) Selection of appropriate scaling criteria for model dimensions, and its operating conditions.

    3) Design and construction of the scaled physical model.

5.2.1.1 Prototype Data

Table 8 lists some of the more important information on the prototype, including the formation characteristics and operating conditions. Figure 1 shows the viscosity-temperature relationship for the prototype oil and model oil, which was a light, refined, MCT-based oil called FAXAM–100. Due to the unavailability of prototype core samples, many difficulties were encountered in trying to satisfy

Table 8: Data of Prototype Reservoir Under Study.

Prototype Parameters

A) Reservoir

1) Pattern Spacing	5.0 ha
2) Pattern Type	Isolated
3) Pay Thickness	18 m
4) Porosity	0.325
5) Permeability	4.0 darcies
6) Initial Reservoir Temperature	19 °C
7) Initial Reservoir Pressure	4.2 MPa
8) Steam Injection Pressure	7.0 MPa
9) Steam Injection Rate	200.0 m^3/d
10) Steam Quality @ Sand Face (assumed)	1.0
11) Oil Viscosity	4400 mPa.s @ 19 °C
12) Oil Density	13 °API (993 kg/m^3)

B) Wells

1) Vertical Wells

- Number of Wells	2
- Type of Wells	Steam Injector

2) Horizontal Well

- Number of Wells	1
- Type of Well	Producer
- Length of Well	404 m
- Diameter of Well	7.0 in
- Type of Well Completion	Slotted Liner
	(400 slots/ft)
	(10.0 in x 0.0084 in)

Figure 1: Viscosity-Temperature Relationships for the Prototype Oil and the Model Oil.
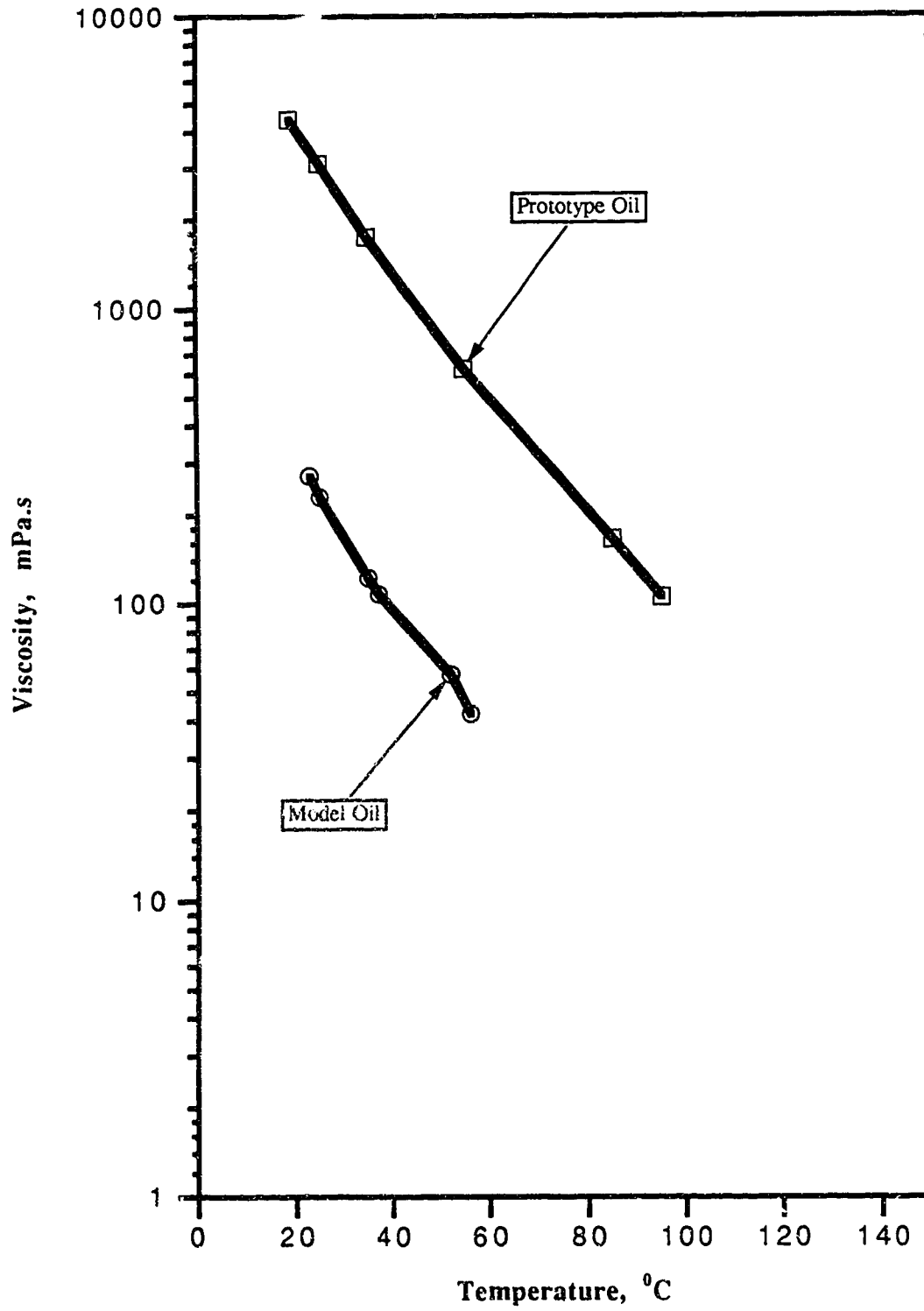
the requirement of different scaling groups. Efforts were made to satisfy, or come close to satisfying as many of the scaling groups as possible. However, a few compromises between practicality and scaling requirements were necessary.

One of the main problems concerned the use of Ottawa sand (mesh size # 70-140) to represent the prototype reservoir. The main result of this was that the porosity and absolute permeability for different laboratory packs were only close to prototype values. This decision, coupled with the use of water and a light, refined oil (FAXAM-100) to represent reservoir fluids meant that the relative permeabilities in the experiments may not be representative of those in the prototype. This problem is endemic to most scaled models of EOR processes. Nevertheless, it is believed that the selection of the above materials for the model reservoir did not have a significant negative impact on the results. First, the prototype reservoir is composed of unconsolidated sand, and has good absolute permeability. Second, in many steam injection recovery processes which utilize a horizontal producer the heated bitumen and steam flow in different regions. As such, relative permeabilities — based upon numerical simulations, and because of the high absolute permeability — might not play as critical a role in these flow processes as they do under normal circumstances. In addition, usually the field relative permeabilities are not known with any great certainty until extensive development has taken place, as in the case of the prototype. Another problem involved the scaling of the prototype horizontal well, which will be discussed in the following sections.

5.2.1.2 Experimental Design

The scaling groups listed in Chapter 4 were used to design the linear physical model. The characteristic reference quantities appearing in these scaling criteria were replaced by representative constant values. First, the scaling factor or ratio of length in the prototype to that in the model, a, had to be determined. It is usually decided by the constraint on available laboratory space. In addition, consideration must be given to the identification of the smallest element of symmetry of the prototype. Scaling down the smallest element of symmetry of the prototype, as opposed to the whole prototype, will permit the duration of an experiment to be shortened without sacrificing the accuracy and reliability of the results. In this case, the smallest element of symmetry was one-half the size of the prototype. Figure 2 shows a plan view of the prototype, with the shaded area denoting the smallest element of symmetry selected for this study. The scaling factor a was determined to be 525, i.e.

$$a = (length\ of\ smallest\ element\ of\ symmetry\ of\ prototype/physical\ model\ length)$$

$$525 = (202\ m/\ physical\ model\ length)$$
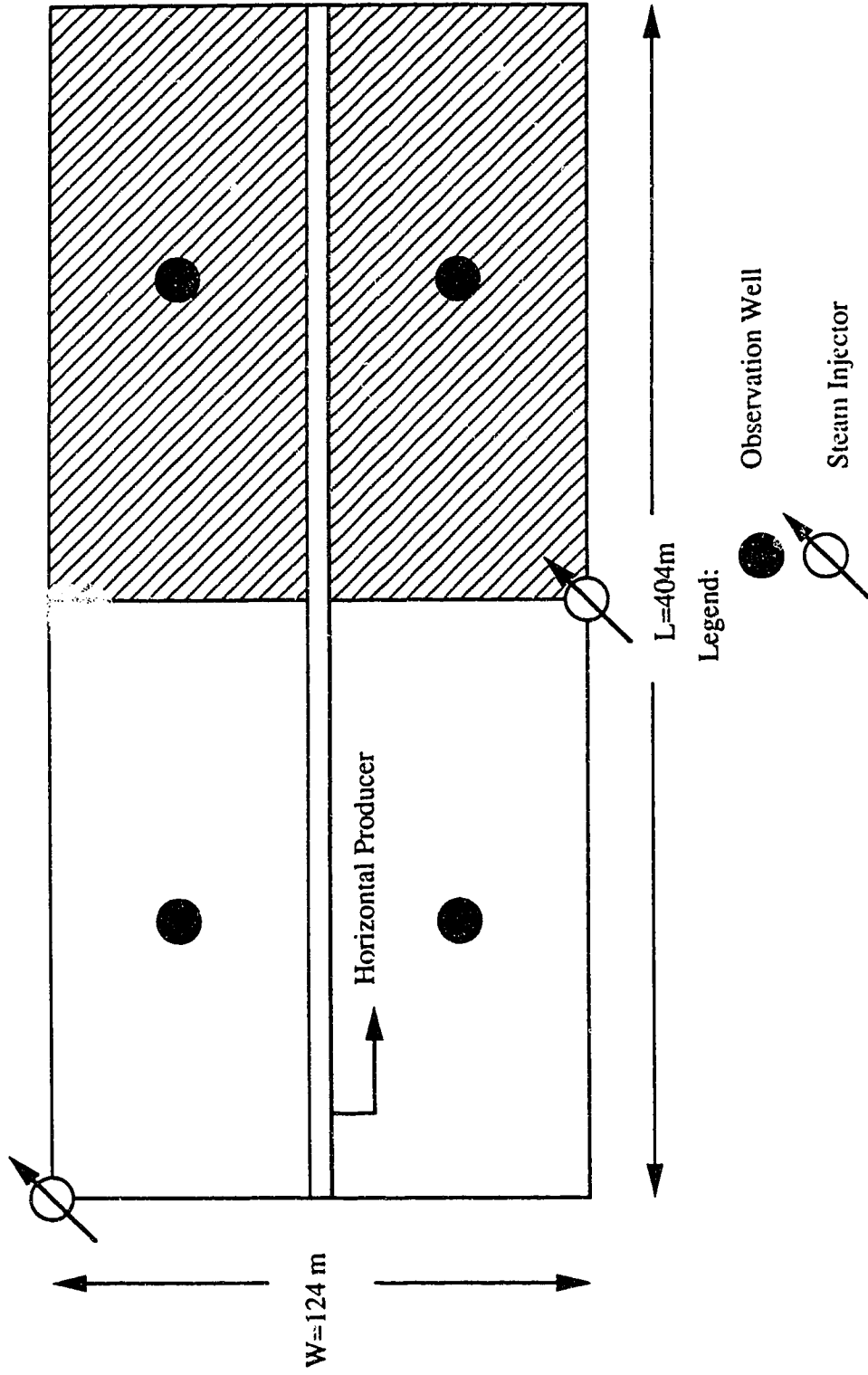
Figure 2: Plan View of Prototype Reservoir.

physical model length $= L_M = 202\ m/\ 525\ =\ 0.385\ m\ =\ 38.5\ cm.$

Since the prototype is an isolated pattern, there may be some end effects affecting flow into the horizontal well. Accordingly, the length of the model was increased from 38.5 cm to 52.6 cm. The extra length at the ends of the model should adequately simulate prototype end effects.

Given that the physical model for this study was linear, and hence circular in geometry, and that the prototype was rectangular, an appropriate approach was needed to reconcile the geometric differences and to determine the lateral extent of the physical model. A satisfactory method may be to scale down the prototype bulk volume, and then use the physical model bulk volume (excluding the extraneous end zones) to calculate its radius/diameter, i.e.

$$\frac{V_{bF}}{V_{bM}} = a^3 \qquad \text{or} \qquad V_{bM} = \frac{V_{bF}}{a^3}$$

$$V_{bM} = \frac{(202\ m\ \cdot 124\ m\ \cdot 18\ m)}{(525^3)} = 0.003116\ m^3$$

$$r_M = \left[V_{bM}/\pi L_M \right]^{0.5}$$

$$r_M = \left[0.003116\ m^3/\pi\ \cdot\ 0.385\ m \right]^{0.5} = 0.0508\ m = 5.08\ cm\ (2\ in).$$

Hence, the linear, high-pressure physical model is a cylinder having a radius equal to 5.08 cm (2 in), and basic length equal to 52.5 cm. To ensure that some radial flow takes place around the horizontal wellbore, the inside wall of the cylinder was lined with a rolled sheet of sintered metal (Figure 3).

Fluid properties Using prototype fluids, and same operating conditions in the prototype and physical model would automatically scale fluid properties such as density, viscosity, and heat capacity — thus satisfying the scaling groups containing these variables. However, water and a light, refined MCT-based oil (FAXAM-100) were chosen to represent reservoir fluids — mainly due to the unavailability of prototype core samples and fluids, as stated before. This particular oil was selected because it exhibits a viscosity-temperature relationship similar to that for the prototype oil, as shown in Figure 1.

Operating pressure limits Due to limitations on apparatus capabilities and laboratory safety concerns, it was decided to operate the physical model at pressure levels not exceeding 3.5 MPag (500 psig). Steam injection pressure was set at 240 kPag (35 psig) for runs carried out in the linear *scaled model*, and at 450 kPag (65 psig) for runs in the *partially scaled model*. The production pressure was set at 105 kPag (15 psig), and at 240 kPag (35 psig), respectively.

Steam injection rate The group $\frac{W_{wR}\mu_{wR}}{\rho_{wR}kk_{rwR}P_{wR}H}$ was to have been used to scale down prototype steam injection rate. However, the capacity for pumps available for the experiments did not lend themselves well to this scaling approach: the scaled down steam injection rate was too low (on

the order of 10^{-3} ml/s) for the pumps to handle. Hence, another approach was used. In this new approach, the lowest permissible rate of the pump was used, and the time scale was adjusted accordingly to maintain dimensional similarity between the prototype and the model.

Time The group $\frac{\phi_R S_{oR} H^2 \mu_{oR}}{4 k k_{roR} P_{oR} t_R}$ was used to scale time. The ratio of prototype time to model time could be determined as follows,

$$\left[\frac{\phi_R S_{oR} H^2 \mu_{oR}}{4 k k_{roR} P_{oR} t_R} \right]_M = \left[\frac{\phi_R S_{oR} H^2 \mu_{oR}}{4 k k_{roR} P_{oR} t_R} \right]_F$$

$$\frac{t_{RF}}{t_{RM}} = \left[\frac{\phi_R S_{oR} H^2 \mu_{oR}}{k_{roR} P_{oR}} \right]_F \Big/ \left[\frac{\phi_R S_{oR} H^2 \mu_{oR}}{k_{roR} P_{oR}} \right]_M .$$

Production rates The experimental oil production rate was scaled up using the group $\frac{q_{oR}^* H^2 \mu_{oR}}{4 P_{oR} k k_{roR} P_{oR}}$. In addition, $\frac{q_{wR}^*}{q_{oR}^*}$ was used to scale up laboratory water production rate vis-à-vis the oil production rate.

Horizontal well Problem was experienced in scaling down the prototype horizontal well. There were several reasons for this. First, there are two factors influencing the scaling down of well size: inflow volume and throughput volume. These two factors interact with one another, as well as contradict each other — resulting in conflicting requirements, i.e. proper scaling of the inflow requirement might result in undersizing or oversizing of the well with respect to the throughput requirement, and vice-versa. The second reason is primarily the lack of treatment of this subject in the available literature. Overwhelmingly, the published studies have dealt only with reservoir flow, and either ignored the inside-well flow process or assumed it to be constant-rate. Ong [94] provided an analysis to scale a horizontal well. The major features of this analysis involved the assumption of laminar flow inside the horizontal well, and thus the application of the Hagen-Poiseuille formula for horizontal pipe flow to describe this flow process. Additionally, by incorporating two previously derived dimensionless scaling groups, B_3 and T' (developed in Ref. 57) into both prototype and model conditions, Ong obtained the final result that if the diameter of the prototype horizontal well was 7.0 inches, then the diameter of the model horizontal well would be approximately 4.0 inches. His analysis was carried out for the steam-assisted gravity drainage process, and hence the well size was mainly a function of the height of the reservoir.

A survey of Table 4 shows that the scaling down of the prototype horizontal well can be effected by the use of the following three groups:

$$\frac{r_{w,inlet}}{r_{w,outlet}} , \quad \frac{3\mu_{mR} r_{w,inlet}^2 v_R U_R}{8\pi J_R L U_{mR} k k_{rmR} P_{mR}} , \quad \frac{r_{w,outlet}^2 (\Delta p)_R}{\mu_{mR} L v_R} .$$

These groups were derived for a variable diameter horizontal well. For a constant diameter horizontal well, they become:

$$\frac{3\mu_{mR}r_w^2 v_R U_R}{8\pi J_R L U_{mR} k k_{rmR} P_{mR}} \quad , \quad \frac{r_w^2 (\Delta p)_R}{\mu_{mR} L v_R} .$$

Considering the constant diameter horizontal well case, an analysis of these two groups shows that one group scales the horizontal well according to the reservoir inflow requirements, and the other group according to the inside-well flow requirements, i.e. $\frac{3\mu_{mR}r_w^2 v_R U_R}{8\pi J_R L U_{mR} k k_{rmR} P_{mR}}$ scales the well radius according to pressure drawdown, while $\frac{r_w^2(\Delta p)_R}{\mu_{mR} L v_R}$ scales the well radius according to pressure drop across its length.

A rearrangement of the pressure-drawdown scaling group yields:

$$v_R = \frac{8\pi J_R L U_{mR} k k_{rmR} P_{mR}}{3\mu_{mR}r_w^2 U_R} \quad ,$$

i.e. the velocity of flow inside a horizontal well is a function of: effective permeability of inflow fluid, pressure drawdown for inflow, viscosity of inflow fluid, and physical resistance to inflow into the wellbore. A higher flow velocity will result if the effective permeability of inflow and pressure drawdown are increased. The velocity will become smaller if the wellbore radius is larger, and/or if the viscosity of inflow fluid is higher.

Second, a rearrangement of the pressure-drop-across-the-well scaling group leads to:

$$(\Delta p)_R = \frac{v_R L \mu_{mR}}{r_w^2} \quad ,$$

i.e. the pressure drop across the horizontal well is primarily a function of: velocity of flow, viscosity of the flowing fluid, length of flow path, and the wellbore internal radius. A higher pressure drop will result when flow is at a higher velocity, has a longer distance to flow through, and the fluid is more viscous. Well pressure drop will be smaller if the well has a larger cross-sectional area. T his analysis agrees with the Poiseuille equation for fluid flow inside a horizontal pipe.

Provided that everything is dimensionally the same in the prototype and model, then the well radius could be first determined from either one of these two scaling groups. The result can then be checked by using the other group.

In the experiments, it was physically easier to fix the pressure drawdown and measure the pressure drop across the horizontal well as a function of well diameter than otherwise. Hence, the horizontal well was scaled down using the pressure drawdown scaling group, i.e.

$$\left[\frac{3\mu_{mR}r_w^2 v_R U_R}{8\pi J_R L U_{mR} k k_{rmR} P_{mR}} \right]_M = \left[\frac{3\mu_{mR}r_w^2 v_R U_R}{8\pi J_R L U_{mR} k k_{rmR} P_{mR}} \right]_F .$$

Rearranging, and assumming $(v_R U_R)_F = (v_R U_R)_M$:

$$r_{w,M} = \left[\frac{r_{w,F}^2 (kk_{rm R}Pm R)_M}{a(kk_{rm R}Pm R)_F}\right]^{0.5} \quad .$$

Let

$(kk_{rm R})_M = 6.5$ (single − phase flow assumption)

$(p_{m R})_M = 0.135$ (experimental pressure drawdown is 135 kf

$(kk_{rm R})_F = 4.0$ (single − phase flow assumption)

$(p_{m R})_F = 3.0$ (prototype pressure drawdown is 3 MPa)

then

$$r_{w,M} = \left[\frac{3.5^2 \cdot 6.5 \cdot 0.200}{525 \cdot 4.0 \cdot 3.0}\right]^{0.5} = 0.041 \; in \quad .$$

In practice, it was difficult − due to several reasons − to satisfy this requirement for scaling down the prototype horizontal well. For one thing, pipes of this size are not readily available. Second, it is physically impossible to perforate these pipes even if they were available. Third, and most important, the horizontal well has to be large enough to accomodate the two pulse-sensing lines (0.0625-in diameter each) of the differential pressure transducer. Without these, the pressure drop across the horizontal well cannot be measured. Therefore, the scaling down of the prototype horizontal well was handled differently. First, the well length was scaled down using the scaling factor, a, i.e.

$$L_{w,M} = \frac{L_{w,F}}{a} = \frac{202 \; m}{525} = 0.385 \; m = 38.5 \; cm \; (\; 15 \; in) \quad .$$

Considering the above limitations, stainless steel tubing of 5/16 inches in diameter was selected for the model horizontal well, which was then slotted. There were 12 slots altogether, the slots being 10.0 mm x 1.0 mm, and evenly spaced along the circumference and the length of the pipe. The dimensions of the slots were determined as follows,

For the prototype horizontal well:

$$\left(\frac{Tot. \; area \; of \; slots}{Tot. \; surface \; area}\right)_F = \frac{(400 slots/ft) \cdot (202m \cdot 3.28 ft/m) \cdot (10.0in \cdot 0.0084in/slot)}{2\pi \cdot 3.5in \cdot 202m \cdot 3.28 ft/m \cdot 12in/ft} = 0.127 \quad .$$

Hence, for the model horizontal well:

$$(Total \; area \; of \; slots)_M = 0.127 \cdot \pi \cdot \frac{38.5cm}{2.54cm/in} \cdot \frac{5}{16}in = 1.89 \; in^2 \; (12.2 \; cm^2) \quad .$$

The above approach is dictated by practical considerations, but it provides only partial scaling of the prototype horizontal well. On the other hand, the two groups involving v_R on the previous page, can be used to estimate the error of such partial scaling.

5.2.2 Construction of the Linear Physical Model

The physical model was fabricated once the dimensions of the model and the horizontal well had been finalized. Plate 1 shows the linear, high-pressure physical model in the horizontal position, with the end caps removed. It was desired to have a tightly packed porous medium for the experiments, so that the absolute permeability would come close to the prototype value (4 darcies). To achieve this, a hydraulic press was incorporated into the overall model design to apply a mechanical load on both ends of the sand pack. In addition, the load also simulated the confining pressure acting on the reservoir. Plate 2 shows the physical model mounted inside the frame of the hydraulic press.

The model (Figure 3) was built by welding a rolled sheet (thickness 1/16 in) of sintered metal to the inside wall of a steel cylinder of length 61.0 cm (24.0 in) — with the extra room needed for the end caps, and diameter 4 in (10.2 cm). Two different types of holes were drilled through the cylinder wall: one for the injection/production wells, and the second one for the thermocouples. The four well openings were 5/8 inches in diameter, and were distributed as follows: two on top, and two in the bottom of the cylinder. Two of the holes – one on top and one in the bottom – were located in the middle of the cylinder length, while the other two holes were placed at either end of the cylinder — offsetting one another. This arrangement provided some flexibility regarding the location and number of injection wells, as well as allowed runs involving a vertical producer. The 16 thermocouple ports were drilled along two rows: one row of eight holes running along the top of the cylinder, and directly facing the second row of the remaining eight holes situated along the bottom of the cylinder. The thermocouple probes which go inside the pack through these ports monitored the growth of the steam zone along the length of the core holder. In addition, phenomena like steam override could be monitored by inserting the thermocouple probes at different depths inside the sand pack.

The model end caps (Figure 4) were machined from solid aluminum blocks. They were 10.5 cm in length, and fitted snuggly inside the core holder. One face of these end caps was flat and fitted with a plate of sintered metals. This was to distribute flow more evenly, and eliminate channelling. The outward-facing side of these caps was machined so that each had five different surfaces. Of these, the central surface was flat and acted as the loading point for the hydraulic press. Openings were made in the four remaining sloping surfaces for equipment purposes, which included the mounting of the flow line for the horizontal well, and the wiring of the pulse-sensing lines of the differential pressure transducer. One of the end caps was used strictly for fluid saturation, while the other acted as the production outlet. Additional thermocouple probes were installed right at the injection and production wells. These were used to monitor the temperature, and quality of the injected steam, as well as to determine the onset of steam breakthrough at the producer.

A slotted constant diameter horizontal well was fabricated from stainless steel tubing. In addition,
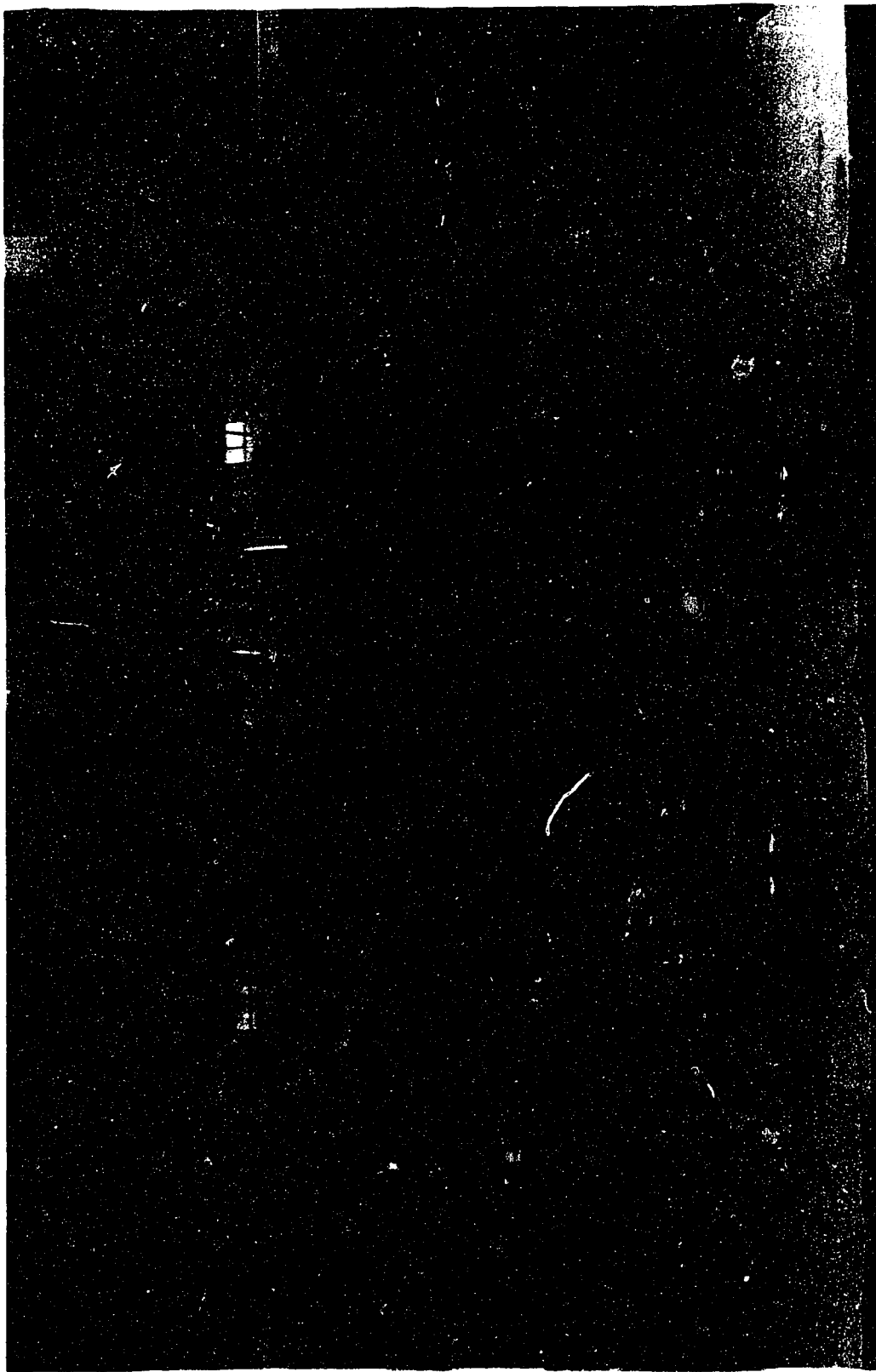
Plate 1: Linear, scaled high-pressure physical model.
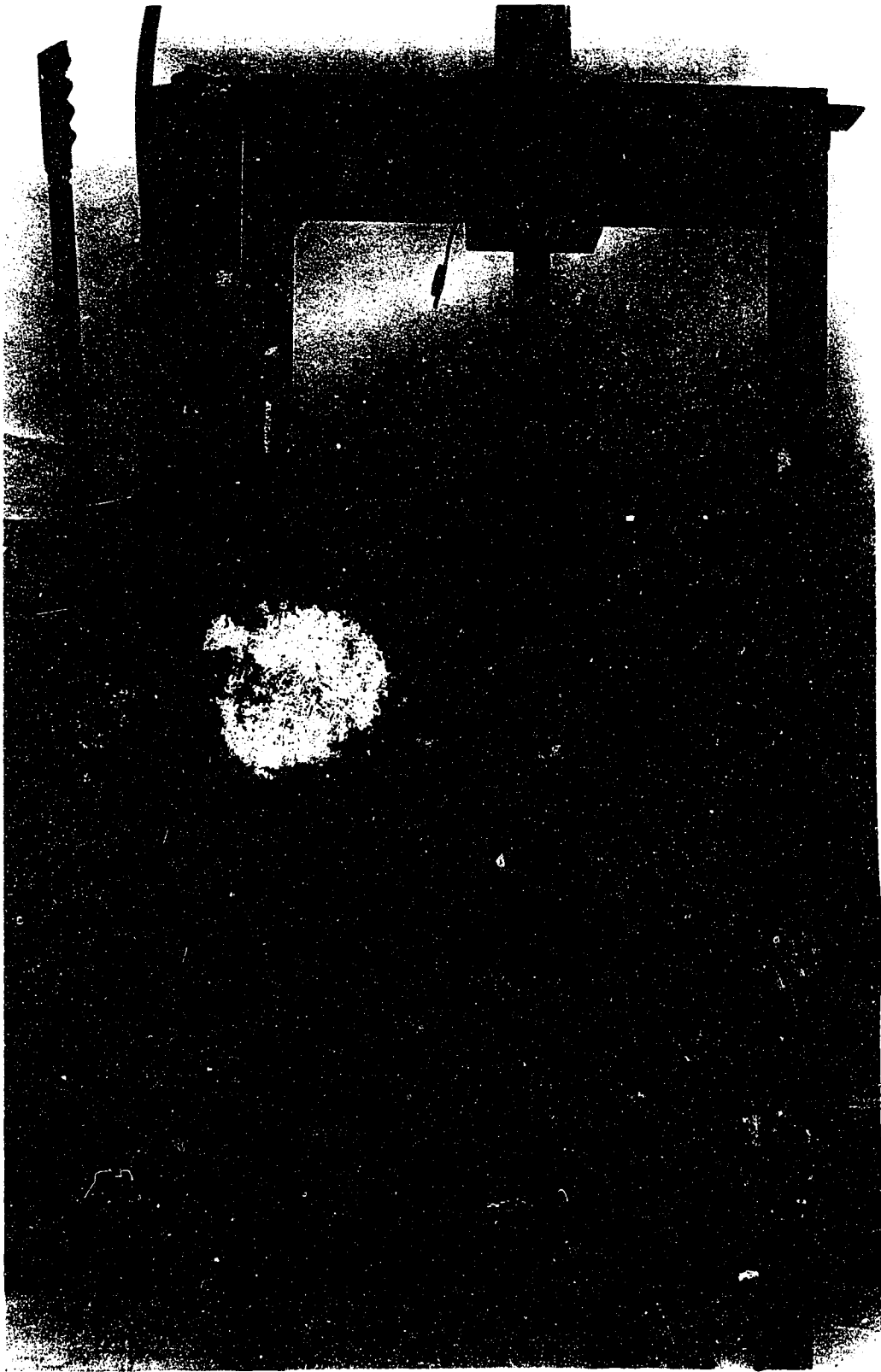
Plate 2: Scaled model mounted inside frame of hydraulic press.
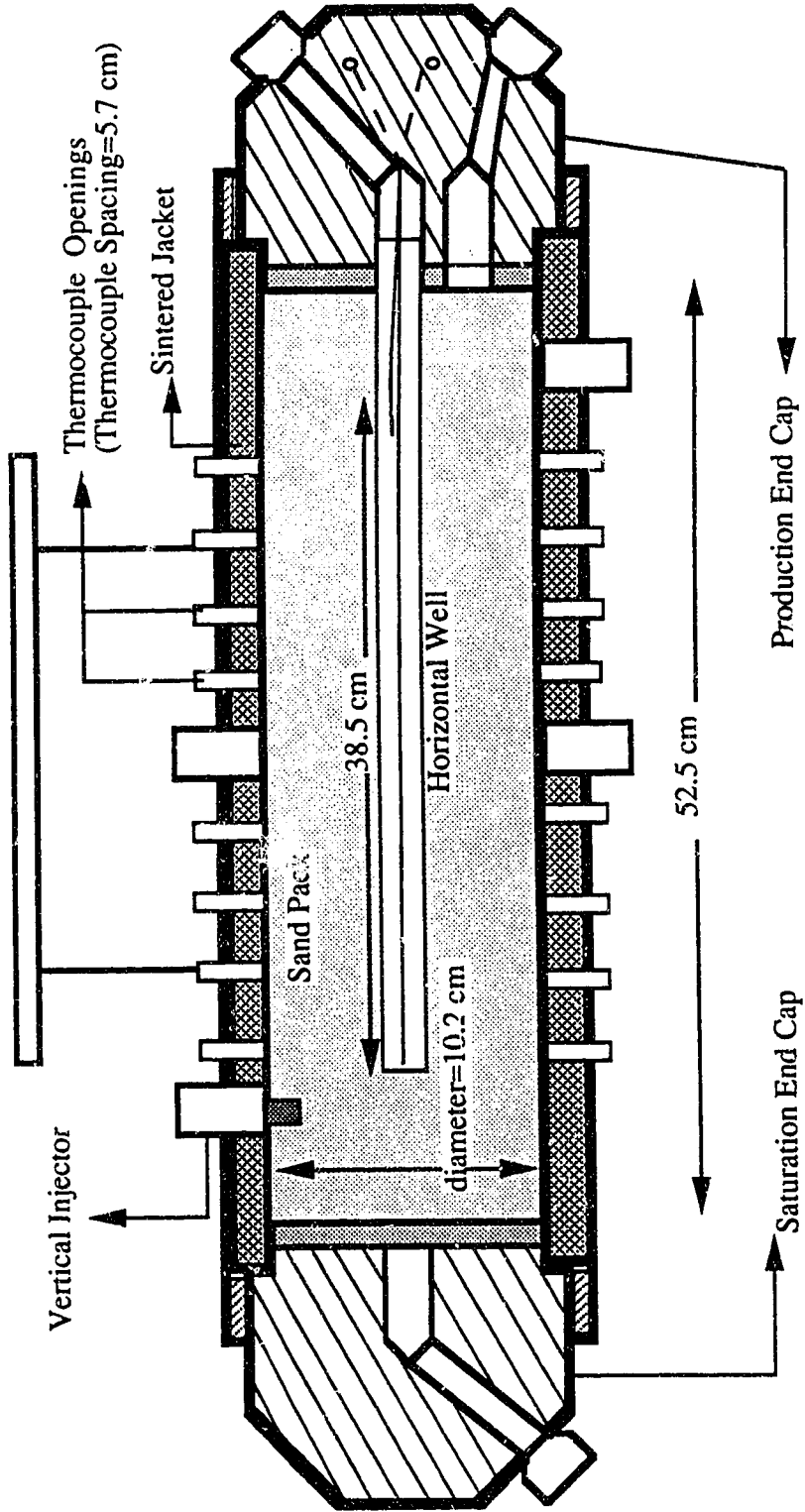
Figure 3: Cross-Sectional View of the Scaled Physical Model.
(Not To Scale)

64

Production End Cap

Quick Connect

Quick Connect

Quick Connect

Boreholes for
Horizontal Wells

Press. transducer
pulse-sensing lines

O-ring Cavities

Sintered flow distribution plate

Saturation End Cap

Quick Connect
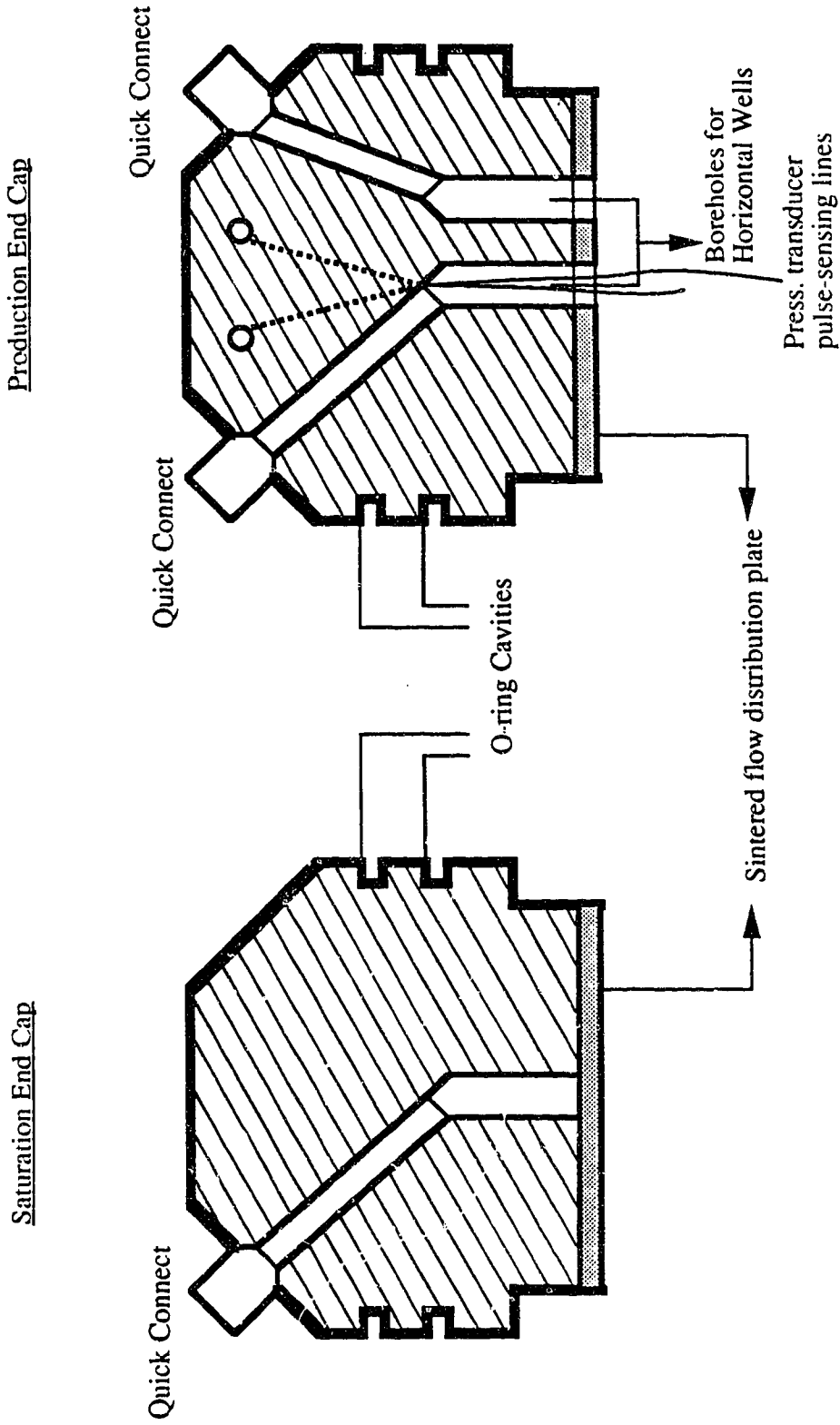
Figure 4: Cross-Sectional View of the End Caps of the Physical Model.

a variable diameter, slotted horizontal well was also made. This well consisted of three equal-length (5 inches each) segments of stainless steel tubing, each having a different diameter size (3/16, 5/16, and 3/8 inches). Tubing size of 7/16 inches diameter was not readily available commercially. The sizes were carefully chosen from the limited available selection so that the total lateral surface area open to inflow was approximately the same for both wells. This was to ensure that the recovery performance for the constant- and variable diameter horizontal well could be compared on the same basis (same lateral area open to inflow for the horizontal wells). Figures 5a, 5b, and 5c provide schematic representations of the vertical steam injection well, constant diameter and variable diameter horizontal wells used in the *scaled model* experiments. To prevent the slotted horizontal wells from being plugged up by sand, it was decided to encase them with sintered metal tubing. Care was taken to make sure that the surface area of the sintered tubes for the two wells was the same. A secondary, but also useful role of the sintered tubes encasing the wells was that they – by having a different permeability from that of the porous medium – could serve to simulate the effects of a permeability-altered (skin) zone around the horizontal wellbore. In this study, the permeability of the sintered metal tubing (about 20 darcies, according to the manufacturer — Motts Metallurgy Corporation) would always be higher than that of the porous packs. Hence, the effects would be akin to those field situations where the horizontal well was stimulated by acid wash, matrix dissolution, or fractured (-ve skin). Once, these effects could be approximated quantitatively they could be assigned a negative value to simulate the reverse situation, when the effects of mud invasion or pore plug-ups predominate (+ve skin). The skin factor can be estimated by carrying out steady-state flow tests in a suitable core holder withe the horizontal well to be tested at the centre.

To evaluate the effect of perforated casing on well recovery performance, four aluminum perforated casings of two different types of design were made. Two of the casings were used in conjunction with the constant diameter horizontal well, while the remaining two casings – tapered – were for use with the variable diameter horizontal well. The casings had exactly the same length as the horizontal wells (38.5 cm), and a perforation density of six holes for every inch of casing length. The size of these holes was 13.5/1000 in, sufficiently small to keep the sand from entering and plugging the well. The first type of casing design (designated type #1) involved the drilling of the holes along the top, and bottom rows of the aluminum casing: three on top, and three in the bottom for every inch of casing. The second type of casing design (designated type #2) had the holes evenly spaced around the periphery of the aluminum casing. Figures 6a and 6b show the two casing pattern designs used in the *scaled model* experiments, while Plates 3 and 4 show the constant and variable diameter horizontal wells used in the *scaled model* experiments, along with their casings.

The *partially scaled model* which was used for a number of experiments was basically a flange-type
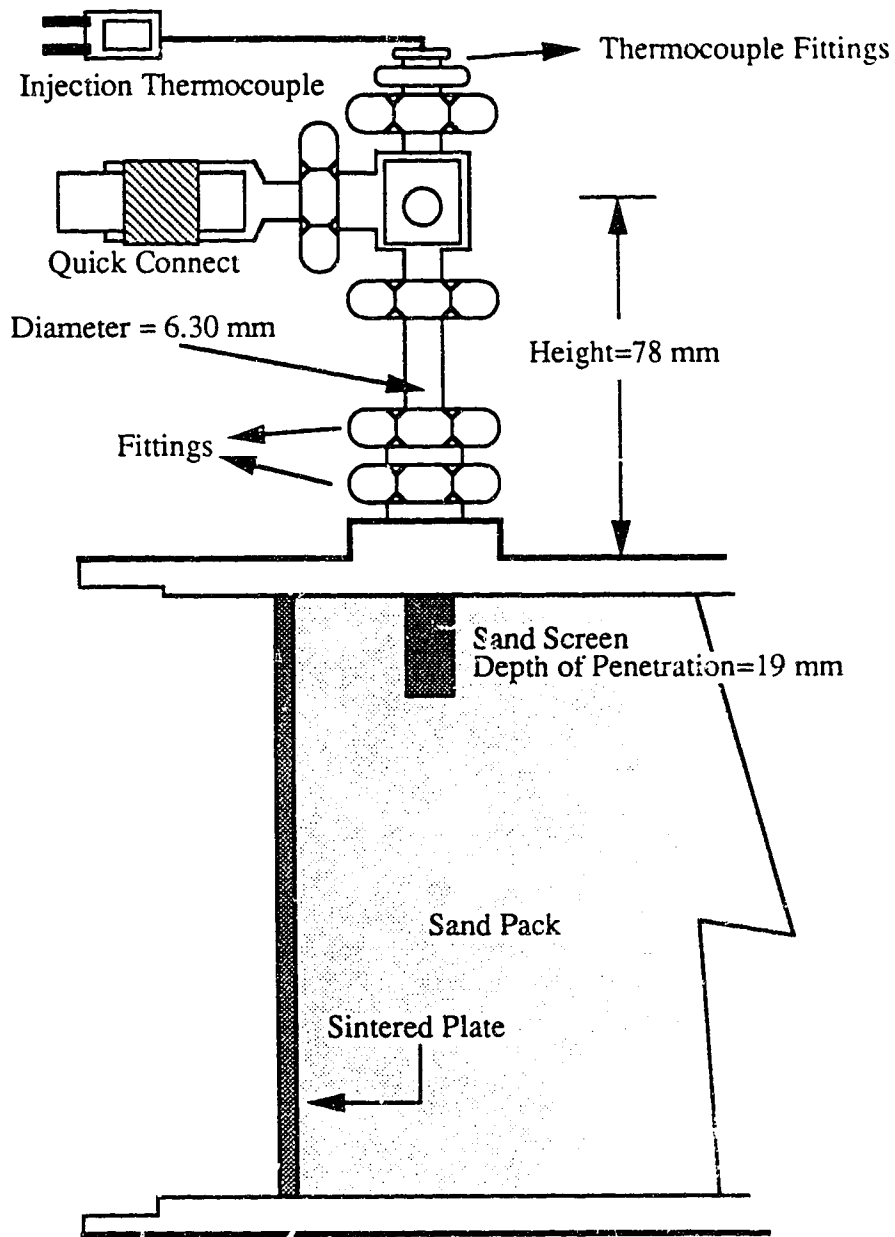
Figure 5a: Schematic Representation of the Vertical Steam Injection Well.

Slots
Size of Slot=10 mm x 1mm

Diameter=7.95 mm (5/16 in)

Length=38.1 cm
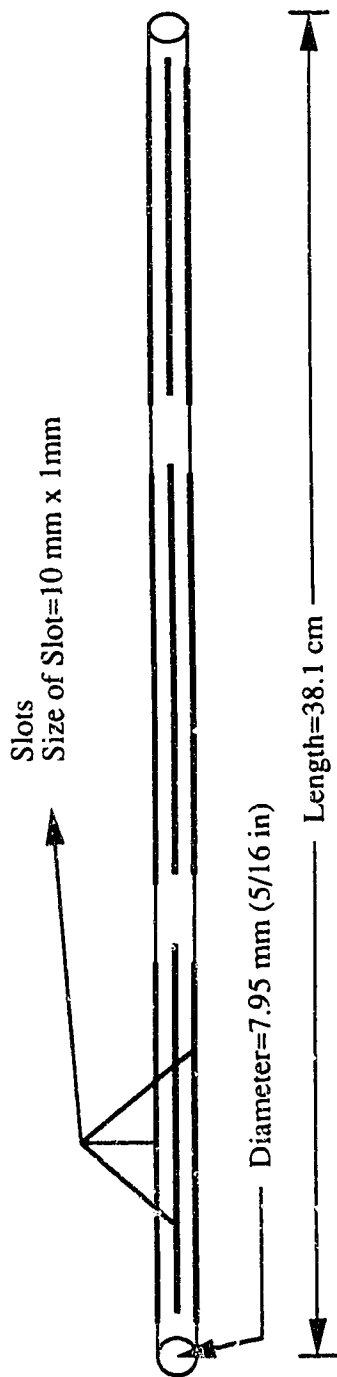
Figure 5b: Schematic Representation of the Constant Diameter Horizontal Well.

Diameter=9.55 mm (3/8 in)

12.7 cm (5 in)

Diameter=7.95 mm (5/16 in)

12.7 cm (5 in)

Length=38.1 cm

Diameter=4.85 mm (3/16 in)

12.7 cm (5 in)
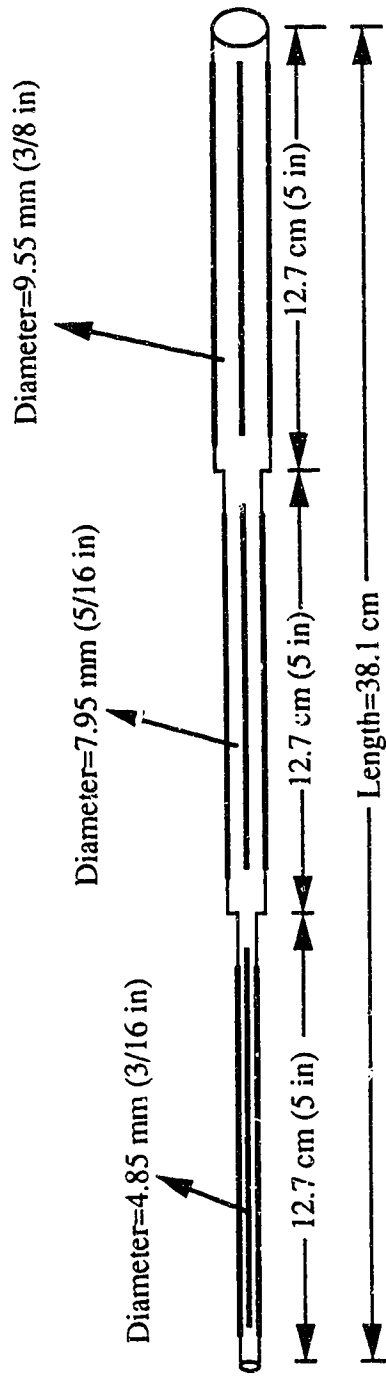
Figure 5c: Schematic Representation of the Variable Diameter Horizontal Well.
(Same Number of Slots, and Same Slot Size as in Figure 5b above)

68

Perforated Holes
Size of Holes=13.5/1000 in (exaggerated size)

Casing Diameter=19.1mm
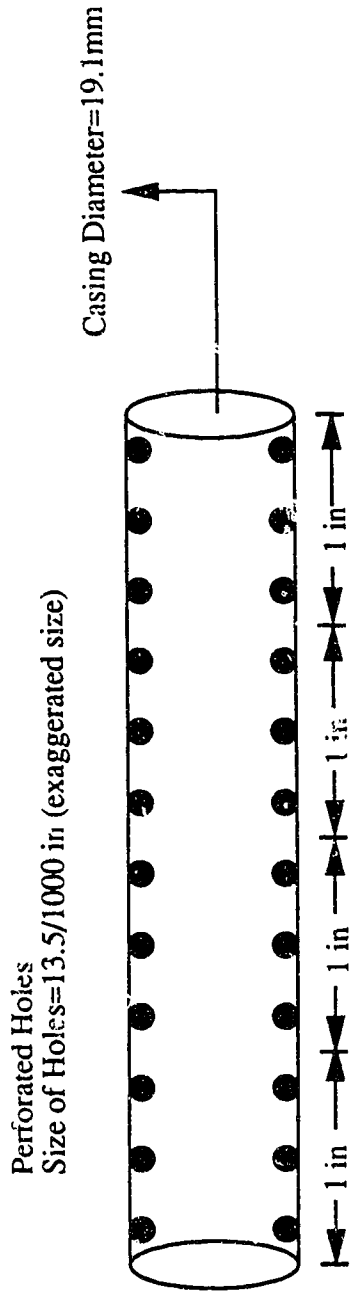
Figure 6a: Distribution of the Perforations for Casing Pattern #1.

Perforated Holes
Size of Holes=13.5/1000 in (exaggerated size)

Holes on the Other Side Not Shown

Casing Diameter=19.1mm
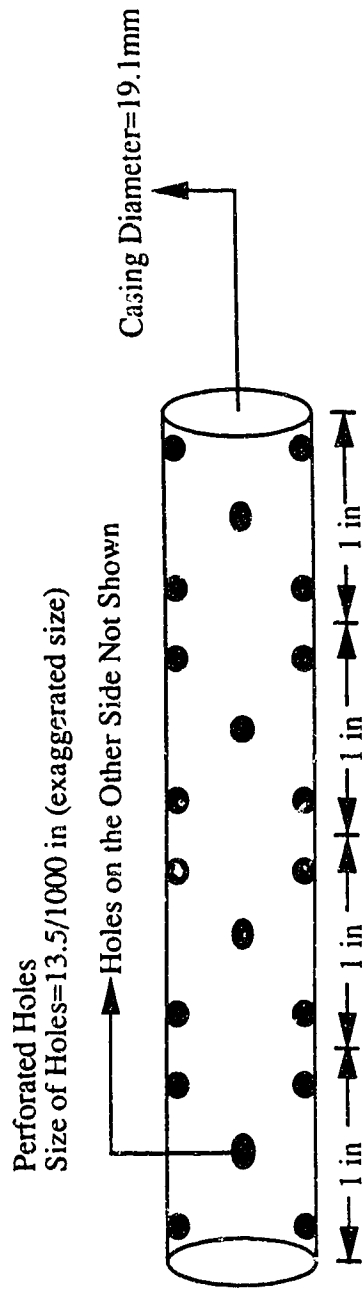
Figure 6b: Distribution of the Perforations for Casing Pattern #2.
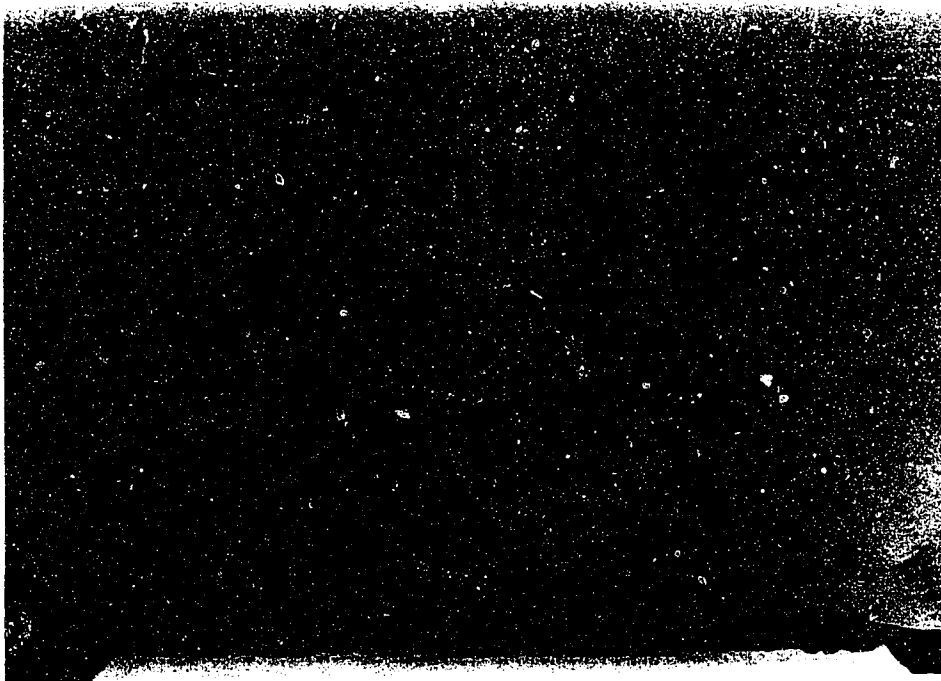
Plate 3: Constant diameter horizontal well for scaled model.
(with its casings)
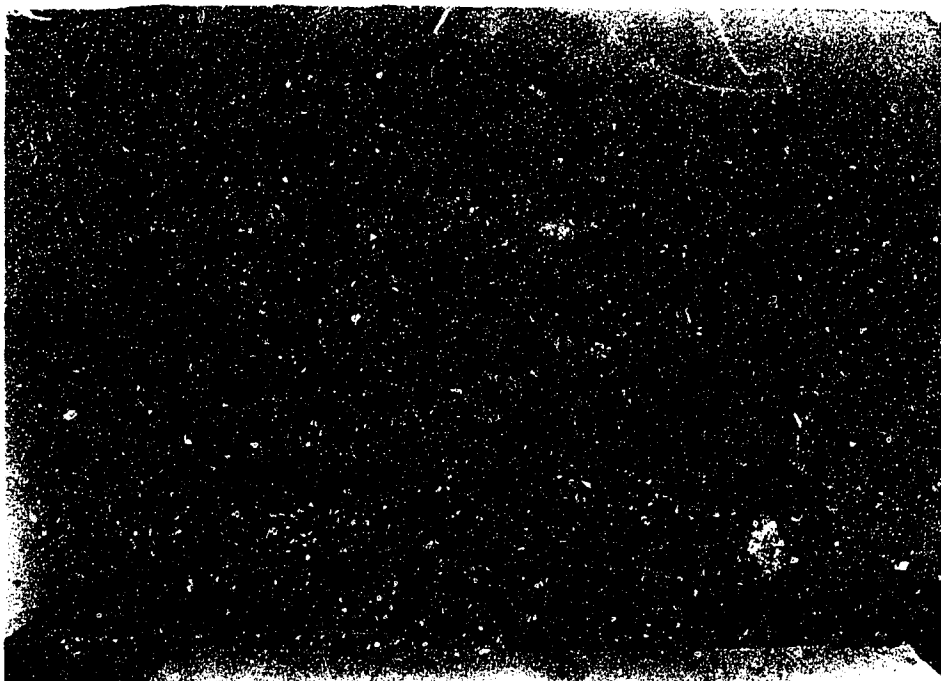
Plate 4: Variable diameter horizontal well for scaled model.
(with its casings)

cylinder. It had an opening for steam injection, and nine openings for the thermocouple probes. A scaling factor of 700 was used for this model — making its diameter to be 7.62 cm (3-in), and length 30.5 cm (12-in). Unlike the *scaled model*, the inside wall of this model was not lined with sintered metal. Again, two different horizontal wells were used: one constant diameter and one variable diameter. In addition, only one type of casing was used. The perforation density in this case was five holes per inch of casing. Furthermore, in the experiments carried out in this model no slotted horizontal well was used. Rather, the sintered tubes were used to simulate the prototype horizontal well. Plates 5 and 6 show the constant and variable diameter horizontal well used in these experiments, along with their casing.

5.3 Experimental Apparatus

The experimental apparatus consisted of four sub-systems: the steam injection facility, the linear physical model, the production facility, and the data acquisition system (DAS). The overall apparatus setup is shown in Figure 7. The steam injection facility supplied steam to the model at the desired pressure, temperature, and quality. It consisted of a feed water pump, a steam generator, a back-pressure regulator, and a water supply container. A constant-rate Milroyal pump was used to pump water from the supply container into the steam generator. The pump was capable of delivering a wide range of rates, from 2.1 gallons (imp.) per hour down to 0.21 gallons/hour. The steam generator was a high-pressure vessel containing an oil bath which served as a heat-transfer medium. Heating rods were used to increase the temperature of the oil bath to as high as 600°C. Immersed in the oil bath were 40 feet of coiled tubing. The feed water injected by the Milroyal pump was heated up and became steam as it made its way through the coiled tubing. A back-pressure regulator of 500-psi rating was employed to set the injected steam pressure to the desired level. Steam pressure and temperature were measured, and adjusted if necessary, before steam was injected into the model. A differential pressure transducer with a 5-psi rating was connected to the horizontal well to measure well pressure drop.

The physical model was always placed in the vertical position during the packing and fluid saturating processes, and horizontally during the determination of the absolute permeability of the sand pack, as well as the actual experiments.

The production sub-system consisted of a back-pressure regulator, cooling bath, and graduated cylinders. The back-pressure regulator was used to set the production pressure, and the graduated cylinders to collect produced fluids at pre-determined time frequencies.

The data acquisition system consisted of two DAS-08 boards, six EXP-16 multiplexers, and the Labtech Notebook Software package from the Metrabyte Corporation. The main advantages of this system included its flexibility (up to 132 channels are available), versatility (users can generate

Plate 5: Constant diameter horizontal well for partially
scaled model.

Plate 6: Variable diameter horizontal well for partially
scaled model.

72
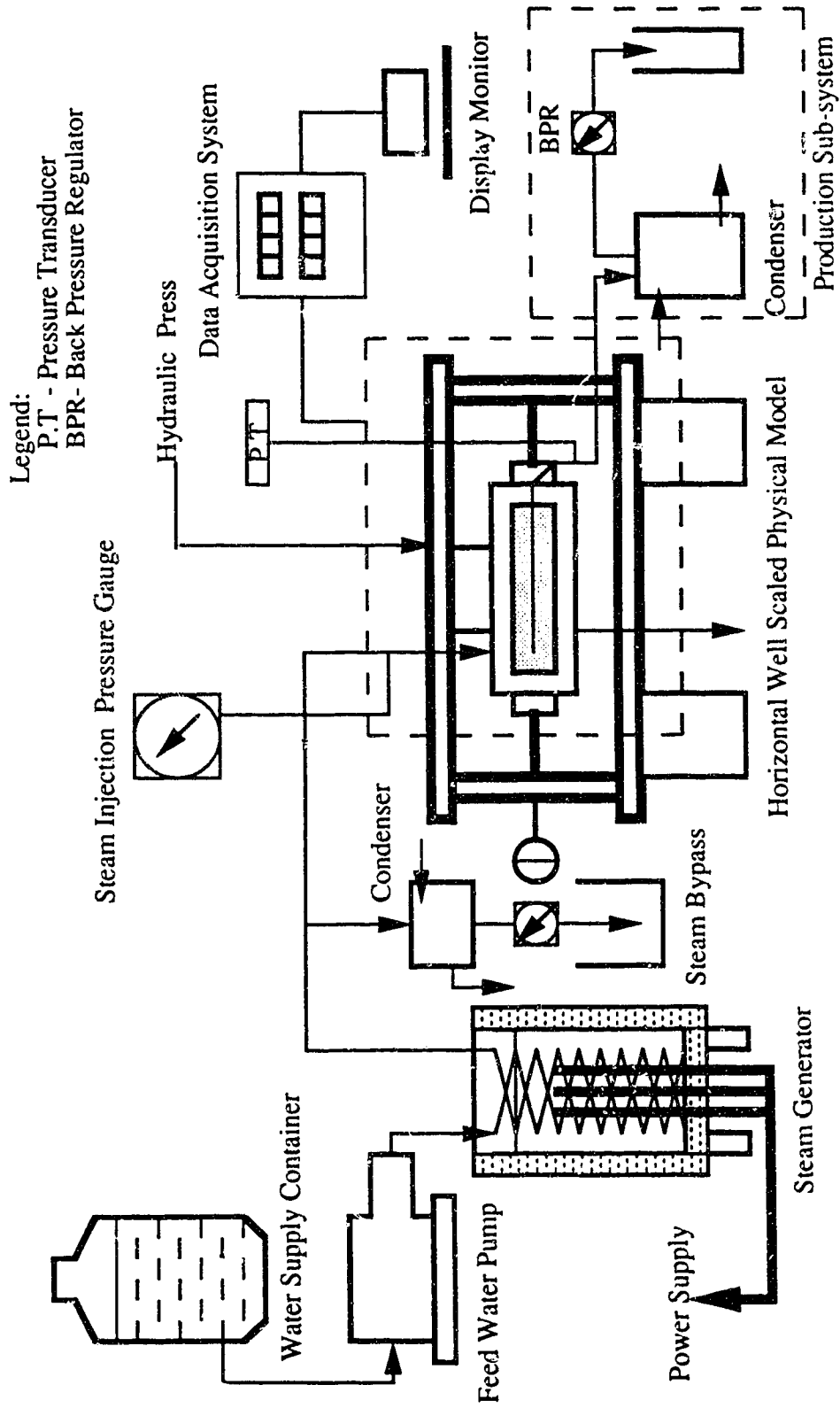
Figure 7: Schematic of Overall Experimental Apparatus Setup.
(Scaled Physical Model)

any program appropriate to any physical model configuration), expansion capability (the number of channels can be increased by adding more DAS-08 boards and EXP-16 panels), and accessibility of repair service. The software package processed all raw thermocouple (mV) and pressure transducer (mV) measurements, converted them into real values of temperature (°C), pressure (kPa) and time (seconds), and if desired displayed them graphically on the IBM monitor. In addition. the data were stored in ASCII file format, and thus were readily analyzed with a spreadsheet-type software (LOTUS 1-2-3).

5.4 Experimental Procedure

Typically, it took about four working days to perform an experiment. Most of this time was devoted to the preparation of the model reservoir. The actual steam injection experiments lasted normally about three hours.

First, before the model could be prepared for an experiment a decision had to be made about the type of run desired. Accordingly, the proper combination and type of vertical/horizontal wells with respective casing was selected and installed. To start the packing process, the production end cap was placed inside one end of the cylindrical core holder. Screws were tightened to keep it in place. The core holder was next mounted vertically in the frame of the mechanical press, with the production end pointing downward, and the open (saturation) end pointing upward. The vertical steam injector and thermocouple probes were secured in their openings. Water was poured into the core holder until it completely filled the inside volume. This, corrected for the volume of the openings for the wells and thermocouple probes, was the bulk volume of the core holder. The water was then removed, and a mechanical vibrator strapped onto the core holder and activated. Water and Ottawa sand were alternately poured into the cylinder. The water was allowed to drain slowly from the core holder through a partially open production valve connected to the horizontal well. The water level was always maintained about 5 cm above the sand column. This was continued until the sand column reached the desired height inside the core holder. The other end cap was put in place. The sand-filled core holder was then swung into the vertical loading position. The production valve was closed, and the screws for the production end cap loosened. Vacuum grease was used to obtain a good seal for the sand pack inside the core holder. A mechanical load of 4500 lbf was then applied to both ends of the sand column through the end cap loading points This mechanical load resulted in a confining pressure of approximately 330 psi acting on the sand and water inside the core holder. The production valve was then opened to allow the water to bleed off. During the packing process, the mechanical vibration of the core holder in combination with the slow, continuous withdrawal of water by gravity from the pack should lead to the desirable effect of settling the matrix material (Ottawa sand in this case) uniformly, and thus resulting in a homogeneous and isotropic porous

medium.

High-pressure air was then passed through the core holder to remove all of the water from the pack. This process typically took about 12–16 hours for the sand to dry completely. Following this, the core holder was evacuated for several hours. At the end of this period there was a vacuum inside the core holder, and water was then allowed to be drawn into the sand pack by this vacuum. The volume of water drawn in, adjusted to account for the volumes due to the thermocouple and well openings, was the pore volume. This was divided by the model bulk volume to give the porosity of the porous pack.

Next, the absolute permeability of the porous sand pack was determined. At this stage the pack was fully saturated with water, and that the pressure inside the core holder was atmospheric. The core holder was placed in its horizontal position, and a pressure differential of known magnitude was applied to the core holder. This was done by introducing a stream of water under pressure into one end of the horizontal cylinder. A waiting period followed to allow the pressure to equalize throughout the porous pack. At this time, the pressure inside the core holder was the same as the pressure applied on the injected water stream. Water was then allowed to discharge through the other end. The water flow rate was measured, and recorded along with the applied fluid pressure. This procedure was repeated a dozen times at different pressure settings — giving correspondingly different flow rates. Darcy's linear flow equation was rearranged and used to calculate the absolute permeability of the porous pack for each pressure setting, i.e.

$$k = \frac{q\mu L}{A\Delta p} \quad .$$

Given that

$L = 0.525 \ m$

$\mu = 1.0 \ mPa.s \ (viscosity \ of \ water \ at \ normal \ conditions)$

$A = 0.0C811 \ m^2 \ (12.57 \ in^2) \ (cross - sectional \ area \ of \ sand \ pack)$

then

$$k = \frac{0.0647q}{\Delta p}, \qquad with \ q \ in \ m^3/sec, \ \Delta p \ in \ Pa, \ and \ k \ in \ m^2 \quad .$$

The average absolute permeability of the porous pack was determined by arithmetically averaging the permeability values. At the end of the above process the porous pack was still fully saturated with water, but the pressure inside the core holder was no longer atmospheric. Instead, the pressure now was close to the last fluid pressure applied to the porous medium. The initial oil saturation and irreducible water saturation values for the porous medium must be known before any experiment

could be carried out. To do this, the core holder was moved to its vertical position. FAXAM-100 oil was then pumped into the porous pack from the top of the vertical core holder, and water was produced through the bottom. This was to ensure a uniform displacement front and prevent the possible formation of viscous fingers. The oil injection was continued, and stopped only when oil breakthrough at the production outlet was noticed. The difference between the volume of water drawn in initially and the volume of water displaced by oil, when divided by the pore volume gave the irreducible water saturation. The ratio between the total volume of oil injected into the core holder and the pore volume gave the initial oil saturation for the porous pack. The sum of these two saturation figures always added up to one, as expected in the absence of any gas saturation.

Once all of the above work had been done, and the model reservoir had been prepared the experiment was ready to be carried out. The thermocouple probes were connected to the EXP-16 panels, the pressure transducers were re-calibrated, and the steam generator was turned on. Usually, it was necessary to wait approximately one hour for the temperature of the oil bath inside the steam generator to rise to the desired level. During this waiting period, several tasks were performed: the water supply container was filled up, the feed water injection rate was set for the Milroyal pump, the numbered graduated cylinders were assembled to collect soon-to-be-produced fluids, and the scanning rate for the data acquisition system was programmed. Plate 7 shows the scaled linear model all set up and ready for an experiment, while Plate 8 shows the partially scaled model in a similar situation. The experiment began when steam at the desired pressure and temperature started to be injected into the core holder. Produced fluids were collected into graduated cylinders at pre-determined time frequencies to give fluid production rates. The experiment continued for about three hours, or until it was deemed that the cumulative steam-oil-ratio had reached the economic limit of 15 : 1. Then the experiment was terminated.

After the termination of the experiment, the core holder was opened and the porous sand pack removed and discarded. The core holder was then cleaned, dried, and readied for the next experiment. The data collected, including thermocouple and pressure transducer readings, were analyzed to determine various parameters indicative of the overall performance of the experiment.

Plate 7: Scaled model set up for an experiment.
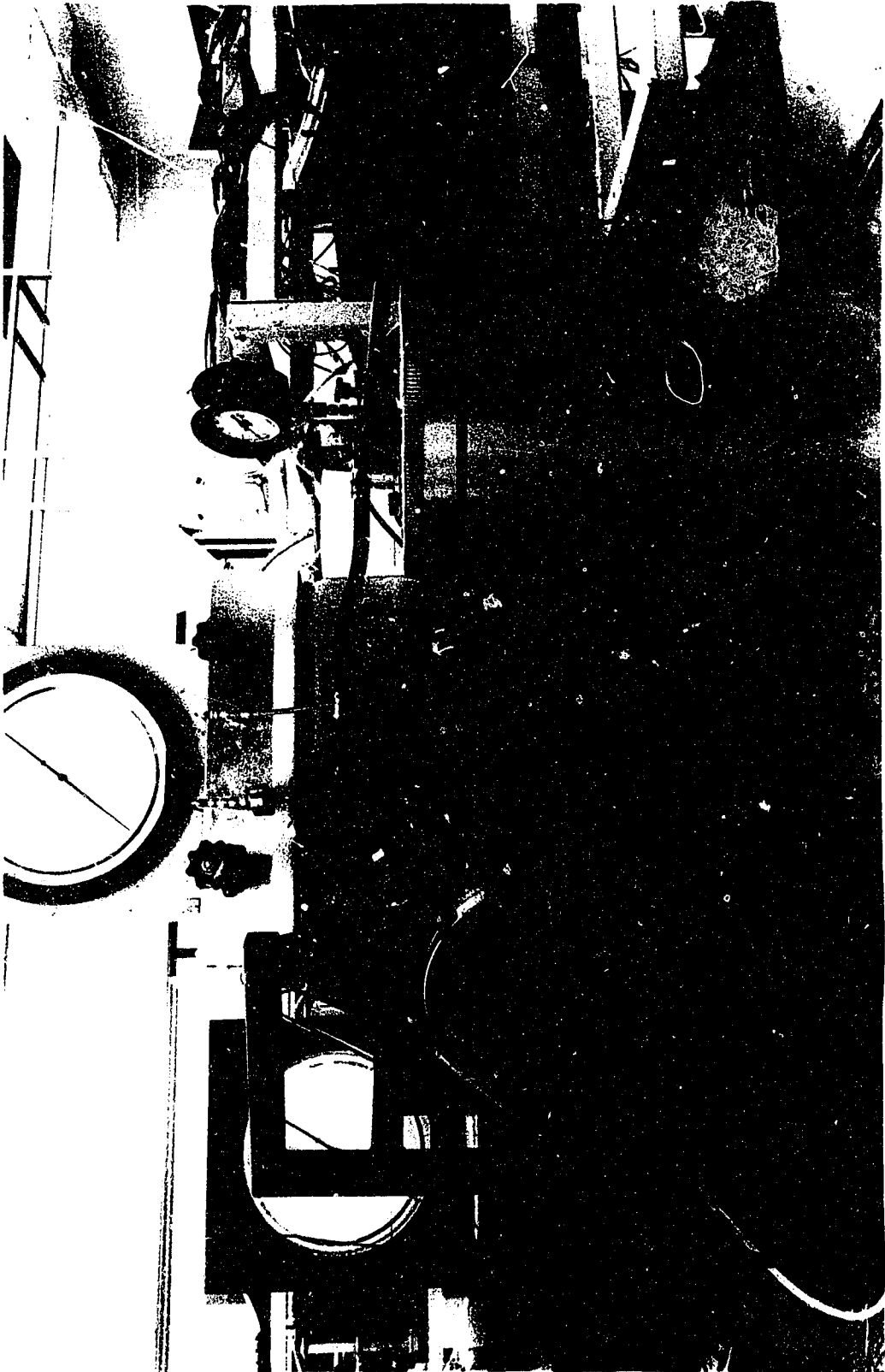
Plate 8: Partially scaled model set up for an experiment.

6. DISCUSSION OF EXPERIMENTAL RESULTS

6.1 Introduction

The objectives of this study, as stated previously, were to investigate the fluid flow behaviour in the vicinity of, and inside, a horizontal wellbore. This involved determining the effects of wellbore geometry and well completion (open well vs. cased well) on oil recovery performance. In addition, a wide range of recovery performance for different types and combinations of steam injectors and producers was examined.

Ideally, physical simulation of a horizontal well in a reservoir should employ a model of the reservoir as well as the horizontal well, with proper treatment of the boundary conditions. This is impractical, even though the scaling criteria needed for such a model have been developed in this work. To make the problem more tractable, an element or microcosm of the real system is modelled instead. This approach is pratical in that only the immediate vicinity of a horizontal well needs to be scaled, and furthermore, the large scale preserves flow behaviour within the wellbore itself. On the other hand, the boundary conditions for such an element must be reconstructed on the basis of practical experience as well as insight gained 'i om simpler analytical approaches to the cyclic steam stimulation problem.

In this work, the physical system being modelled has a constant steam flux at the external boundaries. In this respect, the physical system is akin to a horizontal well fully surrounded by a steam envelope. In a real system, perhaps only a part of the porous system periphery is covered by steam. Physical systems very closely related to the present models are those involving the HASDi.'e (Heated Annulus Steam Drive) process, and the process being used by Mobil Oil in Cold Lake. Within these limitations, the present physical model is a first attempt to investigate flow behaviour within the formation surrounding a horizontal well and within the horizontal well itself, for several types of completion.

Table 9 provides a summary of the 22 experiments carried out during this study. These experiments were carried out in two different models: a *partially scaled model*, and a *scaled model*. In terms of satisfying the scaling criteria derived previously, the *scaled model* experiments – due to the tightness of its sand packs – satisfied the scaling groups containing the absolute permeability parameter more than the *partially scaled model* experiments which had considerably looser sand packs.

Different steam injection rates were used, leading to a wide range of cumulative steam volumes injected in the experiments. In most cases, the total steam volume injected was less than one pore volume (PV), mainly because of the small pressure differential between the injection and production points. In runs utilizing a vertical producer, this was always less than one-quarter of a pore volume.

Table 9: Summary of Experiments.

Run	Model	Injector	Producer	Porosity	Absolute k darcy	Water Sat. %PV	Steam Inj. Rate ml/s (CWE)	Pore Volume ml	Steam Vol. Inj. (CWE) %PV	Cum. Oil Rec. % IOIP
PS3	Part.-Scaled	Vertical	C-D Hor., NC	0.381	17.7	7.5	0.111	1060.0	40.6	23.8
PS4	Part.-Scaled	Vertical	C-D Hor., NC	0.354	8.5	5.7	0.094	985.0	55.2	21.4
PS5	Part.-Scaled	Vertical	V-D Hor., NC	0.362	15.0	10.2	0.089	1007.0	39.7	25.9
PS5A	Part.-Scaled	Vertical	V-D Hor., NC	0.356	15.8	3.2	0.109	991.0	58.0	27.8
PS6	Part.-Scaled	Vertical	V-D Hor., NC	0.342	9.6	6.0	0.078	951.0	42.1	31.2
PS7	Part.-Scaled	Vertical	C-D Hor., WC	0.406	16.3	17.8	0.095	1129.0	47.7	21.5
PS8	Part.-Scaled	Vertical	C-D Hor., WC	0.404	14.3	13.0	0.120	1123.0	60.1	26.9
PS9	Part.-Scaled	Vertical	V-D Hor., WC	0.370	16.3	31.1	0.091	1030.0	48.5	30.2
PS10	Part.-Scaled	Vertical	V-D Hor., WC	0.386	15.8	11.9	0.100	1073.0	51.3	32.1
FS1	Scaled	Vertical	Vertical	0.448	4.4	11.9	0.031	1908.0	10.7	0.9
FS1R	Scaled	Vertical	Vertical (IC)	0.445	5.1	9.0	0.025	1895.0	14.0	7.3
FS2R	Scaled	Vertical	C-D Hor., NC	0.439	5.0	7.3	0.144	1868.0	82.9	56.1
FS3H	Scaled	Vertical	C-D Hor., WC(1)	0.410	5.2	8.8	0.067	1744.0	41.0	20.8
FS3R	Scaled	Vertical	C-D Hor., WC(1)	0.448	6.1	9.0	0.139	1907.0	75.8	52.4
FS4A	Scaled	Vertical	C-D Hor., WC(2)	0.424	6.6	10.8	0.148	1804.0	86.6	65.0
FS5H	Scaled	Vertical	V-D Hor., NC	0.426	4.9	7.0	0.070	1811.0	34.2	28.0
FS5A	Scaled	Vertical	V-D Hor., NC	0.440	6.7	8.3	0.166	1871.0	88.4	64.6
FS5R	Scaled	Vertical	V-D Hor., NC	0.369	6.9	8.9	0.143	1570.0	105.7	71.8
FS6	Scaled	Vertical	V-D Hor., WC(1)	0.451	7.2	8.3	0.128	1920.0	71.6	55.1
FS7	Scaled	Vertical	V-D Hor., WC(2)	0.442	6.7	8.0	0.116	1881.0	66.5	43.8
FS8	Scaled	C-D Hor., NC	V-D Hor., NC	0.415	5.5	6.7	0.443	1767.0	45.2	27.2
FS9	Scaled	C-D Hor., NC	Vertical	0.415	4.6	9.6	0.006	1765.0	3.7	3.0

Legend:

IC - Injector In Communication With Producer
NC - With No Casing (Open well)
WC(1) - With Perforated Casing (Pattern #1)
WC(2) - With Perforated Casing (Pattern #2)
C-D Hor. - Constant Diameter Horizontal Well
V-D Hor. - Variable Diameter Horizontal Well

The cumulative oil recovery also varied greatly from experiment to experiment. Table 10 provides a chart describing the types of experiments carried out, as well as the location of their results, in graphical and tabular form.

The nine experiments conducted in the flange-type, *partially scaled model* can be divided into four groups: those using a constant diameter horizontal producer with no casing, a variable diameter horizontal producer with no casing, the constant diameter horizontal producer encased in a perforated casing, and the variable diameter horizontal producer also encased in a casing. In all of these experiments, a vertical steam injector was used. The experiments were designed to investigate primarily the effects of the geometry and completion of the horizontal producer on oil recovery performance. The steam injection pressure in these runs, as mentioned in Chapter 5, was set at 450 kPag (65 psig), and the production pressure was set at 240 kPag (35 psig).

The remaining 13 experiments in the *scaled model* were also intended to investigate the effects of wellbore geometry and well completion (two different types of perforated casing design were used) on oil recovery, as well as to examine the potential effectiveness of a horizontal steam injector when used in conjunction with a vertical producer, or a horizontal producer. For these runs, the steam injection pressure was kept constant at 205 kPag (30 psig), and the production pressure was allowed to vary between 105-0 kPag (15-0 psig).

The sand packs prepared for experiments in the *scaled model* had a higher porosity and lower absolute permeability than those in the *partially scaled model*. The lower absolute permeability value for the *scaled model* sand packs is due to the compaction of the sand grains by the mechanical load applied to both ends of the sand column. Thus, the incorporation of a hydraulic press into the overall design of the scaled physical model successfully served the purpose of improving the tightness of the sand pack. It is also suspected that the high porosity values for these packs may have been caused by the entrapment of some water in the sintered jacket surrounding the sand pack.

The results of these experiments are presented in tabular form, and are listed in Appendix E (Tables E1 - E22). The tables contain data for the sand pack used in each experiment such as porosity, absolute permeability, initial oil and water saturations, steam injection rate, as well as recovery performance data, such as instantaneous fluid production rate, oil production volume per sample, instantaneous water-oil ratio (WOR), cumulative oil recovery, and cumulative oil-steam ratio (OSR). The steam injection rate shown in each of the tables is the average, cold-water-equivalent (CWE) steam injection rate. It was calculated by dividing the difference between the total volume of feed water pumped into the steam generator and the volume of the bypassed steam condensate during the experiment by the length of the experiment. Based upon visual observation, the actual steam injection rate was approximately constant (and probably close to the calculated average rate) for
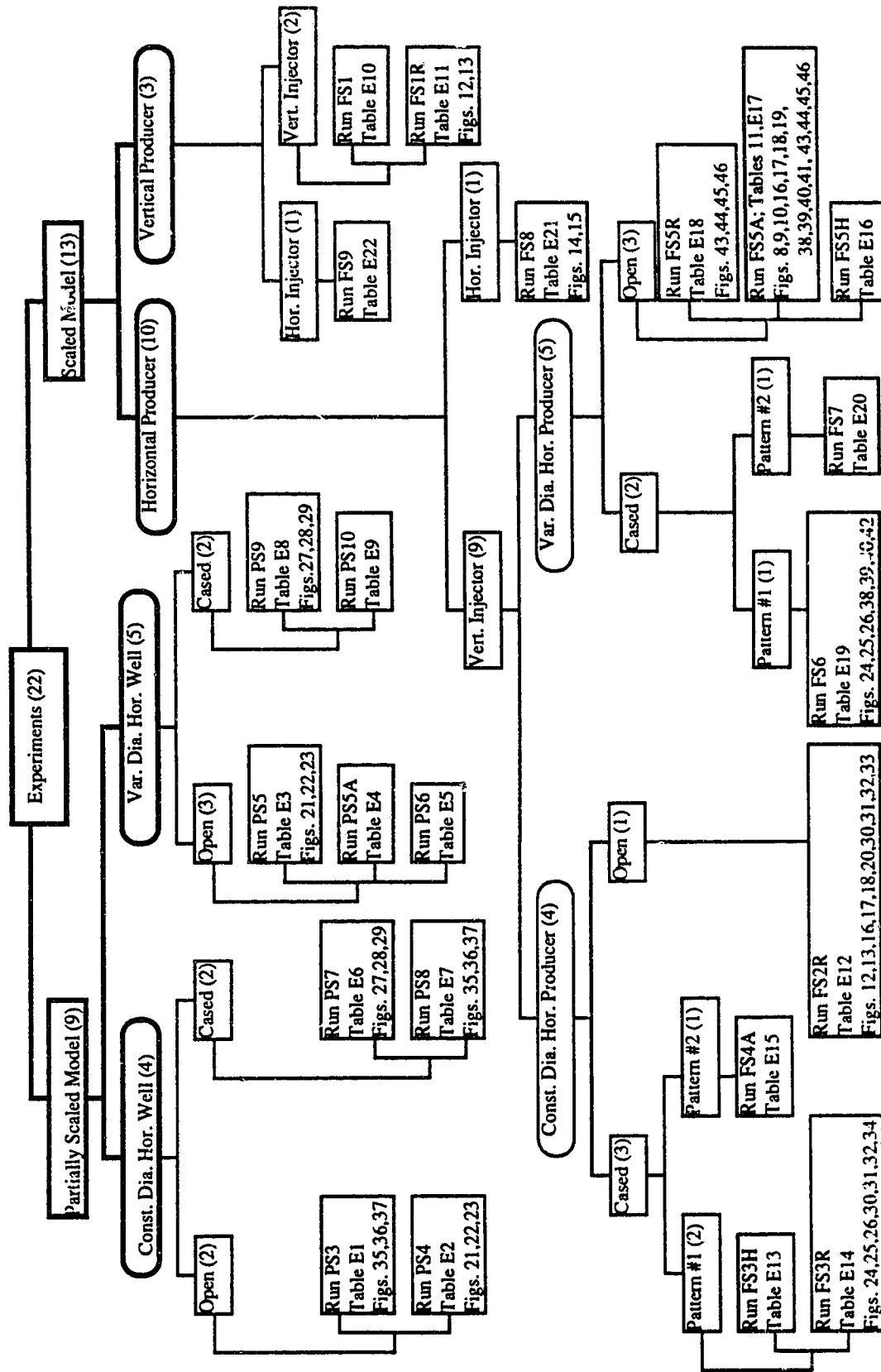
Table 10: Illustration of Experiments Carried Out and Their Results.

most of the experiments. The only time it deviated from the average rate was just after the start of steam injection. During these initial moments of an experiment, the resistance to the formation of a steam zone by the overall system — consisting of the sand matrix, cold fluids (oil and water), and the production back-pressure regulator (BPR) — was too great for the steam to enter the sand pack. As a consequence, most of the steam condensed and was bypassed to a collecting vessel by the injection BPR. It took some time for the sand and fluids to be heated up, the resistance to decrease, and the steam zone to form and propagate. Once the steam zone developed and advanced, the actual steam injection rate stopped fluctuating and stabilized. Such an experimental setup/strategy helped to ensure that steam was actually injected at a constant, pre-set steam injection pressure. In addition, outside of the early part of an experiment, it also helped to maintain and stabilize the steam injection rate.

2 Production History of a Typical Run

Figures 8-10 illustrate graphically the production history of a typical experiment utilizing a vertical steam injector and a horizontal producer. This will be discussed in detail, as an example. The experiment selected is Run FS5A, which was carried out in the *scaled* physical model. For this run, a variable diameter horizontal producer was used, with no casing. The porosity and absolute permeability of the sand pack were 44.0% and 6.7 darcies, respectively. The average steam injection rate was calculated to be 0.166 ml/s (CWE). About 0.9 PV of superheated steam (2-3 °C above saturation temperature) was injected into the sand pack. This resulted in a recovery of 65% of the initial oil in place (IOIP). It was one of the more successful runs, both in ter , of il recovery performance and also in terms of the fewer problems occurring during the actual exp ment. Table 11 is reproduced from Appendix E (Table E17) to present the run results, which were used to generate the graphs in Figures 8, 9, and 10.

Fig re 8 plots instantaneous oil production volume per sample, cumulative oil recovery (both on the left vertical axis), instantaneous WOR, and cumulative OSR (both on the right vertical axis), all versus steam volume injected. An examination of the instantaneous oil production volume per sample profile (bar graphs) reveals several interesting features. First, there was no production for ap oximately the first 0.10 PV of steam injected. As explained , e, during this time there was little actual steam injected into the model reservoir. Most of the steam condensed and was bypassed, and as a result there was no steam zone to mobilize and displace the FAXAM-100 oil. There was no noticeable production until the start of the formation of a steam zone, which began after about 0.10 PV of steam had been injected. Second, the production volume profile did not have a "typical" horizontal-well production profile of high initial production which declines rapidly during the later stages of the recovery process. The main reason for this was that the experiment

Table 11: Run FS5A (Variable Diameter Horizontal Well with No Casing, Scaled Model).

Pore Volume of Sand Pack: 1871.0 ml
Irreducible Water Saturation: 8.3 %PV
Initial Oil Saturation: 91.7 %PV

Porosity of Sand Pack: 44.0 %
Absolute Permeability of Pack: 6.7 darcies
Steam Injection Rate: 0.166 ml/s (CWE)

Sample no.	Steam Vol. Inj. ml (CWE)	Steam Vol. Inj. %PV (CWE)	Inst. Prod. Rate ml/s	Inst. Oil Prod. ml	Inst. WOR ml/ml	Cum. Oil Prod. ml	Cum. Oil Rec. %IOIP	Cum. OSR ml/ml (CWE)
1	179.3	9.6	0.066	71.1	0.00	71.1	4.1	0.40
2	239.1	12.8	0.204	73.3	0.00	144.4	8.4	0.60
3	298.9	16.0	0.195	60.9	0.15	205.3	12.0	0.69
4	358.7	19.2	0.194	52.5	0.33	257.8	15.0	0.72
5	418.5	22.4	0.209	49.4	0.53	307.2	17.9	0.73
6	478.3	25.6	0.220	48.1	0.65	355.3	20.7	0.74
7	538.0	28.8	0.226	47.9	0.70	403.2	23.5	0.75
8	597.8	32.0	0.215	44.8	0.73	448.0	26.1	0.75
9	657.6	35.1	0.219	45.2	0.75	493.2	28.8	0.75
10	717.4	38.3	0.229	47.6	0.74	540.8	31.5	0.76
11	777.2	41.5	0.260	47.6	0.96	588.4	34.3	0.75
12	837.0	44.7	0.253	42.9	1.13	631.3	36.8	0.75
13	896.7	47.9	0.245	36.5	1.42	667.8	38.9	0.74
14	956.5	51.1	0.229	32.6	1.53	700.4	40.8	0.73
15	1016.3	54.3	0.221	35.4	1.25	735.8	42.9	0.72
16	1076.1	57.5	0.252	36.1	1.51	771.9	45.0	0.72
17	1135.9	60.7	0.260	33.5	1.79	805.4	47.0	0.71
18	1195.7	63.9	0.208	25.3	1.95	830.7	48.4	0.69
19	1255.4	67.1	0.186	21.1	2.18	851.8	49.7	0.68
20	1315.2	70.3	0.155	20.7	1.70	872.5	50.9	0.66
21	1375.0	73.5	0.211	24.9	2.06	897.4	52.3	0.65
22	1434.8	76.7	0.232	21.8	2.83	919.2	53.6	0.64
23	1454.7	77.8	2.150	41.7	5.19	960.9	56.0	0.66
24	1574.3	84.1	0.253	42.3	3.31	1003.2	58.5	0.64
25	1654.0	88.4	0.618	104.3	1.84	1107.5	64.6	0.67

Figure 8: Production History of a Typical Experiment (Run FS5A);
Instantaneous Oil Production Volume, Cumulative Oil Recovery,
Instantaneous WOR, and Cumulative OSR vs. Steam Volume Injected.
(Experiment Conducted in Scaled Model)
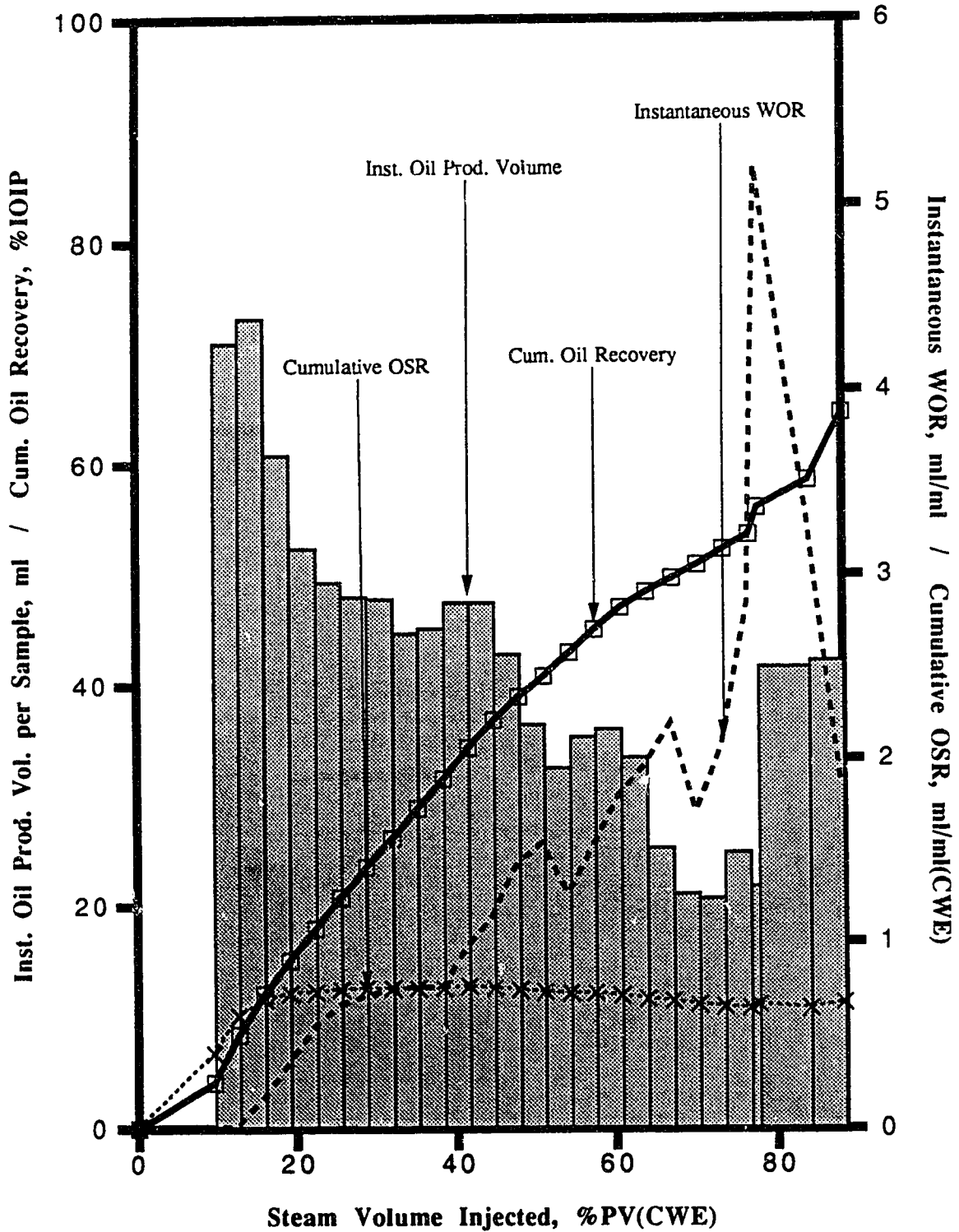
did not last long enough for the decline in production to be really recognizable (only about 0.90 PV of steam had been injected for the whole 3-hour duration of the experiment). The duration of this experiment, like that of all other experiments, was about three hours (real time). In most cases, this time dura:ion resulted in the injection of 0.9-1.0 PV of steam. The relatively small cumulative volume of superheated steam injected in the experiments was due to the small pressure gradie. ' which existed between the injection and production points. A higher pressure gradient would have resulted in a larger volume of steam injected for the same time duration. Furthermore, the effect of near wellbore, and inside wellbore conditions on the flow behaviour would be most pronounced in the initial production period. During the later stages of the experiment (after about 0.75 PV of steam had been injected), fluid production did drop off and it was necessary to lower the production pressure to boost oil production to an acceptable level again.

The instantaneous WOR curve shows that the water content per sample, on average, increased constantly with time. The three instances when it declined (0.55, 0.70, and 0.80 PV of steam injected) were probably caused by fluctuations in the production pressure setting. It is postulated that when the production pressure was set lower, water – due to its lower viscosity and higher mobility – responded to the higher pressure driving force faster than oil (when both were flowing inside the horizontal well), and as such led to a higher water content, and thus higher instantaneous WOR for these samples (liquid hold-up phenomenon). Additionally, the same curve shows that there was little or no water in the first few (two to three) samples. Coupled with this are observations of a large pressure drop across the horizontal well (Figure 9). In addition, low temperature readings were recorded for the produced fluids by the production thermocouple. These observations, altogether, indicate that the produced fluids during the initial production period consisted mainly of cold, not yet fully mobilized oil. It is thought that the production mechanism during this stage of the recovery process was mainly warm (40-60 °C) waterflooding. This perhaps explains the low fluid production rate, large pressure drop across the horizontal well, and the low water content of the samples.

The cumulative OSR curve remained below a value of one for the entire period: on average, between 0.6-0.7 ml of oil was produced for every 1 ml (CWE) of steam injected. The confining geometry of the model most likely contributed to this high thermal efficiency. Additionally, the use of a BPR to control the production pressure also ensured that the steam front moved forward slowly, and that the steam zone swept the sand pack more uniformly. This was confirmed by an analysis of the temperature data from the thermocouples placed at various positions inside the sand pack.

Figure 9 compares the instantaneous fluid production rate curve and well pressure drop curve for this run. In general, there is good correlation between the two curves. As explained above, during the early production period the oil produced was still cold and viscous — leading to large energy

Figure 9: Production History of a Typical Experiment (Run FS5A)
Instantaneous Fluid Production Rate and Well Pressure Drop vs.
Steam Volume Injected. (Experiment Conducted in Scaled Model)
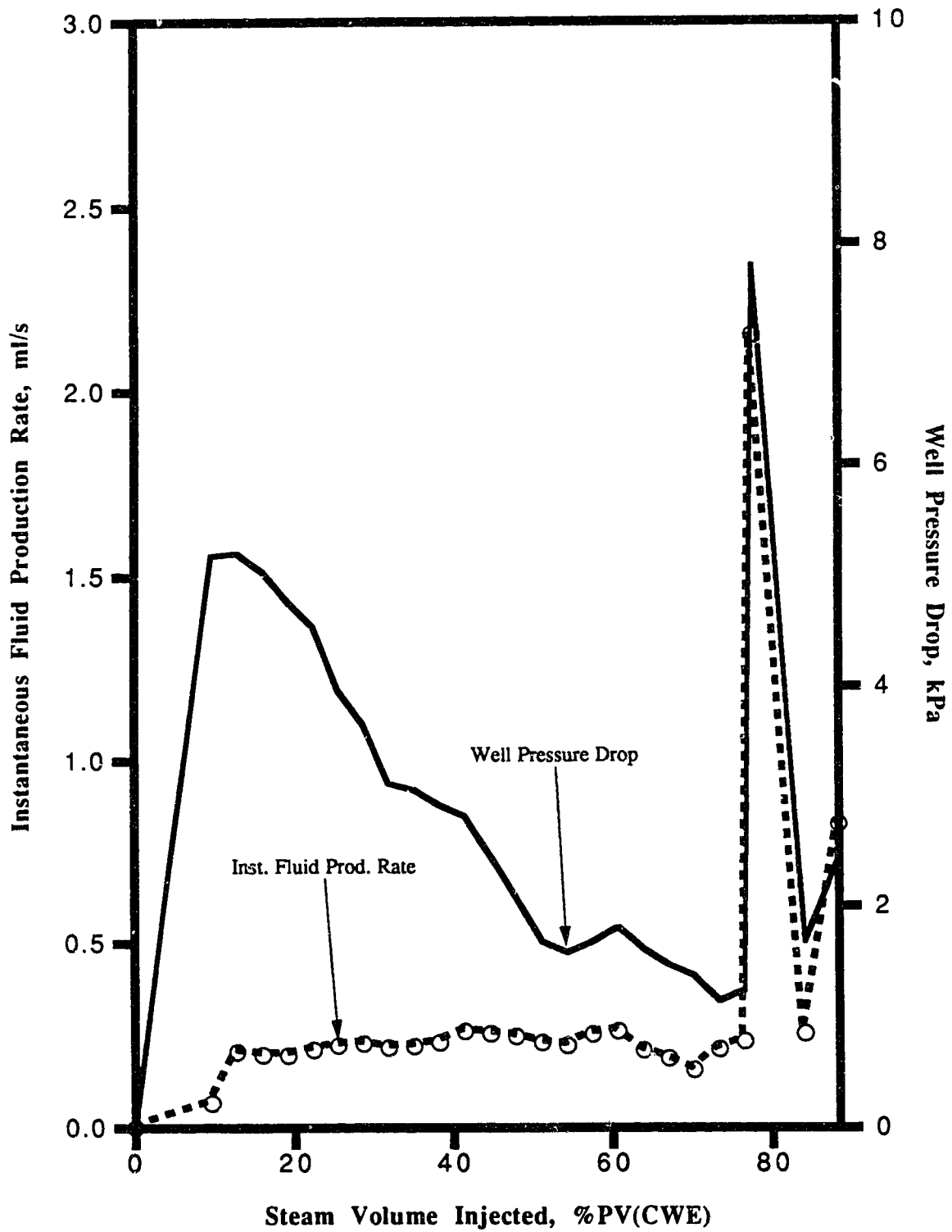
dissipation due to viscous forces, which was manifested as a large pressure drop across the well. As the steam zone developed, more and more of the oil was heated, mobilized, and produced through the horizontal well. The flow of less viscous oil resulted in higher production rates, and lower well pressure drops. Near the end of the experiment (0.75 PV of steam injected), both curves briefly increased significantly, declined, and then increased slightly. The explanation for this behaviour is that the production pressure was lowered from 12 psi to 4 psi (83 kPa to 28 kPa), at this instant (0.75 PV of steam injected), to boost the production. This lowering of the production pressure resulted in a higher pressure driving force which, in turn, led to a higher fluid production rate. The higher pressure driving force, however, also resulted in the mixed flow of hot oil, steam condensate, and cold oil into, and through the horizontal producer. The flow of cold oil caused the observed high pressure drop across the well.

Figure 10 compares the instantaneous fluid production rate behaviour and the set production pressure. There is, as expected, a correlation between the two curves, particularly during the first stage of the recovery process. As explained before, the production pressure controlled the rate of growth of the steam zone via the pressure driving force. The growth rate of the steam zone, in turn, determined how much oil was mobilized, and how fast it flowed into and was produced through the horizontal well. A high production pressure corresponded to a low fluid production rate, and low production pressures resulted in high fluid production rates. This correlation is especially good during early production periods when the flow inside the horizontal well was mostly single-phase. As multiphase flow (heated oil, steam condensate, steam) developed, the above correlation became less precise. The main reason for this was that the BPR used to set the production pressure was built to handle single-phase (liquid) flow only. This point is discussed in detail in Section 6.8 on the reproducibility of experimental results. Fluid production rate responses to the production pressure setting became sluggish (i.e. slower) for multiphase flow.

6.3 Recovery Performance of a Vertical Producer

It was important to know the recovery performance of a vertical producer in place of a horizontal producer for comparison purposes. In essence, this would permit an evaluation of the potentially superior or inferior recovery performance of different types of horizontal wells (i.e. constant diameter, variable diameter) as compared to that for a conventional vertical well. Accordingly, Runs FS1, FS1R, and FS9 were carried out in the *scaled model*. In Runs FS1 and FS1R, two vertical wells were used: one for steam injection, and one for fluid production. Run FS9 utilized a horizontal steam injector and a vertical producer. The results of these runs are contained in Tables E10, E11, and E22, respectively.

As can be seen from the tables, in all three cases the steam injection rate was very low, and the

Figure 10: Production History of a Typical Experiment (Run FS5A);
Instantaneous Fluid Production Rate and Production Pressure vs.
Steam Volume Injected. (Experiment Conducted in Scaled Model)
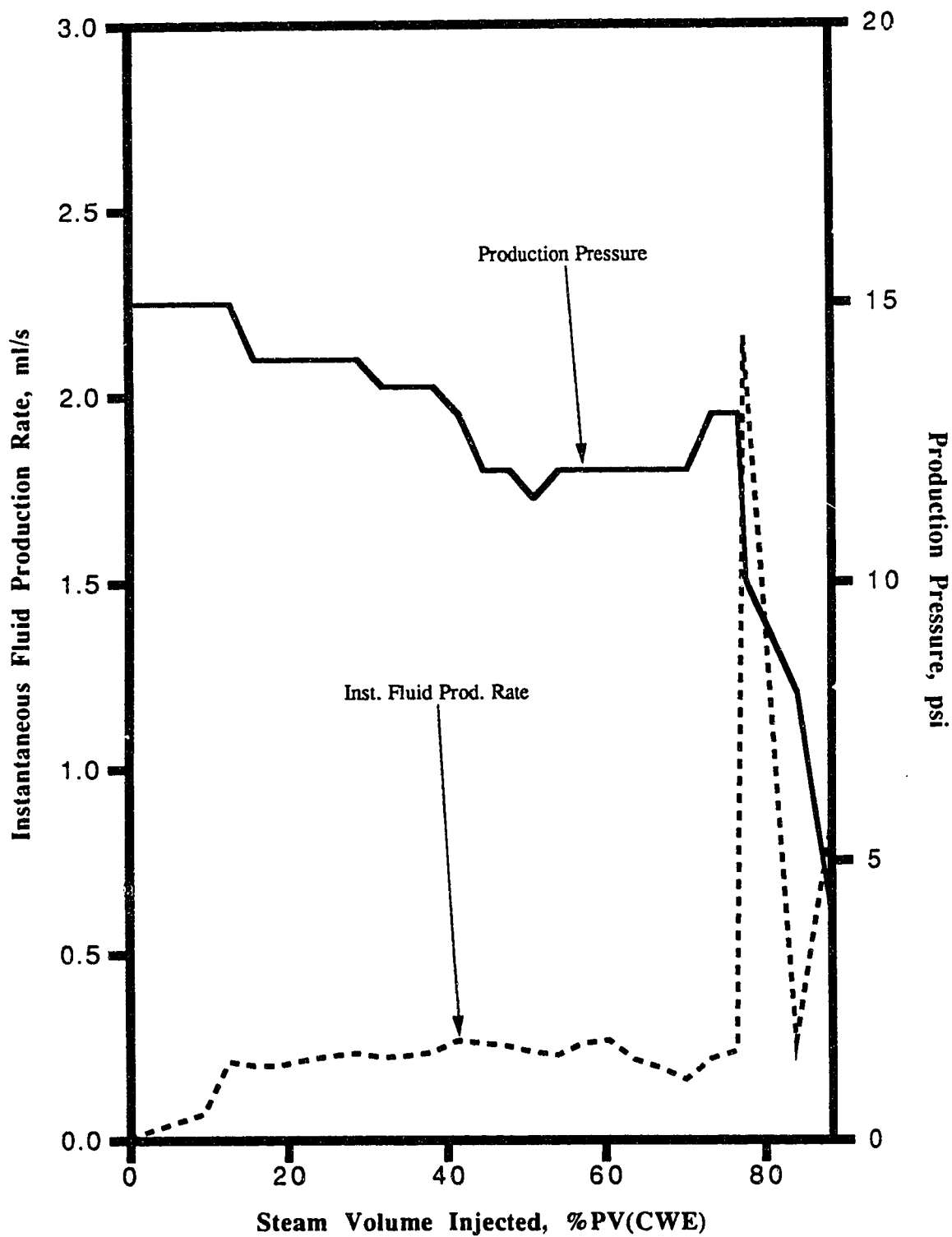
cumulative volume of steam injected into the model was rather small (less than 0.20 PV) — despite the fact that each of these experiments lasted close to three hours. The recovery performance for Run FS1 was disappointingly poor: only 0.9% of the oil in place was recovered after the injection of about 0.11 PV of superheated steam. In addition, the instantaneous fluid recovery rate and the cumulative OSR were small. Run FS1R was an attempt to improve the recovery performance of a vertical producer. In this case, a sintered metal plate, 31 cm x 4 cm, was placed inside the sand pack between the two vertical wells to simulate inter-well communication (i.e. a vertical fracture between the injector and producer). It was hoped that the simulated fracture would accelerate the reservoir response to steam injection and lead to improved recovery. This was indeed the case, as shown in Table 9 (page 79) which shows a much improved cumulative oil recovery (7.3% as opposed to 0.9% of the IOIP) for a modest increase in the total volume of steam injected (0.14 rather than 0.11 PV), as well as in Table E11 which shows higher instantaneous fluid production and better cumulative OSR's. The use of a horizontal steam injector in Run FS9 did not result in any improvement in the recovery performance of the vertical producer: high cumulative OSR's were achieved, but the fluid production rate and cumulative oil recovery were still disappointingly low.

It is speculated that the lower recovery in the case of the vertical producer was due to the slower advance of the steam front, occasioned by the high radial flow resistance. As stated in the previous section, the performance of a steam recovery process depends significantly on the formation and expansion of a steam zone which mobilizes and displaces the viscous oil towards the producer. This, in turn, is a function of the parameters which control the heat transfer and fluid displacement processes, including: oil viscosity, reservoir (including the fluids inside the pores) temperature, thermal conductivity and heat capacity of reservoir and cap rock, steam injection pressure and quality, and production pressure. For example, given a reservoir which has a high initial temperature (e.g. 25°C), contains a medium-viscosity oil, high thermal conductivity and capacity, and the adjoining cap rock has a low thermal diffusivity, it would be relatively easy for a steam zone to form and expand in different directions — mobilizing and driving the oil towards the producer. On the other hand, given another reservoir which has low initial temperature (20°C), highly viscous oil, low thermal conductivity and low heat capacity for the reservoir rock, and high thermal diffusivity for the cap rock, it would certainly be much more difficult for a steam zone to form and expand — resulting in a less efficient process.

It is speculated that the smaller contact area between the vertical producer and the porous medium, as opposed to the case of a horizontal producer, imposed a significant resistance to the formation and growth of the steam zone in the above runs. For a horizontal producer, the mobilized oil flows more easily into, and is produced through it. The steam zone then expands into the already-heated

regions previously occupied by the oil, and heats up more of the surrounding cold oil (Figure 11b). It is different for a vertical producer, as shown in Figure 11a. In this situation, there is a hot oil bank which is driven forward towards the producer by the following hot water zone, formed by the condensation of steam, and the steam zone. The steam injected does not come into direct contact with the cold oil. Rather, most of the steam energy is used to heat up the hot water zone and hot oil bank ahead of it, causing the steam to condense. As such, the rate of expansion of the steam zone is severely restricted by the slow heat conduction – due to small temperature differences – between the hot and cold oil regions.

The above hypothesis regarding the low recovery performance of a vertical producer is supported by experimental observation of large volumes of bypassed steam condensate throughout the runs. In conclusion, it can be said that the productivity of a vertical producer is much less than that of a horizontal producer in a steam drive process.

Figures 12 and 13 compare the recovery performance of a horizontal and a vertical producer. The runs selected were Runs FS1R which used a vertical producer in communication with the vertical injector, and FS2R which had an uncased conventional horizontal producer. First, it should be noted that the two runs lasted for more or less the same length of time. Yet, much more steam was injected in Run FS2R than in Run FS1R. This was due primarily to the large volume of bypassed steam condensate, and the low steam injection rate in Run FS1R. The horizontal producer outperformed the vertical producer in all respects: higher fluid production rate, lower instantaneous WOR, higher cumulative OSR, and cumulative oil recovery. In particular, the overall recovery performance of the horizontal producer still exceeded that of the vertical producer for the same volume of steam injected into the sand pack. Summarizing, under the laboratory conditions described, the recovery performance of a horizontal producer surpassed by a wide margin that of a vertical producer.

6.4 Vertical Injector vs. Horizontal Injector

To evaluate the effectiveness of a horizontal steam injector, Run FS8 was carried out, and its results were compared with those for Run FS5A. Both runs employed an uncased variable diameter horizontal producer, but Run FS5A had a vertical steam injector while Run FS8 used a constant diameter horizontal well for steam injection. In Run FS8, the horizontal injector was placed parallel to, and 1-in (2.54 cm) above the horizontal producer. The run was terminated after 0.45 PV of superheated steam was injected, mainly because steam breakthrough was observed in the horizontal producer. Table E21 contains the data for this run. The instantaneous fluid production rates were higher (about 3-4 times the average fluid production rates of other horizontal well runs) corresponding to a higher average steam injection rate (3-4 times the average steam injection rate of other horizontal well runs in the *scaled model*). The higher steam injection rate and fluid production rates were most
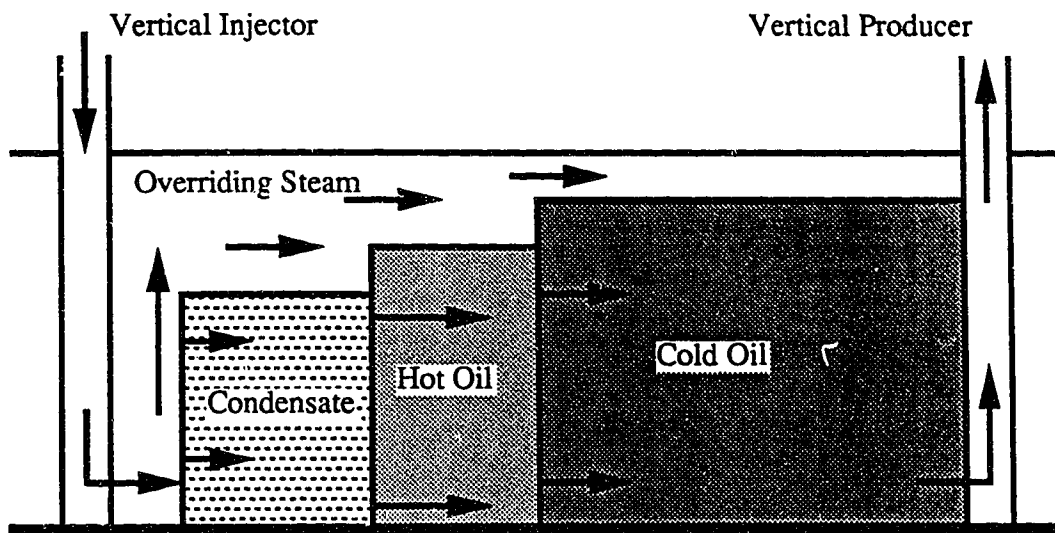
Figure 11a: Schematic of Steamflooding with a Vertical Producer.
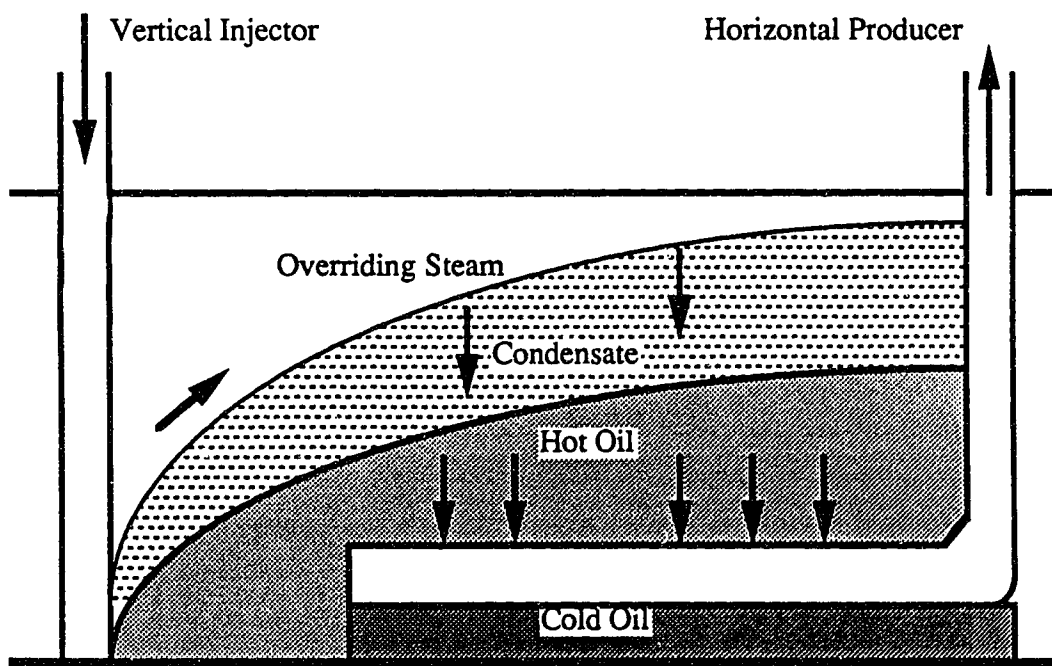
Figure 11b: Schematic of Steamflooding with a Horizontal Producer.

Figure 12: Recovery Performance of a Vertical Producer (Run FS1R) and
Recovery Performance of a Horizontal Producer (Run FS2R);
Instantaneous Fluid Production Rate and Cumulative Oil Recovery vs.
Steam Volume Injected. (Scaled Model Experiments)
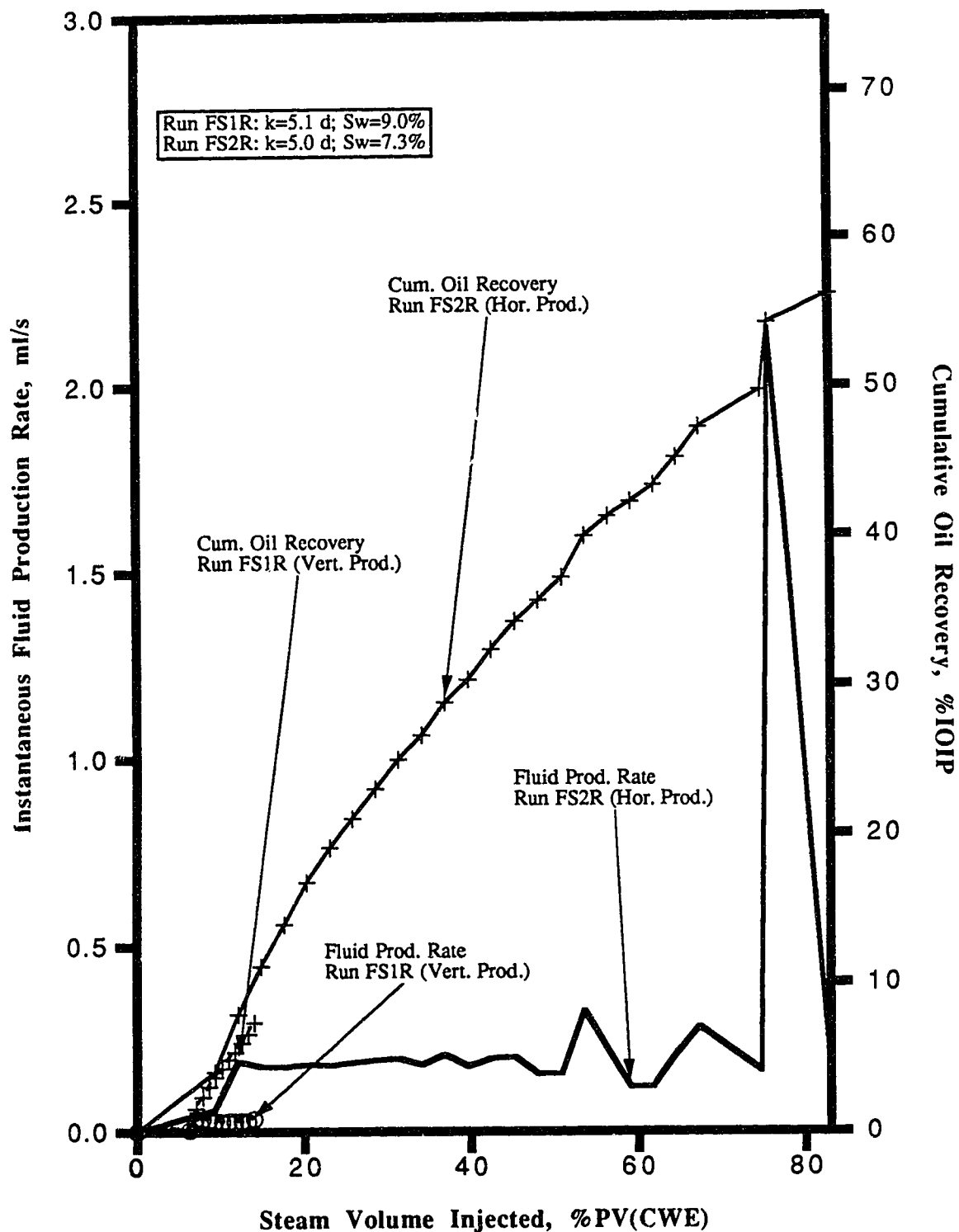
Figure 13: Recovery Performance of a Vertical Producer (Run FS1R) and
Recovery Performance of a Horizontal Producer (Run FS2R);
Cumulative OSR and Instantaneous WOR vs. Steam Volume Injected.
(Scaled Model Experiments)

Cumulative OSR
Run FS2R (Hor. Prod.)

Cumulative OSR
Run FS1R (Vert. Prod.)

Inst. WOR
Run FS2R (Hor. Prod.)

Inst. WOR
Run FS1R (Vert. Prod.)

Run FS1R: k=5.1 d; Sw=9.0%
Run FS2R: k=5.0 d; Sw=7.3%

Cumulative OSR, ml/ml(CWE)

Instantaneous WOR, ml/ml

Steam Volume Injected, %PV(CWE)
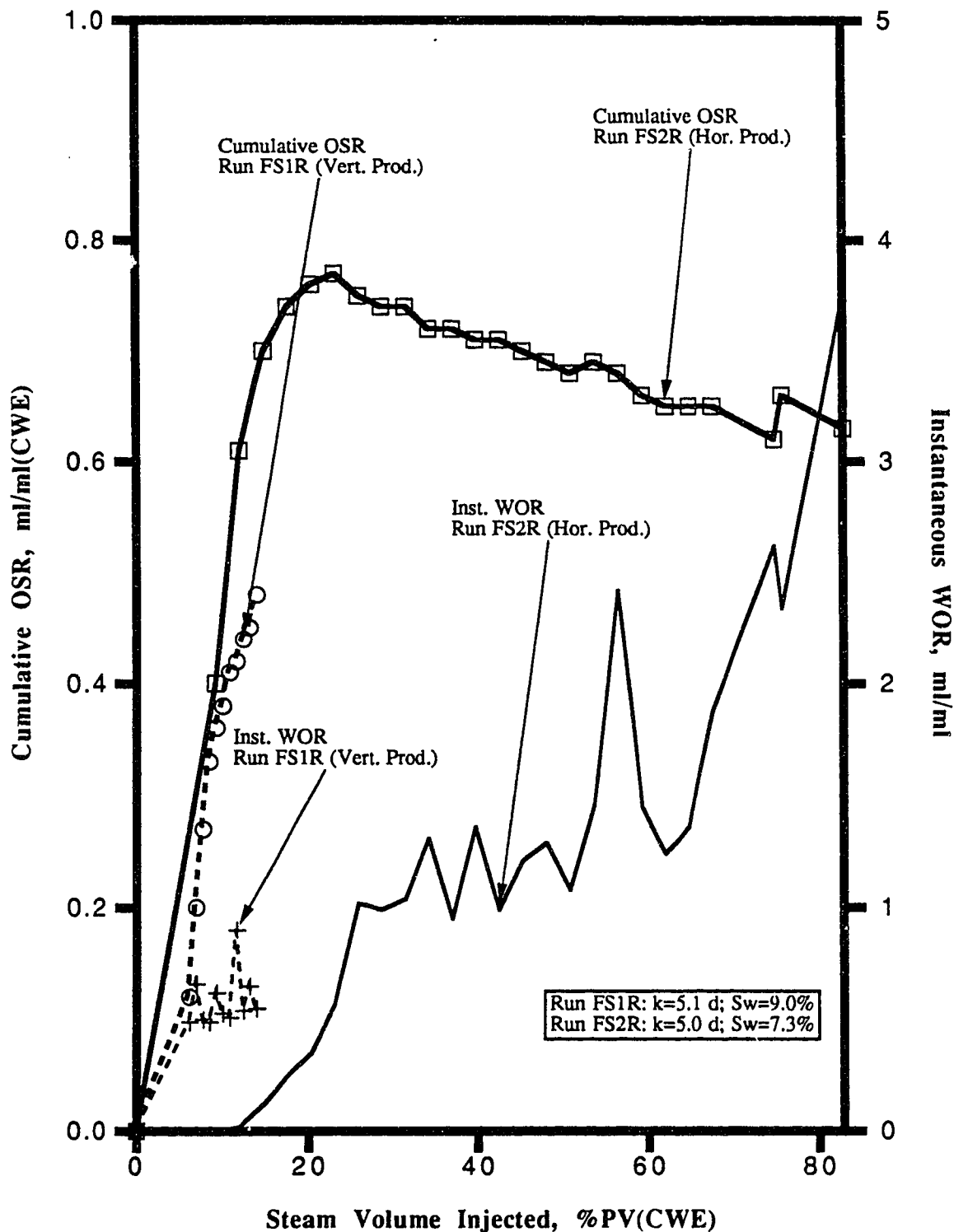
probably a result of the large contact area between the horizontal wells and the reservoir — which accelerated the reservoir response to steam injection. Specifically, the horizontal injector allowed the injected steam to reach and come into contact with a much larger portion of the sand pack than otherwise possible with a vertical injector. This resulted in the mobilization and displacement of a much larger volume of oil, and led to higher fluid production rates.

The cumulative OSR and instantaneous WOR curves in Figure 15, as well as the cumulative oil recovery curve in Figure 14 show that for the same volume of steam injected, a horizontal steam injector yielded lower oil recovery, lower cumulative OSR's and higher instantaneous WOR's than those obtained when a vertical injector was used (Run FS5A). Altogether, these indicated that Run FS8 which used a horizontal injector–horizontal producer well combination — despite achieving higher instantaneous fluid production rates — was not as thermally efficient as a vertical steam injector and a horizontal producer combination (Run FS5A). A possible explanation for the inferior performance in Run FS8 was the small vertical separation (1 in or 2.54 cm) between the horizontal injector and producer. As noted above, given the extended contact between the wells and the reservoir, it did not take long for large volumes of oil to become mobilized and produced, as well as for steam to break through into the horizontal producer. In addition, it is also probable that the geometrical set-up of placing the horizontal producer in the centre of the sand pack, and the horizontal injector 1-in (2.54 cm) above it (also 1-in or 2.54 cm away from the top of the sand pack) contributed to the relatively poor recovery performance. This set-up physically excluded the steam from sweeping the lower half portion of the sand pack (below the central horizontal producer) without breaking into the horizontal producer first. A different set-up, with the wells placed lower in the sand pack, would improve the thermal efficiency of the process and result in a better recovery performance.

Summarizing, the use of a horizontal injector and a horizontal producer did lead to high instantaneous fluid production rates, but also resulted in lower overall recovery efficiency.

6.5 Effect of Wellbore Geometry

Several different experiments were carried out in both physical models to evaluate the effect of the geometry of a horizontal producer (open or cased) on oil recovery. For the case of an open horizontal producer, the results of Runs FS2R and FS5A which were conducted in the *scaled model* were selected for evaluation. Similarly, the results of Run PS4 were compared against those of Run PS5. Both of these experiments were carried out in the *partially scaled model*. For the other case of a cased horizontal producer, Runs FS3R and FS6 in the *scaled model*, and Runs PS7 and PS9 in the *partially scaled model* were chosen.

Figure 14: Recovery Performance due to a Horizontal Injector (Run FS8) and
Recovery Performance due to a Vertical Injector (Run FS5A);
Instantaneous Fluid Production Rate and Cumulative Oil Recovery vs.
Steam Volume Injected. (Scaled Model Experiments)
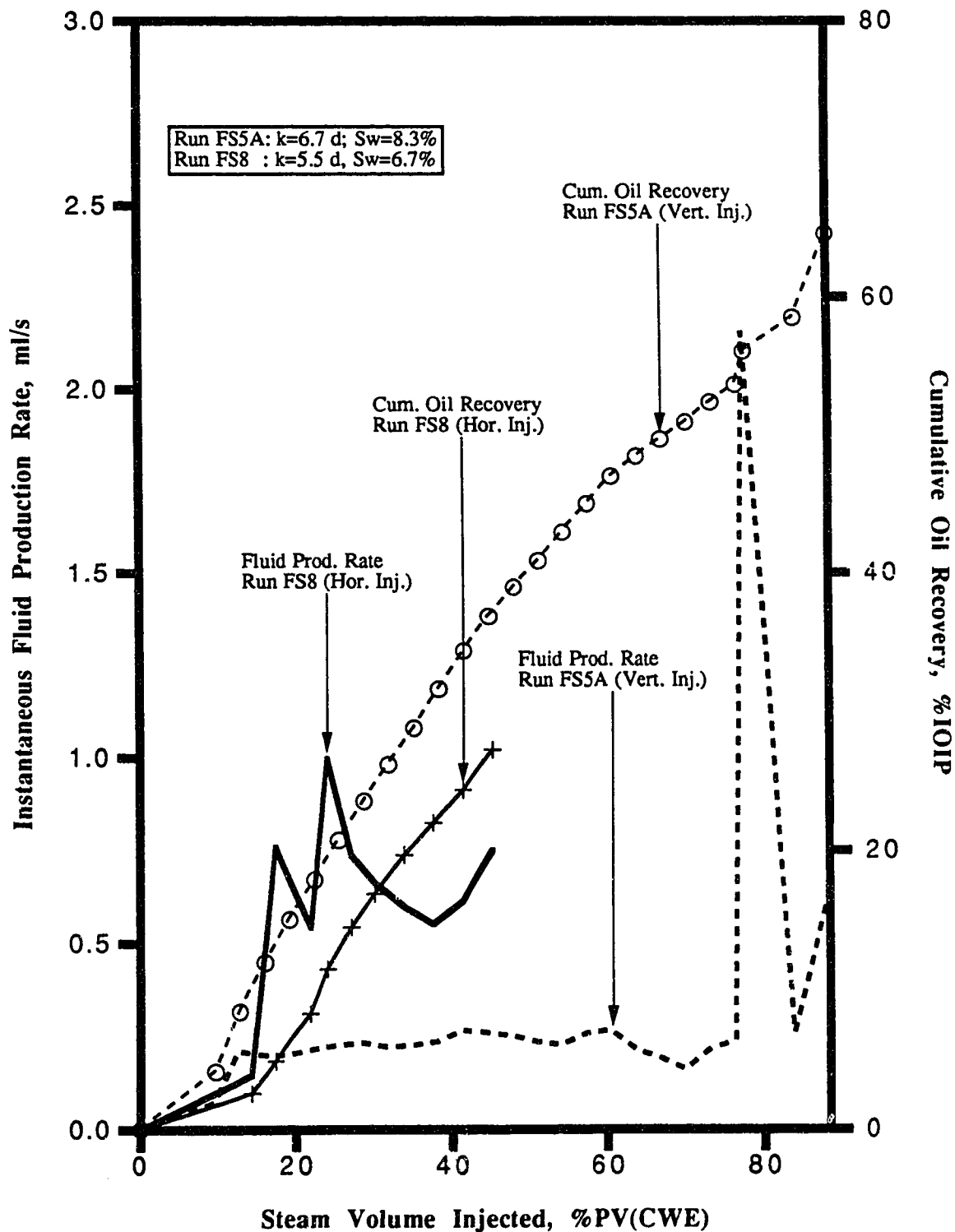
Figure 15: Recovery Performance due to a Horizontal Injector (Run FS8) and
Recovery Performance due to a Vertical Injector (Run FS5A);
Cumulative OSR and Instantaneous WOR vs. Steam Volume Injected.
(Scaled Model Experiments)
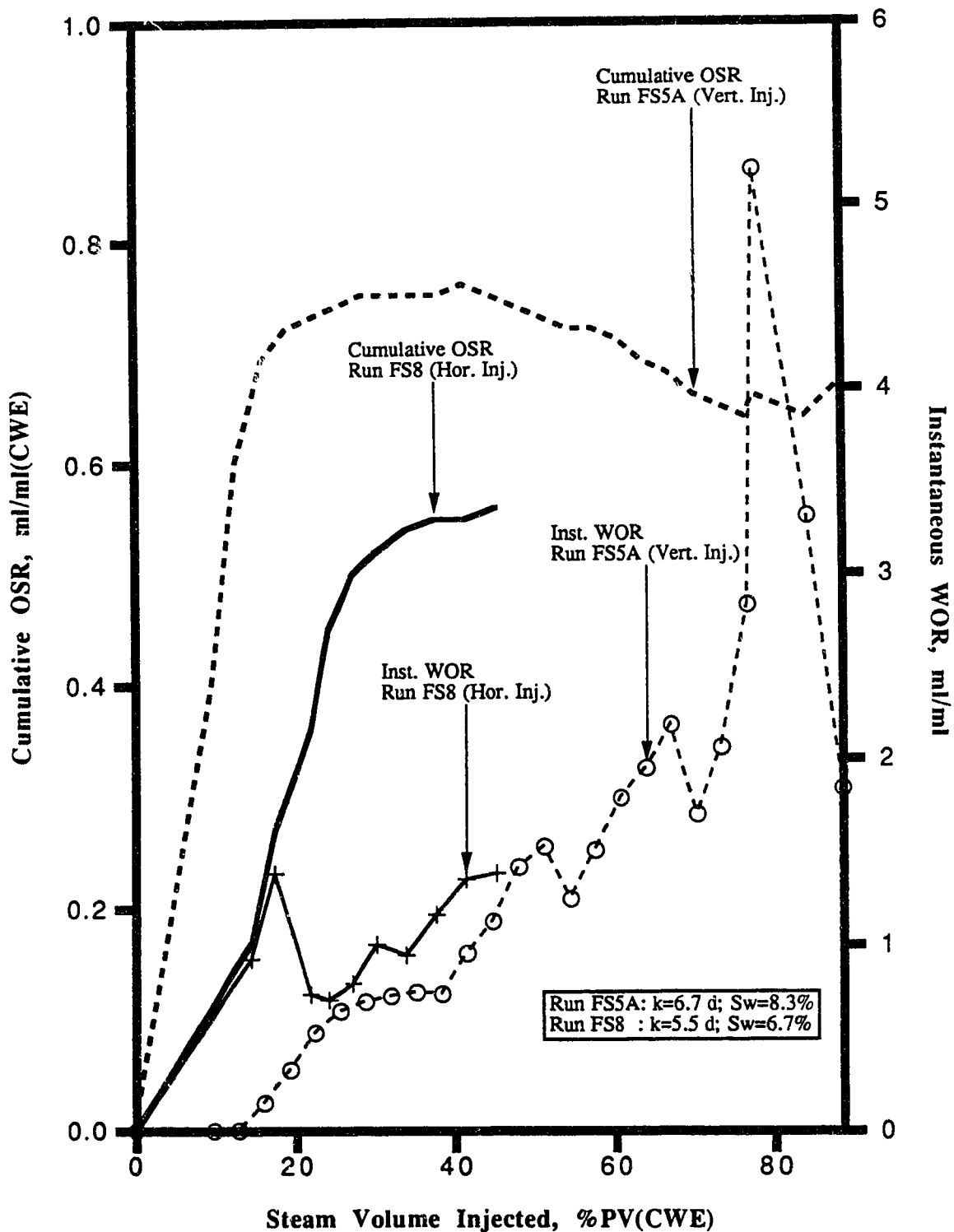
6.5.1 Open Horizontal Producer

6.5.1.1 Scaled Model Experiments

Three experiments were performed in the *scaled physical model* to evaluate the effect of the internal wellbore geometry for an open horizontal producer on oil recovery. These were Runs FS2R, FS5H, and FS5A. Run FS2R used a constant diameter horizontal producer, while Runs FS5H and FS5A had a variable diameter well. Run FS5A was carried out mainly because the recovery process taking place in Run FS5H was hot waterflooding rather than steamflooding, and thus the results could not be compared against those of Run FS2R. All three runs used the same vertical injector.

Tables E12, E16, and E17 contain the results of the three runs, and Figures 16-18 provide a comparison of the different performance indicators of Runs FS2R and FS5A which are necessary to determine the superiority or inferiority, in terms of recovery performance, of one type of horizontal producer to the other type. The comparison of the performance indicators is relative, and not on a one-to-one basis, because the production pressure profiles for the two experiments were slightly different.

Figure 16 shows that the instantaneous fluid production rate curve for Run FS5A (variable diameter) was generally higher than that in Run FS2R (constant diameter). Although the difference is small, it is greater than the experimental error (in reference to Figure 43). The sharp increase exhibited by both curves (after the injection of approximately 0.80 PV of steam) was, in all probability, due to a sudden lowering of the production back pressure. The increased pressure driving force directly led to a higher fluid production rate. An explanation for the higher fluid production rate by the variable diameter horizontal producer lies in the well pressure drop curves for the two cases. These curves show that not only was the well pressure drop curve for Run FS5A always lower than that for Run FS2R, but it also declined at a faster rate. Taking into account the explanations given previously (Section 6.2), these observations cumulatively indicate that the mobilized oil was produced faster through the variable diameter horizontal well than through the conventional, constant diameter well. A likely reason for this observation of better production rate by the variable diameter horizontal well is that the well, because of its internal wellbore geometry, reduced the resistance to the fluid flow inside it. Specifically, as mobilized oil and steam condensate flowed from the narrow inlet end of the variable diameter horizontal well to its wider outlet the cross-sectional area available for flow became larger. This led to a reduction in the wellbore resistance to the fluid flow (as mentioned in Chapter 5), and consequently, less energy dissipation. This latter result manifested itself as lower pressure drop across the horizontal well. The direct result of all this was a higher fluid production rate for a comparable pressure drawdown. Furthermore, this explanation relates readily to the analysis of the pressure-drop-across-the-well scaling group (Chapter 5), i.e. it was commented

Figure 16: Effect of Internal Wellbore Geometry on Recovery Performance;
Instantaneous Fluid Production Rate and Well Pressure Drop vs.
Steam Volume Injected (Scaled Model Experiments),
Constant Diameter Horizontal Well (Run FS2R) vs.
Variable Diameter Horizontal Well (Run FS5A).
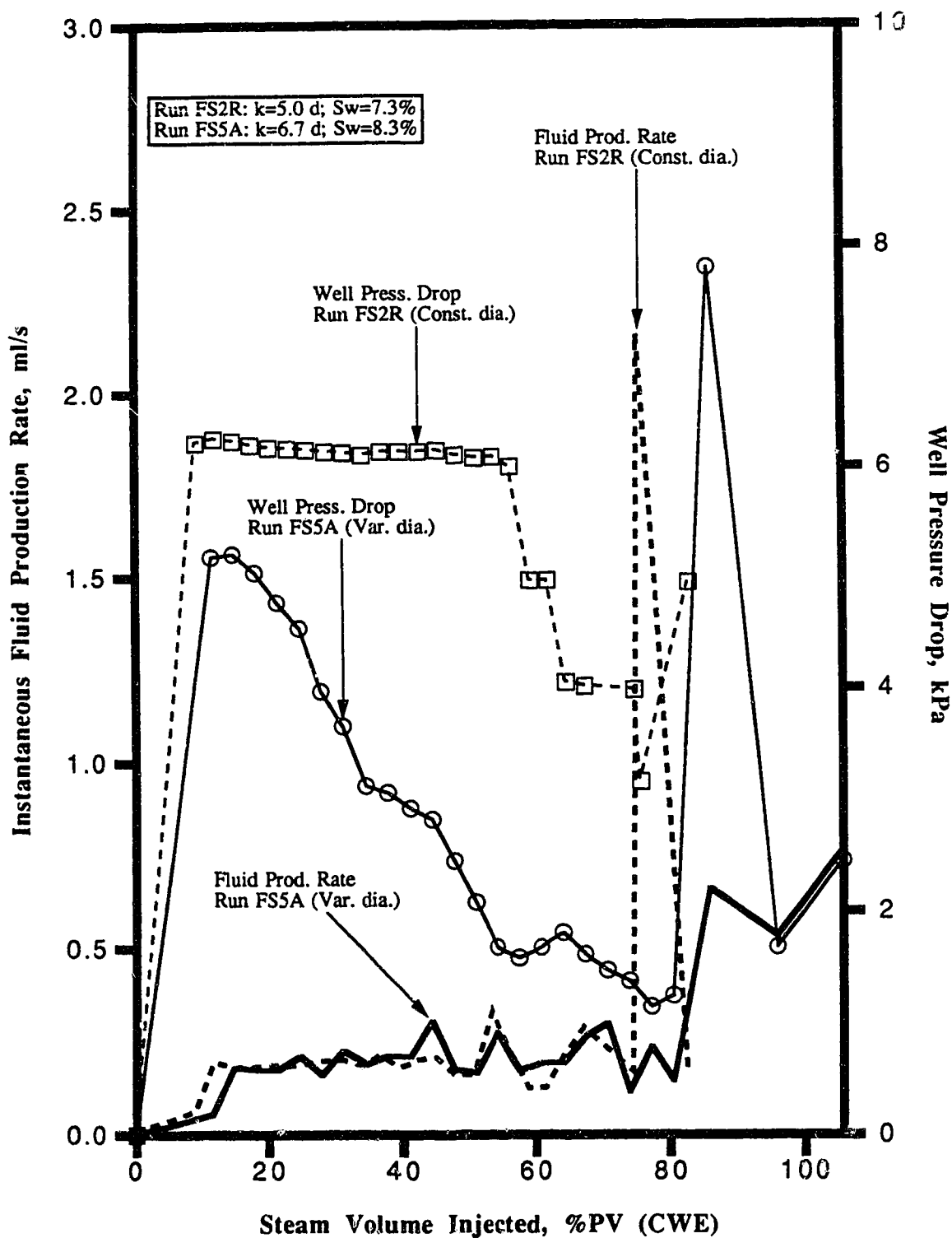
that, according to the equation which resulted from a rearrangement of the above scaling group, the velocity of flow inside the horizontal well will be greater if the well has a larger cross-sectional area of flow at the outlet. This also means that for a constant velocity of flow, the pressure drop across the horizontal well will be smaller if the well has a larger outlet. This is supported by the experimental data presented.

Figure 17 shows that until steam breakthrough (0.80 PV), the cumulative recovery for the variable diameter horizontal producer, for the same volume of steam injected, was for the most part – especially between 0.30 to 0.75 PV of steam injected – higher (3-4 %) than that for the conventional, constant diameter well. In addition, the cumulative OSR curves in Figure 18 show that during the steam zone growth phase (0.20 to 0.60 PV), the OSR for Run FS5A exceeded that for Run FS2R — indicating a higher thermal efficiency for the process using the variable diameter horizontal well. This improved efficiency for the tapered well may be attributed directly to the reduction in the pressure drop across it. Lower axial pressure gradients lead to a higher fluid flow velocity, and also cause – for the same pressure drawdown – more oil and steam condensate drawn into the well, leading to higher recovery and improved thermal efficiency.

Although the improvement in cumulative oil recovery attributed to the variable diameter horizontal well (3-4 %) is close to the experimental error shown in Figure 45 (± 2%), the trend of higher cumulative oil recovery was present in all variable diameter horizontal well experiments. In fact, in Runs FS6, PS5, and PS9 the cumulative oil recoveries for the variable diameter horizontal well were consistently higher – 4 to 6% – than those for the constant diameter horizontal well (Runs FS3R, PS4, and PS7). Further comparison of the results of these experiments is found in Sections 6.5.1.2, 6.5.2.1, and 6.5.2.2.

No serious attempt was made to determine the superior or inferior performance of the two types of horizontal producers based upon their instantaneous WOR curves. This was due to the fact that the production pressure profiles for the two cases were not exactly identical, which makes it improper to compare the two instantaneous WOR curves since, as was explained previously, the WOR's are greatly influenced by the production pressure setting. It is believed that the instantaneous fluid production rate, being composed of both oil and water, was not affected to the same extent by the production pressure as was the instantaneous WOR.

An examination of the temperature profiles of the sand pack after the injection of different volumes of superheated steam for Run FS5A (Figures 19 a, b, c, d), and the corresponding temperature profiles for Run FS2R (Figures 20 a, b, c, d) showed that the steam zone expanded faster in Run FS5A. In addition, it grew more uniformly (i.e. the effect of steam override was less pronounced) in different directions, and in different regions of the model reservoir in the presence of a variable

Figure 17: Effect of Internal Wellbore Geometry on Recovery Performance;
  Cumulative Oil Recovery vs. Steam Volume Injected (Scaled Model Experiments),
  Constanst Diameter Horizontal Well (Run FS2R) vs.
  Variable Diameter Horizontal Well (Run FS5A).

Figure 18: Effect of Internal Wellbore Geometry on Recovery Performance: Cumulative OSR and Instantaneous WOR vs. Steam Volume Injected (Scaled Model Experiments), Constant Diameter Horizontal Well (Run FS2R) vs. Variable Diameter Horizontal Well (Run FS5A).
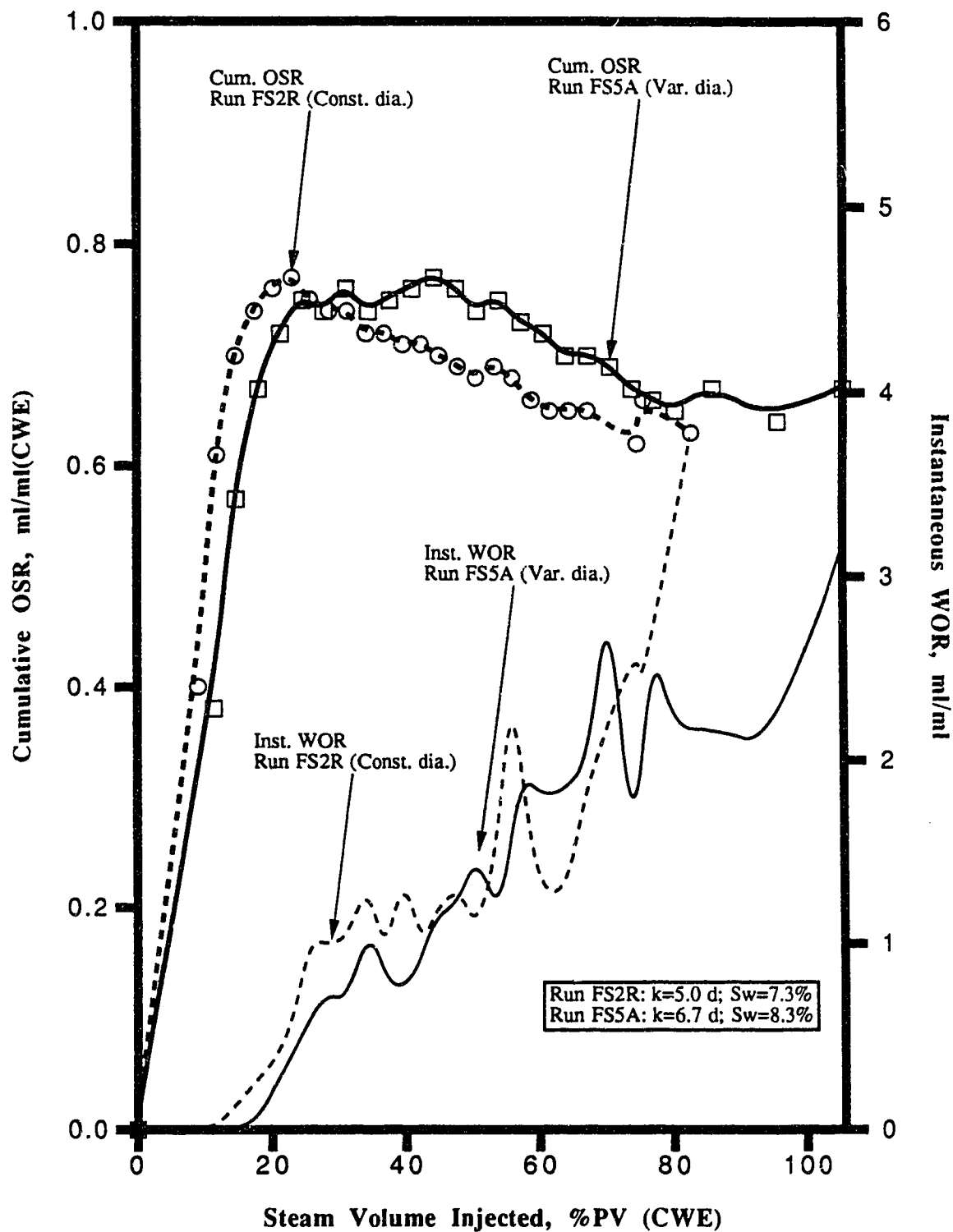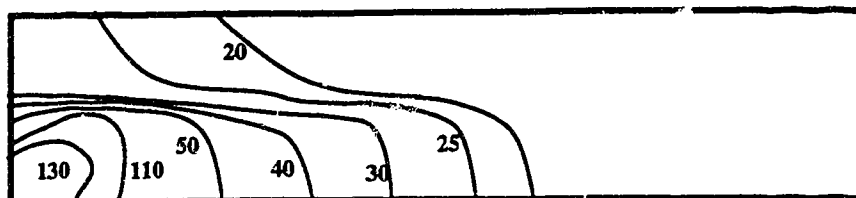
a) 0.10 PV of superheated steam injected.
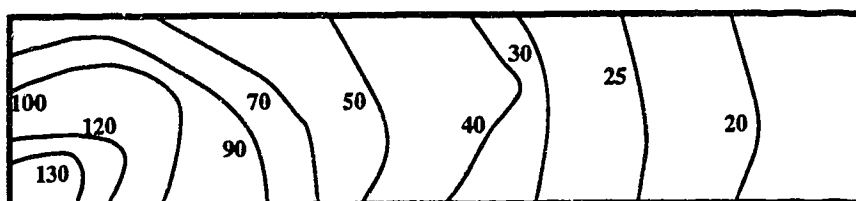
b) 0.25 PV of superheated steam injected.
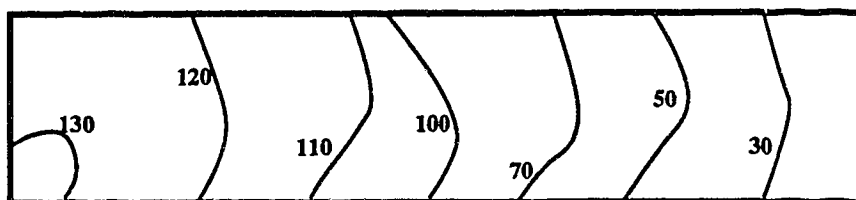
c) 0.50 PV of superheated steam injected.
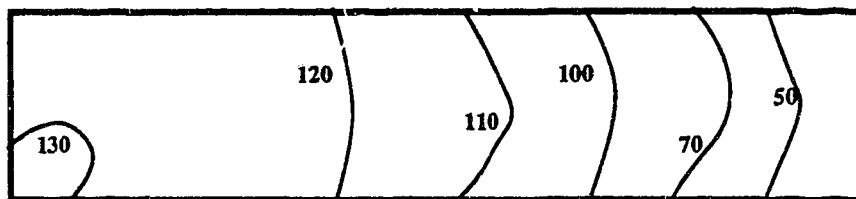
d) 0.75 PV of superheated steam injected.

Figure 19: Temperature (°C) profiles of the sand pack after the injection of 0.10 (a), 0.25 (b), 0.50 (c), and 0.75 (d) PV of superheated steam. Variable diameter horizontal producer case (Run FS5A).
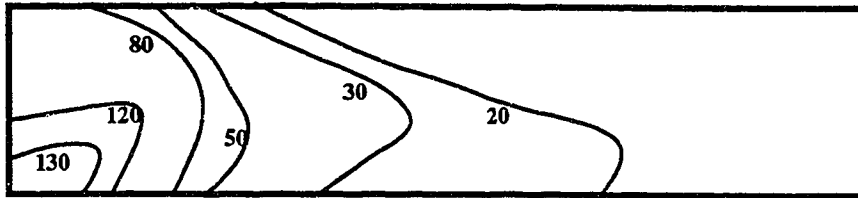
a) 0.10 PV of superheated steam injected.
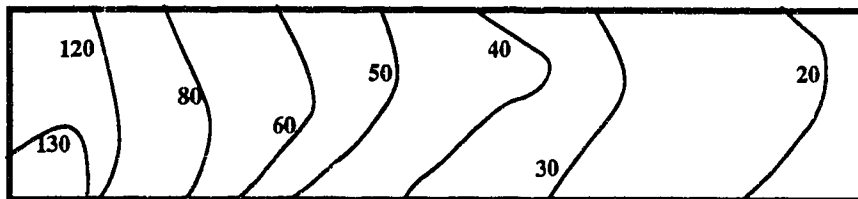
b) 0.25 PV of superheated steam injected.
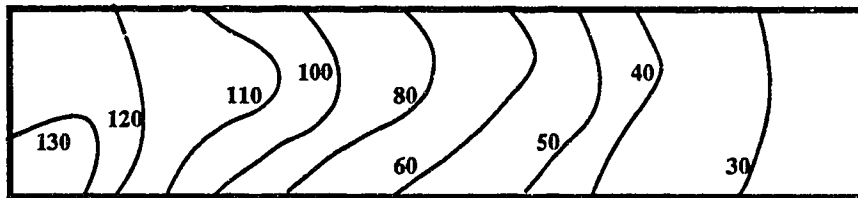
c) 0.50 PV of superheated steam injected.
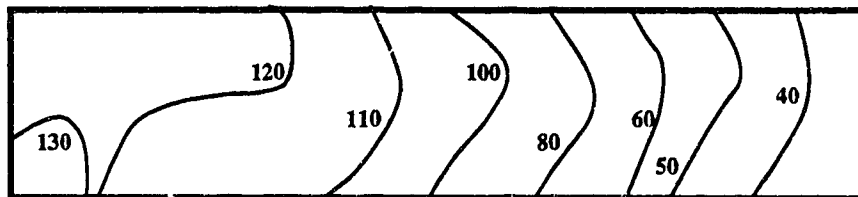
d) 0.75 PV of superheated steam injected.

Figure 20: Temperature (°C) profiles of the sand pack after the injection of 0.10 (a), 0.25 (b), 0.50 (c), and 0.75 (d) PV of superheated steam. Constant diameter horizontal producer case (Run FS2R).

diameter horizontal producer than a constant diameter well. In this sense, the use of a variable diameter horizontal well possibly led to the higher sweep efficiency than that obtained when a constant diameter horizontal well was used.

6.5.1.2 Partially Scaled Model Experiments

Five experiments were carried out in the *partially scaled model* , again for evaluating the effect of wellbore geometry on oil recovery performance. Of these, Runs PS3 and PS4 used a constant diameter sintered-tube horizontal well while Runs PS5, PS5A, and PS6 used a variable diameter sintered-tube well. The results of these runs are listed in Tables E1-E5. The results of two representative runs, one used the constant diameter well and the other the variable diameter producer (Runs PS4 and PS5, respectively) were selected for the comparison of recovery performance indicators, which are graphically illustrated in Figures 21 to 23.

Figure 21 shows that the instantaneous fluid production rate for the variable diameter horizontal producer, despite exhibiting more fluctuations, was relatively higher than that for the constant diameter producer — particularly when less than 0.25 PV of steam had been injected. It is important to note that the absolute permeability in Run PS4 (constant diameter well) was 8.5 darcies, and its initial water saturation was 0.057 PV, while the absolute permeability and initial water saturation for Run PS5 (variable diameter well) were 15.0 darcies and 0.102 PV, respectively. The higher permeability in Run PS5 could have also contributed to its higher fluid production rate in the early period, as well as larger pressure drop across the horizontal well when compared to Run PS4 — especially in reference to previous discussion on the production mechanism during the early period of a recovery process (Section 6.3). This result differs from that for the *scaled model* experiments (Runs FS2R and FS5A) which showed smaller pressure drop across the variable diameter horizontal well.

Figures 22 and 23 show that Run PS5 yielded higher cumulative oil recovery and cumulative OSR than Run PS4, even though its initial oil saturation was less than that for Run PS4. The improvement in the final cumulative oil recovery due to the use of a variable diameter horizontal well (at 0.40 PV of steam injected) was about 10%. Furthermore, not only the variable diameter horizontal well recovered more oil, it also resulted in accelerated recovery — compared to a regular horizontal well, it required a smaller volume of steam to produce a comparable volume of oil. These two results agree closely with those obtained for the *scaled model*.

In conclusion, it is seen from the results of both types of experiments – *scaled and partially scaled* – that the internal wellbore geometry of a horizontal production well can have a significant effect on the recovery performance of a steam injection process. Variable diameter horizontal wells, with narrow inlet ends and wider production ends, could effectively reduce the axial well pressure gradient

Figure 21: Effect of Internal Wellbore Geometry on Recovery Performance;
Instantaneous Fluid Production Rate and Well Pressure Drop vs.
Steam Volume Injected (Partially Scaled Model),
Constant Diameter Horizontal Well (Run PS4) vs.
Variable Diameter Horizontal Well (Run PS5).
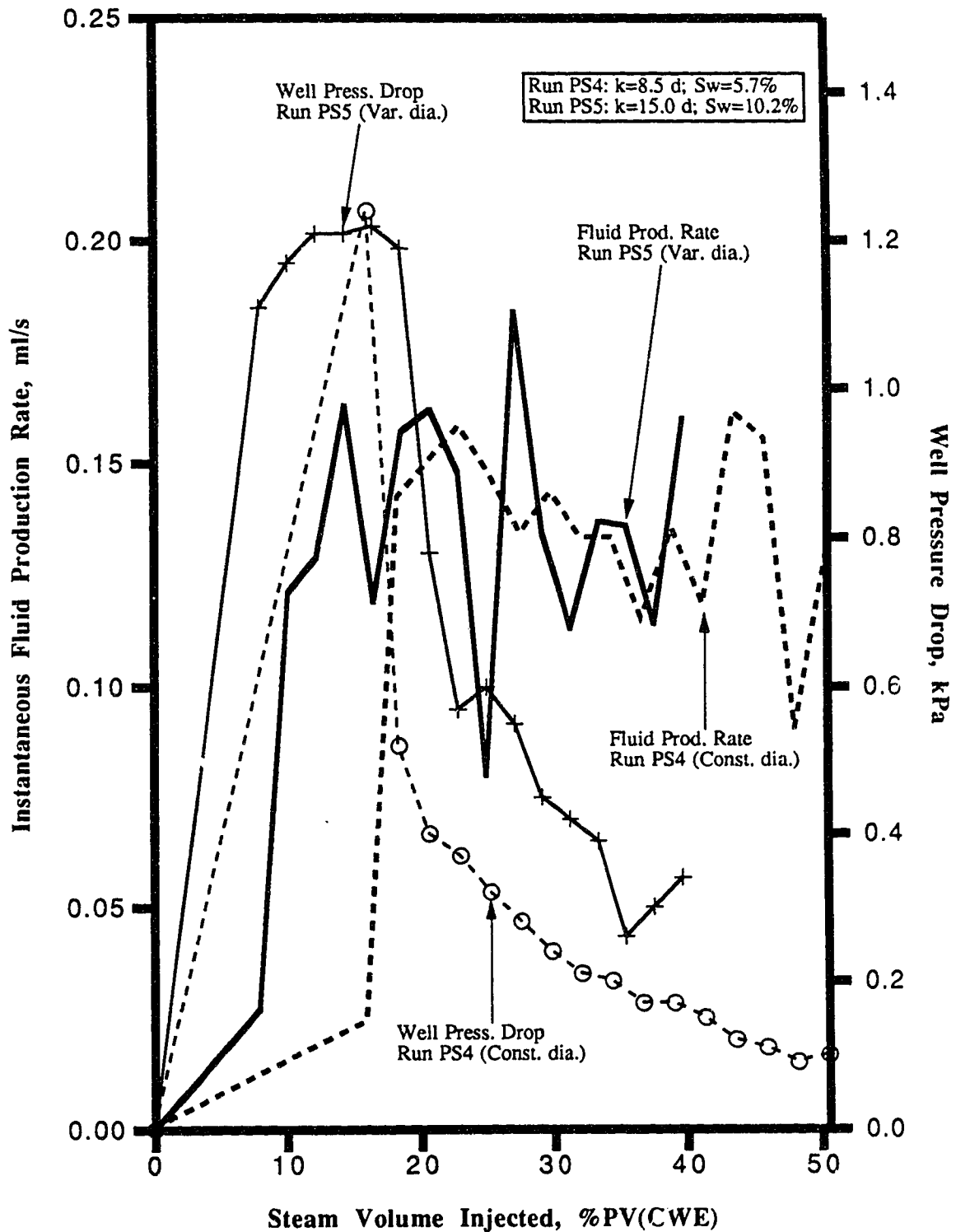
Figure 22: Effect of Internal Wellbore Geometry on Recovery Performance;
Cumulative Oil Recovery vs. Steam Volume Injected (Partially Scaled Model),
Constant Diameter Horizontal Well (Run PS4) vs.
Variable Diameter Horizontal Well (Run PS5).

Figure 23: Effect of Internal Wellbore Geometry on Recovery Performance; Cumulative OSR and Instantaneous WOR vs. Steam Volume Injected (Partially Scaled Model), Constant Diameter Horizontal Well (Run PS4) vs. Variable Diameter Horizontal Well (Run PS5).

and yield higher oil recovery and OSR than constant diameter wells.

6.5.2 Cased Horizontal Producer

Keeping in view the increasingly popular field practice of protecting horizontal wells with perforated casing, it was necessary to determine the potential effectiveness of a variable diameter horizontal well to improve the recovery performance of cased horizontal wells. To do this, the following runs were performed: FS3R and FS6 in the *scaled model*, and PS7 and PS9 in the *partially scaled model*.

6.5.2.1 Scaled Model Experiments

Run FS3R used a constant diameter, slotted horizontal well encased in the perforated casing of design pattern #1 (reference Figures 6a and 6b), whereas Run FS6 had the variable diameter, slotted horizontal well encased in its own tapered casing , also of design pattern #1. The results are given in Tables E14 and E18.

Figure 24 compares the instantaneous fluid production rate and well pressure drop for the runs. It can be seen that the respective fluid production rates were more or less identical for the most part, but Run FS6 showed a higher rate later (> 0.60 PV of steam injected).

An examination of the well pressure drop curves for the two runs shows a characteristic form similar to that seen previously (Section 6.5.1.1): lower pressure drops across the variable diameter horizontal producer (Run FS6). Keeping in mind that the pressure drop across a horizontal well in this study was determined by measuring and subtracting the pressure at two points inside the well at each extremity, the well pressure drops were not affected by the casing, which was external to the well.

Figure 25 shows that even when the horizontal wells were cased, the variable diameter horizontal producer still recovered more oil for the same volume of steam injected than the regular, constant diameter well. Figure 26 demonstrates that the cumulative OSR for Run FS6, beyond 0.20 PV), was higher than that for Run FS3R.

6.5.2.2 Partially Scaled Model Experiments

In this case, Run PS7 used a cased constant diameter, sintered-tube horizontal well, while Run PS9 had a cased variable diameter horizontal producer. Tables E6 and E8 list the results of these two experiments.

Figures 27 to 29 compare several recovery performance indicators for these two runs. Briefly stated, it can be seen that, except for the instantaneous fluid production rate curves which showed large fluctuations in both cases, all of the remaining parameters behaved in the same fashion as those observed in the runs in the *scaled model*: the cased variable diameter horizontal well led to a lower pressure drop across the well, higher cumulative oil recovery and cumulative OSR. The fluctuations in both the instantaneous fluid production rate and instantaneous WOR curves for both runs, not amenable to any definitive interpretation of the performance potential of either type of well

Figure 24: Effect of Internal Wellbore Geometry on Recovery Performance; Instantaneous Fluid Production Rate and Well Pressure Drop vs. Steam Volume Injected (Scaled Model Experiments), Constant Diameter Horizontal Well (Run FS3R) vs. Variable Diameter Horizontal Well (Run FS6).

Figure 25: Effect of Internal Wellbore Geometry on Recovery Performance;
Cumulative Oil Recovery vs. Steam Volume Injected (Scaled Model Experiments),
Constant Diameter Horizontal Well (Run FS3R) vs.
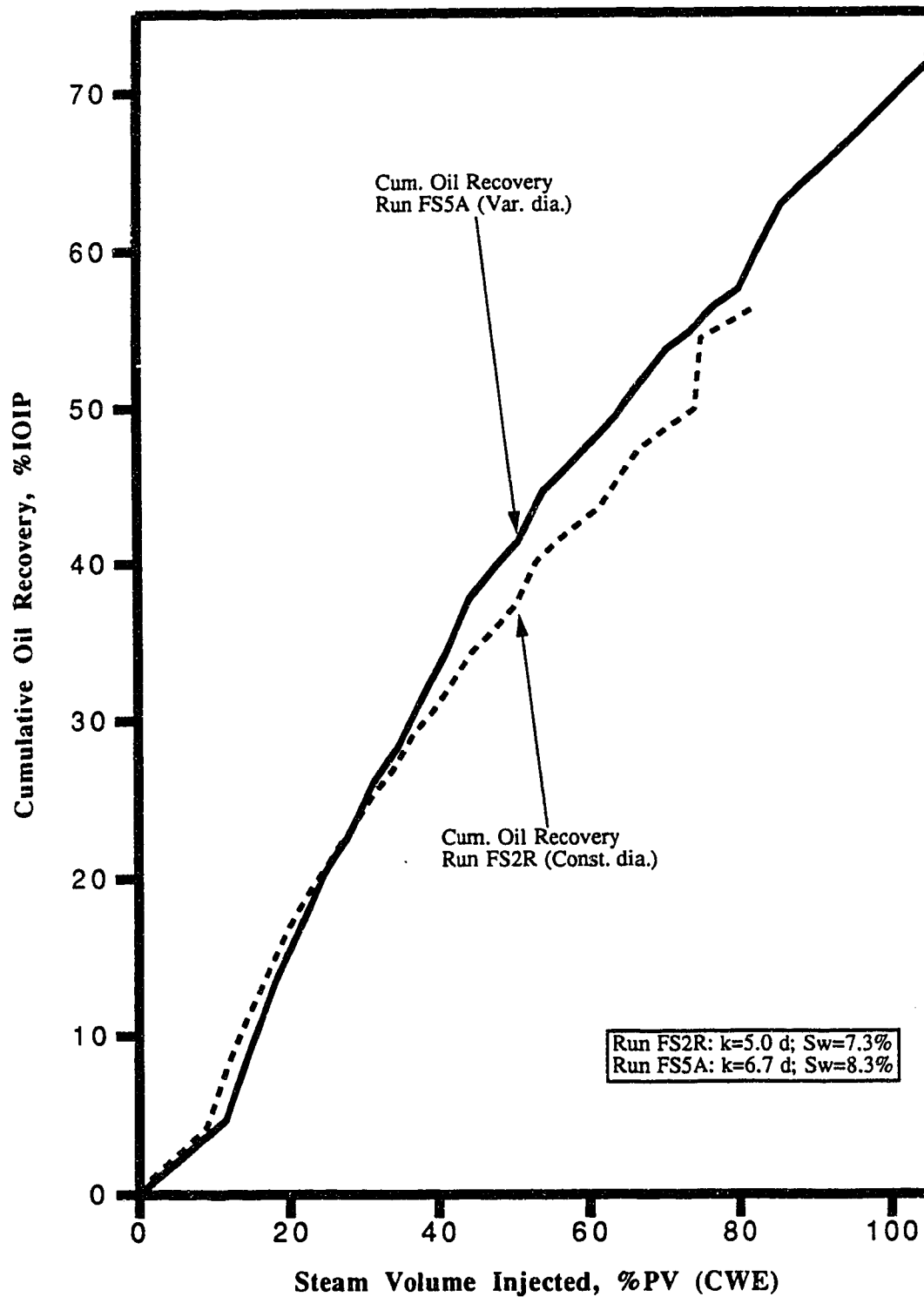Variable Diameter Horizontal Well (Run FS6).

Figure 26: Effect of Internal Wellbore Geometry on Recovery Performance;
Cumulative OSR and Instantaneous WOR vs. Steam Volume Injected
(Scaled Model Experiments),
Constant Diameter Horizontal Well (Run FS3R) vs.
Variable Diameter Horizontal Well (Run FS6).

Figure 27: Effect of Internal Wellbore Geometry on Recovery Performance:
Instantaneous Fluid Production Rate and Well Pressure Drop vs.
Steam Volume Injected (Partially Scaled Model Experiments),
Cased Constant Diameter Horizontal Well (Run PS7) vs.
Cased Variable Diameter Horizontal Well (Run PS9).
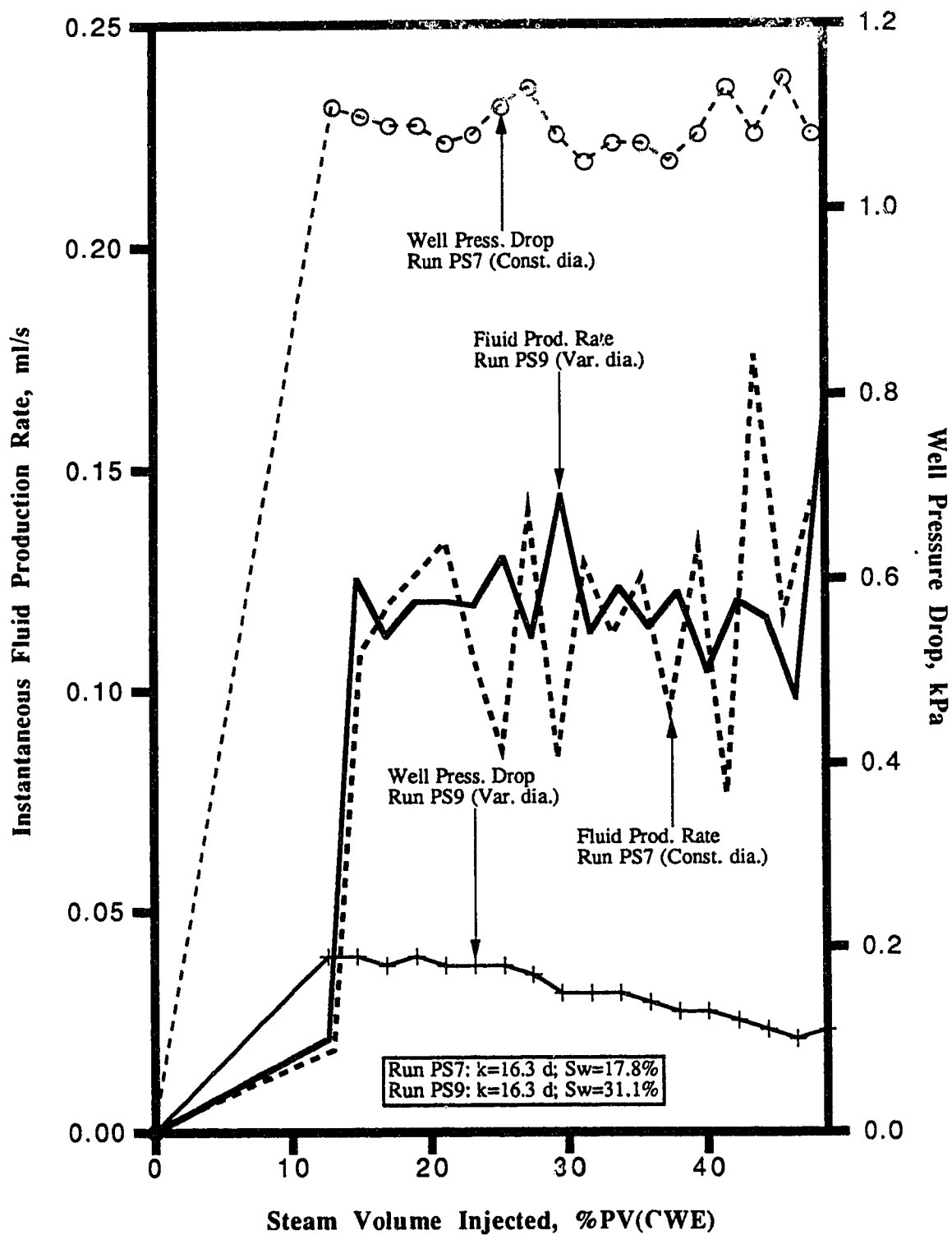
Figure 28: Effect of Internal Wellbore Geometry on Recovery Performance;
Cumulative Oil Recovery vs. Steam Volume Injected (Partially Scaled Model),
Cased Constant Diameter Horizontal Well (Run PS7) vs.
Cased Variable Diameter Horizontal Well (Run PS9).
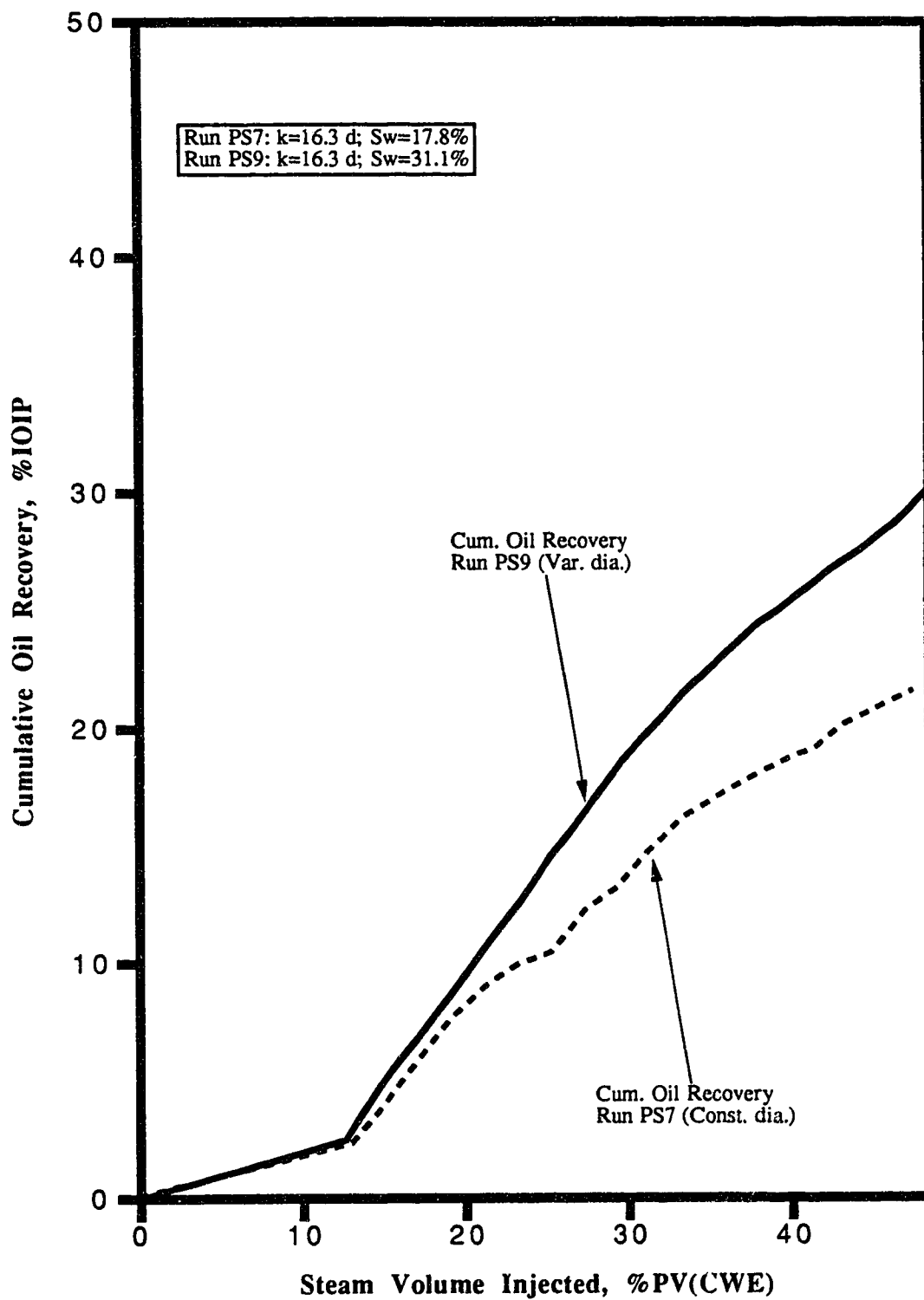
Figure 29: Effect of Internal Wellbore Geometry on Recovery Performance;
Cumulative OSR and Instantaneous WOR vs. Steam Volume Injected
(Partially Scaled Model Experiments),
Cased Constant Diameter Horizontal Well (Run PS7) vs.
Cased Variable Diameter Horizontal Well (Run PS9).
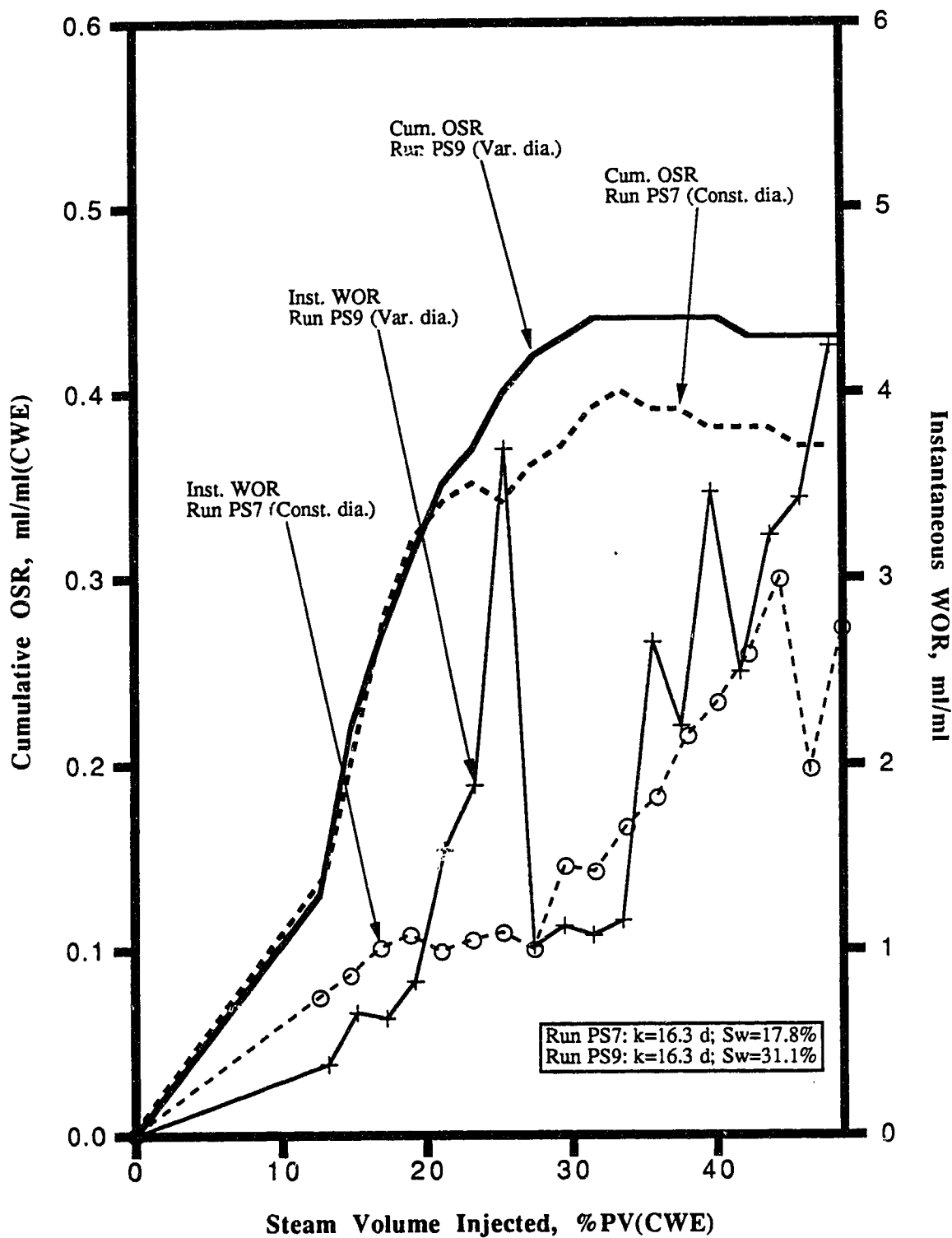
– constant or variable diameter – were due to changes in the production pressure setting. It was noticed that in a few experiments the production back pressure regulator (BPR) – possibly because of the accumulation of deposits inside its different parts – was not responsive, and therefore required continual adjustments to maintain a nominal production pressure.

Summarizing, it is seen from the results obtained for all of the cases considered (cased vs. open horizontal producer, and *scaled model* vs. *partially scaled model*) that the inside-wellbore geometry of a horizontal producer can affect the recovery performance of the steamflood process significantly.

6.6 Effect of Perforated Casing

A variety of experiments were performed in both physical models to determine the role played by a perforated casing on the steamflood oil recovery process. Three different situations were considered: 1) effect of casing on a constant diameter horizontal producer in the *scaled*, and 2) *partially scaled model*, and 3) effect of casing on a variable diameter horizontal producer in the *scaled model*. For the first case, the results of Runs FS2R and FS3R were compared against one another. For the second case, two runs were chosen: PS3 and PS8. And for the last case, Run FS5A and Run FS6 were selected.

6.6.1 Constant Diameter Horizontal Well

6.6.1.1 Scaled Physical Model Experiments

Table E12 contains the results of Run FS2R which used an open, constant diameter horizontal producer, and Table E14 is for Run FS3R which had the above well encased in an aluminum perforated casing of design pattern #1 (reference Figure 6a).

Figures 30 to 32 provide plots of instantaneous fluid production rate, well pressure drop, cu   lative oil recovery, cumulative OSR, and instantaneous WOR for the runs. As shown in Figure 30, the pressure drop across the horizontal producer was lower for the open well for almost the entire duration of the experiment. The instantaneous fluid production rate of Run FS2R, for the early part of the process, was higher than the corresponding rate of Run FS3R. After some time, however, the two production rates started to fluctuate so that at times one rate was higher than the other.

Perhaps the most telling indications of the effect of a casing on oil recovery performance are illustrated in Figures 31 and 32. It can be seen clearly that the cased horizontal producer in Run FS3R recovered less of the oil in place, and had a lower cumulative OSR than the open well in Run FS2R. It is believed that the lower thermal efficiency of Run FS3R was due mostly to the presence of the perforated casing which was believed to behave, in some way, as a channel — diverting some of the injected steam away from the porous medium. A comparison of the instantaneous WOR curves for the two runs shows that in general Run FS3R had a higher instantaneous WOR than Run FS2R, giving another indication of the negative impact of a perforated casing on the recovery performance

Figure 30: Effect of Perforated Casing on Recovery Performance;
Instantaneous Fluid Production Rate and Well Pressure Drop vs.
Steam Volume Injected (Scaled Model Experiments),
Open Constant Diameter Horizontal Well (Run FS2R) vs.
Cased Constant Diameter Horizontal Well (Run FS3R).
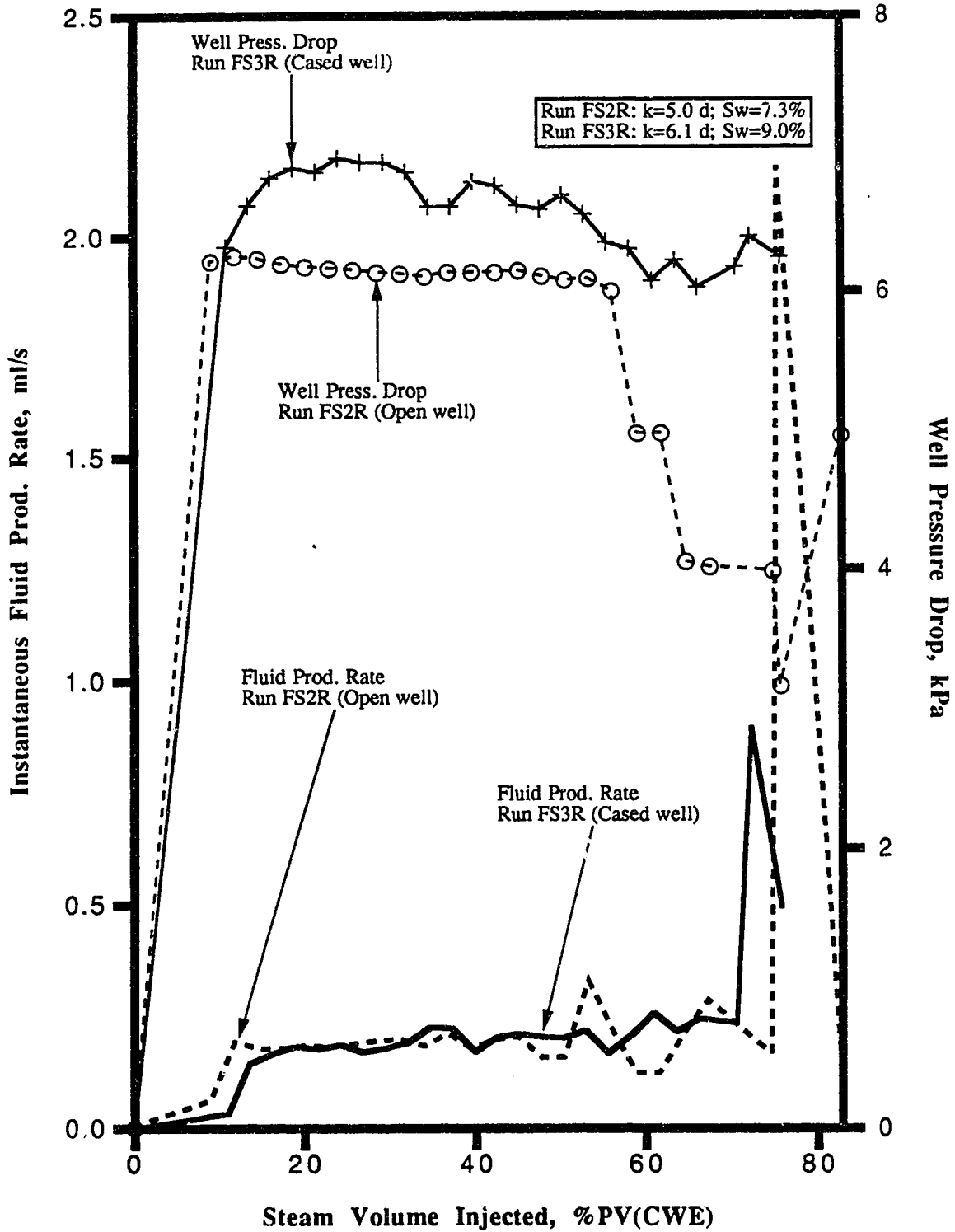
Figure 31: Effect of Perforated Casing on Recovery Performance;
   Cumulative Oil Recovery vs. Steam Volume Injected (Scaled Model Experiments),
   Open Constant Diamter Horizontal Well (Run FS2R) vs.
   Cased Constant Diameter Horizontal Well (Run FS3R).

Run FS2R: k=5.0 d; Sw=7.3%
Run FS3R: k=6.1 d; Sw=9.0%

Cum. Oil Recovery
Run FS2R (Open well)

Cum. Oil Recovery
Run FS3R (Cased well)

Cumulative Oil Recovery, %IOIP

Steam Volume Injected, %PV(CWE)
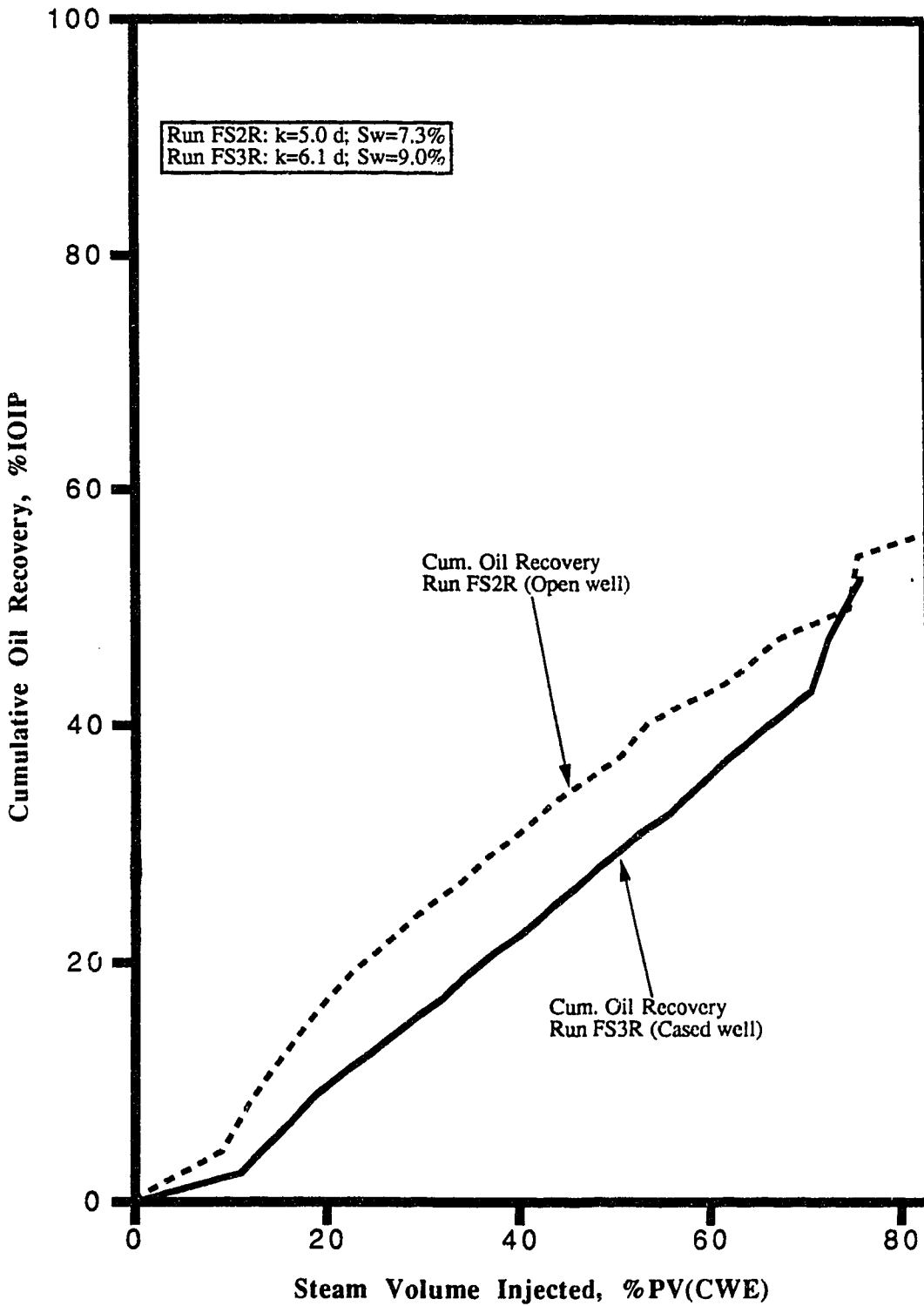
Figure 32: Effect of Perforated Casing on Recovery Performance;
   Cumulative OSR and Instantaneous WOR vs. Steam Volume Injected
   (Scaled Model Experiments),
   Open Constant Diameter Horizontal Well (Run FS2R) vs.
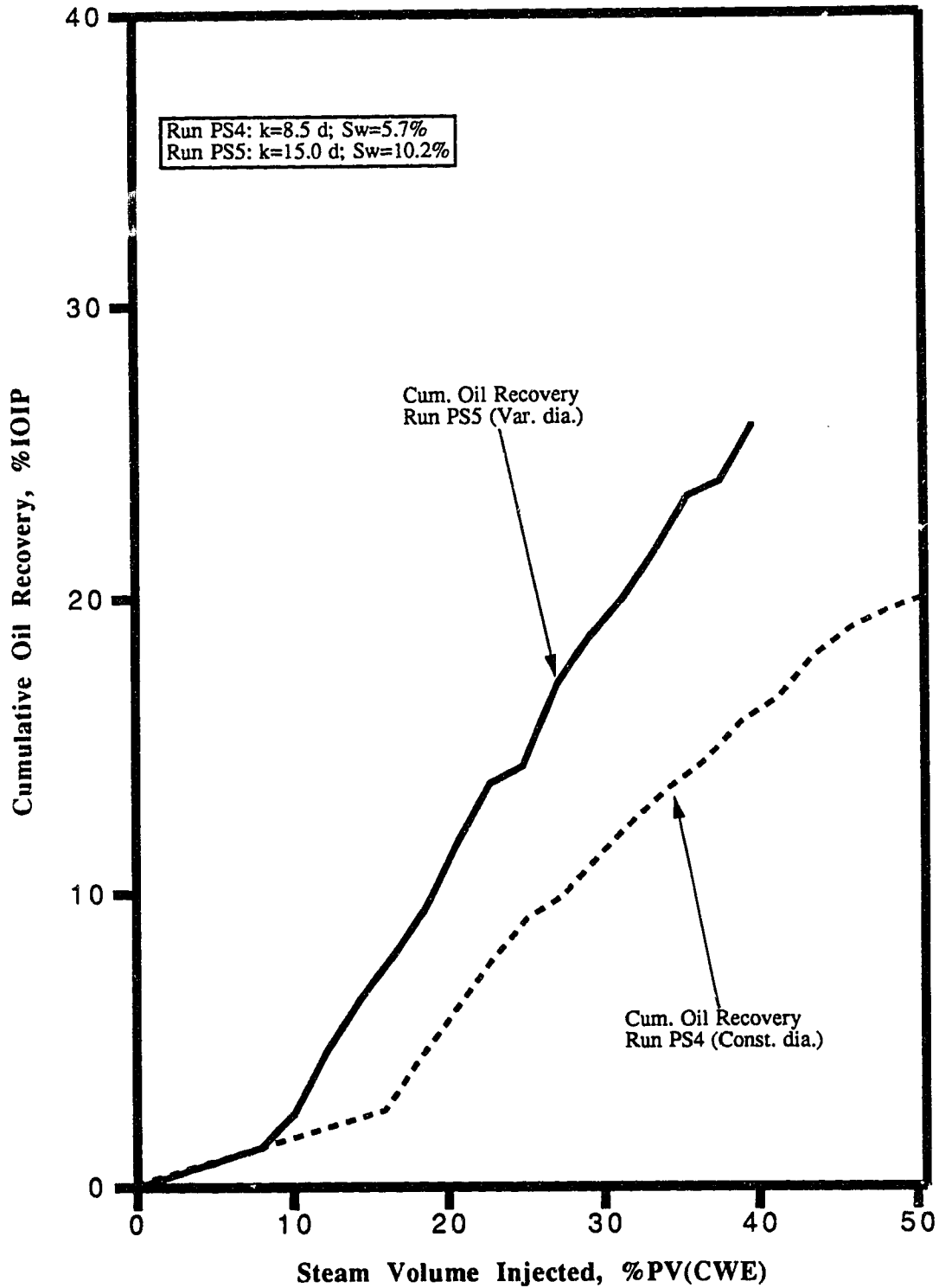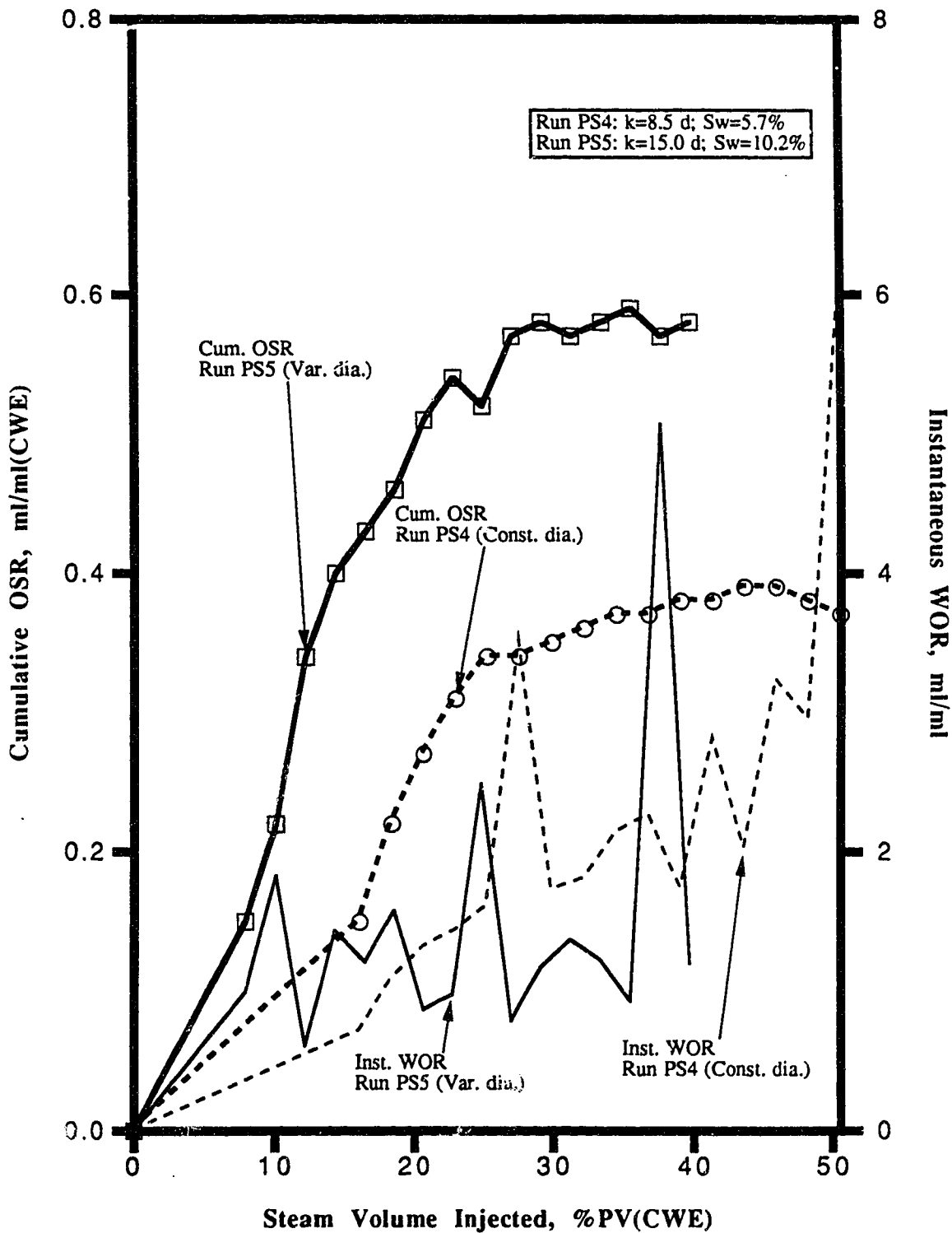   Cased Constant Diameter Horizontal Well (Run FS3R).
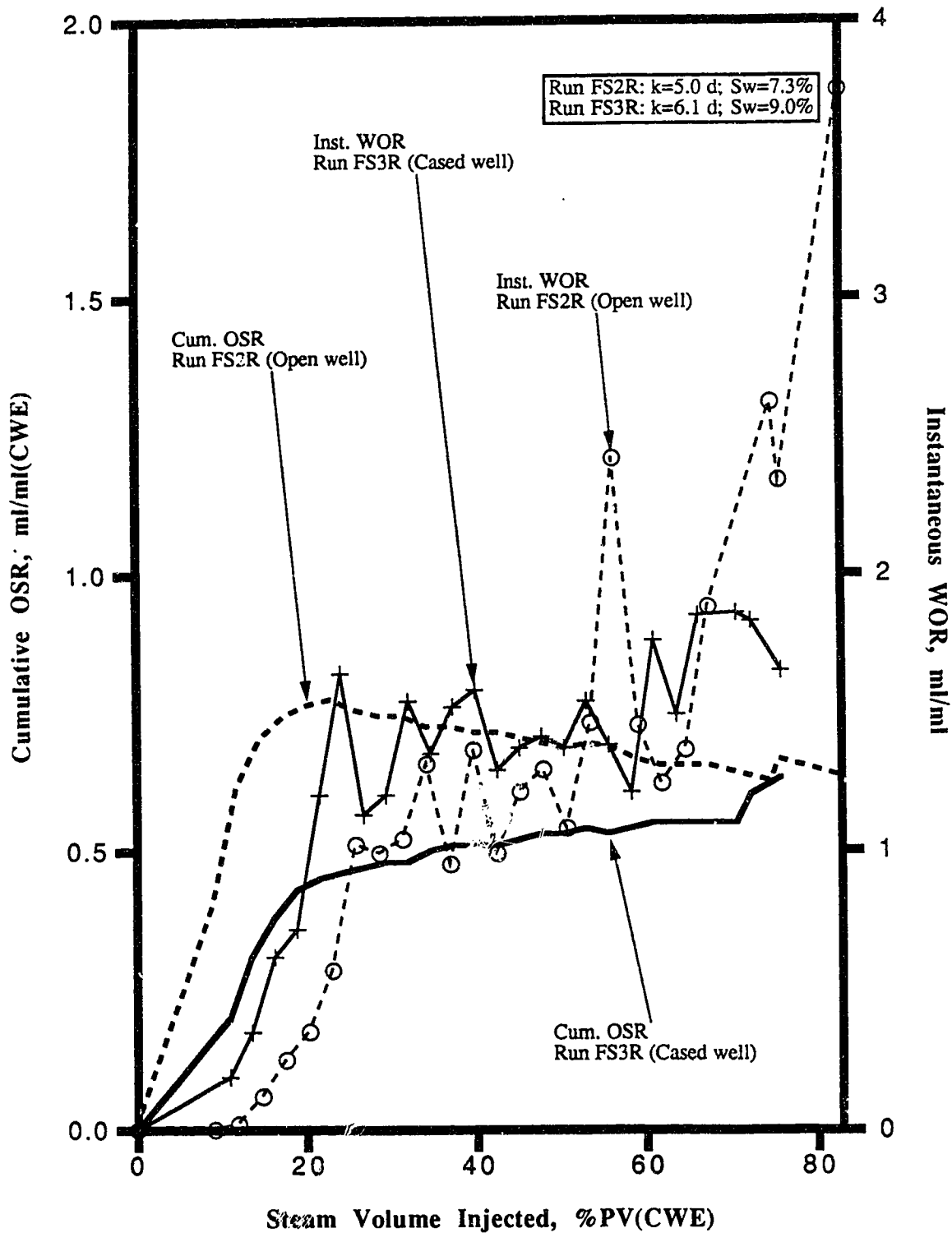
of a horizontal well.

Analyzing the temperature profiles of the sand pack for these two runs (Figure 33 and Figure 34) showed that the effect of casing on steam sweep efficiency was inconclusive. When there was less than 0.50 PV of superheated steam injected, the casing seemed to slow down the expansion rate of the steam zone. However, the steam zone expanded faster during the later stage of the experiment (Figure 34d). It was believed that the faster growth of the steam zone during this stage (0.75 PV of superheated steam injected) was due to the breakthrough of steam in the annulus between the horizontal well and its casing. This was confirmed by a higher reading of the production thermocouple temperature for Run FS3R (64°C) than that for Run FS2R (45°C). More importantly, it can be seen that steam override effect was more pronounced in Run FS3R, when the constant diameter horizontal producer was encased. In this respect, the perforated casing could have led to poorer sweep efficiency in the lower part of the model reservoir.

6.6.1.2 Partially Scaled Physical Model Experiments

In this case, Run PS3 had the constant diameter sintered-tube horizontal well, and Run PS8 was carried out with this well encased in its associated casing. The results are contained in Tables E1 and E7, and displayed graphically in Figures 35 to 37.

Contrary to the results obtained from the *scaled model* experiments which showed a lower well pressure drop for the cased well, Figure 35 shows that the well pressure drop in Run PS8 was less than that in Run PS3. Furthermore, the fluid production rate in Run PS3 was always higher than that in Run PS8.

Regarding the cumulative oil recovery and cumulative OSR results, it can be seen that the cased horizontal well recovered less oil (Figure 36), and was less efficient (Figure 37) than the open well. For these indicators, the results were identical to those obtained from the *scaled model* experiments — supporting, once again, the evidence of the negative impact caused by the perforated casing on the oil recovery performance.

6.6.2 Variable Diameter Horizontal Well

To evaluate the effect of a tapered perforated casing on the recovery performance of a variable diameter horizontal producer, four runs were performed in the *scaled model*: FS5H, FS5A, FS6 (casing pattern #1), and FS7 (casing pattern #2) (reference Figures 6a and 6b). The results of FS5A and FS6 were chosen to compare against one another. Tables E17 and E19 contain these results.

It can be seen from Figure 38 that, in general, the behaviour of the instantaneous fluid pro   n rate and well pressure drop curves for these variable diameter horizontal producer runs fo   ved those for the constant diameter horizontal well runs in the *scaled model*. In addition, Figures 39 and
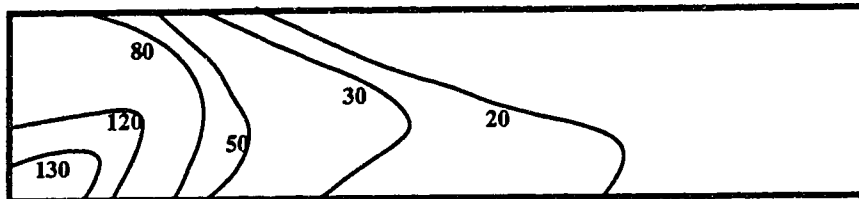
a) 0.10 PV of superheated steam injected.
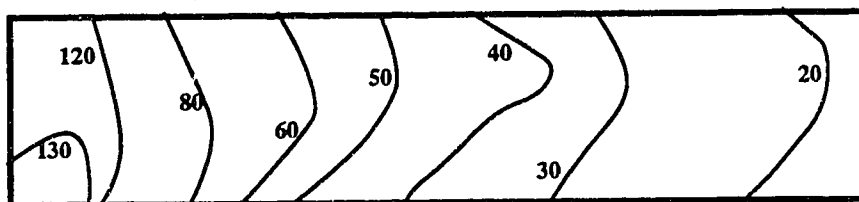
b) 0.25 PV of superheated steam injected.
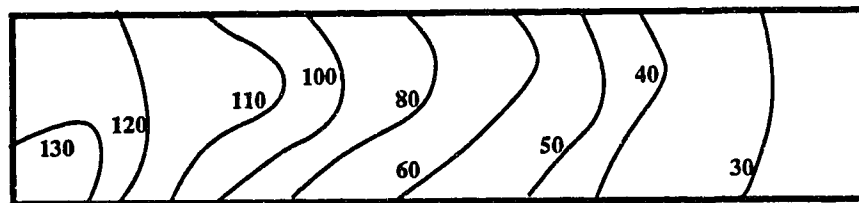
c) 0.50 PV of superheated steam injected.
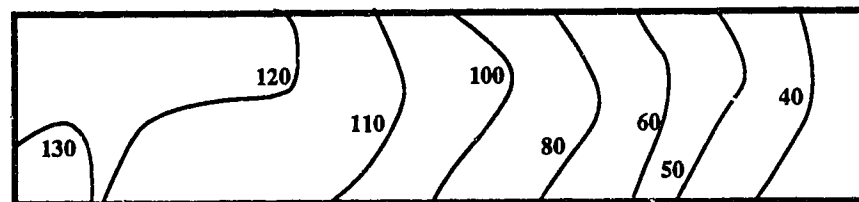
d) 0.75 PV of superheated steam injected.

Figure 33: Temperature (°C) profiles of the sand pack after the injection of 0.10 (a), 0.25 (b), 0.50 (c), and 0.75 (d) PV of superheated steam. Constant diameter horizontal producer case (Run FS2R).
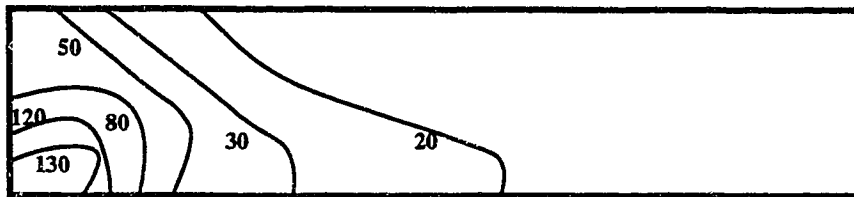
a) 0.10 PV of superheated steam injected.
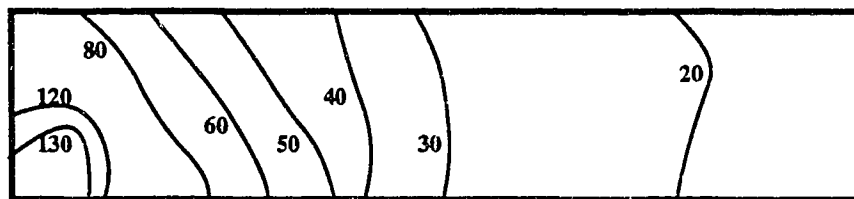
b) 0.25 PV of superheated steam injected.
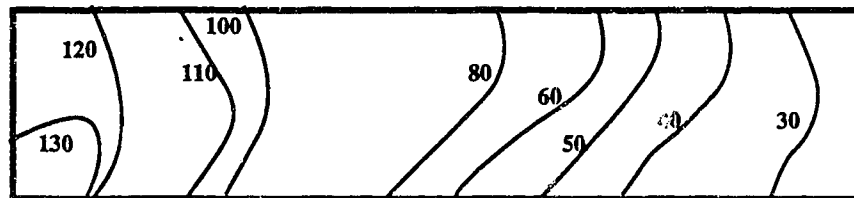
c) 0.50 PV of superheated steam injected.

d) 0.75 PV of superheated steam injected.

Figure 34: Temperature (°C) profiles of the sand pack after the injection of 0.10 (a),
0.25 (b), 0.50 (c), and 0.75 (d) PV of superheated steam.
Constant diameter horizontal producer case with casing (Run FS3R).

Figure 35: Effect of Perforated Casing on Recovery Performance;
Instantaneous Fluid Production Rate and Well Pressure Drop vs.
Steam Volume Injected (Partially Scaled Model Experiments),
Open Constant Diameter Horizontal Well (Run PS3) vs.
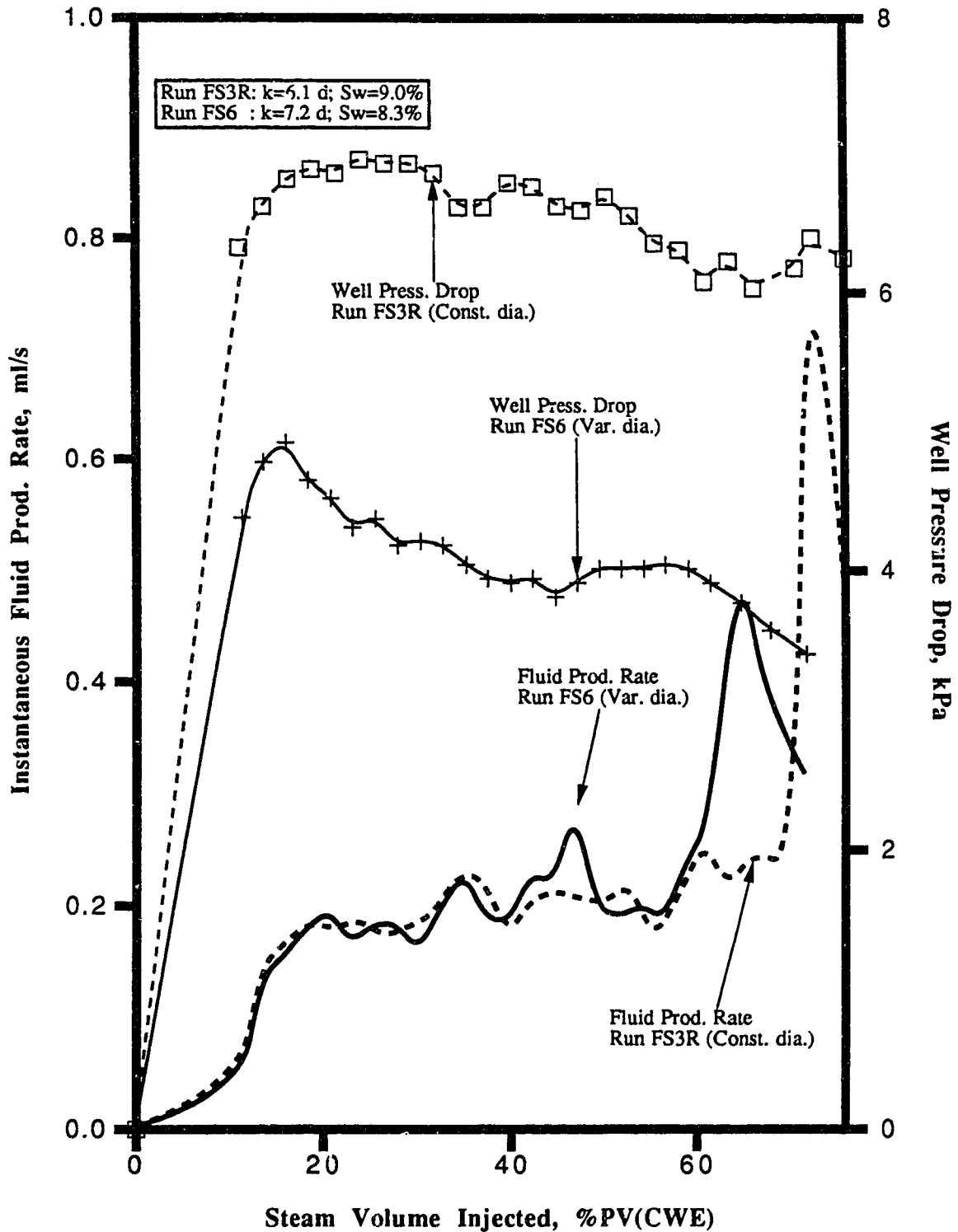Cased Constant Diameter Horizontal Well (Run PS8).
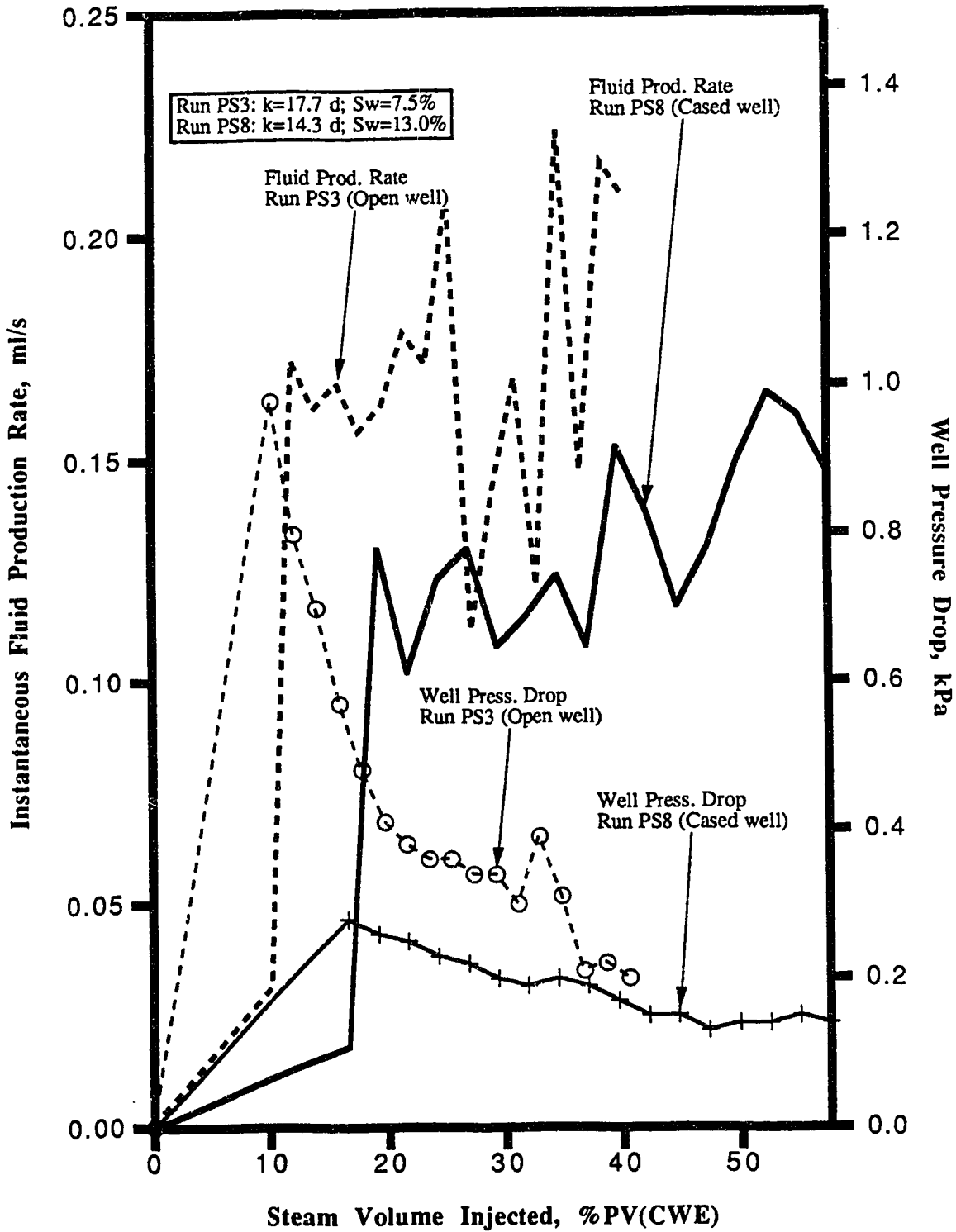
Figure 36: Effect of Perforated Casing on Recovery Performance;
  Cumulative Oil Recovery vs. Steam Volume Injected
  (Partially Scaled Model Experiments),
  Open Constant Diameter Horizontal Well (Run PS3) vs.
  Cased Constant Diameter Horizontal Well (Run PS8).

Run PS3: k=17.7 d; Sw=7.5%
Run PS8: k=14.3 d; Sw=13.0%

Cum. Oil Recovery
Run PS3 (Open well)

Cum. Oil Recovery
Run PS8 (Cased well)

Steam Volume Injected, %PV(CWE)

Cumulative Oil Recovery, %IOIP
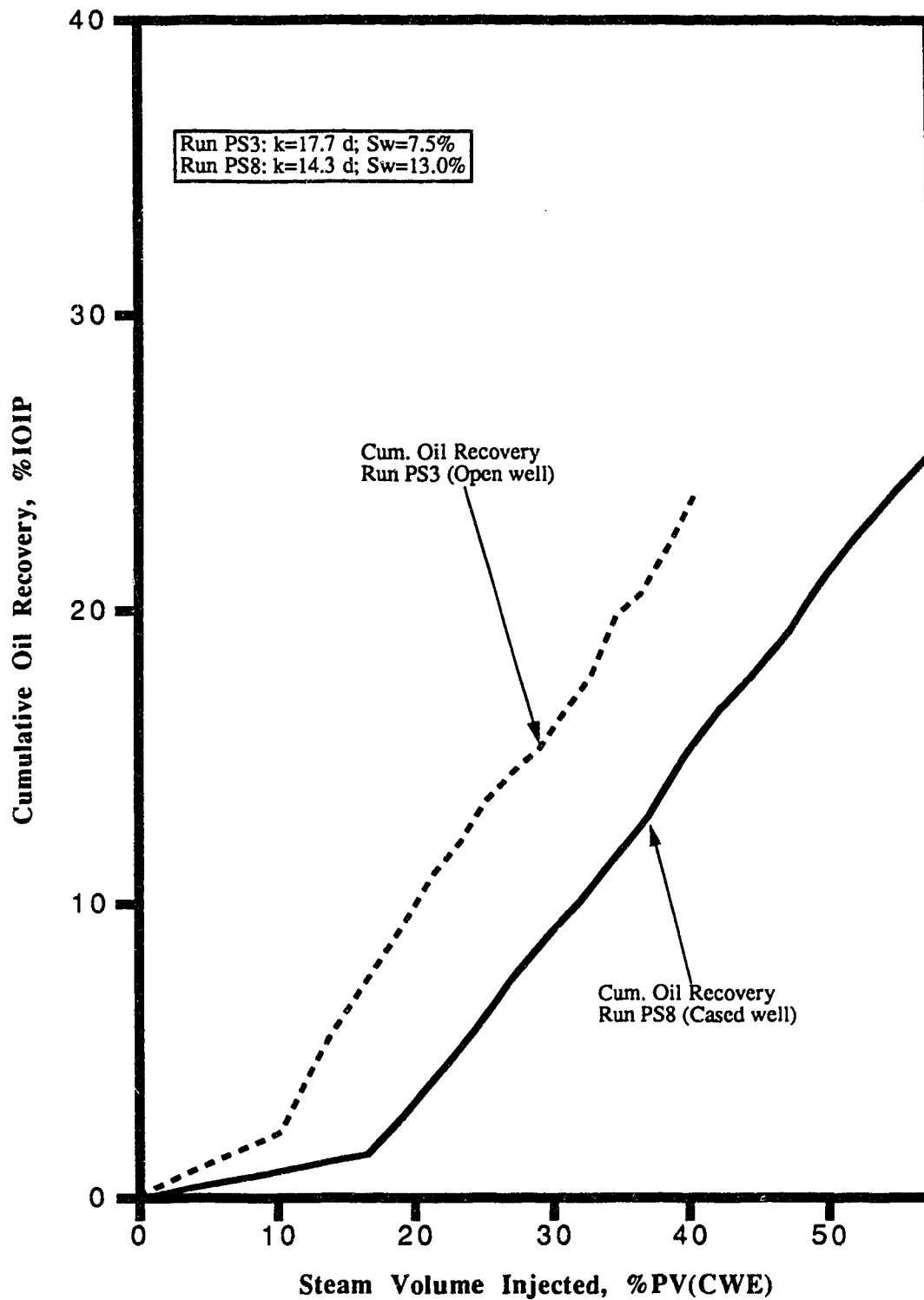
Figure 37: Effect of Perforated Casing on Recovery Performance;
Cumulative OSR and Instantaneous WOR vs. Steam Volume Injected
(Partially Scaled Model Experiments),
Open Constant Diameter Horizontal Well (Run PS3) vs.
Cased Constant Diameter Horizontal Well (Run PS8).
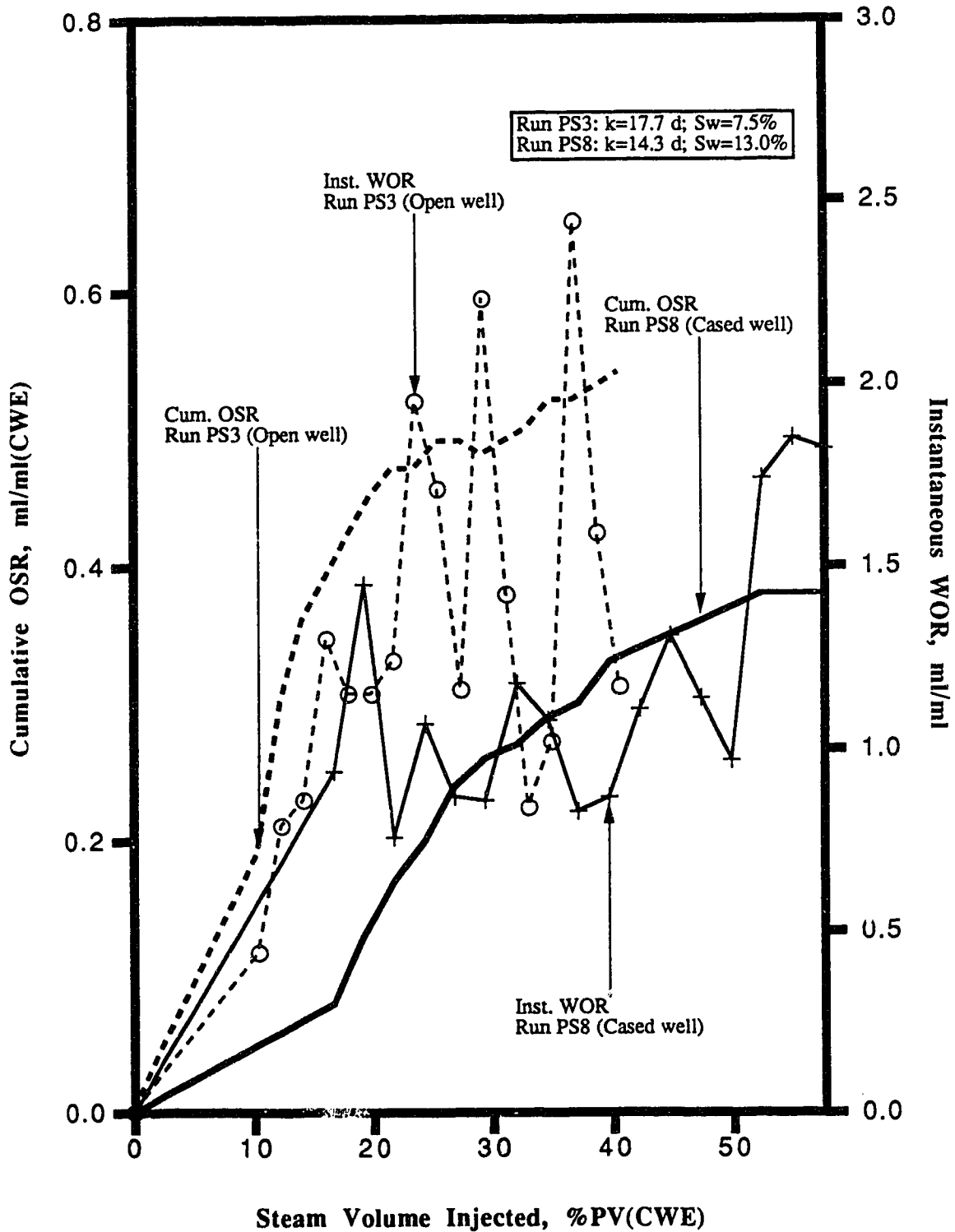
Figure 38: Effect of Perforated Casing on Recovery Performance;
Instantaneous Fluid Production Rate and Well Pressure Drop vs.
Steam Volume Injected (Scaled Model Experiments),
Open Variable Diameter Horizontal Well (Run FS5A) vs.
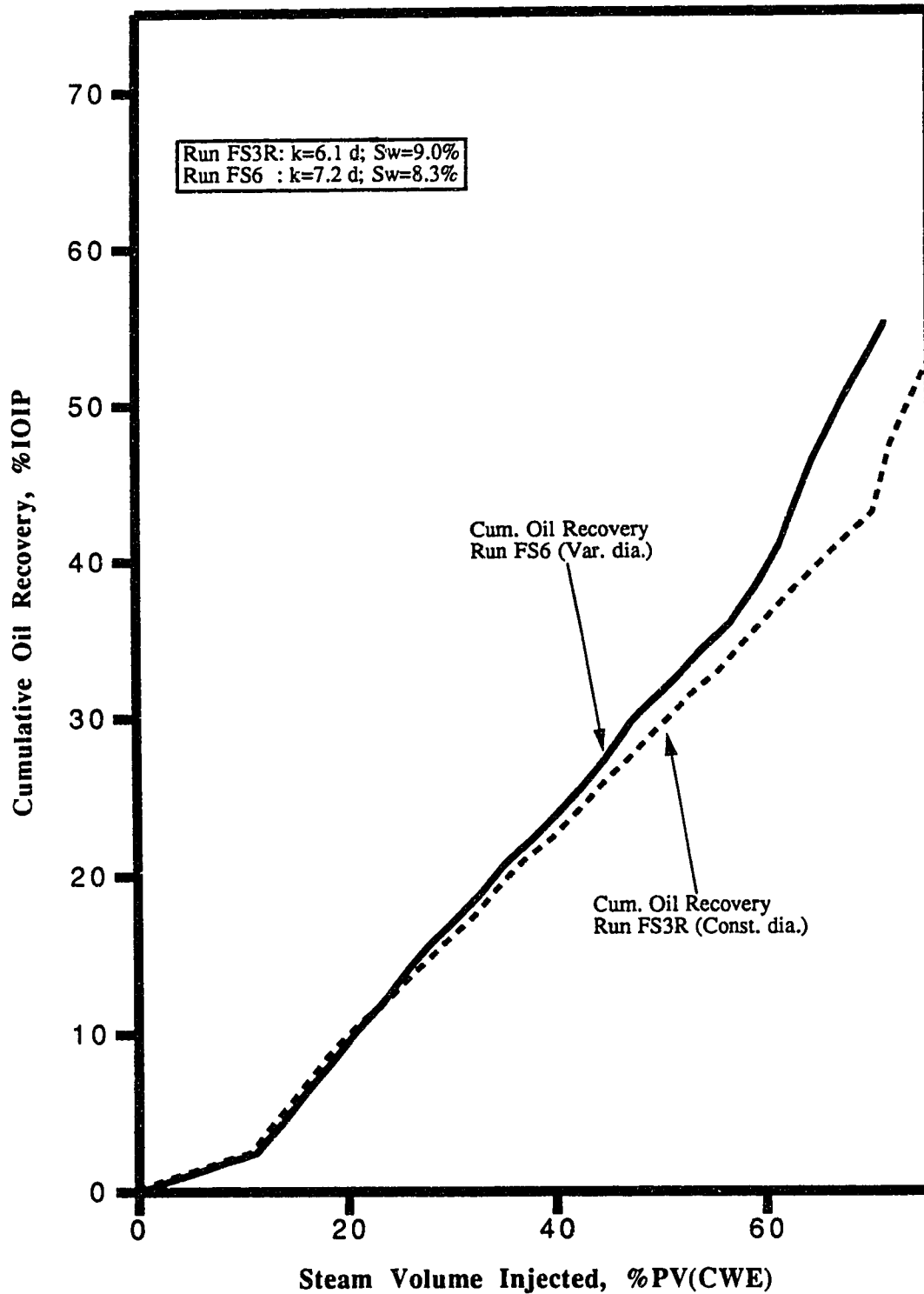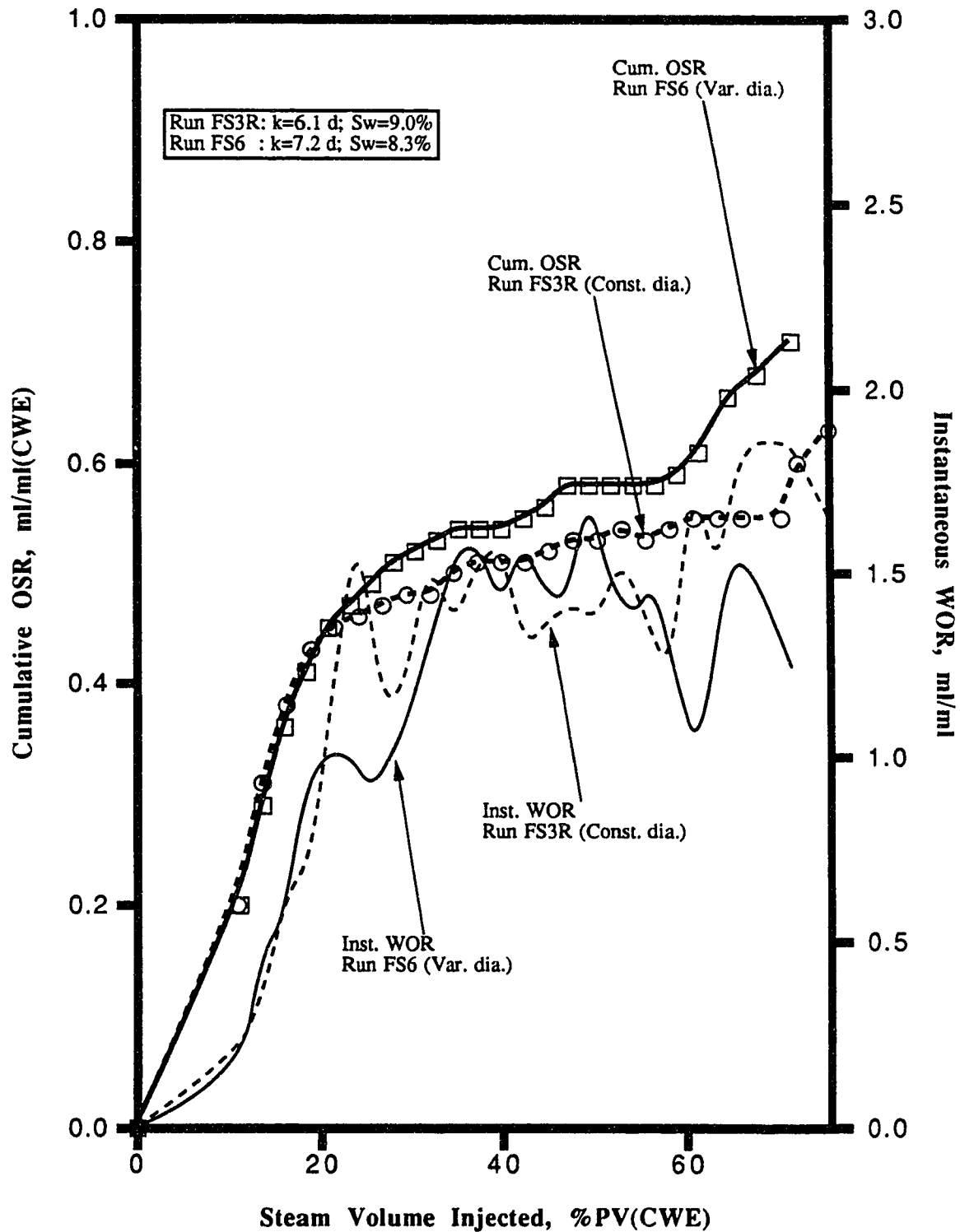Cased Variable Diameter Horizontal Well (Run FS6).
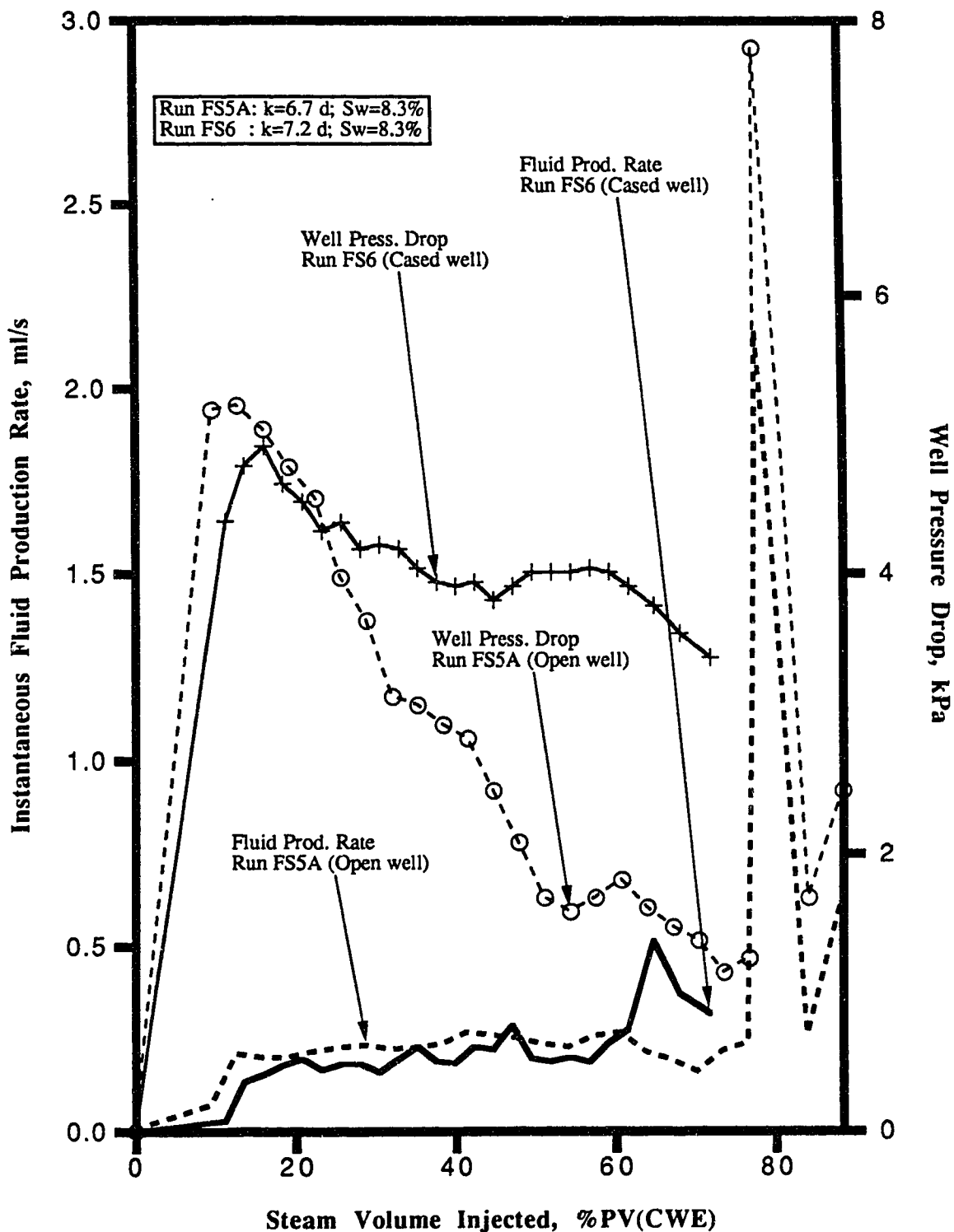
Figure 39: Effect of Perforated Casing on Recovery Performance;
  Cumulative Oil Recovery vs. Steam Volume Injected (Scaled Model Experiments),
  Open Variable Diameter Horizontal Well (Run FS5A) vs.
  Cased Variable Diameter Horizontal Well (Run FS6).

Run FS5A: k=6.7 d; Sw=8.3%
Run FS6 : k=7.2 d; Sw=8.3%

Cum. Oil Recovery
Run FS5A (Open well)

Cum. Oil Recovery
Run FS6 (Cased well)
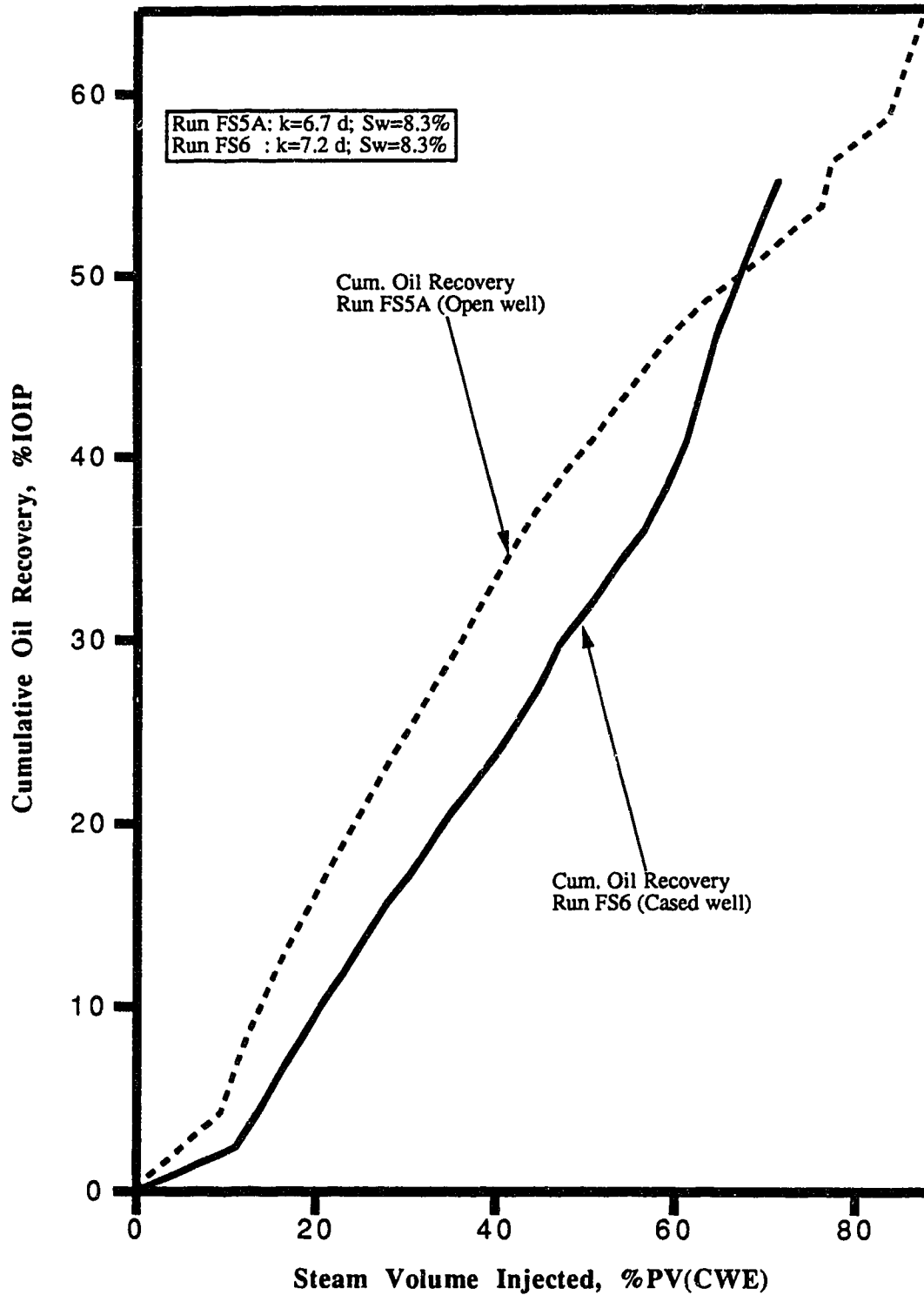
40 show that the effect of perforated casing (tapered in this case) on the recovery performance of a variable diameter horizontal producer also mirrored that of a constant diameter horizontal well: lower cumulative oil recovery and cumulative OSR when the casing was present.

Observing the temperature profiles of the sand pack after the injection of different volumes of superheated steam for these two experiments (Figures 41 and 42), it can be seen that the effect of the perforated casing in this case followed closely those observed when a constant diameter horizontal well was used: the casing seemed to slow down the expansion rate of the steam zone in the initial period of production, and accelerated the growth of the steam zone during the later stage of the recovery process. As for the case of the constant diameter horizontal well, the production thermocouple temperature reading in the later period of the recovery process was higher when the casing was present (65°C for Run FS6, as opposed to 52°C for Run FS5A). This showed that steam had broken through in the annulus between the variable diameter horizontal well and its tapered casing. Again, the effect of steam override was observed more clearly for the experiment utilizing the cased horizontal producer (Run FS6).

Summarizing, it can be concluded that a perforated casing decreased the production performance of a horizontal well. In most instances, it led to lower fluid production rate, cumulative oil recovery, and cumulative OSR. Its achievement of lower well pressure loss was due mostly to the impediment to the inflow of reservoir fluids into the horizontal well.

6.7 Reproducibility of Experimental Results

An important aspect of the experimental part of this physical modelling study concerns the reproducibility of the experimental results — considering the relatively small number of experiments conducted, and the many parameters involved in the recovery process. It is believed that the reproducibility of the results was good, based upon the consistent trends observed. Additionally, portions of certain runs could be evaluated for repeatability.

Repeatability of the runs was examined further by conducting Run FS5R, to check the reproducibility of the results obtained for Run FS5A, which utilized a variable diameter horizontal producer with no casing. Table E18 contains the results of this experiment. These two experiments, except for small differences in the production pressure at different stages of the recovery process, had identical operating conditions (e.g. same steam injection pressure and temperature). The average steam injection rate for this experiment was 0.143 ml/s (CWE), as opposed to 0.166 ml/s (CWE) for Run FS5A. Furthermore, the total volume of steam injected into the model reservoir for Run FS5R was 1.06 PV, compared to 0.88 PV for Run FS5A. The instantaneous fluid production rate, instantaneous WOR, cumulative oil recovery, and cumulative OSR for these two experiments are plotted in Figures 43 to 46.

Figure 40: Effect of Perforated Casing on Recovery Performance;
Cumulative OSR and Instantaneous WOR vs. Steam Volume Injected
(Scaled Model Experiments),
Open Variable Diameter Horizontal Well (Run FS5A) vs.
Cased Variable Diameter Horizontal Well (Run FS6).
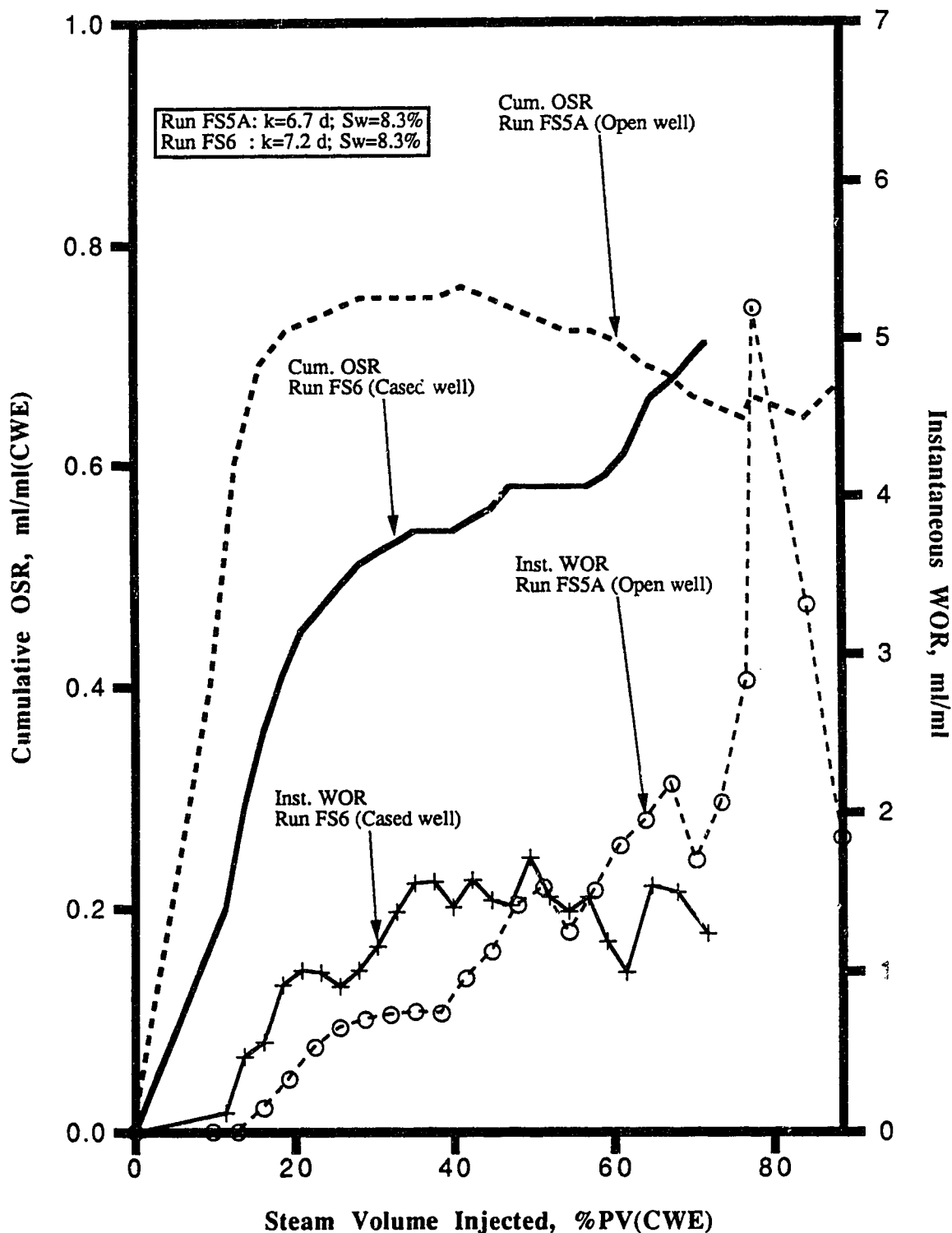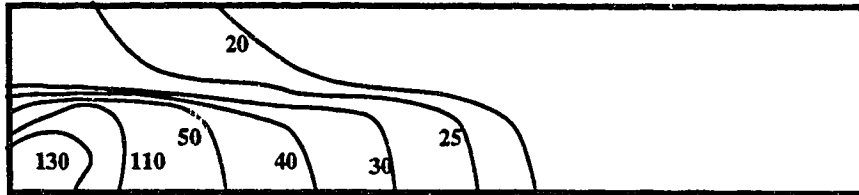
a) 0.10 PV of superheated steam injected.
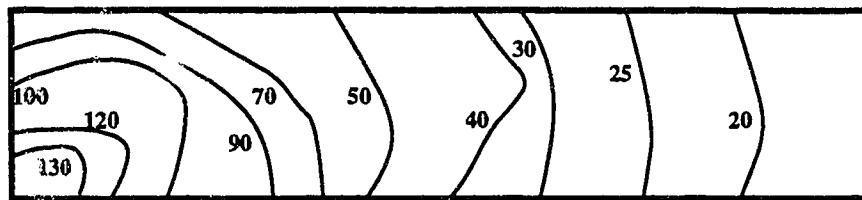
b) 0.25 PV of superheated steam injected.
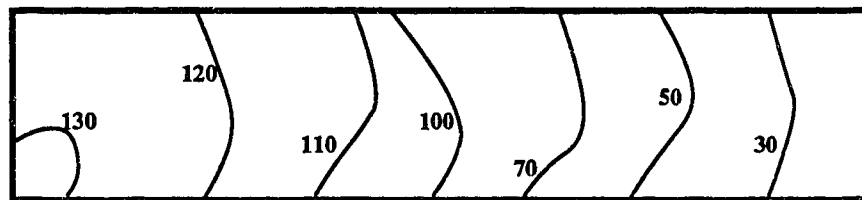
c) 0.50 PV of superheated steam injected.
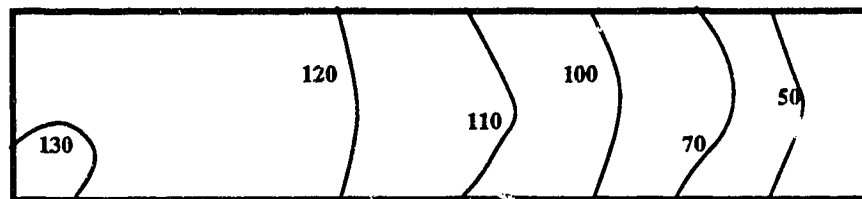
d) 0.75 PV of superheated steam injected.

Figure 41: Temperature (°C) profiles of the sand pack after the injection of 0.10 (a), 0.25 (b), 0.50 (c), and 0.75 (d) PV of superheated steam. Variable diameter horizontal producer case (Run FS5A).
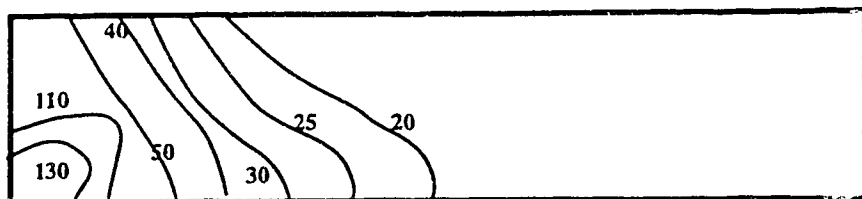
a) 0.10 PV of superheated steam injected.
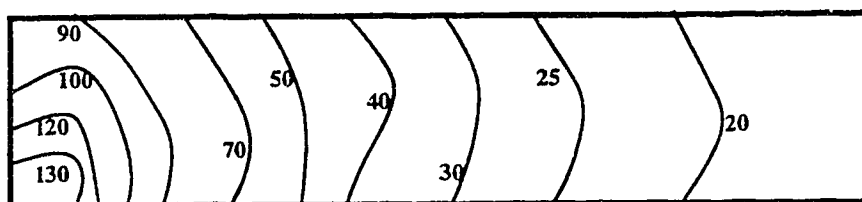
b) 0.25 PV of superheated steam injected.
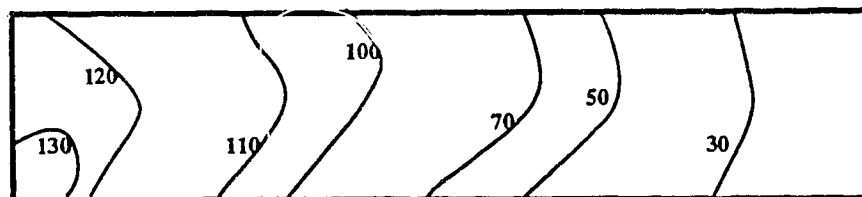
c) 0.50 PV of superheated steam injected.
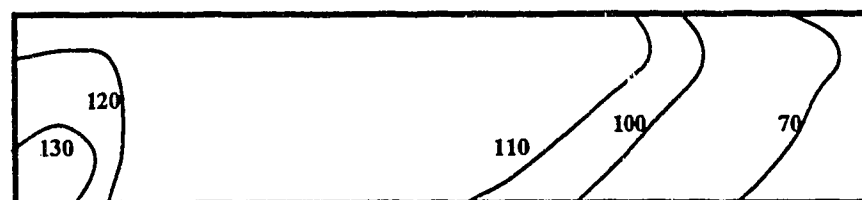
d) 0.75 PV of superheated steam injected.

Figure 42: Temperature (°C) profiles of the sand pack after the injection of 0.10 (a), 0.25 (b), 0.50 (c), and 0.75 (d) PV of superheated steam. Variable diameter horizontal producer case with casing (Run FS6).

Figures 43 and 44 show that, in general, the reproducibility of the instantaneous fluid production rate and instantaneous WOR was good. It is believed that the discrepancy in the two curves in the later part of the runs was due to the slight difference in the production pressure profiles. The use of a back pressure regulator (BPR) to control the production pressure of the experiments had several advantages and disadvantages. The main advantage is the ability to set, vary and/or maintain a nominal fluid production pressure, and hence the driving force for the steam displacement process and the duration of the experiment prior to steam breakthrough at the producer. Other types of pressure regulators are not as capable of handling these requirements as a back pressure regulator. This is not to suggest that a back pressure regulator is perfect for the experimental requirements of this study.

The biggest disadvantages of a back pressure regulator are – due to its nature, design and construction – its inability to handle multiphase flow and the non-instantaneous response. Basically, a back pressure regulator consists of a piston pushing down on a "seat" which covers a "release opening". The piston is, in turn, pushed on from above by a spring or gas dome. The pressure exerted on the piston by the spring or gas dome is set to the desired production pressure. Incoming fluids, if at a pressure less than the production pressure, will not be produced through the release opening and instead will accumulate inside the regulator. When the pressure becomes greater than the pre-set production pressure, the piston will be pushed upward and in the process lift the seat and allow the release of these fluids through the opening. Steam, because of its large compressibility and low viscosity (leading to greater conformance), will take longer to exceed the production pressure, but will also exit the back pressure regulator at a much higher velocity. Heated oil and steam condensate, on the other hand, will take some time to be released. For this reason, the back pressure regulator will not work well in the presence of multiphase flow (i.e. the release rate will fluctuate significantly, resulting in the need to adjust continually the production pressure). In addition, the response of the back pressure regulator is neither easily nor readily quantifiable. A small rotation of the regulating knob can lead to a large change in the reading of the pressure gauge.

Combining the above discussion about the limitations of experimental apparatus and previous discussion (Sections 6.2, 6.3, and 6.5) regarding the influence of the production back pressure on the expansion of the steam zone, fluid production rate, and instantaneous WOR for the production samples it can be concluded that, overall, the reproducibility of the results for these two recovery performance indicators was good, and the small discrepancies in the results were due mostly to the limitations of the back pressure regulator.

Figures 45 and 46 compare the cumulative oil recovery and cumulative OSR for the two experiments. It can be seen that in both cases, the results for Run FS5A were reproduced in Run FS5R. Not

Figure 43: Reproducibility of Experimental Results (Scaled Physical Model),
Instantaneous Fluid Production Rate vs. Steam Volume Injected,
Run FS5A (Variable Diameter Horizontal Producer with No Casing) vs.
Run FS5R (Variable Diameter Horizontal Producer with No Casing).
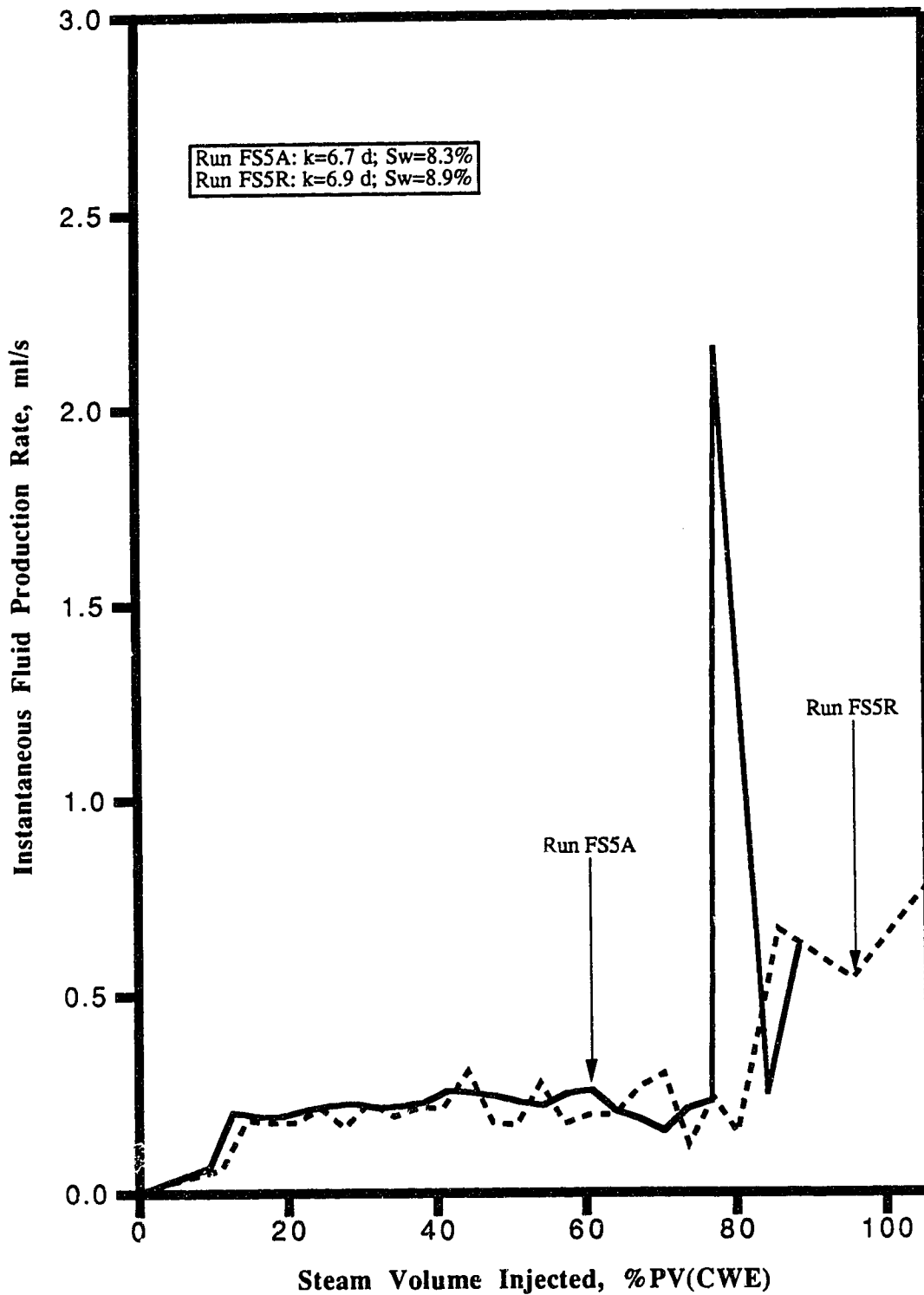
Figure 44: Reproducibility of Experimental Results ,
Instantaneous WOR vs. Steam Volume Injected (Scaled Physical Model),
Run FS5A (Variable Diameter Horizontal Producer with No Casing) vs.
Run FS5R (Variable Diameter Horizontal Producer with No Casing).
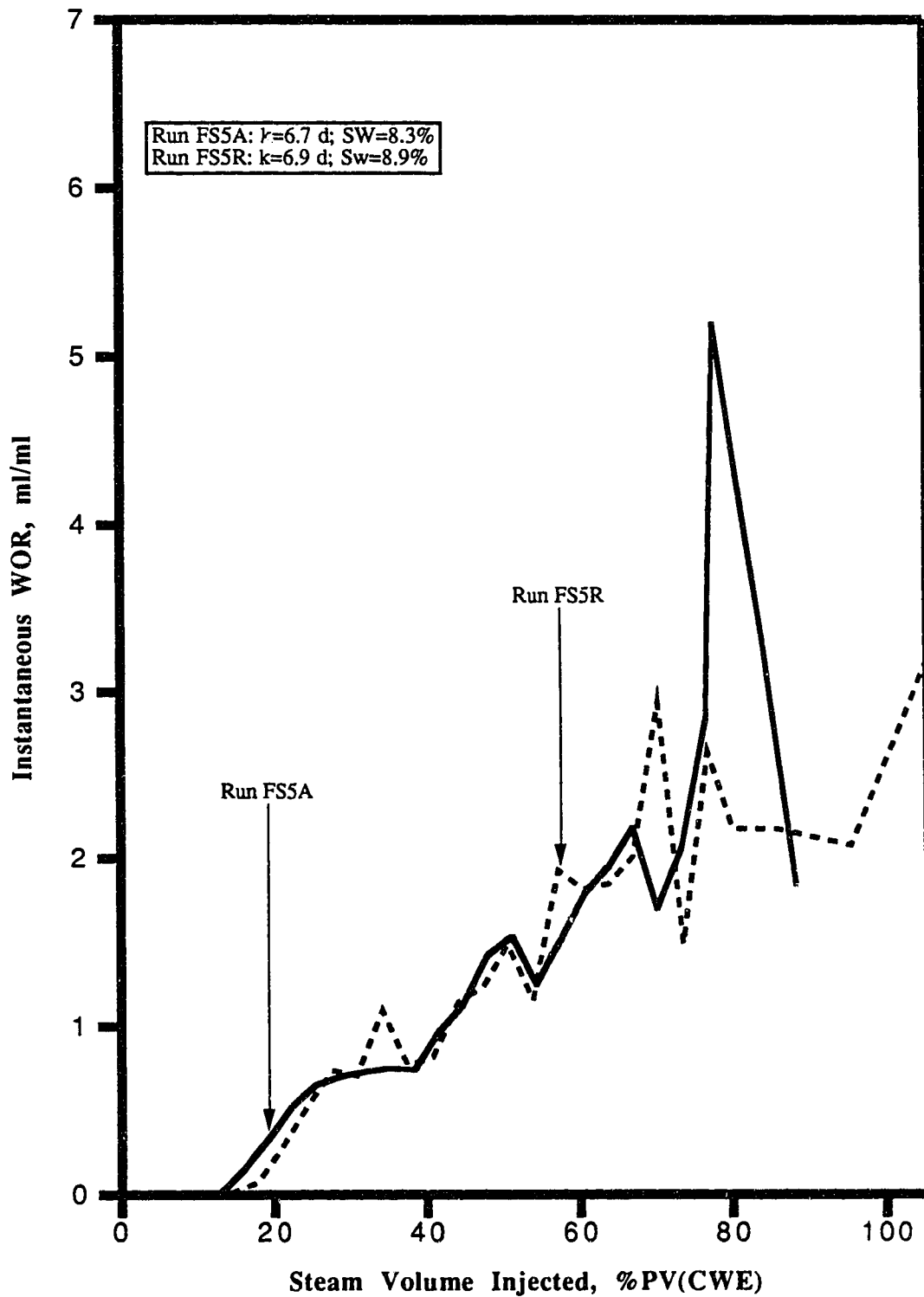
Figure 45: Reproducibility of Experimental Results,
   Cumulative Oil Recovery vs. Steam Volume Injected (Scaled Physical Model),
   Run FS5A (Variable Diameter Horizontal Producer with No Casing) vs.
   Run FS5R (Variable Diameter Horizontal Producer with No Casing).
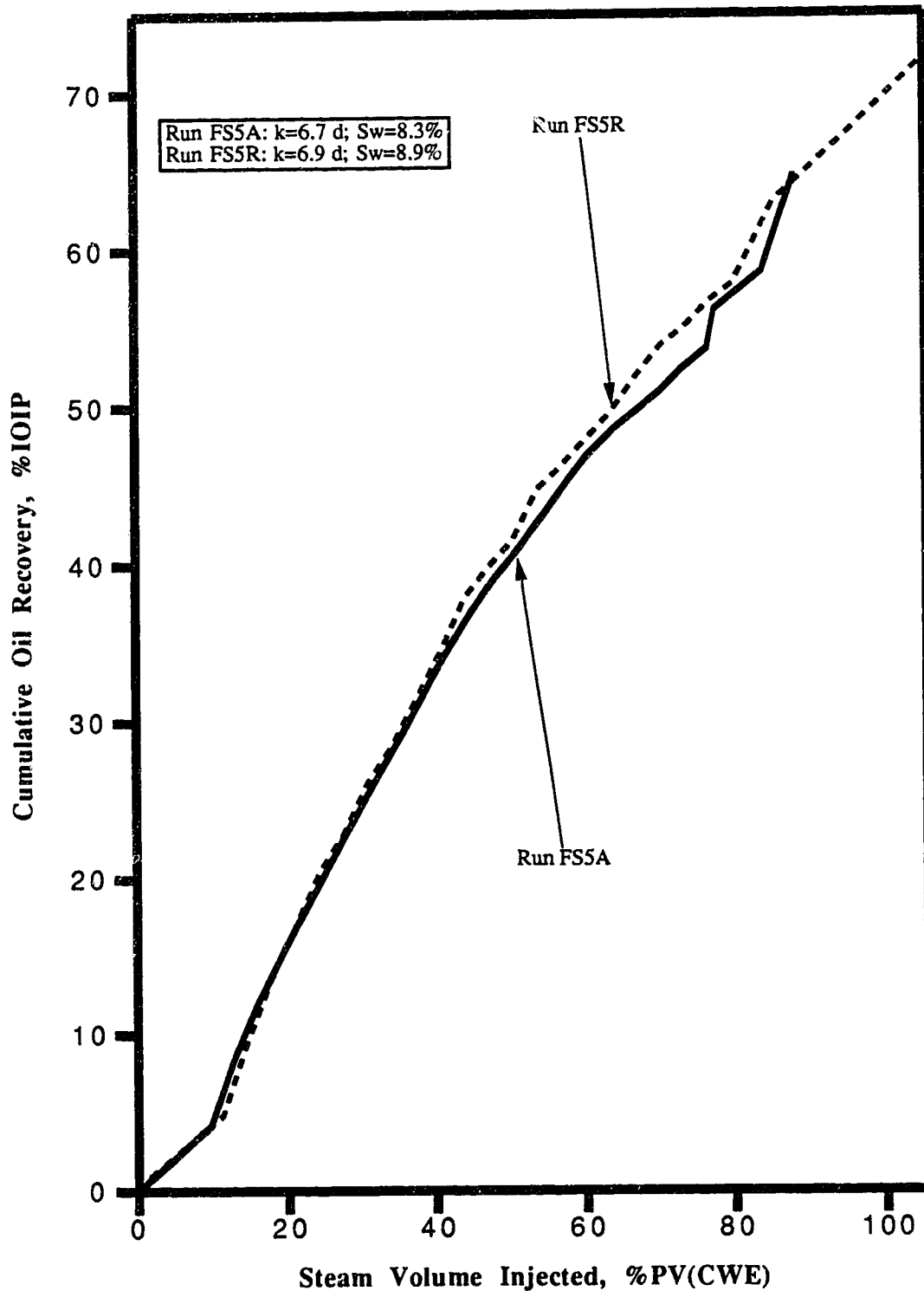
Figure 46: Reproducibility of Experimental Results,
Cumulative OSR vs. Steam Volume Injected (Scaled Physical Model),
Run FS5A (Variable Diameter Horizontal Producer with No Casing) vs.
Run FS5R (Variable Diameter Horizontal Producer with No Casing).

Run FS5A: k=6.7 d; Sw=8.3%
Run FS5R: k=6.9 d; Sw=8.9%

Run FS5R

Run FS5A

Cumulative OSR, ml/ml(CWE)

Steam Volume Injected, %PV(CWE)
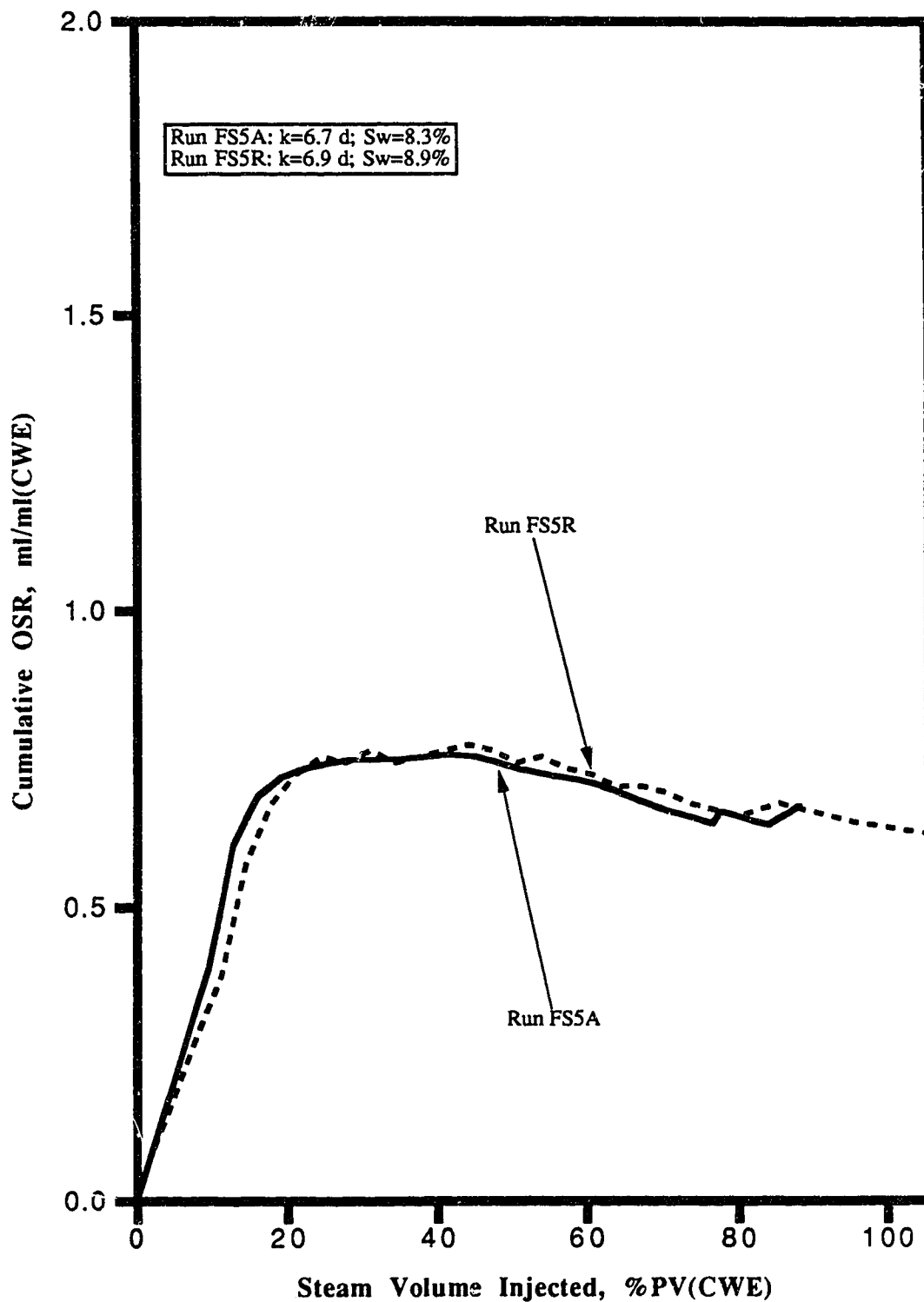
only were the trends the same for the recovery process, but in many instances the magnitudes were identical. An explanation for the excellent reproducibility of the results for these two recovery performance parameters, as compared to that for the two previous parameters, is that these parameters were averaged quantities and were thus not greatly affected by the limitations of the back pressure regulator. They were determined exclusively by the volume of produced fluids collected, and steam injected for a set period of time. As such, the effect of the fluctuations in the production rate was damped out.

In conclusion, the reproducibility of results for the experiments carried out was good, given the limitations of the experimental apparatus.

6.8 Implications of the Experimental Results for the Prototype

One of the important questions arising from this study is with regard to the implications of experimental results, i.e. can these laboratory results be used to predict the behaviour of the prototype reservoir ? After all, the underlying purpose of a scaled model study is not just to scale down field processes to laboratory conditions, but also to scale up laboratory results to predict the actual performance of the prototype. Furthermore, if the laboratory results can be used to predict the recovery performance of the prototype, how reliable and accurate would this prediction be ?

6.8.1 Scaling Up the Laboratory Results

Recalling the scaling groups derived in Chapter 4, and how some of these scaling groups were used to design the physical model, and determine various parameters for the experiments in Chapter 5, it can be seen that the groups $\frac{q_{oR}^{*} H^2 \mu_{oR}}{4 P_{oR} k k_{roR} P_{oR}}$ and $\frac{\phi_R S_{oR} H^2 \mu_{oR}}{4 k k_{roR} P_{oR} t_R}$ can be used to scale up laboratory oil production rate, and predict an oil production rate vs. time profile for the prototype reservoir. Keeping in mind that the prototype horizontal well was of the conventional, constant diameter type, it is appropriate to scale up the results of Run FS2R (Table E12) to predict the recovery performance of the prototype reservoir. The followings provide an illustration of the calculation procedure employed to scale up laboratory oil production rate to field scale. Production sample No. 3 of Run FS2R is selected. The oil production volume for this sample was 56.2 ml over 6 minutes. Hence, the laboratory volumetric oil production rate was:

$$\left(q_{or}^{*}\right)_M = \frac{56.2 \times 10^{-6}\ m^3}{6 \cdot 60\ s} = 15.6 \times 10^{-8}\ m^3/s \quad .$$

Since $\left(\rho_{oR}\right)_M$ =879.9 kg/m^3, then the oil production rate, on a mass basis, is:

$$\left(q_{or}^{*}\right)_M = 15.6 \times 10^{-8}\ \frac{m^3}{s} \cdot 879.9\ \frac{kg}{m^3} = 13.73 \times 10^{-5}\ kg/s \quad .$$

Now,

$$\left[\frac{q_{oR}^{*}H^2\mu_{oR}}{4\rho_{oR}kk_{roR}P_{oR}}\right]_F = \left[\frac{q_{oR}^{*}H^2\mu_{oR}}{4\rho_{oR}kk_{roR}P_{oR}}\right]_M \quad ,$$

thus,

$$\left(q_{oR}^{*}\right)_F = \frac{\left(q_{oR}^{*}H^2\mu_{oR}\right)_M}{\left(H^2\mu_{oR}\right)_F} \cdot \frac{\left(\rho_{oR}kk_{roR}P_{oR}\right)_F}{\left(\rho_{oR}kk_{roR}P_{oR}\right)_M} \quad .$$

Given that the steam injection pressure for the prototype reservoir is 7 MPa, and that the viscosity-temperature function for the prototype oil can be approximated by $\left(\mu_{oR}\right)_F = 0.0001002e^{\left(5130.3/T^{*}\right)}$, then the steam temperature at the steam-bitumen interface is $T_S = 179.81(7)^{0.2376} = 285.5$ °C, and the viscosity of the mobilized oil is $\left(\mu_{oR}\right)_F = 0.0001002e^{\left(5130.3/(273.1+285.5)\right)} = 0.979$ $mPa.s$.

Substituting these values into the above equation for $\left(q_{oR}^{*}\right)_F$, and knowing that $\left(\rho_{oR}\right)_F$=993 kg/m^3, $\left(\rho_{oR}\right)_M$=879.9 kg/m^3, $\left(P_{oR}\right)_F$ =2.0 MPa (field pressure drawdown), $\left(P_{oR}\right)_M$ =0.2 MPa (laboratory pressure drawdown), and $\left(\mu_{oR}\right)_M \approx 12$ $mPa.s$ @ 130°C (steam temperature in the experiments) led to:

$$\left(q_{oR}^{*}\right)_F = \frac{(13.73\text{x}10^{-5}\ kg/s)(0.1\ m)^2(12\ mPa.s)}{(18\ m)^2(0.979\ mPa.s)} \cdot \frac{(993\ kg/m^3)(4.0\ darcies)(2.0\ MPa)}{(879.9\ kg/m^3)(5.0\ darcies)(0.2\ MPa)}$$

$$= 4.69\text{x}10^{-7}\ kg/s \quad ,$$

but this is the oil production rate per unit pore volume, and hence the total oil production rate for the prototype reservoir is:

$$\left(q_{oR}^{*}\right)_F = (4.69\text{x}10^{-7}\ kg/s.m^3) \cdot (0.5 \cdot 5.0\text{x}10^4\ m^2 \cdot 18\ m \cdot 0.325)$$

$$= 0.0686\ kg/s = 5926.3\ kg/day = 5.97\ m^3/day = 37.5\ bpd \quad .$$

The field water production rate could be determined by using the group $\left[\frac{q_{wR}^{*}}{q_{oR}^{*}}\right]$ to scale up the laboratory water production rate. However, keeping in mind the previous discussion regarding the influence of the back production pressure on water production and instantaneous WOR's in the experiments (Sections 6.2 and 6.5.1.1), water production and WOR for the prototype reservoir based on the laboratory data may be unreliable, unless analogous back pressures are maintained in the prototype also.

The total volume of superheated steam injected into the sand pack for sample No. 3 was 0.12 its pore volume (PV). This same volume of steam in field scale will be:

$$(0.12\ PV)_F = 0.12 \cdot 0.5(5.0\text{x}10^4\ m^2 \cdot 18\ m \cdot 0.325) = 17550\ m^3 \quad .$$

Given that the average steam injection rate for the prototype was 100 m^3/day (CWE), then the actual time it took to inject this volume is:

$$(time)_F = \frac{17550 \ m^3}{100 \ m^3/day} = 176 \ days \quad .$$

Table 12 contains the scaled up time and oil production rate for the prototype reservoir, and these are displayed graphically in Figure 47.

6.8.2 Implications of Laboratory Results for the Prototype Reservoir

The previous section illustrated the calculation procedure used to predict oil production rate as a function of time for the prototype reservoir. But how reliable is this prediction ? It is believed that this prediction should provide an estimate for predicting the actual production of the prototype reservoir, if the boundary conditions and the well operating conditions of the prototype are scaled to the laboratory experiments. Several observations in this regard are in order.

First, the fluid production rates (both oil and water) in the experiments were directly controlled by the back pressure at the production end. There are advantages and disadvantages of using back pressure to control the production. The main advantages include a slow and uniform expansion of the steam zone which led to a delay in the steam breakthrough at the producer, high sweep efficiency, and high thermal efficiency for the recovery process (as evidenced by the high cumulative OSR). The confined geometry of the physical model also contributed significantly to the high thermal efficiency obtained in the experiments — mainly by inhibiting steam dispersion in the lateral direction, and reducing steam override and gravity segregation. More will be discussed about the effect of the geometry in the following paragraphs.

The chief disadvantage of using back pressure to control fluid production is the relatively low fluid production rate, which is a direct result of the slow expansion of the steam zone. In the field, quite often out of the economic necessity to generate a high cash flow, it is not always possible or practical to slow down the expansion rate of the steam zone to obtain high (close to perfect) sweep efficiency for a given well spacing. More likely, efforts are required to promote and accelerate the steam zone expansion. Furthermore, due to the large physical extent of the prototype reservoir, the use of back pressure to control fluid production and sweep performance would, most likely, not have the same level of success as that achieved in the confined, cylindrical physical model. Steam dispersion effect, along with steam override would certainly be more pronounced under field conditions, and they would lead to a lower thermal efficiency for field processes. Again, it is believed that if the boundary conditions are scaled, the model results will indeed reflect the prototype performance.

Second, the sand packs used in the experiments were homogeneous and isotropic. As such, the steam zone was able to expand uniformly in the model reservoir, leading to high steam sweep efficiency. Shale barriers and/or vertical/horizontal fractures in the prototype reservoir, if present, could either inhibit or promote the expansion of the steam zone, which in turn will influence the oil production

Table 12: Field Prediction of Oil Production Rate.

Field Time days	Oil Production Rate m3/day	Oil Production Rate _pd
134.6	2.22	14.00
175.5	7.09	44.50
216.5	5.97	37.50
255.9	5.26	33.00
296.9	5.09	32.00
337.8	4.30	27.00
378.8	3.4	21.80
418.3	3.6s	23.10
459.2	3.65	23.00
500.2	2.97	18.70
539.7	4.06	25.50
580.6	2.83	17.70
621.6	3.75	23.60
661.1	3.46	21.80
702.0	2.56	16.10
743.0	2.85	17.90
783.9	5.04	31.60
823.4	2.43	15.30
864.3	1.85	11.60
905.3	2.05	12.90
944.8	3.37	21.20
985.7	3.74	23.50
1094.0	1.71	10.70
1107.1	24.67	154.90
1212.4	1.37	8.60

Figure 47. Prediction of Oil Production Rate for the Prototype Reservoir, Constant Diameter Horizontal Well with No Perforated Casing.
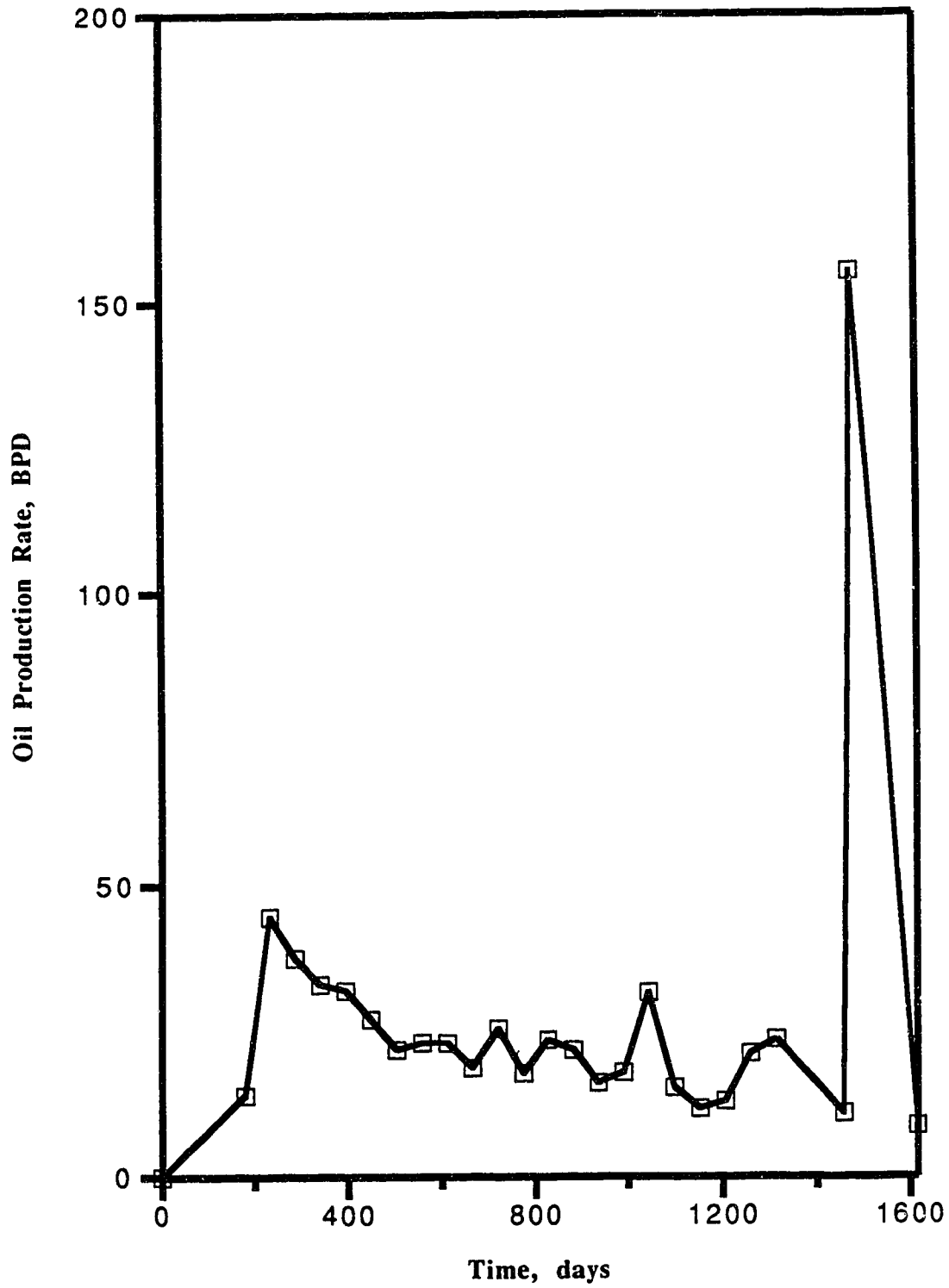
rate, cumulative oil recovery, instantaneous WOR, cumulative OSR, and the pressure drop across the horizontal producer. In this sense, this or any other physical model (or numerical simulation), will be rather limited in forecasting the prototype recovery performance.

Third, in this experiment (Run FS2R) the constant diameter horizontal producer – to prevent sand plugging – was encased in a sintered tube with a permeability ($\approx$ 20 darcies) much higher than that of the porous pack ($\approx$ 5 darcies). As a result of this "negative skin", it is suspected that the inflow of reservoir fluids (oil and water) from the pack into the model horizontal producer was hindered less than would have been the case if the skin factor was positive — as is often the case in the field. Hence, the scaled up oil production rate could prove to be high.

Last, the inflow and flow inside the horizontal well was assumed to be single-phase. As observed and discussed previously (Sections 6.2, 6.3, 6.5, and 6.7), this assumption worked fairly well during the initial stage of the recovery process when most of the produced fluids consisted of cold, viscous oil. As multiphase flow (oil, steam condensate, and steam) started to develop, the correlation between the fluid production rate and the production back pressure became less precise. As such, the predicted oil production rate for the prototype reservoir in the later periods of its life will not be truly indicative of the actual prototype performance.

Summarizing, the present scaling groups can be used to scale up laboratory results and predict the performance of the prototype reservoir. However, due to differences in the geometry and the production strategy between the physical model and the prototype reservoir the scaled up laboratory results could prove to be either optimistic or pessimistic, and as such, should only be used to provide an estimate of the prototype reservoir production.

7. SUMMARY AND CONCLUSIONS

Equations were developed to model flow in the vicinity of, and inside a horizontal wellbore. Scaling criteria were then derived from these equations to determine the scaling requirements for these two flow processes. The criteria were used in the design and construction of high-pressure, linear physical models, as well as in the operation of different steam injection experiments in these models. A variety of experiments were carried out in two physical models: partially scaled and scaled, designed to determine experimentally the effect of the inside-wellbore geometry of a horizontal producer, as well as the role played by perforated casing on oil recovery performance. In addition, the production performances of different combinations of injector and producer were established to permit an evaluation of the effectiveness of a horizontal steam injector.

The following conclusions are reached on the basis of the experimental observations:

1) It is important in the development of the scaling criteria to treat the flow inside the horizontal well separately from the reservoir flow process. An improved criterion was developed in this work, which helped to ensure that the model horizontal well was scaled down properly, according to the requirements resulting from its own flow process. Two scaling groups are derived to determine the size of the model horizontal well: the first scaling group scales the well radius according to the inflow requirement, and the other group scales its radius according to the pressure drop across it.

2) There is a correlation between the experimental fluid production rate of a horizontal well and the pressure drop across it. This correlation was predicted by one of the scaling groups for the horizontal well, involving the flow velocity inside the well, the length of flow path, the viscosity of the flowing fluid, and the cross-sectional area of the wellbore. This is true for both constant and variable diameter horizontal wells.

3) There is a direct experimental correlation between the production rate of a horizontal well and the production pressure in early production period, when the flow inside the horizontal well is single-phase. The back pressure at the production end controlled the rate of growth of the steam zone, which in turn determined how much oil was mobilized, and how fast it was drawn into, and produced through the horizontal well. Overall, a high back pressure led to a low fluid production rate.

4) The pressure drop across a horizontal well can be large, especially in the initial production period due to the high oil viscosity and the predominance of hot waterflooding, resulting from steam condensation.

5) The internal wellbore geometry of a horizontal producer can have a significant effect on the recovery performance. The experimental results of the *scaled model* runs generally agreed with those of the *partially scaled model* — even though it was found that the improved oil recovery due

to the use of a variable diameter horizontal well was greater for runs in the *partially scaled model* (8-10%) than for runs in the *scaled model* (3-5%). The variable diameter (small at the inlet end, larger at the outlet end) horizontal wells used in the experiments consistently outperformed the constant-diameter wells. They appear to reduce the pressure drop across the well and lead to higher fluid production rates, cumulative recovery, and thermal efficiency.

6) Perforated casing can restrict the flow of reservoir fluids into a horizontal producer, and lower its recovery performance. In most of the cases studied, a well encased in a perforated casing recovered less oil (6-10% range in both the *partially scaled and scaled* models), had a lower fluid production rate and cumulative OSR than an open, uncased well.

8. RECOMMENDATIONS FOR FURTHER RESEARCH

Based on the results of this study, the following recommendations are offered to extend the scope of the research, as well as to improve the overall quality of the work for the next phase of the research project.

1) Multiphase flow model should be incorporated into the mathematical equations simulating the inflow between the reservoir and the horizontal well, and inside the horizontal well. The scaling criteria for inside-well flow developed from the model presented in this study were for single-phase flow only, and as such, cannot properly scale and predict multiphase flow phenomena such as liquid holdup, and the different flow regimes that could play a role in the production capability of a horizontal producer in the field.

2) Regarding the lack of correlation between the production pressure and the instantaneous fluid production rate of a horizontal producer when there is multiphase flow inside the well, a phase separator could be incorporated into the production sub-system (i.e. tied in to the production back pressure regulator, BPR) to provide instantaneous response of multiphase fluid production rates vis-à-vis the changes in the production pressure, and lead to improved correlation between these two parameters during the recovery process. In addition, this would also allow a more relevant comparison of the recovery performance of different types of wells and recovery strategies based upon the instantaneous WOR.

3) Regarding the potential problems associated with using an average steam injection rate in the experiments, multiple collecting vessels can be used to collect the volume of steam condensate bypass for different periods of an experiment. This would permit the determination of an instantaneous steam injection rate at different times during the experiment — leading to a more accurate correlation between the steam injection rate and various recovery performance variables. Unless such a system is automated it would be very labour-intensive.

4) A method should be devised to determine qualitatively the skin effect due to the perforated casing used in various experiments in this study. As such, a better prediction of the performance of prototype cased horizontal producers can be made.

5) Regarding the relatively poor recovery performance for the combination of a horizontal injector and a horizontal producer, a better strategy of testing the recovery performance would be to move the wells further down inside the sand pack. This would allow the injected steam to sweep a larger area of the reservoir model, without having it break through into the horizontal producer early. This type of modification to the physical setup could also be done for other experiments involving a single horizontal well.

6) Experiments using more viscous oils should be carried out.

7) Other recovery strategies and processes, such as injecting steam with a gas or solvent slug, or any type of steam additive, should be tested. This will establish a wider range of recovery efficiencies for different processes for the physical model, as well as serve as a test for possible recovery strategies for the prototype.

8) The length and size of the horizontal wells could be varied to determine the effect on oil recovery strategy. As well, these could serve as the basis for some new production strategy which could prove practical for field application.

146

REFERENCES

1) Anonymous:"Horizontal Drilling – A Means for Greater Oil Recovery", *The Petroleum Engineer*, October 1945, pp. 196 – 208.

2) Hyland, C.R.:"Drain Hole Drilling - An Old Idea Whose Time is Now", paper SPE 12792, presented at the 1984 California Regional Meeting, Long Beach, CA April 11-13, 1984.

3) Harding, T.G. and Farouq Ali, S.M.:"Mine-Assisted Heavy Oil Recovery Technology", paper SPE 12787, presented at the 1984 California Regional Meeting, Long Beach, CA April 11-13, 1984.

4) Haston, J., O'Rourke, J., Kovalsky, J., Luhning, R., Greenwell, J., and Bohme, C.:"AOSTRA Underground Test Facility: Mining Access for Research and Production", paper no. 126, proceedings of the Fourth UNITAR/UNDP Conference on Heavy Crude and Tar Sands, Edmonton, Alberta,August 7-12, 1988.

5) Pendleton, L. and Ramesh, A.B.:"Bechtel Develops Innovative Method for Horizontal Drilling", *Oil & Gas Journal*, May 27 1985, pp.95 – 99.

6) Dickinson, W. and Dickinson, R.W.:"Horizontal Radial Drilling System", paper SPE 13949, presented at the 1985 California Regional Meeting, Bakersfield, California, March 27-29, 1985.

7) Dech, J.A., Hearn, D.D., Schuh, F.J., and Lenhart, B.:"New Tools Allow Medium-Radius Horizontal Drilling", *Oil & Gas Journal*, July 14 1986, pp. 95 – 99.

8) Prevedel, B.:"New Techniques in Horizontal and Drainhole Drilling Optimization: Lehrte 41 Lateral Drilling Project", paper SPE 15694, presented at the Fifth SPE Middle East Oil Show, Manama, Bahrain, March 7-10, 1987.

9) Joshi, S.D.:"A Review of Horizontal Well and Drainhole Technology", paper SPE 16868, presented at the 62nd Annual Technical Conference and Exhibition of the Society of Petroleum Engineers, Dallas, Texas, September 27-30, 1987.

10) Bardin, C.A.:"Remote-controlled Bent Sub Aids Directional Drilling by Allowing Bent-angle Change", *Oil & Gas Journal*, January 30 1989, pp. 76 – 80.

11) Karlsson, H., Cobbley, R., and Jacques, G.E.:"New Developments in Short-, Medium-, and Long-radius Lateral Drilling", paper SPE 18706, presented at the 1989 SPE/IADC Drilling Conference, New Orleans, Louisiana, February 28 - March 3, 1989.

12) Giannesi, F. and Bosio, J.:"Horizontal Wells Cut Offshore Production Costs", paper SPE 17656/OSEA 88127, presented at the 7th Offshore South East Asia Conference, Singapore, February 2-5, 1988.

13) Dorel, M.:"Horizontal Drilling Methods Proven in Three Test Wells", *World Oil*, May 1983, pp.

127 – 135.

14) Spreux, A., Georges, C., and Lessi. J.:"Most Problems in Horizontal Completions Are Resolved", *Oil & Gas Journal*, June 13 1988, pp. 48 – 52.

15) Dickinson, W., Anderson, R.R., Dickinson, W., and Dykstra, H.:"Gravel Packing of Horizontal Wells", paper SPE 16931, presented at the 62nd Annual Technical Conference and Exhibition of the Society of Petroleum Engineers, Dallas, Texas, September 27-30, 1987.

16) Zaleski,Jr., T.E. and Spatz, E.:"Horizontal Completions Challenge for Industry", *Oil & Gas Journal*, May 2 1988, pp. 58 –70.

17) Lessi, J. and Spreux, A.:"Completion of Horizontal Drainholes", paper SPE 17572, presented at the SPE International Meeting on Petroleum Engineering, Tianjin, China, November 1-4, 1988.

18) Cooper, R.E. and Troncoso, J.C.:"An Overview of Horizontal Well Completion Technology", paper SPE 17582, presented at the SPE Internal Meeting on Petroleum Engineering, Tianjin, China, November 1-4, 1988.

19) Weirich, J.B., Zaleski,Jr., T.E., and Mulcahy, P.M.:"Perforating the Horizontal Well: Designs and Techniques Prove Successful", paper SPE 16929, presented at the 62nd Annual Technical Conference and Exhibition of the Society of Petroleum Engineers, Dallas, Texas, September 27-30, 1987.

20) Soliman, M., Hunt, J.L., and El Rabaa, W.:"On Fracturing Horizontal Wells", paper SPE 18542, presented at the SPE Eastern Regional Meeting, Charleston, WV, November 1-4, 1988.

21) Economides, M.J. and Nolte, K.G.:*Reservoir Stimulation*, Prentice-Hall, 1989, Chapter 19, pp. 19-1 – 19-28.

22) Wilkirson, J.P., Smith, J.H., Stagg, T.O., and Walters, D.A.:"Horizontal Drilling Techniques at Prudhoe Bay, Alaska", paper SPE 15372, presented at the 61st Annual Technical Conference and Exhibition of the Society of Petroleum Engineers, New Orleans, LA, October 5-8, 1986.

23) MacDonald, R.R.:"Drilling the Cold Lake Horizontal Well Pilot No.2", *SPE Drilling Engineering*, September 1987, pp. 193 – 198.

24) Sheikholeslami, B.A., Schlottman, B.W., Siedel, F.A., and Button, D.M.:"Drilling and Production Aspects of Horizontal Wells in the Austin Chalk", paper SPE 19825, presented at the 64th Annual Technical Conference and Exhibition of the Society of Petroleum Engineers, San Antonio, Texas, October 8-11, 1989.

25) Reiley, R.H., Black, J.W., Stagg, T.O., Walters, D.A., and Atol, G.R.:"Cementing of Liners in Horizontal and High-angle Wells at Prudhoe Bay, Alaska", paper SPE 16682, presented at the 62nd Annual Technical Conference and Exhibition of the Society of Petroleum Engineers, Dallas, Texas, September 27-30, 1987.

26) Ashton, J.P., Liput, J., Lemons, R., and Summerlin, J.:"Gravel Packing Horizontal and Highly Deviated Openhole Completions Using a Single-screen Prepacked Liner in Offshore California Field", paper SPE 19718, presented at the 64th Annual Technical Conference and Exhibition of the Society of Petroleum Engineers, San Antonio, Texas, October 8-11, 1989.

27) Perrine, R.L.:"Well Productivity Increase from Drainholes as Measured by Model Studies", Petroleum Transactions, AIME Vol. 204, 1955, pp. 30 – 34.

28) Borisov, Ju. P.:"Oil Field Production Using Horizontal and Multiple-Deviation Wells", Moskva, Nedra, 1964. Translated into French by Institut Français du Pétrole, August 1980. Translated into English by J. Strauss, Phillips Petroleum Company.

29) Giger, F.M., Reiss, L.H., and Jourdan, A.P.:"The Reservoir Engineering Aspects of Horizontal Drilling", paper SPE 13024, presented at the 59th Annual Technical Conference and Exhibition of the Society of Petroleum Engineers, Houston, Texas, September 16-19, 1984.

30) Giger, F.M.:"Horizontal Wells Production Techniques in Heterogeneous Reservoirs", paper SPE 13710, presented at the SPE 1985 Middle East Oil Technical Conference and Exhibition, Bahrain, March 11-14, 1985.

31) Joshi, S.D.:"Augmentation of Well Productivity Using Slant and Horizontal Wells", paper SPE 15375, presented at the 61st Annual Technical Conference and Exhibition of the Society of Petroleum Engineers, New Orleans, LA, October 5-8, 1986.also Journal of Pet. Tech., June 1988, pp. 729 – 739.

32) Karcher, B.J., Giger, F.M., and Combe, J.:"Some Practical Formulas to Predict Horizontal Well Behavior", paper SPE 15430, presented at the 61st Annual Technical Conference and Exhibition of the Society of Petroleum Engineers, New Orleans, LA, October 5-8, 1986.

33) Plahn, S.V., Startzman, R.A., and Wattenbarger, R.A.:"A Method for Predicting Horizontal Well Performance in Solution-Gas-Drive Reservoirs", paper SPE 16201, presented at the SPE Production Operations Symposium, Oklahoma City, Oklahoma, March 8-10, 1987.

34) Giger, F.:"Low-Permeability Reservoir Development Using Horizontal Wells", paper SPE/DOE 16406, presented at the SPE/DOE Low Permeability Reservoirs Symposium, Denver, Colorado, May 18-19, 1987.

35) Sung, W. and Ertekin, T.:"Performance Comparison of Vertical and Horizontal Hydraulic Fractures and Horizontal Boreholes in Low Permeability Reservoirs: A Numerical Study", paper SPE/DOE 16407, presented at the SPE/DOE Low Permeability Reservoirs Symposium, Denver, Colorado, May 18-19, 1987.

36) Ozkan, E. and Raghavan, R.:"Performance of Horizontal Wells Subject to Bottom Water Drive", paper SPE 18545, presented at the SPE Symposium on Energy, Finance and Taxation Policies,

Washington, DC., September 19-20, 1988.

37) Babu, D.K. and Odeh, A.S.:"Productivity of a Horizontal Well", paper SPE 18298, presented at the 63rd Annual Technical Conference and Exhibition of the Society of Petroleum Engineers, Houston, Texas, October 2-5, 1988. also *SPE Reservoir Engineering*, November 1989, pp. 417 – 421.

38) Mutalik, P.N., Godbole, S.P., and Joshi, S.D.:"Effect of Drainage Area Shapes on the Productivity of Horizontal Wells", paper SPE 18301, presented at the 63rd Annual Technical Conference and Exhibition of the Society of Petroleum Engineers, Houston, Texas, October 2-5, 1988.

39) Mukherjee, H. and Economides, M.J.:"A Parametric Comparison of Horizontal and Vertical Well Performance", paper SPE 18303, presented at the 63rd Annual Technical Conference and Exhibition of the Society of Petroleum Engineers, Houston, Texas, October 2-5, 1988.

40) Joshi, S.D.:"Production Forecasting Methods for Horizontal Wells", paper SPE 17580, presented at the SPE International Meeting on Petroleum Engineering, Tianjin, China, November 1-4, 1988.

41) Van Dijkum, C.E.:"Enhanced Recovery by Horizontal Drainholes", paper SPE 18005, presented at the SPE Middle East Oil Technical Conference and Exhibition, Manama, Bahrain, March 11-14, 1989.

42) Chang, M-M., Tomutsa, L., and Tham, M.K.:"Predicting Horizontal/Slanted Well Production by Mathematical Modelling", paper SPE 18854, presented at the SPE Production Operations Symposium, Oklahoma City, Oklahoma, March 13-14, 1989.

43) Bendakhlia, H. and Aziz, K.:"Inflow Performance Relationships for Solution-Gas Drive Horizontal Wells", paper SPE 19823, presented at the 64th Annual Technical Conference and Exhibition of the Society of Petroleum Engineers, San Antonio, Texas, October 8-11, 1989.

44) Dikken, B.J.:"Pressure Drop in Horizontal Wells and Its Effect on Their Production Performance", paper SPE 19824, presented at the 64th Annual Technical Conference and Exhibition of the Society of Petroleum Engineers, San Antonio, Texas, October 8-11, 1989.also *SPE Journal of Pet. Tech.*, November 1990, pp. 1426 – 1433.

45) Chaperon, I.:"Theoretical Study of Coning Toward Horizontal and Vertical Wells in Anisotropic Formations: Subcritical and Critical Rates", paper SPE 15377, presented at the 61st Annual Technical Conference and Exhibition of the Society of Petroleum Engineers, New Orleans, LA, October 5-8, 1986.

46) Papatzacos, P., Herring, T.R., Martinsen, R., and Skjaeveland, S.M.:"Cone Breakthrough Time for Horizontal Wells", paper SPE 19822, presented at the 64th Annual Technical Conference and Exhibition of the Society of Petroleum Engineers, San Antonio, Texas, October 8-11, 1989.

47) Goode, P.A. and Thambynayagam, R.K.M.:"Pressure Drawdown and Buildup Analysis of Horizontal Wells in Anisotropic Media", paper SPE 14250, presented at the 60th Annual Technical Conference and Exhibition of the Society of Petroleum Engineers, Las Vegas, NV, September 22-25, 1985.also SPE Formation Evaluation, December 1987, pp. 683 – 697.

48) Daviau. F., Mouronval, G., Bourdarot, G., and Curutchet, P.:"Pressure Analysis for Horizontal Wells", paper SPE 14251, presented at the 60th Annual Technical Conference and Exhibition of the Society of Petroleum Engineers, Las Vegas, NV, September 22-25, 1985.also SPE Formation Evaluation, December 1988, pp. 716 – 724.

49) Clonts, M.D. and Ramey,Jr., H.J.:"Pressure Transient Analysis for Wells with Horizontal Drainholes", paper SPE 15116, presented at the 56th California Regional Meeting of the Society of Petroleum Engineers, Oakland, CA, April 2-4, 1986.

50) Rosa, A.J. and de Souza Carvalho, R.:"A Mathematical Model for Pressure Evaluation in an Infinite Conductivity Horizontal Well", unsolicited paper SPE 15967, June 26 1986.also SPE Formation Evaluation, December 1989, pp. 559 – 566.

51) Ozkan, E., Raghavan, R., and Joshi, S.:"Horizontal Well Pressure Analysis", paper SPE 16378, presented at the California Regional Meeting of the Society of Petroleum Engineers, Ventura, CA, April 8-10, 1987.also SPE Formation Evaluation, December 1989, pp. 567 – 575.

52) Kuchuk, F.J., Goode, P.A., Wilkinson, D.J., and Thambynayagam, R.K.M.:"Pressure Transient Behavior of Horizontal Wells with and without Gas Cap or Aquifer", paper SPE 17413, presented at the California Regional Meeting of the Society of Petroleum Engineers, Long Beach, CA, March 23-25, 1988.

53) Kuchuk, F.J., Goode, P.A., Brice, B., Sherrard, D., and Thambynayagam, R.K.M.:"Pressure Transient Analysis and Inflow Performance for Horizontal Wells", paper SPE 18300, presented at the 63rd Annual Technical Conference and Exhibition of the Society of Petroleum Engineers, Houston, Texas, October 2-5, 1988.also Journal of Pet. Techn., August 1990, pp. 974 – 979 and 1028 – 1031.

54) de Souza Carvalho, R. and Rosa, A.J.:"Transient Pressure Behavior for Horizontal Wells in Naturally Fractured Reservoirs", paper SPE 18302, presented at the 63rd Annual Technical Conference and Exhibition of the Society of Petroleum Engineers, Houston, Texas, October 2-5, 1988.

55) Aguilera, R. and Ng, M.C.:"Transient Pressure Analysis of Horizontal Wells in Anisotropic Naturally Fractured Reservoirs", paper SPE 19002, presented at the SPE Joint Rocky Mountain Regional/Low Permeability Reservoirs Symposium and Exhibition, Denver, Colorado, March 6-8, 1989.

56) Odeh, A.S. and Babu, D.K.:"Transient Flow Behavior of Horizontal Wells: Pressure Drawdown, and Buildup Analysis", paper SPE 18802, presented at the California Regional Meeting of the Society of Petroleum Engineers, Bakersfield, CA, April 5-7, 1989. also *SPE Formation Evaluation*, March 1990, pp. 7 - 15.

57) Butler, R.M., McNab, G.S., and Lo, H.Y.:"Theoretical Studies on the Gravity Drainage of Heavy Oil during In-situ Steam Heating", paper presented at the 29th Canadian Chemical Engineering Conference, Sarnia, Ontario, October 1, 1979.also *The Can. Journ. of Chemical Engg.*, Vol 59, August 1981, pp. 455 - 460.

58) Butler, R.M. and Stephens, D.J.:"The Gravity Drainage of Steam-heated Heavy Oil to Parallel Horizontal Wells", paper no. 80-31-31, presented at the 31st Annual Technical Meeting of the Petroleum Society of the CIM, Calgary, May 25-28, 1980.also *The Journ. of Can. Petroleum Technology*, April-June 1981, pp. 90 - 96.

59) Butler, R.M., Stephens, D.J., and Weiss, M.:"The Vertical Growth of Steam Chambers in the In-situ Thermal Recovery of Heavy Oils", Proceedings of the 30th Canadian Chemical Engineering Conference, Edmonton, Alberta, Volume 4, pp. 1152 - 1167, October, 19-22, 1980.

60) Griffin, P.J. and Trofimenkoff, P.N.:"Laboratory Studies of the Steam-assisted Gravity Drainage Process", paper presented at the AOSTRA 5th Annual 'Advances in Petroleum Recovery & Upgrading Technology' Conference, June 14-15 1984, Calgary, Alberta.also AOSTRA Journal of Research, Vol. 2, No. 4, 1986, pp. 197 - 203.

61) Butler, R.M.:"A New Approach to the Modelling of Steam-assisted Gravity Drainage", *The Journ. of Can. Petroleum Technology*, May-June 1985, pp. 42 - 51.

62) Joshi, S.D.:"A Laboratory Study of Thermal Oil Recovery Using Horizontal Wells", paper SPE 14916, presented at the SPE/DOE Fifth Symposium on Enhanced Oil Recovery of the Society of Petroleum Engineers and the Dept. of Energy, Tulsa, OK, April 20-23, 1986.

63) Butler, R.M.:"The Rise of Interfering Steam Chambers", paper no. 86-37-23, presented at the 37th Annual Technical Meeting of the Petroleum Society of CIM, Calgary, June 8-11, 1986.

64) Edmunds, N.R., Haston, J.A., and Best, D.A.:"Analysis and Implementation of the Steam-assisted Gravity Drainage Process at the AOSTRA UTF", paper no. 125, proceedings of the Fourth UNITAR/UNDP Conference on Heavy Crude and Tar Sands, Edmonton, August 7-12, 1988.

65) Chung, K.H. and Butler, R.M.:"A Theoretical and Experimental Study of Steam-assisted Gravity Drainage Process", paper no. 89, proceedings of the Fourth UNITAR/UNDP Conference on Heavy Crude and Tar Sands, Edmonton, August 7-12, 1988.

66) Huygen, H.H.A. and Black, J.B.:"Steaming Through Horizontal Wells and Fractures - Scaled

Model Tests", proceedings of 2nd European Symposium on Enhanced Oil Recovery, Paris, 8-10 November 1982, pp. 507 – 517.

67) Coates, R.:"Physical Simulator for Horizontal Well", proceedings of the WRI-DOE Tar Sand Symposium, sponsored by Western Research Institute and US Department of Energy, June 26-29 1984, Vail, Colorado.

68) Toma, P., Redford, D., and Livesey, D.:"The Laboratory Simulation of Bitumen Recovery by Steam Stimulation of Horizontal Wells", proceedings of the WRI-DOE Tar Sand Symposium, sponsored by Western Research Institute and US Department of Energy, June 26-29 1984, Vail, Colorado.

69) Chang, H., Farouq Ali, S.M., and George, A.E.:"Performance of Horizontal-Vertical Well Combination for Steamflooding Bottom Water Formations", paper CIM/SPE no. 90-86, presented at the International Technical Meeting of the Petroleum Society of CIM and the Society of Petroleum Engineers, Calgary, Alberta, June 10-13, 1990.

70) Rial, R.M.:"3D Thermal Simulation Using a Horizontal Wellbore for Steamflooding", paper SPE 13076, presented at the 59th Annual Technical Conference and Exhibition of the Society of Petroleum Engineers, Houston, Texas, September 16-19, 1984.

71) Jain, S. and Khosla, A.:"Predicting Steam Recovery of Athabasca Oil Through Horizontal Wells", paper no. 85-36-28, presented at the 36th Annual Technical Meeting of the Petroleum Society of CIM, Edmonton, Alberta, June 2-5, 1985.

72) Huang, W.-S. and Hight, M.A.:"Evaluation of Steamflood Processes Using Horizontal Wells", paper SPE 14130, presented at the SPE 1986 International Meeting on Petroleum Engineering, Beijing, China, March 17-20, 1986.

73) Hsueh, L.:"Numerical Simulation of the HAS Drive Process", paper SPE 15088, presented at the 56th California Regional Meeting of the Society of Petroleum Engineers, Oakland, CA, April 2-4, 1986.

74) Dietrich, J.K.:"The Kern River Horizontal-Well Steam Pilot", paper SPE 16346, presented at the 1987 SPE California Regional Meeting, Ventura, CA, April 8-10, 1987.also SPE Reservoir Engineering, August 1988, pp. 935 – 944.

75) Folefac, A.N. and Archer, J.S.:"Application of Horizontal Wells in the Simulation of Heavy Oil Recovery Process", paper SPE 17078, presented at the SPE Symposium on Reservoir Simulation, San Antonio, Texas, February 1-4, 1987.

76) Combe, J., Burger, J., Renard, G., and Valentin, E.:"New Technologies in Thermal Recovery: Contribution of Horizontal Wells", paper no. 117, proceedings of the Fourth UNITAR/UNDP Conference on Heavy Crude and Tar Sands, Edmonton, August 7-12, 1988.

77) Chen, S.M. and Olynyk, J.:"Sweep Efficiency Improvement Using Horizontal Wells or Tilted Horizontal Wells in Miscible Floods", paper no. 85-36-62, presented at the 36th Annual Technical Meeting of the Petroleum Society of CIM, Edmonton, Alberta, June 2-5, 1985.

78) Butler, R.M. and Mokrys, I.J.:"A New Process (VAPEX) for Recovering Heavy Oils using Hot Water and Hydrocarbon Vapour", paper CIM/SPE no.90-133, presented at the International Technical Meeting of the Petroleum Society of CIM and the Society of Petroleum Engineers, Calgary, Alberta, June 10-13, 1990.

79) Langhaar, H.L.:*Dimensional Analysis and Theory of Models*, John Wiley & Sons, New York 1951.

80) Leverett, M.C., Lewis, W.B., and True, M.E.: Petroleum Transactions, **AIME** Vol. 146, 1942, 175.

81) Rapoport, L.A. and Leas, W.J.: Petroleum Transactions, **AIME** Vol. 198, 1953, 139.

82) Croes, G.A. and Schwarz, N.: Petroleum Transactions, **AIME** Vol. 204, 1955, 35.

83) Offeringa, J. and van der Poel, C.: Petroleum Transactions, **AIME** Vol. 201, 1954, 310.

84) Geertsma, J., Croes, G., and Schwarz, N.:"Theory of Dimensionally Scaled Models of Petroleum Reservoirs", Petroleum Transactions, **AIME** Vol. 207, 1956, pp. 118 – 127.

85) Rojas, G.A. and Farouq Ali, S.M.:"Dynamics of Subcritical CO_2/Brine Floods for Heavy-Oil Recovery", paper SPE 13598, presented at the 1985 California Regional Meeting, Bakersfield, March 27-29, 1985.

86) Rojas, G.A. and Farouq Ali, S.M.:"Scaled Model Studies of Carbon Dioxide/Brine Injection Strategies for Heavy Oil Recovery from Thin Formations", *The Journ. of Can. Petroleum Technology*, January-February 1986, pp. 85 – 94.

87) Pujol, L. and Boberg, T.C.:"Scaling Accuracy of Laboratory Steam Flooding Models", paper SPE 4191, presented at the California Regional Meeting of the Society of Petroleum Engineers, Bakersfield, November 8-10, 1972.

88) Stegemeier, G.L., Laumbach, D.D., and Volek, C.W.:" Representing Steam Processes with Vacuum Models", *Society of Petroleum Engineers Journal*, June 1980, pp. 151 – 174.

89) Farouq Ali, S.M. and Redford, D.A.:"Physical Modeling of *In Situ* Recovery Methods for Oil Sands", proceedings of the Canada-Venezuela Oil Sands Symposium, Edmonton, Canada, CIM Special Volume No.17, pp. 319 – 326, 1977.

90) Kimber, K. and Farouq Ali, S.M.:"Application of New Scaling Approaches for Steam Injection Experiments", AIChE Symposium Series, Vol. 84, No. 263 (1988), pp. 191 – 196.

91) Kimber, K., Farouq Ali, S.M., and Puttagunta, V.R.:'Verification of Scaling Approaches for Steam Injection Experiments", CIM paper no. 88-39-17, presented at the 39th Annual Technical

Meeting of the Petroleum Society of CIM, Calgary, June 12-16, 1988.

92) Kimber, K., Farouq Ali, S.M.:"New Options for Scaling Steam Injection Experiments", paper SPE 18751, presented at the SPE California Regional Meeting, Bakersfield, CA, April 5-7, 1989.

93) Bird, R.B., Stewart, W.E., and Lightfoot, E.N.:_Transport Phenomena_, John Wiley & Sons, New York 1960.

94) Ong, T.S.:"Recovery of Heavy Oil by Steam-Assisted Gravity Drainage — A Three-Dimensional Approach", M.Sc. Thesis, The University of Calgary, 1988.

APPENDIX A

DERIVATION OF EQUATIONS FOR RESERVOIR FLOW

General statement of material balance:

$$Net\ throughput\ +\ Net\ change\ =\ 0$$

$$(Leaving\ -\ Entering)\ +\ (Conc.\ @\ t + \Delta t\ -\ Conc.\ @\ t)\ =\ 0.$$

1) Mass balance of Oil component (Oleic phase):

Referring to Figure 48:

Mass leaving:

$$-\rho_o C_{oo} v_{or}(r\Delta\theta\Delta z) + \rho_o C_{oo} v_{o\theta+\Delta\theta}(\Delta r\Delta z) + \rho_o C_{oo} v_{oz+\Delta z}(r\Delta r\Delta\theta) - (r\Delta r\Delta\theta\Delta z)q_o^*.$$

Mass entering:

$$-\rho_o C_{oo} v_{or+\Delta r}((r+\Delta r)\Delta\theta\Delta z) + \rho_o C_{oo} v_{o\theta}(\Delta r\Delta z) + \rho_o C_{oo} v_{oz}(r\Delta r\Delta\theta).$$

Mass concentration @ $t + \Delta t$:

$$r\Delta r\Delta\theta\Delta z(\phi S_o\rho_o C_{oo})\Big|_{t+\Delta t}.$$

Mass concentration @ t:

$$r\Delta r\Delta\theta\Delta z(\phi S_o\rho_o C_{oo})\Big|_{t}.$$

Therefore,

$$\Big\{ -\rho_o C_{oo} v_{or}(r\Delta\theta\Delta z) + \rho_o C_{oo} v_{o\theta+\Delta\theta}(\Delta r\Delta z) + \rho_o C_{oo} v_{oz+\Delta z}(r\Delta r\Delta\theta) - (r\Delta r\Delta\theta\Delta z)q_o^*$$

$$+ \rho_o C_{oo} v_{or+\Delta r}(r\Delta\theta\Delta z) + \rho_o C_{oo} v_{or+\Delta r}(\Delta r\Delta\theta\Delta z) - \rho_o C_{oo} v_{o\theta}(\Delta r\Delta z) - \rho_o C_{oo} v_{oz}(r\Delta r\Delta\theta)\Big\}\Delta t$$

$$= -(r\Delta r\Delta\theta\Delta z)\Big[(\phi S_o\rho_o C_{oo})_{t+\Delta t} - (\phi S_o\rho_o C_{oo})_t\Big].$$

Dividing through by $r\Delta r\Delta\theta\Delta z\Delta t$, and taking limit as $\Delta r, \Delta\theta, \Delta z, \Delta t \to 0$,

$$\frac{\partial}{\partial r}(\rho_o C_{oo} v_{or}) + \frac{1}{r}(\rho_o C_{oo} v_{or+\Delta r}) + \frac{1}{r}\frac{\partial}{\partial\theta}(\rho_o C_{oo} v_{o\Delta\theta}) + \frac{\partial}{\partial z}(\rho_o C_{oo} v_{oz}) - q_o^* = -\frac{\partial}{\partial t}(\phi S_o\rho_o C_{oo}).$$

Simplifying the expression above leads to,

$$-\frac{1}{r}\frac{\partial}{\partial r}(r\rho_o C_{oo} v_{or}) - \frac{1}{r}\frac{\partial}{\partial\theta}(\rho_o C_{oo} v_{o\Delta\theta}) - \frac{\partial}{\partial z}(\rho_o C_{oo} v_{oz}) + q_o^* = \frac{\partial}{\partial t}(\phi S_o\rho_o C_{oo}).$$

Define the following Darcian velocities:

$$v_{or} = -\frac{kk_{ro}}{\mu_o}\cdot\frac{\partial\Phi_o}{\partial r} = -\frac{kk_{ro}}{\mu_o}\cdot\frac{\partial}{\partial r}(p_o + \rho_o grsin\theta),$$

$$v_{o\theta} = -\frac{kk_{ro}}{\mu_o}\cdot\frac{1}{r}\frac{\partial\Phi_o}{\partial\theta} = -\frac{kk_{ro}}{\mu_o}\cdot\frac{1}{r}\cdot\frac{\partial}{\partial\theta}(p_o + \rho_o grsin\theta),$$

$$v_{oz} = -\frac{kk_{ro}}{\mu_o}\cdot\frac{\partial p_o}{\partial z}.$$
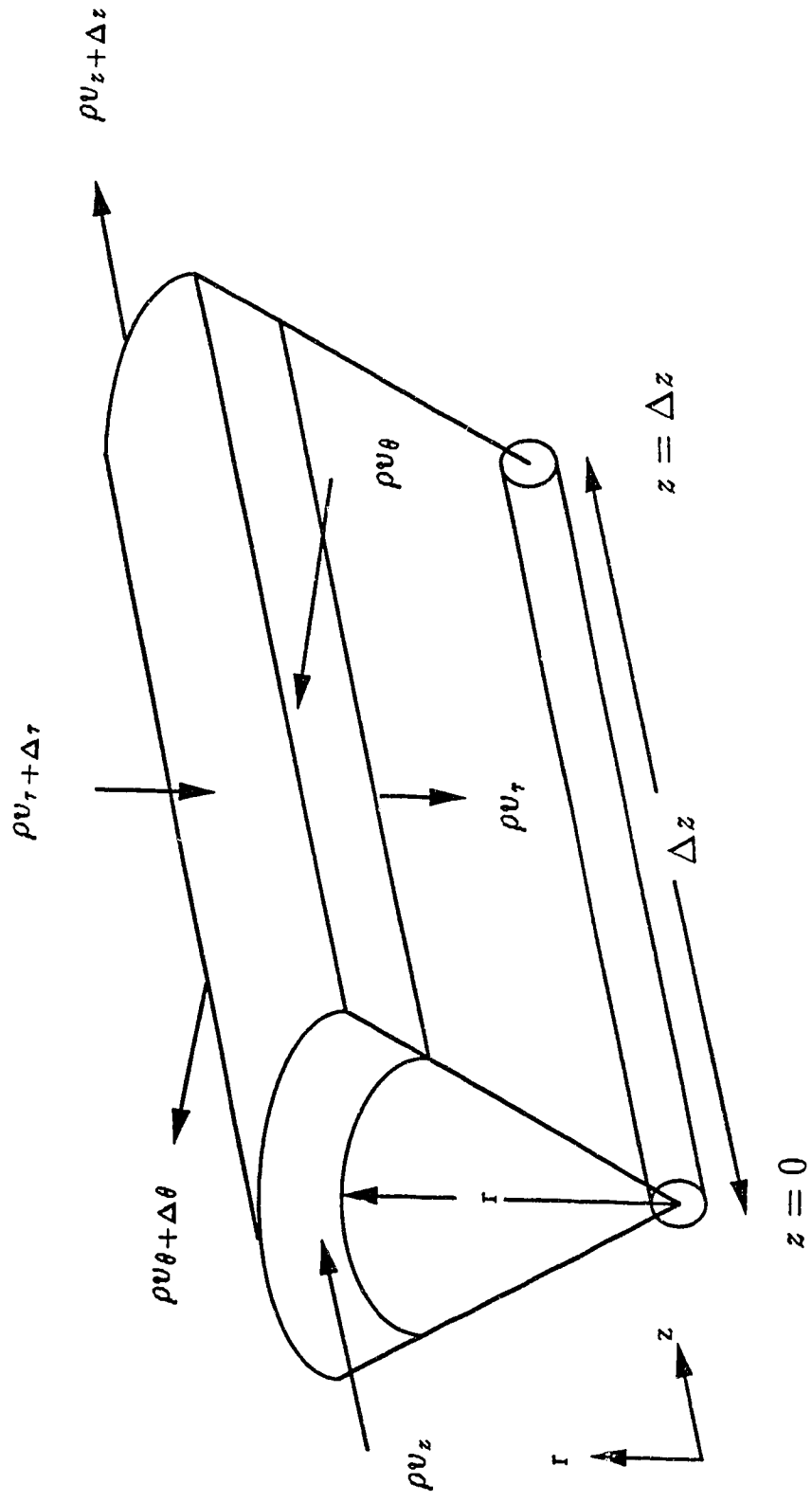
Figure 48: Schematic of Control Volume (CV) for Reservoir Flow.

Substituting these velocities int the partial differential equation above results in,

$$\frac{1}{r}\frac{\partial}{\partial r}\left[r\rho_o C_{oo}\frac{kk_{ro}}{\mu_o}\cdot\left(\frac{\partial p_o}{\partial r}+\rho_o g\frac{\partial(r sin\theta)}{\partial r}\right)\right]$$

$$+\frac{1}{r^2}\frac{\partial}{\partial\theta}\left[\rho_o C_{oo}\frac{kk_{ro}}{\mu_o}\cdot\left(\frac{\partial p_o}{\partial\theta}+\rho_o g\frac{\partial(r sin\theta)}{\partial\theta}\right)\right]$$

$$+\frac{\partial}{\partial z}\left[\rho_o C_{oo}\frac{kk_{ro}}{\mu_o}\cdot\frac{\partial p_o}{\partial z}\right]+q_o^{*}=\frac{\partial}{\partial t}\left(\phi S_o\rho_o C_{oo}\right)\quad. \tag{1}$$

Similarly,

2) Mass balance for water (for both aqueous and vapour phases):

$$\frac{1}{r}\frac{\partial}{\partial r}\left[r\rho_w\frac{kk_{rw}}{\mu_w}\cdot\left(\frac{\partial p_w}{\partial r}+\rho_w g\frac{\partial(r sin\theta)}{\partial r}\right)\right]$$

$$+\frac{1}{r}\frac{\partial}{\partial r}\left[r\rho_g C_{gw}\frac{kk_{rg}}{\mu_g}\cdot\left(\frac{\partial p_g}{\partial r}+\rho_g g\frac{\partial(r sin\theta)}{\partial r}\right)\right]$$

$$+\frac{1}{r^2}\frac{\partial}{\partial\theta}\left[\rho_w\frac{kk_{rw}}{\mu_w}\cdot\left(\frac{\partial p_w}{\partial\theta}+\rho_w g\frac{\partial(r sin\theta)}{\partial\theta}\right)\right]$$

$$+\frac{1}{r^2}\frac{\partial}{\partial\theta}\left[\rho_g C_{gw}\frac{kk_{rg}}{\mu_g}\cdot\left(\frac{\partial p_g}{\partial\theta}+\rho_g g\frac{\partial(r sin\theta)}{\partial\theta}\right)\right]$$

$$+\frac{\partial}{\partial z}\left[\rho_w\frac{kk_{rw}}{\mu_w}\cdot\frac{\partial p_w}{\partial z}\right]+\frac{\partial}{\partial z}\left[\rho_g C_{gw}\frac{kk_{rg}}{\mu_g}\cdot\frac{\partial p_g}{\partial z}\right]$$

$$+q_w^{*}+q_g^{*}C_{gw}^{*}=\frac{\partial}{\partial t}\left(\phi S_w\rho_w+\phi S_g\rho_g C_{gw}\right)\quad. \tag{2}$$

3) Mass balance for steam additive:

$$\frac{1}{r}\frac{\partial}{\partial r}\left[r\rho_o C_{oa}\frac{kk_{ro}}{\mu_o}\cdot\left(\frac{\partial p_o}{\partial r}+\rho_o g\frac{\partial(r sin\theta)}{\partial r}\right)\right]$$

$$+\frac{1}{r}\frac{\partial}{\partial r}\left[r\rho_g C_{ga}\frac{kk_{rg}}{\mu_g}\cdot\left(\frac{\partial p_g}{\partial r}+\rho_g g\frac{\partial(r sin\theta)}{\partial r}\right)\right]$$

$$+\frac{1}{r^2}\frac{\partial}{\partial\theta}\left[\rho_o C_{oa}\frac{kk_{ro}}{\mu_o}\cdot\left(\frac{\partial p_o}{\partial\theta}+\rho_o g\frac{\partial(r sin\theta)}{\partial\theta}\right)\right]$$

$$+\frac{1}{r^2}\frac{\partial}{\partial\theta}\left[\rho_g C_{ga}\frac{kk_{rg}}{\mu_g}\cdot\left(\frac{\partial p_g}{\partial\theta}+\rho_g g\frac{\partial(r sin\theta)}{\partial\theta}\right)\right]$$

$$+\frac{\partial}{\partial z}\left[\rho_o C_{oa}\frac{kk_{ro}}{\mu_o}\cdot\frac{\partial p_w}{\partial z}\right]+\frac{\partial}{\partial z}\left[\rho_g C_{ga}\frac{kk_{rg}}{\mu_g}\cdot\frac{\partial p_g}{\partial z}\right]$$

$$+q_o^{*}C_{oa}^{*}+q_g^{*}C_{ga}^{*}=\frac{\partial}{\partial t}\left(\phi S_o\rho_o C_{oa}+\phi S_g\rho_g C_{ga}\right)\quad. \tag{3}$$

4) Energy balance:

$$\frac{1}{r}\frac{\partial}{\partial r}(rk_{hr}\cdot\frac{\partial T}{\partial r})+\frac{1}{r^2}\frac{\partial}{\partial\theta}(k_{hr}\cdot\frac{\partial T}{\partial\theta})+\frac{\partial}{\partial z}(k_{hr}\cdot\frac{\partial T}{\partial z})$$

$$+ \frac{1}{r}\frac{\partial}{\partial r}\left[r\rho_o \frac{h_o k k_{ro}}{\mu_o} \cdot \left(\frac{\partial p_o}{\partial r} + \rho_o g \frac{\partial (r sin\theta)}{\partial r} \right) \right]$$

$$+ \frac{1}{r^2}\frac{\partial}{\partial \theta}\left[\rho_o \frac{h_o k k_{ro}}{\mu_o} \cdot \left(\frac{\partial p_o}{\partial \theta} + \rho_o g \frac{\partial (r sin\theta)}{\partial \theta} \right) \right] + \frac{\partial}{\partial z}\left[\rho_o \frac{h_o k k_{ro}}{\mu_o} \cdot \frac{\partial p_o}{\partial z} \right]$$

$$+ \frac{1}{r}\frac{\partial}{\partial r}\left[r\rho_w \frac{h_w k k_{rw}}{\mu_w} \cdot \left(\frac{\partial p_w}{\partial r} + \rho_w g \frac{\partial (r sin\theta)}{\partial r} \right) \right]$$

$$+ \frac{1}{r^2}\frac{\partial}{\partial \theta}\left[\rho_w \frac{h_w k k_{rw}}{\mu_w} \cdot \left(\frac{\partial p_w}{\partial \theta} + \rho_w g \frac{\partial (r sin\theta)}{\partial \theta} \right) \right] + \frac{\partial}{\partial z}\left[\rho_w \frac{h_w k k_{rw}}{\mu_w} \cdot \frac{\partial p_w}{\partial z} \right]$$

$$+ \frac{1}{r}\frac{\partial}{\partial r}\left[r\rho_g \frac{h_g k k_{rg}}{\mu_g} \cdot \left(\frac{\partial p_g}{\partial r} + \rho_g g \frac{\partial (r sin\theta)}{\partial r} \right) \right]$$

$$+ \frac{1}{r^2}\frac{\partial}{\partial \theta}\left[\rho_g \frac{h_g k k_{rg}}{\mu_g} \cdot \left(\frac{\partial p_g}{\partial \theta} + \rho_g g \frac{\partial (r sin\theta)}{\partial \theta} \right) \right] + \frac{\partial}{\partial z}\left[\rho_g \frac{h_g k k_{rg}}{\mu_g} \cdot \frac{\partial p_g}{\partial z} \right]$$

$$+ q_h^* - q_l^* = \frac{\partial}{\partial t}\left[(1-\phi)\rho_r U_r + \phi S_o \rho_o U_o + \phi S_w \rho_w U_w + \phi S_g \rho_g U_g \right] \quad . \tag{4}$$

APPENDIX B

INITIAL AND BOUNDARY CONDITIONS FOR RESERVOIR FLOW

B.1 Initial conditions

$$S_o(r,\theta,z,t=0) = S_{oi} \quad.$$

$$S_w(r,\theta,z,t=0) = S_{wi} \quad.$$

$$p_o(r,\theta,z,t=0) = p_{oi} \quad.$$

$$T(r,\theta,z,t=0) = T_i \quad.$$

B.2 Boundary conditions

B.2.1 Outer boundaries

B.2.1.1 No flow across top&bottom of reservoir, (r = ±H/2)

$$\frac{kk_{ro}}{\mu_o}\cdot\left(\frac{\partial p_o}{\partial r}-\rho_o g\frac{\partial(r\sin\theta)}{\partial r}\right)\Big|_{r=\pm H/2}=0 \quad.$$

$$\frac{kk_{rw}}{\mu_w}\cdot\left(\frac{\partial p_w}{\partial r}-\rho_w g\frac{\partial(r\sin\theta)}{\partial r}\right)\Big|_{r=\pm H/2}=0 \quad.$$

$$\frac{kk_{rg}}{\mu_g}\cdot\left(\frac{\partial p_g}{\partial r}-\rho_g g\frac{\partial(r\sin\theta)}{\partial r}\right)\Big|_{r=\pm H/2}=0 \quad.$$

B.2.1.2 No fluid flow across the end boundaries of the pattern, (z = 0,L)

$$\frac{kk_{ro}}{\mu_o}\cdot\frac{\partial p_o}{\partial z}\Big|_{z=0,L}=0 \quad.$$

$$\frac{kk_{rw}}{\mu_w}\cdot\frac{\partial p_w}{\partial z}\Big|_{z=0,L}=0 \quad.$$

$$\frac{kk_{rg}}{\mu_g}\cdot\frac{\partial p_g}{\partial z}\Big|_{z=0,L}=0 \quad.$$

B.2.1.3 Heat loss to overburden and surrounding formations

$$\frac{1}{r}\frac{\partial}{\partial r}\left(rk_{hob}\frac{\partial T_{ob}}{\partial r}\right)+\frac{1}{r^2}\frac{\partial}{\partial\theta}\left(k_{ob}\frac{\partial T_{ob}}{\partial\theta}\right)+\frac{\partial}{\partial z}\left(k_{ob}\frac{\partial T_{ob}}{\partial z}\right)+q_L^*=\rho_{ob}C_{ob}\frac{\partial T_{ob}}{\partial t} \quad.$$

B.2.2 Inner boundaries

B.2.2.1 Fluids production at the production well

$$q_o^*\big|_{r_w}=-\frac{\rho_o A_w kk_{ro}}{V_b\mu_o}\cdot\frac{\partial p_o}{\partial r} \quad.$$

$$q_w^*\big|_{r_w}=-\frac{\rho_w A_w kk_{rw}}{V_b\mu_w}\cdot\frac{\partial p_w}{\partial r} \quad.$$

$$q_g^*\big|_{r_w}=-\frac{\rho_g A_w kk_{rg}}{V_b\mu_g}\cdot\frac{\partial p_g}{\partial r} \quad.$$

Therefore,

$$q_w^* = q_o^* \frac{\rho_w k_{rw} \mu_o}{\rho_o k_{ro} \mu_w} \quad .$$

$$q_g^* = q_o^* \frac{\rho_g k_{rg} \mu_o}{\rho_o k_{ro} \mu_g} \quad .$$

B.2.2.2 Heat production at the production well

$$q_{hprod}^* = h_{oprod}^* q_{oprod}^* + h_{wprod}^* q_{wprod}^* + h_{sprod}^* C_{gwprod}^* q_{gprod}^* + h_{aprod}^* C_{gaprod}^* q_{gprod}^* \quad .$$

B.2.2.3 Mass injection rate of water at the injection well

$$W_{ww} = \int_{Ainj} \frac{\rho_w k k_{rw}}{\mu_w} \cdot \left(\nabla p_w + \rho_w g \nabla r \right) dA_w \quad .$$

B.2.2.4 Mass injection rate of steam and additive in the vapour phase

$$W_{gw} + W_{ga} = \int_{Ainj} \frac{\rho_g k k_{rg}}{\mu_g} \cdot \left(\nabla p_g + \rho_g g \nabla r \right) dA_w \quad .$$

B.2.2.5 Heat injection rate at the steam injection well

$$W_{ga} h_{gainj} + W_{gw} h_{gwinj} + W_{ww} h_{wwinj} =$$

$$\int_{Ainj} \left[k_{hr} \nabla T + \frac{\rho_g h_g k k_{rg}}{\mu_g} \cdot \left(\nabla p_g + \rho_g g \nabla r \right) + \frac{\rho_w h_w k k_{rw}}{\mu_w} \cdot \left(\nabla p_w + \rho_w g \nabla r \right) \right] dA_w \quad .$$

APPENDIX C

RESERVOIR FLOW EQUATIONS IN DIMENSIONLESS FORM

C.1 Water mass balance

$$\left[\frac{\rho_{wR}kk_{rw}RP_{wR}}{r_R^2\mu_{wR}}\right]\frac{1}{r_D}\frac{\partial}{\partial r_D}\left(\frac{r_D\rho_{wD}kk_{rwD}}{\mu_{wD}}\cdot\frac{\partial p_{wD}}{\partial r_D}\right)$$

$$+\left[\frac{\rho_{gR}C_{gwR}kk_{rg}RP_{gR}}{r_R^2\mu_{gR}}\right]\frac{1}{r_D}\frac{\partial}{\partial r_D}\left(\frac{r_D\rho_{gD}C_{gwD}kk_{rgD}}{\mu_{gD}}\cdot\frac{\partial p_{gD}}{\partial r_D}\right)$$

$$+\left[\frac{\rho_{wR}^2kk_{rw}Rg_Rr_Rsin\theta_R}{r_R\theta_R^2\mu_{wR}}\right]\frac{1}{r_D}\frac{\partial}{\partial r_D}\left(\frac{r_D\rho_{wD}^2kk_{rwD}g_D}{\mu_{wD}}\cdot\frac{\partial(r_Dsin\theta_D)}{\partial r_D}\right)$$

$$+\left[\frac{\rho_{gR}^2C_{gwR}kk_{rg}Rg_Rr_Rsin\theta_R}{r_R^2\mu_{gR}}\right]\frac{1}{r_D}\frac{\partial}{\partial r_D}\left(\frac{r_D\rho_{gD}^2C_{gwD}kk_{rgD}g_D}{\mu_{gD}}\cdot\frac{\partial(r_Dsin\theta_D)}{\partial r_D}\right)$$

$$+\left[\frac{\rho_{wR}kk_{rw}RP_{wR}}{r_R^2\theta_R^2\mu_{wR}}\right]\frac{1}{r_D^2}\frac{\partial}{\partial\theta_D}\left(\frac{\rho_{wD}kk_{rwD}}{\mu_{wD}}\cdot\frac{\partial p_{wD}}{\partial\theta_D}\right)$$

$$+\left[\frac{\rho_{gR}C_{gwR}kk_{rg}RP_{gR}}{r_R^2\theta_R^2\mu_{gR}}\right]\frac{1}{r_D^2}\frac{\partial}{\partial\theta_D}\left(\frac{\rho_{gD}C_{gwD}kk_{rgD}}{\mu_{gD}}\cdot\frac{\partial p_{gD}}{\partial\theta_D}\right)$$

$$+\left[\frac{\rho_{wR}^2kk_{rw}Rg_Rr_Rsin\theta_R}{r_R\theta_R^2\mu_{wR}}\right]\frac{1}{r_D^2}\frac{\partial}{\partial\theta_D}\left(\frac{\rho_{wD}^2kk_{rwD}g_D}{\mu_{wD}}\cdot\frac{\partial(r_Dsin\theta_D)}{\partial\theta_D}\right)$$

$$+\left[\frac{\rho_{gR}^2C_{gwR}kk_{rg}Rg_Rr_Rsin\theta_R}{r_R\theta_R^2\mu_{gR}}\right]\frac{1}{r_D^2}\frac{\partial}{\partial\theta_D}\left(\frac{\rho_{gD}^2C_{gwD}kk_{rgD}g_D}{\mu_{gD}}\cdot\frac{\partial(r_Dsin\theta_D)}{\partial\theta_D}\right)$$

$$+\left[\frac{\rho_{wR}kk_{rw}RP_{wR}}{z_R^2\mu_{wR}}\right]\frac{\partial}{\partial z_D}\left(\frac{\rho_{wD}^2kk_{rwD}g_D}{\mu_{wD}}\cdot\frac{\partial p_{wD}}{\partial z_D}\right)$$

$$+\left[\frac{\rho_{gR}C_{gwR}kk_{rg}RP_{gR}}{z_R^2\mu_{gR}}\right]\frac{\partial}{\partial z_D}\left(\frac{\rho_{gD}^2C_{gwD}kk_{rgD}g_D}{\mu_{gD}}\cdot\frac{\partial p_{gD}}{\partial z_D}\right)$$

$$+q_{wR}^*q_{wD}^*+C_{gwR}^*q_{gR}^*C_{gwD}^*q_{gD}^*$$

$$=\left[\frac{\phi_RS_{wR}\rho_{wR}}{t_R}\right]\frac{\partial}{\partial t_D}\left(\phi_DS_{wD}\rho_{wD}\right)+\left[\frac{\phi_RS_{gR}\rho_{gR}C_{gwR}}{t_R}\right]\frac{\partial}{\partial t_D}\left(\phi_DS_{gD}\rho_{gD}C_{gwD}\right). \quad (C\text{-}1)$$

Dividing through by the first coefficient of the left side leads to,

$$\frac{\partial}{\partial r_D}\left(\frac{r_D\rho_{wD}kk_{rwD}}{\mu_{wD}}\cdot\frac{\partial p_{wD}}{\partial r_D}\right)$$

$$+\left[\frac{\rho_{gR}C_{gwR}k_{rg}R\mu_{wR}P_{gR}}{\rho_{wR}k_{rw}R\mu_{gR}P_{wR}}\right]\frac{\partial}{\partial r_D}\left(\frac{r_D\rho_{gD}C_{gwD}kk_{rgD}}{\mu_{gD}}\cdot\frac{\partial p_{gD}}{\partial r_D}\right)$$

$$+\left[\frac{\rho_{wR}g_Rr_Rsin\theta_R}{P_{wR}}\right]\frac{\partial}{\partial r_D}\left(\frac{r_D\rho_{wD}^2kk_{rwD}g_D}{\mu_{wD}}\cdot\frac{\partial(r_Dsin\theta_D)}{\partial r_D}\right)$$

$$+\left[\frac{\rho_{gR}^2C_{gwR}k_{rg}R\mu_{wR}g_Rr_Rsin\theta_R}{\rho_{wR}k_{rw}R\mu_{gR}P_{wR}}\right]\frac{\partial}{\partial r_D}\left(\frac{r_D\rho_{gD}^2C_{gwD}kk_{rgD}g_D}{\mu_{gD}}\cdot\frac{\partial(r_Dsin\theta_D)}{\partial r_D}\right)$$

$$+\left[\frac{1}{\theta_R^2}\right]\frac{1}{r_D}\frac{\partial}{\partial\theta_D}\left(\frac{\rho_{wD}kk_{rwD}}{\mu_{wD}}\cdot\frac{\partial p_{wD}}{\partial\theta_D}\right)$$

$$+ \left[\frac{\rho_{gR}C_{gwR}k_{rgR}\mu_{wR}p_{gR}}{\rho_{wR}k_{rwR}\mu_{gR}p_{wR}\theta_R^2}\right]\frac{1}{r_D}\frac{\partial}{\partial\theta_D}\left(\frac{\rho_{gD}C_{gwD}kk_{rgD}}{\mu_{gD}}\cdot\frac{\partial p_{gD}}{\partial\theta_D}\right)$$

$$+ \left[\frac{r_R^2\rho_{wR}g_R sin\theta_R}{\theta_R^2 p_{wR}}\right]\frac{1}{r_D}\frac{\partial}{\partial\theta_D}\left(\frac{\rho_{wD}^2 kk_{rwD}g_D}{\mu_{wD}}\frac{\partial(r_D sin\theta_D)}{\partial\theta_D}\right)$$

$$+ \left[\frac{\rho_{gR}^2 C_{gwR}k_{rgR}\mu_{wR}g_R r_R^2 sin\theta_R}{\rho_{wR}k_{rwR}\mu_{gR}p_{wR}\theta_R^2}\right]\frac{1}{r_D}\frac{\partial}{\partial\theta_D}\left(\frac{\rho_{gD}^2 C_{gwD}kk_{rgD}g_D}{\mu_{gD}}\cdot\frac{\partial(r_D sin\theta_D)}{\partial\theta_D}\right)$$

$$+ \left[\frac{r_R^2}{z_R^2}\right]r_D\frac{\partial}{\partial z_D}\left(\frac{\rho_{wD}kk_{rwD}}{\mu_{wD}}\cdot\frac{\partial p_{wD}}{\partial z_D}\right)$$

$$+ \left[\frac{\rho_{gR}C_{gwR}k_{rgR}\mu_{wR}p_{gR}r_R^2}{\rho_{wR}k_{rwR}\mu_{gR}p_{wR}z_R^2}\right]r_D\frac{\partial}{\partial z_D}\left(\frac{\rho_{gD}^2 C_{gwD}kk_{rgD}g_D}{\mu_{gD}}\cdot\frac{\partial p_{gD}}{\partial z_D}\right)$$

$$+ \left[\frac{q_{wR}^* r_R^2 \mu_{wR}}{\rho_{wR}kk_{rwR}p_{wR}}\right]r_D q_{wD}^* + \left[\frac{C_{gwR}^* q_{gR}^* r_R^2 \mu_{wR}}{\rho_{wR}kk_{rwR}p_{wR}}\right]r_D C_{gwD}^* q_{gD}^*$$

$$= \left[\frac{\phi_R S_{wR} r_R^2 \mu_{wR}}{kk_{rwR}p_{wR}t_R}\right]r_D\frac{\partial}{\partial t_D}\left(\phi_D S_{wD}\rho_{wD}\right)$$

$$+ \left[\frac{\phi_R S_{gR} r_R^2 \mu_{wR}C_{gwR}\rho_{gR}}{kk_{rwR}p_{wR}\rho_{wR}t_R}\right]r_D\frac{\partial}{\partial t_D}\left(\phi_D S_{gD}\rho_{gD}C_{gwD}\right). \tag{C-2}$$

C.2 Steam — additive mass balance

$$\left[\frac{\rho_{oR}C_{oaR}kk_{roR}p_{oR}}{r_R^2\mu_{oR}}\right]\frac{1}{r_D}\frac{\partial}{\partial r_D}\left(\frac{r_D\rho_{oD}C_{oaD}kk_{roD}}{\mu_{oD}}\cdot\frac{\partial p_{oD}}{\partial r_D}\right)$$

$$+ \left[\frac{\rho_{gR}C_{gaR}kk_{rgR}p_{gR}}{r_R^2\mu_{gR}}\right]\frac{1}{r_D}\frac{\partial}{\partial r_D}\left(\frac{r_D\rho_{gD}C_{gaD}kk_{rgD}}{\mu_{gD}}\cdot\frac{\partial p_{gD}}{\partial r_D}\right)$$

$$+ \left[\frac{\rho_{oR}^2 C_{oaR}kk_{roR}g_R r_R sin\theta_R}{r_R^2\mu_{oR}}\right]\frac{1}{r_D}\frac{\partial}{\partial r_D}\left(\frac{r_D\rho_{oD}^2 C_{oaD}kk_{roD}g_D}{\mu_{oD}}\cdot\frac{\partial(r_D sin\theta_D)}{\partial r_D}\right)$$

$$+ \left[\frac{\rho_{gR}^2 C_{gaR}kk_{rgR}g_R r_R sin\theta_R}{r_R^2\mu_{gR}}\right]\frac{1}{r_D}\frac{\partial}{\partial r_D}\left(\frac{r_D\rho_{gD}^2 C_{gaD}kk_{rgD}g_D}{\mu_{gD}}\cdot\frac{\partial(r_D sin\theta_D)}{\partial r_-}\right)$$

$$+ \left[\frac{\rho_{oR}C_{oaR}kk_{roR}p_{oR}}{r_R^2\theta_R^2\mu_{oR}}\right]\frac{1}{r_D^2}\frac{\partial}{\partial\theta_D}\left(\frac{\rho_{oD}C_{oaD}kk_{roD}}{\mu_{oD}}\cdot\frac{\partial p_{oD}}{\partial\theta_D}\right)$$

$$+ \left[\frac{\rho_{gR}C_{gaR}kk_{rgR}p_{gR}}{r_R^2\theta_R^2\mu_{gR}}\right]\frac{1}{r_D^2}\frac{\partial}{\partial\theta_D}\left(\frac{\rho_{gD}C_{gaD}kk_{rgD}}{\mu_{gD}}\cdot\frac{\partial p_{gD}}{\partial\theta_D}\right)$$

$$+ \left[\frac{\rho_{oR}^2 C_{oaR}kk_{roR}g_R r_R sin\theta_R}{r_R\theta_R^2\mu_{oR}}\right]\frac{1}{r_D^2}\frac{\partial}{\partial\theta_D}\left(\frac{\rho_{oD}^2 C_{oaD}kk_{roD}g_D}{\mu_{oD}}\cdot\frac{\partial(r_D sin\theta_D)}{\partial\theta_D}\right)$$

$$+ \left[\frac{\rho_{gR}^2 C_{gaR}kk_{rgR}g_R r_R sin\theta_R}{r_R\theta_R^2\mu_{gR}}\right]\frac{1}{r_D^2}\frac{\partial}{\partial\theta_D}\left(\frac{\rho_{gD}^2 C_{gaD}kk_{rgD}g_D}{\mu_{gD}}\cdot\frac{\partial(r_D sin\theta_D)}{\partial\theta_D}\right)$$

$$+ \left[\frac{\rho_{oR}C_{oaR}kk_{roR}p_{oR}}{z_R^2\mu_{oR}}\right]\frac{\partial}{\partial z_D}\left(\frac{\rho_{oD}^2 C_{oaD}kk_{roD}g_D}{\mu_{oD}}\cdot\frac{\partial p_{oD}}{\partial z_D}\right)$$

$$+ \left[\frac{\rho_{gR}C_{gaR}kk_{rgR}p_{gR}}{z_R^2\mu_{gR}}\right]\frac{\partial}{\partial z_D}\left(\frac{\rho_{gD}^2 C_{gaD}kk_{rgD}g_D}{\mu_{gD}}\cdot\frac{\partial p_{gD}}{\partial z_D}\right)$$

$$+ C_{oaR}^* q_{oR}^* C_{oaD}^* q_{oD}^* + C_{gaR}^* q_{gR}^* C_{gaD}^* q_{gD}^* = \left[\frac{\phi_R S_{oR}\rho_{oR}C_{oaR}}{t_R}\right]\frac{\partial}{\partial t_D}\left(\phi_D S_{oD}\rho_{oD}C_{oaD}\right)$$

$$+ \left[\frac{\phi_R S_{gR}\rho_{gR}C_{gaR}}{t_R}\right]\frac{\partial}{\partial t_D}\left(\phi_D S_{gD}\rho_{gD}C_{gaD}\right). \tag{C-3}$$

Dividing through by the first coefficient of the left side leads to,

$$\frac{\partial}{\partial r_D}\left(\frac{r_D \rho_{oD} C_{oaD} k k_{roD}}{\mu_{oD}} \cdot \frac{\partial p_{oD}}{\partial r_D}\right)$$

$$+ \left[\frac{\rho_{gR} C_{gaR} k_{rgR} \mu_{oR} p_{gR}}{\rho_{oR} C_{oaR} k_{roR} \mu_{gR} p_{oR}}\right] \frac{\partial}{\partial r_D}\left(\frac{r_D \rho_{gD} C_{gaD} k k_{rgD}}{\mu_{gD}} \cdot \frac{\partial p_{gD}}{\partial r_D}\right)$$

$$+ \left[\frac{\rho_{oR} g_R r_R \sin\theta_R}{p_{oR}}\right] \frac{\partial}{\partial r_D}\left(\frac{r_D \rho_{oD}^2 C_{oaD} k k_{roD} g_D}{\mu_{oD}} \cdot \frac{\partial(r_D \sin\theta_D)}{\partial r_D}\right)$$

$$+ \left[\frac{\rho_{gR}^2 C_{gaR} k_{rgR} \mu_{oR} g_R r_R \sin\theta_R}{\rho_{oR} C_{oaR} k_{roR} \mu_{gR} p_{oR}}\right] \frac{\partial}{\partial r_D}\left(\frac{r_D \rho_{gD}^2 C_{gaD} k k_{rgD} g_D}{\mu_{gD}} \cdot \frac{\partial(r_D \sin\theta_D)}{\partial r_D}\right)$$

$$+ \left[\frac{1}{\theta_R^2}\right] \frac{1}{r_D} \frac{\partial}{\partial \theta_D}\left(\frac{\rho_{oD} C_{oaD} k k_{roD}}{\mu_{oD}} \cdot \frac{\partial p_{oD}}{\partial \theta_D}\right)$$

$$+ \left[\frac{\rho_{gR} C_{gaR} k_{rgR} \mu_{oR} p_{gR}}{\rho_{oR} C_{oaR} k_{roR} \mu_{gR} p_{oR} \theta_R^2}\right] \frac{1}{r_D} \frac{\partial}{\partial \theta_D}\left(\frac{\rho_{gD} C_{gaD} k k_{rgD}}{\mu_{gD}} \cdot \frac{\partial p_{gD}}{\partial \theta_D}\right)$$

$$+ \left[\frac{r_R^2 \rho_{oR} g_R \sin\theta_R}{\theta_R^2 p_{oR}}\right] \frac{1}{r_D} \frac{\partial}{\partial \theta_D}\left(\frac{\rho_{oD}^2 C_{oaD} k k_{roD} g_D}{\mu_{oD}} \cdot \frac{\partial(r_D \sin\theta_D)}{\partial \theta_D}\right)$$

$$+ \left[\frac{\rho_{gR}^2 C_{gaR} k_{rgR} \mu_{oR} g_R r_R^2 \sin\theta_R}{\rho_{oR} C_{oaR} k_{roR} \mu_{gR} p_{oR} \theta_R^2}\right] \frac{1}{r_D} \frac{\partial}{\partial \theta_D}\left(\frac{\rho_{gD}^2 C_{gaD} k k_{rgD} g_D}{\mu_{gD}} \cdot \frac{\partial(r_D \sin\theta_D)}{\partial \theta_D}\right)$$

$$+ \left[\frac{r_R^2}{z_R^2}\right] r_D \frac{\partial}{\partial z_D}\left(\frac{\rho_{oD} C_{oaD} k k_{roD}}{\mu_{oD}} \cdot \frac{\partial p_{oD}}{\partial z_D}\right)$$

$$+ \left[\frac{\rho_{gR} C_{gaR} k_{rgR} \mu_{oR} p_{gR} r_R^2}{\rho_{oR} C_{oaR} k_{roR} \mu_{gR} p_{oR} z_R^2}\right] r_D \frac{\partial}{\partial z_D}\left(\frac{\rho_{gD} C_{gaD} k k_{rgD}}{\mu_{gD}} \cdot \frac{\partial p_{gD}}{\partial z_D}\right)$$

$$+ \left[\frac{C_{oaR}^* q_{oR}^* r_R^2 \mu_{oR}}{C_{oaR} \rho_{oR} k_{roR} p_{oR}}\right] r_D C_{oaD}^* q_{oD}^* + \left[\frac{C_{gaR}^* q_{gR}^* r_R^2 \mu_{oR}}{C_{oaR} \rho_{oR} k_{roR} p_{oR}}\right] r_D C_{gaD}^* q_{gD}^*$$

$$= \left[\frac{\phi_R S_{oR} r_R^2 \mu_{oR}}{k k_{roR} p_{oR} t_R}\right] r_D \frac{\partial}{\partial t_D}\left(\phi_D S_{oD} \rho_{oD} C_{oaD}\right)$$

$$+ \left[\frac{\phi_R S_{gR} r_R^2 \mu_{oR} \rho_{gR} C_{gaR}}{k k_{roR} p_{oR} \rho_{oR} t_R C_{oaR}}\right] r_D \frac{\partial}{\partial t_D}\left(\phi_D S_{gD} \rho_{gD} C_{gaD}\right). \tag{C-4}$$

C.3 Energy balance

$$\left[\frac{k_{hrR} T_R}{r_R^2}\right] \frac{\partial}{\partial r_D}\left(\frac{r_D k_{hrD} \cdot \partial T_D}{\partial r_D}\right) + \left[\frac{k_{hrR} T_R}{r_R^2 \theta_R^2}\right] \frac{\partial}{\partial \theta_D}\left(\frac{k_{hrD} \partial T_D}{\partial \theta_D}\right) + \left[\frac{k_{hrR} T_R}{z_R^2}\right] \frac{\partial}{\partial z_D}\left(\frac{k_{hrD} \partial T_D}{\partial z_D}\right)$$

$$+ \left[\frac{\rho_{oR} h_{oR} k k_{roR} p_{oR}}{r_R^2 \mu_{oR}}\right] \frac{1}{r_D} \frac{\partial}{\partial r_D}\left(\frac{r_D \rho_{oD} h_{oD} k k_{roD}}{\mu_{oD}} \cdot \frac{\partial p_{oD}}{\partial r_D}\right)$$

$$+ \left[\frac{\rho_{oR}^2 h_{oR} k k_{roR} g_R r_R \sin\theta_R}{r_R^2 \mu_{oR}}\right] \frac{1}{r_D} \frac{\partial}{\partial r_D}\left(\frac{r_D \rho_{oD}^2 h_{oD} k k_{roD} g_D}{\mu_{oD}} \cdot \frac{\partial(r_D \sin\theta_D)}{\partial r_D}\right)$$

$$+ \left[\frac{\rho_{oR} h_{oR} k k_{roR} p_{oR}}{r_R^2 \theta_R^2 \mu_{oR}}\right] \frac{1}{r_D^2} \frac{\partial}{\partial \theta_D}\left(\frac{\rho_{oD} h_{oD} k k_{roD}}{\mu_{oD}} \cdot \frac{\partial p_{oD}}{\partial \theta_D}\right)$$

$$+ \left[\frac{\rho_{oR}^2 h_{oR} k k_{roR} g_R r_R \sin\theta_R}{r_R \theta_R^2 \mu_{oR}}\right] \frac{1}{r_D^2} \frac{\partial}{\partial \theta_D}\left(\frac{\rho_{oD}^2 h_{oD} k k_{roD} g_D}{\mu_{oD}} \cdot \frac{\partial(r_D \sin\theta_D)}{\partial \theta_D}\right)$$

$$+ \left[\frac{\rho_{oR} h_{oR} k k_{roR} p_{oR}}{z_R^2 \mu_{oR}}\right] \frac{\partial}{\partial z_D}\left(\frac{\rho_{oD} h_{oD} k k_{roD}}{\mu_{oD}} \cdot \frac{\partial p_{oD}}{\partial z_D}\right)$$

$$+ \left[\frac{\rho_{wR} h_{wR} k k_{rwR} p_{wR}}{r_R^2 \mu_{wR}}\right] \frac{1}{r_D} \frac{\partial}{\partial r_D}\left(\frac{r_D \rho_{wD} h_{wD} k k_{rwD}}{\mu_{wD}} \cdot \frac{\partial p_{wD}}{\partial r_D}\right)$$

$$+ \left[\frac{\rho_{wR}^2 h_{wR} k k_{rwR} g_R r_R sin\theta_R}{r_R^2 \mu_{wR}}\right] \frac{1}{r_D} \frac{\partial}{\partial r_D} \left(\frac{r_D \rho_{wD}^2 h_{wD} k k_{rwD} g_D}{\mu_{wD}} \cdot \frac{\partial(r_D sin\theta_D)}{\partial r_D}\right)$$

$$+ \left[\frac{\rho_{wR} h_{wR} k k_{rwR} P_{wR}}{r_R^2 \theta_R^2 \mu_{wR}}\right] \frac{1}{r_D^2} \frac{\partial}{\partial\theta_D} \left(\frac{\rho_{wD} h_{wD} k k_{rwD}}{\mu_{wD}} \cdot \frac{\partial p_{vD}}{\partial\theta_D}\right)$$

$$+ \left[\frac{\rho_{wR}^2 h_{wR} k k_{rwR} g_R r_R sin\theta_R}{r_R \theta_R^2 \mu_{wR}}\right] \frac{1}{r_D^2} \frac{\partial}{\partial\theta_D} \left(\frac{\rho_{wD}^2 h_{wD} k k_{rwD} g_D}{\mu_{wD}} \cdot \frac{\partial(r_D sin\theta_D)}{\partial\theta_D}\right)$$

$$+ \left[\frac{\rho_{wR} h_{wR} k k_{rwR} P_{wR}}{z_R^2 \mu_{wR}}\right] \frac{\partial}{\partial z_D} \left(\frac{\rho_{wD} h_{wD} k k_{rwD}}{\mu_{wD}} \cdot \frac{\partial p_{wD}}{\partial z_D}\right)$$

$$+ \left[\frac{\rho_{gR} h_{gR} k k_{rgR} P_{gR}}{r_R^2 \mu_{gR}}\right] \frac{1}{r_D} \frac{\partial}{\partial r_D} \left(\frac{r_D \rho_{gD} h_{gD} k k_{rgD}}{\mu_{gD}} \cdot \frac{\partial p_{gD}}{\partial r_D}\right)$$

$$+ \left[\frac{\rho_{gR}^2 h_{gR} k k_{rgR} g_R r_R sin\theta_R}{r_R^2 \mu_{gR}}\right] \frac{1}{r_D} \frac{\partial}{\partial r_D} \left(\frac{r_D \rho_{gD}^2 h_{gD} k k_{rgD} g_D}{\mu_{gD}} \cdot \frac{\partial(r_D sin\theta_D)}{\partial r_D}\right)$$

$$+ \left[\frac{\rho_{gR} h_{gR} k k_{rgR} P_{gR}}{r_R^2 \theta_R^2 \mu_{gR}}\right] \frac{1}{r_D^2} \frac{\partial}{\partial\theta_D} \left(\frac{\rho_{gD} h_{gD} k k_{rgD}}{\mu_{gD}} \cdot \frac{\partial p_{gD}}{\partial\theta_D}\right)$$

$$+ \left[\frac{\rho_{gR}^2 h_{gR} k k_{rgR} g_R r_R sin\theta_R}{r_R \theta_R^2 \mu_{gR}}\right] \frac{1}{r_D^2} \frac{\partial}{\partial\theta_D} \left(\frac{\rho_{gD}^2 h_{gD} k k_{rgD} g_D}{\mu_{gD}} \cdot \frac{\partial(r_D sin\theta_D)}{\partial\theta_D}\right)$$

$$+ \left[\frac{\rho_{gR} h_{gR} k k_{rgR} P_{gR}}{z_R^2 \mu_{gR}}\right] \frac{\partial}{\partial z_D} \left(\frac{\rho_{gD} h_{gD} k k_{rgD}}{\mu_{gD}} \cdot \frac{\partial p_{gD}}{\partial z_D}\right)$$

$$+ \dot{q}_{hR} \dot{q}_{hD} - \dot{q}_{iR} \dot{q}_{iD} = \left[\frac{(1-\phi_R)\rho_{rR} U_{rR}}{t_R}\right] \frac{\partial}{\partial t_D}\left((1-\phi_D)\rho_{rD} U_{rD}\right)$$

$$+ \left[\frac{\phi_R S_{oR} \rho_{oR} U_{oR}}{t_R}\right] \frac{\partial}{\partial t_D}\left(\phi_D S_{oD} \rho_{oD} U_{oD}\right) + \left[\frac{\phi_R S_{wR} \rho_{wR} U_{wR}}{t_R}\right] \frac{\partial}{\partial t_D}\left(\phi_D S_{wD} \rho_{wD} U_{wD}\right)$$

$$+ \left[\frac{\phi_R S_{gR} \rho_{gR} U_{gR}}{t_R}\right] \frac{\partial}{\partial t_D}\left(\phi_D S_{gR} \rho_{gR} U_{gR}\right). \tag{C-5}$$

Dividing through by the first coefficient of the left side leads to,

$$\left[\frac{k_{hrR} T_R \mu_{oR}}{\rho_{oR} k k_{roR} h_{oR} P_{oR}}\right] \frac{\partial}{\partial r_D} \left(\frac{r_D k_{hrD} \cdot \partial T_D}{\partial r_D}\right) + \left[\frac{k_{hrR} T_R \mu_{oR}}{\rho_{oR} k k_{roR} h_{oR} P_{oR} \theta_R^2}\right] \frac{1}{r_D} \frac{\partial}{\partial\theta_D} \left(\frac{k_{hrD} \partial T_D}{\partial\theta_D}\right)$$

$$+ \left[\frac{k_{hrR} T_R \mu_{oR} r_R^2}{\rho_{oR} k k_{roR} h_{oR} P_{oR} z_R^2}\right] r_D \frac{\partial}{\partial z_D} \left(\frac{k_{hrD} \partial T_D}{\partial z_D}\right) + \frac{\partial}{\partial r_D} \left(\frac{r_D \rho_{oD} h_{oD} k k_{roD}}{\mu_{oD}} \cdot \frac{\partial p_{oD}}{\partial r_D}\right)$$

$$+ \left[\frac{\rho_{oR} g_R r_R sin\theta_R}{P_{oR}}\right] \frac{\partial}{\partial r_D} \left(\frac{r_D \rho_{oD}^2 h_{oD} k k_{roD} g_D}{\mu_{oD}} \cdot \frac{\partial(r_D sin\theta_D)}{\partial r_D}\right)$$

$$+ \left[\frac{1}{\theta_R^2}\right] \frac{1}{r_D} \frac{\partial}{\partial\theta_D} \left(\frac{\rho_{oD} h_{oD} k k_{roD}}{\mu_{oD}} \cdot \frac{\partial p_{oD}}{\partial\theta_D}\right)$$

$$+ \left[\frac{r_R^2 \rho_{oR} g_R sin\theta_R}{\theta_R^2 P_{oR}}\right] \frac{1}{r_D} \frac{\partial}{\partial\theta_D} \left(\frac{\rho_{oD}^2 h_{oD} k k_{roD} g_D}{\mu_{oD}} \cdot \frac{\partial(r_D sin\theta_D)}{\partial\theta_D}\right)$$

$$+ \left[\frac{r_R^2}{z_R^2}\right] r_D \frac{\partial}{\partial z_D} \left(\frac{\rho_{oD} h_{oD} k k_{roD}}{\mu_{oD}} \cdot \frac{\partial p_{oD}}{\partial z_D}\right)$$

$$+ \left[\frac{\rho_{wR} h_{wR} k_{rwR} \mu_{oR} P_{wR}}{\rho_{oR} h_{oR} k_{roR} \mu_{wR} P_{oR}}\right] \frac{\partial}{\partial r_D} \left(\frac{r_D \rho_{wD} h_{wD} k k_{rwD}}{\mu_{wD}} \cdot \frac{\partial p_{wD}}{\partial r_D}\right)$$

$$+ \left[\frac{\rho_{wR}^2 h_{wR} k_{rwR} \mu_{oR} g_R r_R sin\theta_R}{\rho_{oR} h_{oR} k_{roR} \mu_{wR} P_{oR}}\right] \frac{\partial}{\partial r_D} \left(\frac{r_D \rho_{wD}^2 h_{wD} k k_{rwD} g_D}{\mu_{wD}} \cdot \frac{\partial(r_D sin\theta_D)}{\partial r_D}\right)$$

$$+ \left[\frac{\rho_{wR} h_{wR} k_{rwR} \mu_{oR} P_{wR}}{\rho_{oR} h_{oR} k_{roR} \mu_{wR} P_{oR} \theta_R^2}\right] \frac{1}{r_D} \frac{\partial}{\partial\theta_D} \left(\frac{\rho_{wD} h_{wD} k k_{rwD}}{\mu_{wD}} \cdot \frac{\partial p_{wD}}{\partial\theta_D}\right)$$

$$+ \left[\frac{\rho_{wR}^2 h_{wR} k_{rwR} \mu_{oR} g_R r_R^2 \sin\theta_R}{\rho_{oR} h_{oR} k_{roR} \mu_{wR} P_{oR} \theta_R^2}\right] \frac{1}{r_D} \frac{\partial}{\partial\theta_D} \left(\frac{\rho_{wD}^2 h_{wD} k k_{rwD} g_D}{\mu_{wD}} \cdot \frac{\partial(r_D \sin\theta_D)}{\partial\theta_D}\right)$$

$$+ \left[\frac{\rho_{wR} h_{wR} k_{rwR} \mu_{oR} P_{wR} r_R^2}{\rho_{oR} h_{oR} k_{roR} \mu_{wR} P_{oR} z_R^2}\right] r_D \frac{\partial}{\partial z_D} \left(\frac{\rho_{wD} h_{wD} k k_{rwD}}{\mu_{wD}} \cdot \frac{\partial p_{wD}}{\partial z_D}\right)$$

$$+ \left[\frac{\rho_{gR} h_{gR} k_{rgR} \mu_{oR} P_{gR}}{\rho_{oR} h_{oR} k_{roR} \mu_{gR} P_{oR}}\right] \frac{\partial}{\partial r_D} \left(\frac{r_D \rho_{gD} h_{gD} k k_{rgD}}{\mu_{gD}} \cdot \frac{\partial p_{gD}}{\partial r_D}\right)$$

$$+ \left[\frac{\rho_{gR}^2 h_{gR} k_{rgR} \mu_{oR} g_R r_R \sin\theta_R}{\rho_{oR} h_{oR} k_{roR} \mu_{gR} P_{oR}}\right] \frac{\partial}{\partial r_D} \left(\frac{r_D \rho_{gD}^2 h_{gD} k k_{rgD} g_D}{\mu_{gD}} \cdot \frac{\partial(r_D \sin\theta_D)}{\partial r_D}\right)$$

$$+ \left[\frac{\rho_{gR} h_{gR} k_{rgR} \mu_{oR} P_{gR}}{\rho_{oR} h_{oR} k_{roR} \mu_{gR} P_{oR} \theta_R^2}\right] \frac{1}{r_D} \frac{\partial}{\partial\theta_D} \left(\frac{\rho_{gD} h_{gD} k k_{rgD}}{\mu_{gD}} \cdot \frac{\partial p_{gD}}{\partial\theta_D}\right)$$

$$+ \left[\frac{\rho_{gR}^2 h_{gR} k_{rgR} \mu_{oR} g_R r_R^2 \sin\theta_R}{\rho_{oR} h_{oR} k_{roR} \mu_{gR} P_{oR} \theta_R^2}\right] \frac{1}{r_D} \frac{\partial}{\partial\theta_D} \left(\frac{\rho_{gD}^2 h_{gD} k k_{rgD} g_D}{\mu_{gD}} \cdot \frac{\partial(r_D \sin\theta_D)}{\partial\theta_D}\right)$$

$$+ \left[\frac{\rho_{gR} h_{gR} k_{rgR} \mu_{oR} P}{\rho_{oR} h_{oR} k_{roR} \mu_{gR}}\right] \frac{\partial}{\partial z_D} \left(\frac{\rho_{gD} h_{gD} k k_{rgD}}{\mu_{gD}} \cdot \frac{\partial p_{gD}}{\partial z_D}\right)$$

$$+ \left[\frac{q_{hR} r_R^2 \mu_{oR}}{\rho_{oR} k k_{roR} h_{oR} P_{oR}}\right] r_D \dot{q}_{hD} - \left[\frac{q_{iR} r_R^2 \mu_{oR}}{\rho_{oR} k k_{roR} h_{oR} P_{oR}}\right] r_D \dot{q}_{iD}$$

$$= \left[\frac{(1-\phi_R)\rho_{rR} U_{rR} r_R^2 \mu_{oR}}{\rho_{oR} k k_{roR} h_{oR} P_{oR} t_R}\right] r_D \frac{\partial}{\partial t_D} \left((1-\phi_D)\rho_{rD} U_{rD}\right)$$

$$+ \left[\frac{\phi_R S_{oR} r_R^2 \mu_{oR} U_{oR}}{k k_{roR} h_{oR} P_{oR} t_R}\right] r_D \frac{\partial}{\partial t_D} \left(\phi_D S_{oD} \rho_{oD} U_{oD}\right)$$

$$+ \left[\frac{\phi_R S_{wR} r_R^2 \mu_{oR} U_{wR} \rho_{wR}}{k k_{roR} h_{oR} P_{oR} t_R \rho_{oR}}\right] r_D \frac{\partial}{\partial t_D} \left(\phi_D S_{wD} \rho_{wD} U_{wD}\right)$$

$$+ \left[\frac{\phi_R S_{gR} r_R^2 \mu_{oR} U_{gR} \rho_{gR}}{k k_{roR} h_{oR} P_{oR} t_R \rho_{oR}}\right] r_D \frac{\partial}{\partial t_D} \left(\phi_D S_{gR} \rho_{gR} U_{gR}\right). \tag{C-6}$$

APPENDIX D

DERIVATION OF GOVERNING EQUATIONS FOR INSIDE-WELL FLOW

<u>Mass balance</u> :

General statement of material balance:

$$Net\ throughput\ +\ Net\ change\ =\ 0$$

$$(Leaving\ -\ Entering)\ +\ (Conc.\ @\ t + \Delta t\ -\ Conc.\ @\ t)\ = 0\ \ .$$

For steady-state flow, Net change $= 0$.

Therefore, Rate of mass entering $=$ Rate of mass leaving .

From the drawing of the control volume (CV) in Figure 49:

Mass entering: two components,

1) Mass entering through the inlet $= \rho_m A_{in} v_{in}$.

2) Mass entering through the side $= \rho_m q_m$, where

$$q_m = -\frac{2\pi a_w r_{w,avg} k k_{rm} \Delta z}{\mu_m} \cdot \left[\frac{dp_m}{dr} + \rho_m g \frac{d}{dr}(r sin\theta)\right]\ \ .$$

In the formulation of this equation, radial flow was assumed. As such, Darcy's radial equation was modified for the problem under consideration which had an element orientated in the horizontal direction (as shown in Figure 49), instead of the conventional vertical position. In this case, the area open to inflow was $A = 2\pi a_w r_{w,avg} \Delta z$, with a_w denoting that only a fraction of the peripheral area of the horizontal well was open to the inflow of reservoir fluids. Furthermore, the potential drawdown gradient $\left[\frac{dp_m}{dr} + \rho_m g \frac{d}{dr}(r sin\theta)\right]$ was evaluated between the potential at point r and the wellbore radius, $r_{w,avg}$.

Mass leaving $= \rho_m(A_{in} + \Delta A)v_{out}$.

Hence, the mass balance is:

$$\rho_m A_{in} v_{out} - \rho_m A_{in} v_{in} + \rho_m \Delta A v_{out} + \frac{2\pi \rho_m a_w r_{w,avg} k k_{rm} \Delta z}{\mu_m} \cdot \left[\frac{dp_m}{dr} + \rho_m g \frac{d}{dr}(r sin\theta)\right] = 0\ \ .$$

Dividing through by $\rho_m A_{in} \Delta z$, and take limit as $\Delta z \to 0$:

$$\frac{dv}{dz} + \frac{v_{out}}{A_{in}} \frac{dA}{dz} + \frac{2\pi a_w r_{w,avg} k k_{rm}}{\mu_m A_{in}} \cdot \left[\frac{dp_m}{dr} + \rho_m g \frac{d}{dr}(r sin\theta)\right] = 0\ \ .$$

But $A = \pi r_w^2$, therefore $dA = 2\pi r_w dr_w$,

thus the above equation becomes:

$$\frac{dv}{dz} + \frac{2v_{out} r_w}{r_{w,in}^2} \cdot \frac{dr_w}{dz} + \frac{2a_w r_{w,avg} k k_{rm}}{\mu_m r_{w,in}^2} \cdot \left[\frac{dp_m}{dr} + \rho_m g \frac{d}{dr}(r sin\theta)\right] = 0\ \ .$$
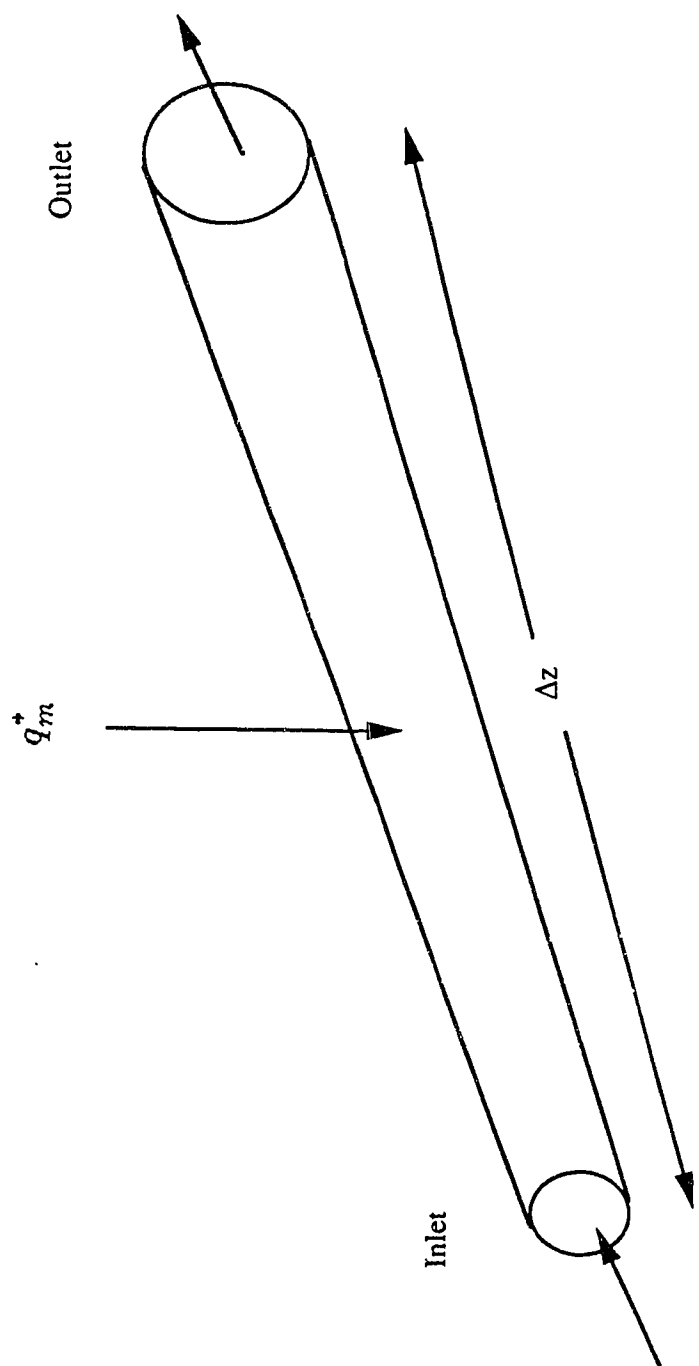
Figure 49: Schematic of Control Volume (CV) for Inside-Well Flow.

This is the same as equation (7) in Chapter 4.

Energy balance :

For the energy balance, it is assumed that the convective heat transfer process due to the movement of fluids from one end of the horizontal producer to the other, as well as from the reservoir into the well is much bigger than the conductive heat transfer taking place due to the temperature gradient between the fluids and the actual horizontal well. According to the First Law of Thermodynamics:

'For any mass system (that is, any identified and unchanging collection of matter) the net heat supplied to the system equals the increase in energy of the system plus all the energy which leaves the system as work is done.'

Or, in algebraic terms,

$$\Delta Q = \Delta E + \Delta W$$

where ΔE represents the energy of the system, ΔQ the heat added to the system, and ΔW the work done by the system while the change ΔE occurs.

1) Rate of energy entering the C.V. $= \rho_m A_{in} v_{in}\left(\frac{U_{in}}{J} + \frac{v_{in}^2}{2J}\right) + \rho_m q_m U_m$, where

$$q_m U_m = -\frac{2\pi a_w r_{w,avg} k k_{rm} \Delta z U_m}{\mu_m} \cdot \left[\frac{dp_m}{dr} + \rho_m g \frac{d}{dr}(r\sin\theta)\right]$$

2) Rate of energy leaving the C.V. $= \rho_m A_{out} v_{out}\left(\frac{U_{out}}{J} + \frac{v_{out}^2}{2J}\right)$.

3) Rate of work done on the fluids by a pump $= -\rho_m \bar{A}\Delta z \cdot W$, where $\bar{A} = \pi r_{w,avg}^2$.

4) Rate of energy accumulation $= \rho_m \bar{A}\Delta z C_H \frac{\Delta T}{\Delta t}$.

Hence, the energy balance is:

$$\rho_m A_{in}\left(\frac{v_{out}U_{out}}{J} - \frac{v_{in}U_{in}}{J}\right) + \rho_m \Delta A \frac{v_{out}U_{out}}{J} + \rho_m A_{in}\left(\frac{v_{out}^3}{2J} - \frac{v_{in}^3}{2J}\right) + \rho_m \Delta A \frac{v_{out}^3}{2J}$$
$$+ \frac{2\pi a_w r_{w,avg} k k_{rm} \Delta z U_m \rho_m}{\mu_m} \cdot \left[\frac{dp_m}{dr} + \rho_m g \frac{d}{dr}(r\sin\theta)\right] - \rho_m \bar{A}\Delta z W = \rho_m \bar{A}\Delta z C_H \frac{\Delta T}{\Delta t}$$

Assume that the kinetic energy effects are negligible compared to thermal energy effects, then the terms $\rho_{in} A_{in}\left(\frac{v_{out}^3}{2J} - \frac{v_{in}^3}{2J}\right)$ and $\rho_m \Delta A \frac{v_{out}^3}{2J}$ disappear, and the energy balance equation becomes:

$$\rho_m A_{in}\left(\frac{v_{out}U_{out}}{J} - \frac{v_{in}U_{in}}{J}\right) + \rho_m \Delta A \frac{v_{out}U_{out}}{J} - \rho_m \bar{A}\Delta z W$$
$$+ \frac{2\pi a_w r_{w,avg} k k_{rm} \Delta z U_m \rho_m}{\mu_m} \cdot \left[\frac{dp_m}{dr} + \rho_m g \frac{d}{dr}(r\sin\theta)\right] = \rho_m \bar{A}\Delta z C_H \frac{\Delta T}{\Delta t}$$

Divide through by $\rho_m \bar{A}\Delta z$, and take limit as $\Delta z, \Delta t \to 0$:

$$\frac{A_{in}}{\bar{A}}\frac{d}{dz}\left(\frac{vU}{J}\right) + \frac{v_{out}U_{out}}{J\bar{A}}\frac{dA}{dz} + \frac{2\pi a_w r_{w,avg} k k_{rm} U_m}{\mu_m \bar{A}} \cdot \left[\frac{dp_m}{dr} + \rho_m g \frac{d}{dr}(r\sin\theta)\right] - W = C_H \frac{\Delta T}{\Delta t}$$

Simplifying the above expression leads to the following,

$$\frac{r_{w,in}^2}{r_{w,avg}^2} \cdot \frac{d}{dz}\left(\frac{vU}{J}\right) + \frac{2v_{out}U_{out}r_w}{Jr_{w,avg}^2} \cdot \frac{dr_w}{dz} + \frac{2a_w kk_{rm}U_m}{\mu_m r_{w,avg}} \cdot \left[\frac{dp_m}{dr} + \rho_m g\frac{d}{dr}(r\sin\theta)\right] - W = C_H\frac{dT}{dt}$$

This is the same as equation (10) in Chapter 4.

Appendix E: Tables of Experimental Results.

Table E1: Run PS3 (Constant Diameter Horizontal Well with No Casing, Partially Scaled Model).

Pore Volume of Sand Pack:	1060.0 ml		Porosity of Sand Pack:	38.1 %	
Irreducible Water Saturation:	7.5 %PV		Absolute Permeability of Pack:	17.7 darcies	
Initial Oil Saturation:	92.5 %PV		Steam Injection Rate:	0.111 ml/s (CWE)	

Sample no.	Steam Vol. Inj. ml (CWE)	Steam Vol. Inj. %PV (CWE)	Inst. Prod. Rate ml/s	Inst. Oil Prod. ml	Inst. WOR ml/ml	Cum. Oil Prod. ml	Cum. Oil Rec. %IOIP	Cum. OSR ml/ml (CWE)
1	110.0	10.4	0.031	21.1	0.44	21.1	2.2	0.19
2	130.0	12.3	0.172	17.3	0.79	38.4	3.9	0.30
3	150.0	14.2	0.161	15.6	0.86	54.0	5.5	0.36
4	170.0	16.0	0.167	13.1	1.30	67.1	6.8	0.39
5	190.0	17.9	0.156	13.0	1.15	80.1	8.2	0.42
6	210.0	19.8	0.162	13.6	1.15	93.7	9.6	0.45
7	230.0	21.7	0.178	14.3	1.24	108.0	11.0	0.47
8	250.0	23.6	0.171	10.4	1.95	118.4	12.1	0.47
9	270.0	25.5	0.209	13.9	1.71	132.3	13.5	0.49
10	290.0	27.4	0.111	9.2	1.16	141.5	14.4	0.49
11	310.0	29.2	0.143	8.0	2.23	149.5	15.2	0.48
12	330.0	31.1	0.168	12.5	1.42	162.0	16.5	0.49
13	350.0	33.0	0.121	11.8	0.84	173.8	17.7	0.50
14	370.0	34.9	0.223	19.9	1.02	193.7	19.7	0.52
15	390.0	36.8	0.147	7.7	2.44	201.4	20.5	0.52
16	410.0	38.7	0.216	15.0	1.59	216.4	22.1	0.53
17	430.0	40.6	0.208	17.2	1.17	233.6	23.8	0.54

Table E2: Run PS4 (Constant Diameter Horizontal Well with No Casing, Partially Scaled Model).

Pore Volume of Sand Pack:	985.0 ml	
Irreducible Water Saturation:	5.7 %PV	
Initial Oil Saturation:	94.3 %PV	
Porosity of Sand Pack:	35.4 %	
Absolute Permeability of Pack:	8.5 darcies	
Steam Injection Rate:	0.094 ml/s (CWE)	

Sample no.	Steam Vol. Inj. ml (CWE)	Steam Vol. Inj. %PV (CWE)	Inst. Prod. Rate ml/s	Inst. Oil Prod. ml	Inst. WOR ml/ml	Cum. Oil Prod. ml	Cum. Oil Rec. %IOIP	Cum. OSR ml/ml (CWE)
1	158.5	16.1	0.024	23.5	0.72	23.5	2.5	0.15
2	181.1	18.4	0.142	16.3	1.09	39.8	4.3	0.22
3	203.8	20.7	0.150	15.5	1.32	55.3	6.0	0.27
4	226.4	23.0	0.158	15.5	1.44	70.8	7.6	0.31
5	249.1	25.3	0.147	13.5	1.61	84.3	9.1	0.34
6	271.7	27.6	0.134	7.1	3.52	91.4	9.8	0.34
7	294.3	29.9	0.143	12.6	1.73	104.0	11.2	0.35
8	317.0	32.2	0.133	11.3	1.81	115.3	12.4	0.36
9	339.6	34.5	0.133	10.2	2.14	125.5	13.5	0.37
10	362.3	36.8	0.115	8.4	2.27	133.9	14.4	0.37
11	384.9	39.1	0.135	11.8	1.74	145.7	15.7	0.38
12	407.5	41.4	0.118	7.4	2.81	153.1	16.5	0.38
13	430.2	43.7	0.161	12.8	2.02	165.9	17.9	0.39
14	452.8	46.0	0.155	8.8	3.24	174.7	18.8	0.39
15	475.5	48.3	0.090	5.5	2.95	180.2	19.4	0.38
16	498.1	50.6	0.129	4.3	6.19	184.5	19.9	0.37
17	520.8	52.9	0.088	3.3	5.36	187.8	20.2	0.36
18	543.4	55.2	0.173	11.1	2.73	198.9	21.4	0.37

Table E3: Run PS5 (Variable Diameter Horizontal Well with No Casing, Partially Scaled Model).

Pore Volume of Sand Pack: 1007.0 ml   Porosity of Sand Pack: 36.2 %

Irreducible Water Saturation: 10.2 %PV   Absolute Permeability of Pack: 15.0 darcies

Initial Oil Saturation: 89.8 %PV   Steam Injection Rate: 0.089 ml/s (CWE)

Sample no.	Steam Vol. Inj. ml (CWE)	Steam Vol. Inj. %PV (CWE)	Inst. Prod. Rate ml/s	Inst. Oil Prod. ml	Inst. WOR ml/ml	Cum. Oil Prod. ml	Cum. Oil Rec. %IOIP	Cum. OSR ml/ml (CWE)
1	80.0	7.9	0.027	12.1	1.00	12.1	1.3	0.15
2	101.3	10.1	0.121	10.3	1.83	22.4	2.5	0.22
3	122.7	12.2	0.129	19.3	0.61	41.7	4.6	0.34
4	144.0	14.3	0.163	16.0	1.44	57.7	6.4	0.40
5	165.3	16.4	0.119	12.9	1.21	70.6	7.8	0.43
6	186.7	18.5	0.157	14.6	1.58	85.2	9.4	0.46
7	208.0	20.7	0.162	20.7	0.87	105.9	11.7	0.51
8	229.3	22.8	0.148	18.0	0.98	123.9	13.7	0.54
9	250.7	24.9	0.080	5.5	2.49	129.4	14.3	0.52
10	272.0	27.0	0.184	24.7	0.79	154.1	17.0	0.57
11	293.3	29.1	0.134	14.7	1.18	168.8	18.7	0.58
12	314.7	31.2	0.113	11.4	1.37	180.2	19.9	0.57
13	336.0	33.4	0.137	14.8	1.22	195.0	21.6	0.58
14	357.3	35.5	0.136	16.9	0.93	211.9	23.4	0.59
15	378.7	37.6	0.114	4.5	5.07	216.4	23.9	0.57
16	400.0	39.7	0.160	17.4	1.20	233.8	25.9	0.58

Table E4: Run PS5A (Variable Diameter Horizontal Well with No Casing, Partially Scaled Model).

Pore Volume of Sand Pack:	991.0 ml	Porosity of Sand Pack:	35.6 %
Irreducible Water Saturation:	3.2 %PV	Absolute Permeability of Pack:	15.8 darcies
Initial Oil Saturation:	96.8 %PV	Steam Injection Rate:	0.109 ml/s (CWE)

Sample no.	Steam Vol. Inj. ml (CWE)	Steam Vol. Inj. %PV (CWE)	Inst. Prod. Rate ml/s	Inst. Oil Prod. ml	Inst. WOR ml/ml	Cum. Oil Prod. ml	Cum. Oil Rec. %IOIP	Cum. OSR ml/ml (CWE)
1	130.7	13.2	0.024	25.2	0.13	25.2	2.6	0.19
2	156.8	15.8	0.122	20.8	0.41	46.0	4.8	0.29
3	183.0	18.5	0.113	16.2	0.67	62.2	6.5	0.34
4	209.1	21.1	0.119	15.8	0.81	78.0	8.1	0.37
5	235.2	23.7	0.117	15.8	0.78	93.8	9.8	0.40
6	261.4	26.4	0.120	16.3	0.77	110.1	11.5	0.42
7	287.5	29.0	0.118	15.2	0.87	125.3	13.1	0.44
8	313.6	31.6	0.118	14.7	0.93	140.0	14.6	0.45
9	339.8	34.3	0.118	14.4	0.70	154.4	16.1	0.45
10	365.9	36.9	0.116	15.0	0.86	169.4	17.7	0.46
11	392.0	39.6	0.115	14.7	0.88	184.1	19.2	0.47
12	418.2	42.2	0.123	15.2	0.93	199.3	20.8	0.48
13	444.3	44.8	0.137	15.1	1.17	214.4	22.4	0.48
14	470.5	47.5	0.145	14.1	1.47	228.5	23.8	0.49
15	496.6	50.1	0.064	4.9	2.12	233.4	24.3	0.47
16	522.7	52.7	0.055	4.1	2.24	237.5	24.8	0.45
17	548.9	55.4	0.135	11.9	1.71	249.4	26.0	0.45
18	575.0	58.0	0.184	17.6	1.51	267.0	27.8	0.46

Table E5: Run PS6 (Variable Diameter Horizontal Well with No Casing, Partially Scaled Model).

Pore Volume of Sand Pack: 951.0 ml
Irreducible Water Saturation: 6.0 %PV
Initial Oil Saturation: 94.0 %PV

Porosity of Sand Pack: 34.2 %
Absolute Permeability of Pack: 9.6 darcies
Steam Injection Rate: 0.078 ml/s (CWE)

Sample no.	Steam Vol. Inj. ml (CWE)	Steam Vol. Inj. %PV (CWE)	Inst. Prod. Rate ml/s	Inst. Oil Prod. ml	Inst. WOR ml/ml	Cum. Oil Prod. ml	Cum. Oil Rec. %IOIP	Cum. OSR ml/ml (CWE)
1	81.9	8.6	0.037	29.7	0.30	29.7	3.3	0.36
2	100.6	10.6	0.139	22.9	0.45	52.6	5.9	0.52
3	119.3	12.5	0.166	20.7	0.93	73.3	8.2	0.61
4	138.0	14.5	0.118	13.1	1.15	86.4	9.7	0.63
5	156.7	16.5	0.168	17.5	1.30	103.9	11.6	0.66
6	175.4	18.4	0.159	16.0	1.38	119.9	13.4	0.68
7	194.2	20.4	0.198	21.6	1.20	141.5	15.8	0.73
8	212.9	22.4	0.123	11.6	1.55	153.1	17.1	0.72
9	231.6	24.4	0.088	9.3	1.27	162.4	18.2	0.70
10	250.3	26.3	0.142	18.6	0.83	181.0	20.2	0.72
11	269.0	28.3	0.162	15.1	1.57	196.1	21.9	0.73
12	287.7	30.3	0.175	16.8	1.51	212.9	23.8	0.74
13	306.4	32.2	0.067	3.1	4.19	216.0	24.2	0.70
14	325.1	34.2	0.130	11.6	1.70	227.6	25.5	0.70
15	343.9	36.2	0.128	14.7	1.10	242.3	27.1	0.70
16	362.6	38.1	0.144	14.8	1.33	257.1	28.8	0.71
17	381.3	40.1	0.128	9.7	2.16	266.8	29.8	0.70
18	400.0	42.1	0.147	12.1	1.92	278.9	31.2	0.70

Table E6: Run PS7 (Constant Diameter Horizontal Well with Perf. Casing, Partially Scaled Model).

Pore Volume of Sand Pack: 1129.0 ml   Porosity of Sand Pack: 40.6 %
Irreducible Water Saturation: 17.8 %PV   Absolute Permeability of Pack: 16.3 darcies
Initial Oil Saturation: 82.2 %PV   Steam Injection Rate: 0.095 ml/s (CWE)

Sample no.	Steam Vol. Inj. ml (CWE)	Steam Vol. Inj. %PV (CWE)	Inst. Prod. Rate ml/s	Inst. Oil Prod. ml	Inst. WOR ml/ml	Cum. Oil Prod. ml	Cum. Oil Rec. %IOIP	Cum. OSR ml/ml (CWE)
1	149.0	13.2	0.018	20.8	0.38	20.8	2.2	0.14
2	171.9	15.2	0.108	15.5	0.66	36.3	3.9	0.21
3	194.8	17.3	0.119	17.5	0.63	53.8	5.8	0.28
4	217.7	19.3	0.126	16.5	0.83	70.3	7.6	0.32
5	240.6	21.3	0.133	12.6	1.54	82.9	8.9	0.34
6	263.5	23.3	0.107	8.9	1.89	91.8	9.9	0.35
7	286.5	25.4	0.086	4.4	3.70	96.2	10.4	0.34
8	309.4	27.4	0.140	16.7	1.02	112.9	12.2	0.36
9	332.3	29.4	0.084	9.5	1.13	122.4	13.2	0.37
10	355.2	31.5	0.128	14.7	1.08	137.1	14.8	0.39
11	378.1	33.5	0.112	12.4	1.16	149.5	16.1	0.40
12	401.0	35.5	0.125	8.2	2.66	157.7	17.0	0.39
13	424.0	37.6	0.095	7.1	2.21	164.8	17.8	0.39
14	446.9	39.6	0.132	7.1	3.46	171.9	18.5	0.38
15	469.8	41.6	0.076	5.2	2.50	177.1	19.1	0.38
16	492.7	43.6	0.175	9.9	3.23	187.0	20.2	0.38
17	515.6	45.7	0.116	6.3	3.43	193.3	20.8	0.37
18	538.5	47.7	0.142	6.5	4.25	199.8	21.5	0.37

Table E7: Run PS8 (Constant Diameter Horizontal Well with Perf. Casing, Partially Scaled Model).

Pore Volume of Sand Pack:	1123.0 ml	Porosity of Sand Pack:	40.4 %
Irreducible Water Saturation:	13.0 %PV	Absolute Permeability of Pack:	14.3 darcies
Initial Oil Saturation:	87.0 %PV	Steam Injection Rate:	0.120 ml/s (CWE)

Sample no.	Steam Vol. Inj. ml (CWE)	Steam Vol. Inj. %PV (CWE)	Inst. Prod. Rate ml/s	Inst. Oil Prod. ml	Inst. WOR ml/ml	Cum. Oil Prod. ml	Cum. Oil Rec. %IOIP	Cum. OSR ml/ml (CWE)
1	186.7	16.6	0.018	14.4	0.94	14.4	1.5	0.08
2	215.4	19.2	0.130	12.7	1.45	27.1	2.8	0.13
3	244.1	21.7	0.102	13.9	0.76	41.0	4.2	0.17
4	272.9	24.3	0.123	14.2	1.07	55.2	5.6	0.20
5	301.6	26.9	0.130	16.6	0.87	71.8	7.3	0.24
6	330.3	29.4	0.108	14.0	0.86	85.8	8.8	0.26
7	359.0	32.0	0.115	12.7	1.18	98.5	10.1	0.27
8	387.8	34.5	0.124	14.3	1.08	112.8	11.5	0.29
9	416.5	37.1	0.108	14.1	0.83	126.9	13.0	0.30
10	445.2	39.6	0.153	19.6	0.87	146.5	15.0	0.33
11	473.9	42.2	0.138	15.7	1.11	162.2	16.6	0.34
12	502.7	44.8	0.117	12.1	1.31	174.3	17.8	0.35
13	531.4	47.3	0.130	14.5	1.14	188.8	19.3	0.36
14	560.1	49.9	0.150	18.3	0.97	207.1	21.2	0.37
15	588.8	52.4	0.165	14.5	1.74	221.6	22.7	0.38
16	617.6	55.0	0.160	13.5	1.85	235.1	24.1	0.38
17	646.3	57.5	0.147	12.5	1.82	247.6	25.3	0.38
18	675.0	60.1	0.166	15.4	1.59	263.0	26.9	0.39

Table E8: Run PS9 (Variable Diameter Horizontal Well with Perf. Casing, Partially Scaled Model).

Pore Volume of Sand Pack: 1030.0 ml
Irreducible Water Saturation: 31.1 %PV
Initial Oil Saturation: 68.9 %PV

Porosity of Sand Pack: 37.0 %
Absolute Permeability of Pack: 16.3 darcies
Steam Injection Rate: 0.091 ml/s (CWE)

Sample no.	Steam Vol. Inj. ml (CWE)	Steam Vol. Inj. %PV (CWE)	Inst. Prod. Rate ml/s	Inst. Oil Prod. ml	Inst. WOR ml/ml	Cum. Oil Prod. ml	Cum. Oil Rec. %IOIP	Cum. OSR ml/inl (CWE)
1	130.4	12.7	0.021	17.6	0.74	17.6	2.5	0.13
2	152.2	14.8	0.125	16.1	0.86	33.7	4.7	0.22
3	173.9	16.9	0.112	13.4	1.01	47.1	6.6	0.27
4	195.7	19.0	0.120	13.8	1.08	60.9	8.6	0.31
5	217.4	21.1	0.120	14.5	0.99	75.4	10.6	0.35
6	239.1	23.2	0.119	13.9	1.05	89.3	12.6	0.37
7	260.9	25.3	0.130	14.9	1.09	104.2	14.7	0.40
8	282.6	27.4	0.112	13.4	1.00	117.6	16.6	0.42
9	304.3	29.5	0.144	14.1	1.45	131.7	18.5	0.43
10	326.1	31.7	0.113	11.2	1.42	142.9	20.1	0.44
11	347.8	33.8	0.123	11.1	1.66	154.0	21.7	0.44
12	369.6	35.9	0.114	9.7	1.82	163.7	23.1	0.44
13	391.3	38.0	0.122	9.3	2.15	173.0	24.4	0.44
14	413.0	40.1	0.104	7.5	2.33	180.5	25.4	0.44
15	434.8	42.2	0.120	8.0	2.59	188.5	26.5	0.43
16	456.5	44.3	0.116	7.0	2.99	195.5	27.5	0.43
17	478.3	46.4	0.098	7.9	1.97	203.4	28.6	0.43
18	500.0	48.5	0.166	10.7	2.73	214.1	30.2	0.43

Table E9: Run PS10 (Variable Diameter Horizontal Well with Perf. Casing, Partially Scaled Model).

Pore Volume of Sand Pack: 1073.0 ml   Porosity of Sand Pack: 38.6 %

Irreducible Water Saturation: 11.9 %PV   Absolute Permeability of Pack: 15.8 darcies

Initial Oil Saturation: 88.1 %PV   Steam Injection Rate: 0.100 ml/s (CWE)

Sample no.	Steam Vol. Inj. ml (CWE)	Steam Vol. Inj. %PV (CWE)	Inst. Prod. Rate ml/s	Inst. Oil Prod. ml	Inst. WOR ml/ml	Cum. Oil Prod. ml	Cum. Oil Rec. %IOIP	Cum. OSR ml/ml (CWE)
1	143.5	13.4	0.020	27.9	0.04	27.9	3.0	0.19
2	167.4	15.6	0.127	26.8	0.13	54.7	5.8	0.33
3	191.3	17.8	0.129	22.9	0.35	77.6	8.2	0.41
4	215.2	20.1	0.125	20.4	0.47	98.0	10.4	0.46
5	239.1	22.3	0.148	22.3	0.60	120.3	12.7	0.50
6	263.0	24.5	0.107	16.3	0.57	136.6	14.5	0.52
7	287.0	26.7	0.130	18.1	0.72	154.7	16.4	0.54
8	310.9	29.0	0.182	23.1	0.89	177.8	18.8	0.57
9	334.8	31.2	0.111	11.7	1.28	189.5	20.1	0.57
10	358.7	33.4	0.130	15.2	1.05	204.7	21.7	0.57
11	382.6	35.7	0.155	18.3	1.03	223.0	23.6	0.58
12	406.5	37.9	0.128	13.8	1.23	236.8	25.1	0.58
13	430.4	40.1	0.148	13.5	1.64	250.3	26.5	0.58
14	454.3	42.3	0.102	6.1	3.02	256.4	27.1	0.56
15	478.3	44.6	0.166	18.1	1.20	274.5	29.0	0.57
16	502.2	46.8	0.198	15.6	2.05	290.1	30.7	0.58
17	526.1	49.0	0.101	5.8	3.19	295.9	31.3	0.56
18	550.0	51.3	0.090	7.8	1.77	303.7	32.1	0.55

Table E10: Run FS1 (Vertical Injector and Vertical Producer, Scaled Model).

Pore Volume of Sand Pack: 1908.0 ml   Porosity of Sand Pack: 44.8 %

Irreducible Water Saturation: 11.9 %PV   Absolute Permeability of Pack: 4.4 darcies

Initial Oil Saturation: 88.1 %PV   Steam Injection Rate: 0.031 ml/s (CWE)

Sample no.	Steam Vol. Inj. ml (CWE)	Steam Vol. Inj. %PV (CWE)	Inst. Prod. Rate ml/s	Inst. Oil Prod. ml	Inst. WOR ml/ml	Cum. Oil Prod. ml	Cum. Oil Rec. %IOIP	Cum. OSR ml/ml (CWE)
1	193.8	10.2	0.001	6.8	0.00	6.8	0.4	0.04
2	205.0	10.7	0.021	7.6	0.00	14.4	0.9	0.07

Table E11: Run FS1R (Vertical Injector in Communication with Vertical Producer, Scaled Model).

Pore Volume of Sand Pack:	1895.0 ml	Porosity of Sand Pack:	44.5 %
Irreducible Water Saturation:	9.0 %PV	Absolute Permeability of Pack:	5.1 darcies
Initial Oil Saturation:	91.0 %PV	Steam Injection Rate:	0.025 ml/s (CWE)

Sample no.	Steam Vol. Inj. ml (CWE)	Steam Vol. Inj. %PV (CWE)	Inst. Prod. Rate ml/s	Inst. Oil Prod. ml	Inst. WOR ml/ml	Cum. Oil Prod. ml	Cum. Oil Rec. %IOIP	Cum. OSR ml/ml (CWE)
1	117.8	6.2	0.004	14.2	0.49	14.2	0.8	0.12
2	132.5	7.0	0.035	12.8	0.66	27.0	1.6	0.20
3	147.2	7.8	0.033	13.3	0.50	40.3	2.3	0.27
4	161.9	8.5	0.031	12.5	0.49	52.8	3.1	0.33
5	176.7	9.3	0.028	10.4	0.62	63.2	3.7	0.36
6	191.4	10.1	0.027	10.4	0.53	73.6	4.3	0.38
7	206.1	10.9	0.026	10.4	0.51	84.0	4.9	0.41
8	220.8	11.7	0.027	8.4	0.90	92.4	5.4	0.42
9	235.6	12.4	0.028	11.0	0.54	103.4	6.0	0.44
10	250.3	13.2	0.027	9.8	0.65	113.2	6.6	0.45
11	265.0	14.0	0.034	13.0	0.55	126.2	7.3	0.48

Table E12: Run FS2R (Constant Diameter Horizontal Well with No Casing, Scaled Model).

Pore Volume of Sand Pack:	1868.0 ml	Porosity of Sand Pack:	43.9 %
Irreducible Water Saturation:	7.3 %PV	Absolute Permeability of Pack:	5.0 darcies
Initial Oil Saturation:	92.7 %PV	Steam Injection Rate:	0.144 ml/s (CWE)

Sample no.	Steam Vol. Inj. ml (CWE)	Steam Vol. Inj. %PV (CWE)	Inst. Prod. Rate ml/s	Inst. Oil Prod. ml	Inst. WOR ml/ml	Cum. Oil Prod. ml	Cum. Oil Rec. %IOIP	Cum. OSR ml/ml (CWE)
1	172.5	9.2	0.058	69.8	0.00	69.8	4.0	0.40
2	224.2	12.0	0.189	66.7	0.02	136.5	7.9	0.61
3	276.0	14.8	0.175	56.2	0.12	192.7	11.1	0.70
4	327.7	17.5	0.173	49.5	0.25	242.2	14.0	0.74
5	379.5	20.3	0.180	47.9	0.35	290.1	16.8	0.76
6	431.2	23.1	0.177	40.5	0.57	330.6	19.1	0.77
7	482.9	25.9	0.184	32.7	1.02	363.3	21.0	0.75
8	534.7	28.6	0.191	34.6	0.99	397.9	23.0	0.74
9	586.4	31.4	0.195	34.4	1.04	432.3	25.0	0.74
10	638.2	34.2	0.179	28.0	1.31	460.3	26.6	0.72
11	689.9	36.9	0.207	38.2	0.95	498.5	28.8	0.72
12	741.7	39.7	0.174	26.6	1.36	525.1	30.3	0.71
13	793.4	42.5	0.195	35.3	0.99	560.4	32.4	0.71
14	845.1	45.2	0.200	32.6	1.21	593.0	34.3	0.70
15	896.9	48.0	0.154	24.1	1.29	617.1	35.6	0.69
16	948.6	50.8	0.155	26.8	1.08	643.9	37.2	0.68
17	1000.4	53.6	0.324	47.4	1.46	691.3	39.9	0.69
18	1052.1	56.3	0.218	22.9	2.42	714.2	41.3	0.68
19	1103.9	59.1	0.119	17.4	1.45	731.6	42.3	0.66
20	1155.6	61.9	0.120	19.3	1.24	750.9	43.4	0.65
21	1207.4	64.6	0.208	31.7	1.36	782.6	45.2	0.65
22	1259.1	67.4	0.281	35.2	1.88	817.8	47.2	0.65
23	1397.1	74.8	0.162	42.9	2.62	860.7	49.7	0.62
24	1414.3	75.7	2.153	77.4	2.34	938.1	54.2	0.66
25	1548.0	82.9	0.170	33.3	3.75	971.4	56.1	0.63

Table E13: Run FS3H (Constant Diameter Horizontal Well with Perf. Casing (#2, Scaled Model).

Pore Volume of Sand Pack: 1744.0 ml
Irreducible Water Saturation: 8.8 %PV
Initial Oil Saturation: 91.2 %PV

Porosity of Sand Pack: 41.0 %
Absolute Permeability of Pack: 5.2 darcies
Steam Injection Rate: 0.067 ml/s (CWE)

Sample no.	Steam Vol. Inj. ml (CWE)	Steam Vol. Inj. %PV (CWE)	Inst. Prod. Rate ml/s	Inst. Oil Prod. ml	Inst. WOR ml/ml	Cum. Oil Prod. ml	Cum. Oil Rec. %IOIP	Cum. OSR ml/ml (CWE)
1	159.8	9.2	0.010	13.7	0.69	13.7	0.9	0.09
2	183.7	10.5	0.056	11.6	0.73	25.3	1.6	0.14
3	207.7	11.9	0.061	12.6	0.75	37.9	2.4	0.18
4	231.7	13.3	0.061	14.3	0.55	52.2	3.3	0.23
5	255.6	14.7	0.062	14.9	0.49	67.1	4.2	0.26
6	279.6	16.0	0.061	14.9	0.47	82.0	5.2	0.29
7	303.6	17.4	0.061	15.7	0.40	97.7	6.1	0.32
8	327.5	18.8	0.066	15.2	0.55	112.9	7.1	0.34
9	351.5	20.2	0.063	12.8	0.78	125.7	7.9	0.36
10	375.5	21.5	0.079	16.1	0.77	141.8	8.9	0.38
11	399.4	22.9	0.070	12.1	1.09	153.9	9.7	0.39
12	423.4	24.3	0.064	11.6	1.00	165.5	10.4	0.39
13	447.4	25.7	0.068	11.9	1.05	177.4	11.2	0.40
14	471.3	27.0	0.064	11.2	1.04	188.6	11.9	0.40
15	495.3	28.4	0.069	12.4	1.00	201.0	12.6	0.41
16	519.3	29.8	0.071	12.8	0.99	213.8	13.4	0.41
17	543.2	31.1	0.071	12.9	0.98	226.7	14.3	0.42
18	567.2	32.5	0.074	13.0	1.05	239.7	15.1	0.42
19	591.2	33.9	0.074	12.1	1.19	251.8	15.8	0.43
20	615.1	35.3	0.076	11.6	1.36	263.4	16.6	0.43
21	639.1	36.6	0.081	9.2	2.15	272.6	17.1	0.43
22	663.1	38.0	0.061	9.5	1.33	282.1	17.7	0.43
23	715.0	41.0	0.136	48.2	1.19	330.3	20.5	0.46

Table E14: Run FS3R (Constant Diameter Horizontal Well with Perf. Casing (#1), Scaled Model).

Pore Volume of Sand Pack: 1907.0 ml
Irreducible Water Saturation: 9.0 %PV
Initial Oil Saturation: 91.0 %PV

Porosity of Sand Pack: 44.8 %
Absolute Permeability of Pack: 6.1 darcies
Steam Injection Rate: 0.139 ml/s (CWE)

Sample no.	Steam Vol. Inj. ml (CWE)	Steam Vol. Inj. %PV (CWE)	Inst. Prod. Rate ml/s	Inst. Oil Prod. ml	Inst. WOR ml/ml	Cum. Oil Prod. ml	Cum. Oil Rec. %IOIP	Cum. OSR ml/ml (CWE)
1	208.8	10.9	0.033	41.3	0.19	41.3	2.4	0.20
2	258.9	13.6	0.144	38.4	0.35	79.7	4.6	0.31
3	309.0	16.2	0.167	37.1	0.62	116.8	6.7	0.38
4	359.2	18.8	0.183	38.3	0.72	155.1	8.9	0.43
5	409.3	21.5	0.177	28.9	1.20	184.0	10.6	0.45
6	459.4	24.1	0.186	25.4	1.64	209.4	12.1	0.46
7	509.5	26.7	0.170	28.8	1.13	238.2	13.7	0.47
8	559.6	29.3	0.179	29.3	1.20	267.5	15.4	0.48
9	609.7	32.0	0.191	27.1	1.54	294.6	17.0	0.48
10	659.9	34.6	0.226	34.6	1.35	329.2	19.0	0.50
11	710.0	37.2	0.223	31.8	1.52	361.0	20.8	0.51
12	760.1	39.9	0.171	23.9	1.58	384.9	22.2	0.51
13	810.2	42.5	0.204	32.2	1.29	417.1	24.0	0.51
14	860.3	45.1	0.211	32.0	1.37	449.1	25.9	0.52
15	910.4	47.7	0.204	30.5	1.41	479.6	27.6	0.53
16	960.5	50.4	0.201	30.4	1.37	510.0	29.4	0.53
17	1010.7	53.0	0.218	30.9	1.54	540.9	31.2	0.54
18	1060.8	55.6	0.167	25.3	1.38	566.2	32.6	0.53
19	1110.9	58.3	0.207	33.7	1.21	599.9	34.6	0.54
20	1161.0	60.9	0.256	33.4	1.76	633.3	36.5	0.55
21	1211.1	63.5	0.215	31.0	1.49	664.3	38.3	0.55
22	1261.2	66.1	0.245	30.9	1.85	695.2	40.1	0.55
23	1344.8	70.5	0.234	49.1	1.86	744.3	42.9	0.55
24	1378.2	72.3	0.893	75.8	1.83	820.1	47.3	0.60
25	1445.0	75.8	0.495	89.8	1.65	909.9	52.4	0.63

Table E15: Run FS4A (Constant Diameter Horizontal Well with Perf. Casing (#2), Scaled Model).

Pore Volume of Sand Pack:	1804.0 ml	Porosity of Sand Pack:	42.4 %
Irreducible Water Saturation:	10.8 %PV	Absolute Permeability of Pack:	6.6 darcies
Initial Oil Saturation:	89.2 %PV	Steam Injection Rate:	0.148 ml/s (CWE)

Sample no.	Steam Vol. Inj. ml (CWE)	Steam Vol. Inj. %PV (CWE)	Inst. Prod. Rate ml/s	Inst. Oil Prod. ml	Inst. WOR ml/ml	Cum. Oil Prod. ml	Cum. Oil Rec. %IOIP	Cum. OSR ml/ml (CWE)
1	218.2	12.1	0.032	33.9	0.37	33.9	2.1	0.16
2	271.6	15.1	0.153	35.1	0.57	69.0	4.3	0.25
3	325.1	18.0	0.171	37.7	0.63	106.7	6.6	0.33
4	378.5	21.0	0.158	40.3	0.41	147.0	9.1	0.39
5	431.9	23.9	0.160	42.2	0.36	189.2	11.8	0.44
6	485.4	26.9	0.193	47.8	0.45	237.0	14.7	0.49
7	538.8	29.9	0.221	39.8	1.00	276.8	17.2	0.51
8	592.2	32.8	0.200	29.6	1.44	306.4	19.0	0.52
9	645.7	35.8	0.217	34.5	1.26	340.9	21.2	0.53
10	699.1	38.8	0.246	35.9	1.47	376.8	23.4	0.54
11	752.6	41.7	0.209	30.6	1.46	407.4	25.3	0.54
12	806.0	44.7	0.213	32.1	1.38	439.5	27.3	0.55
13	859.4	47.6	0.241	35.5	1.45	475.0	29.5	0.55
14	912.9	50.6	0.249	36.8	1.43	511.8	31.8	0.56
15	966.3	53.6	0.214	30.9	1.49	542.7	33.7	0.56
16	1019.7	56.5	0.214	32.4	1.38	575.1	35.7	0.56
17	1073.2	59.5	0.255	38.1	1.41	613.2	38.1	0.57
18	1126.6	62.5	0.257	32.1	1.88	645.3	40.1	0.57
19	1180.0	65.4	0.233	27.6	2.03	672.9	41.8	0.57
20	1233.5	68.4	0.241	36.2	1.39	709.1	44.0	0.57
21	1286.9	71.3	0.264	37.3	1.55	746.4	46.4	0.58
22	1340.4	74.3	0.258	35.5	1.61	781.9	48.6	0.58
23	1376.0	76.3	0.862	74.8	1.76	856.7	53.2	0.62
24	1447.2	80.2	0.455	81.1	1.69	937.8	58.2	0.65
25	1563.0	86.6	0.309	109.5	1.20	1047.3	65.0	0.67

Table E16: Run FS5H (Variable Diameter Horizontal Well with No Casing, Scaled Model).

Pore Volume of Sand Pack: 1811.0 ml
Irreducible Water Saturation: 7.0 %PV
Initial Oil Saturation: 93.0 %PV

Porosity of Sand Pack: 42.6 %
Absolute Permeability of Pack: 4.9 darcies
Steam Injection Rate: 0.070 ml/s (CWE)

Sample no.	Steam Vol. Inj. ml (CWE)	Steam Vol. Inj. %PV (CWE)	Inst. Prod. Rate ml/s	Inst. Oil Prod. ml	Inst. WOR ml/ml	Cum. Oil Prod. ml	Cum. Oil Rec. %IOIP	Cum. OSR ml/ml (CWE)
1	117.1	6.5	0.022	36.8	0.00	36.8	2.2	0.31
2	142.2	7.9	0.101	36.4	0.00	73.2	4.3	0.51
3	167.3	9.2	0.101	36.2	0.00	109.4	6.5	0.65
4	192.4	10.6	0.093	28.2	0.19	137.6	8.2	0.72
5	217.5	12.0	0.095	24.9	0.37	162.5	9.6	0.75
6	242.6	13.4	0.094	23.4	0.45	185.9	11.0	0.77
7	267.7	14.8	0.108	26.5	0.47	212.4	12.6	0.79
8	292.8	16.2	0.120	17.6	1.45	230.0	13.6	0.79
9	317.9	17.6	0.115	19.1	1.16	249.1	14.8	0.78
10	343.0	18.9	0.084	17.1	0.78	266.2	15.8	0.78
11	376.4	20.8	0.107	26.9	0.90	293.1	17.4	0.78
12	393.1	21.7	0.121	12.6	1.31	305.7	18.1	0.78
13	418.2	23.1	0.098	18.8	0.88	324.5	19.3	0.78
14	443.3	24.5	0.103	17.5	1.13	342.0	20.3	0.77
15	468.4	25.9	0.119	22.0	0.95	364.0	21.6	0.78
16	493.5	27.3	0.089	16.7	0.92	380.7	22.6	0.77
17	518.6	28.6	0.119	20.5	1.09	401.2	23.8	0.77
18	543.7	30.0	0.085	16.7	0.83	417.9	24.8	0.77
19	568.8	31.4	0.122	20.2	1.17	438.1	26.0	0.77
20	593.9	32.8	0.098	16.8	1.09	454.9	27.0	0.77
21	619.0	34.2	0.102	16.1	1.27	471.0	28.0	0.76

Table E17: Run FS5A (Variable Diameter Horizontal Well with No Casing, Scaled Model).

Pore Volume of Sand Pack: 1871.0 ml
Irreducible Water Saturation: 8.3 %PV
Initial Oil Saturation: 91.7 %PV

Porosity of Sand Pack: 44.0 %
Absolute Permeability of Pack: 6.7 darcies
Steam Injection Rate: 0.166 ml/s (CWE)

Sample no.	Steam Vol. Inj. ml (CWE)	Steam Vol. Inj. %PV (CWE)	Inst. Prod. Rate ml/s	Inst. Oil Prod. ml	Inst. WOR ml/ml	Cum. Oil Prod. ml	Cum. Oil Rec. %IOIP	Cum. OSR ml/ml (CWE)
1	179.3	9.6	0.066	71.1	0.00	71.1	4.1	0.40
2	239.1	12.8	0.204	73.3	0.00	144.4	8.4	0.60
3	298.9	16.0	0.195	60.9	0.15	205.3	12.0	0.69
4	358.7	19.2	0.194	52.5	0.33	257.8	15.0	0.72
5	418.5	22.4	0.209	49.4	0.53	307.2	17.9	0.73
6	478.3	25.6	0.220	48.1	0.65	355.3	20.7	0.74
7	538.0	28.8	0.226	47.9	0.70	403.2	23.5	0.75
8	597.8	32.0	0.215	44.8	0.73	448.0	26.1	0.75
9	657.6	35.1	0.219	45.2	0.75	493.2	28.8	0.75
10	717.4	38.3	0.229	47.6	0.74	540.8	31.5	0.75
11	777.2	41.5	0.260	47.6	0.96	588.4	34.3	0.76
12	837.0	44.7	0.253	42.9	1.13	631.3	36.8	0.75
13	896.7	47.9	0.245	36.5	1.42	667.8	38.9	0.74
14	956.5	51.1	0.229	32.6	1.53	700.4	40.8	0.73
15	1016.3	54.3	0.221	35.4	1.25	735.8	42.9	0.72
16	1076.1	57.5	0.252	36.1	1.51	771.9	45.0	0.72
17	1135.9	60.7	0.260	33.5	1.79	805.4	47.0	0.71
18	1195.7	63.9	0.208	25.3	1.95	830.7	48.4	0.69
19	1255.4	67.1	0.186	21.1	2.18	851.8	49.7	0.68
20	1315.2	70.3	0.155	20.7	1.70	872.5	50.9	0.66
21	1375.0	73.5	0.211	24.9	2.06	897.4	52.3	0.65
22	1434.8	76.7	0.232	21.8	2.83	919.2	53.6	0.64
23	1454.7	77.8	2.150	41.7	5.19	960.9	56.0	0.66
24	1574.3	84.1	0.253	42.3	3.31	1003.2	58.5	0.64
25	1654.0	88.4	0.618	104.3	1.84	1107.5	64.6	0.67

Table E18: Run FS5R (Variable Diameter Horizontal Well with No Casing, Scaled Model).

Pore Volume of Sand Pack: 1570.0 ml   Porosity of Sand Pack: 3?.9 %
Irreducible Water Saturation: 8.9 %PV   Absolute Permeability of Pack: 6.9 darcies
Initial Oil Saturation: 91.1 %PV   Steam Injection Rate: 0.143 ml/s (CWE)

Sample no.	Steam Vol. Inj. ml (CWE)	Steam Vol. Inj. %PV (CWE)	Inst. Prod. Rate ml/s	Inst. Oil Prod. ml	Inst. WOR ml/ml	Cum. Oil Prod. ml	Cum. Oil Rec. %IOIP	Cum. OSR ml/ml (CWE)
1	180.6	11.5	0.054	67.8	0.00	67.8	4.7	0.38
2	232.2	14.8	0.179	64.5	0.00	132.3	9.3	0.57
3	283.8	18.1	0.173	58.9	0.06	191.2	13.4	0.67
4	335.4	21.4	0.174	48.8	0.28	240.0	16.8	0.72
5	387.0	24.7	0.209	49.8	0.51	289.8	20.3	0.75
6	438.7	27.9	0.160	33.5	0.72	323.3	22.6	0.74
7	490.3	31.2	0.223	47.5	0.69	370.8	25.9	0.76
8	541.9	34.5	0.188	32.5	1.08	403.3	28.2	0.74
9	593.5	37.8	0.210	43.2	0.75	446.5	31.2	0.75
10	645.1	41.1	0.210	42.1	0.80	488.6	34.2	0.76
11	696.7	44.4	0.302	51.1	1.13	539.7	37.7	0.77
12	748.3	47.7	0.173	28.1	1.22	567.8	39.7	0.76
13	799.9	50.9	0.165	24.1	1.47	591.9	41.4	0.74
14	851.5	54.2	0.273	45.9	1.14	637.8	44.6	0.75
15	903.1	57.5	0.170	21.0	1.91	658.8	46.1	0.73
16	954.7	60.8	0.191	24.6	1.80	683.4	47.8	0.72
17	1006.3	64.1	0.191	24.3	1.83	707.7	49.5	0.70
18	1057.9	67.4	0.261	31.4	1.99	739.1	51.7	0.70
19	1109.5	70.7	0.296	27.2	2.92	766.3	53.6	0.69
20	1161.1	74.0	0.115	16.7	1.47	783.0	54.8	0.67
21	1212.7	77.2	0.235	23.4	2.62	806.4	56.4	0.66
22	1264.4	80.5	0.144	16.4	2.16	822.8	57.5	0.65
23	1350.4	86.0	0.659	75.2	2.16	898.0	62.8	0.67
24	1505.2	95.9	0.532	62.5	2.06	960.5	67.2	0.64
25	1660.0	105.7	0.765	66.4	3.15	1026.9	71.8	0.62

Table E19: Run FS6 (Variable Diameter Horizontal Well with Perf. Casing (#1), Scaled Model).

Pore Volume of Sand Pack: 1920.0 ml
Irreducible Water Saturation: 8.3 %PV
Initial Oil Saturation: 91.7 %PV
Porosity of Sand Pack: 45.1 %
Absolute Permeability of Pack: 7.2 darcies
Steam Injection Rate: 0.128 ml/s (CWE)

Sample no.	Steam Vol. Inj. ml (CWE)	Steam Vol. Inj. %PV (CWE)	Inst. Prod. Rate ml/s	Inst. Oil Prod. ml	Inst. WOR ml/ml	Cum. Oil Prod. ml	Cum. Oil Rec. %IOIP	Cum. OSR ml/ml (CWE)
1	214.5	11.2	0.028	42.7	0.12	42.7	2.4	0.20
2	260.4	13.6	0.133	32.4	0.47	75.1	4.3	0.29
3	306.4	16.0	0.154	35.6	0.56	110.7	6.3	0.36
4	352.4	18.4	0.177	33.2	0.92	143.9	8.2	0.41
5	398.3	20.7	0.194	34.8	1.01	178.7	10.2	0.45
6	444.3	23.1	0.165	29.7	1.00	208.4	11.8	0.47
7	490.3	25.5	0.181	34.2	0.91	242.6	13.8	0.49
8	536.2	27.9	0.182	32.6	1.01	275.2	15.6	0.51
9	582.2	30.3	0.158	26.3	1.16	301.5	17.1	0.52
10	628.1	32.7	0.195	29.5	1.38	331.0	18.8	0.53
11	674.1	35.1	0.228	32.1	1.56	363.1	20.6	0.54
12	720.1	37.5	0.187	26.1	1.57	389.2	22.1	0.54
13	766.0	39.9	0.183	27.3	1.41	416.5	23.7	0.54
14	812.0	42.3	0.226	31.5	1.58	448.0	25.5	0.55
15	857.9	44.7	0.219	32.2	1.45	480.2	27.3	0.56
16	903.9	47.1	0.284	42.3	1.42	522.5	29.7	0.58
17	949.9	49.5	0.196	26.0	1.72	548.5	31.2	0.58
18	995.8	51.9	0.188	27.3	1.47	575.8	32.7	0.58
19	1041.8	54.3	0.198	29.9	1.38	605.7	34.4	0.58
20	1087.7	56.7	0.186	27.1	1.47	632.8	36.0	0.58
21	1133.7	59.0	0.237	38.9	1.19	671.7	38.2	0.59
22	1179.7	61.4	0.272	49.0	1.00	720.7	40.9	0.61
23	1240.9	64.6	0.515	97.3	1.54	818.0	46.5	0.66
24	1302.2	67.8	0.370	71.1	1.50	889.1	50.5	0.68
25	1375.0	71.6	0.316	80.6	1.24	969.7	55.1	0.71

Table E20: Run FS7 (Variable Diameter Horizontal Well with Perf. Casing (#2), Scaled Model).

Pore Volume of Sand Pack:	1881.0 ml		Porosity of Sand Pack:		44.2 %
Irreducible Water Saturation:	8.0 %PV		Absolute Permeability of Pack:		6.7 darcies
Initial Oil Saturation:	92.0 %PV		Steam Injection Rate:		0.116 ml/s (CWE)

Sample no.	Steam Vol. Inj. ml (CWE)	Steam Vol. Inj. %PV (CWE)	Inst. Prod. Rate ml/s	Inst. Oil Prod. ml	Inst. WOR ml/ml	Cum. Oil Prod. ml	Cum. Oil Rec. %IOIP	Cum. OSR ml/ml (CWE)
1	204.9	10.9	0.022	37.3	0.06	37.3	2.2	0.18
2	246.5	13.1	0.112	30.3	0.33	67.6	3.9	0.27
3	288.2	15.3	0.136	27.5	0.77	95.1	5.5	0.33
4	329.9	17.5	0.144	32.7	0.59	127.8	7.4	0.39
5	371.5	19.8	0.137	29.5	0.67	157.3	9.1	0.42
6	413.2	22.0	0.139	22.2	1.25	179.5	10.4	0.43
7	454.9	24.2	0.135	23.9	1.03	203.4	11.8	0.45
8	496.5	26.4	0.138	23.2	1.14	226.6	13.1	0.46
9	538.2	28.6	0.136	18.1	1.71	244.7	14.1	0.45
10	579.9	30.8	0.146	23.2	1.27	267.9	15.5	0.46
11	621.5	33.0	0.158	22.4	1.54	290.3	16.8	0.47
12	663.2	35.3	0.159	21.7	1.65	312.0	18.0	0.47
13	704.9	37.5	0.183	25.4	1.59	337.4	19.5	0.48
14	746.5	39.7	0.198	29.3	1.43	366.7	21.2	0.49
15	788.2	41.9	0.185	20.9	2.19	387.6	22.4	0.49
16	829.9	44.1	0.159	23.1	1.47	410.7	23.7	0.49
17	871.5	46.3	0.162	25.6	1.28	436.3	25.2	0.50
18	913.2	48.5	0.183	22.5	1.93	458.8	26.5	0.50
19	954.9	50.8	0.183	25.2	1.62	484.0	28.0	0.51
20	996.5	53.0	0.152	20.9	1.61	504.9	29.2	0.51
21	1038.2	55.2	0.173	26.9	1.31	531.8	30.7	0.51
22	1079.9	57.4	0.204	26.4	1.79	558.2	32.3	0.52
23	1121.5	59.6	0.484	83.6	1.08	641.8	37.1	0.57
24	1225.7	65.2	0.261	91.1	1.58	732.9	42.4	0.60
25	1250.0	66.5	0.249	24.8	1.11	757.7	43.8	0.61

Table E21: Run FS8 (Horizontal Steam Injector and Horizontal Producer, Scaled Model).

Pore Volume of Sand Pack: 1767.0 ml
Irreducible Water Saturation: 6.7 %PV
Initial Oil Saturation: 93.3 %PV

Porosity of Sand Pack: 41.5 %
Absolute Permeability of Pack: 5.5 darcies
Steam Injection Rate: 0.443 ml/s (CWE)

Sample no.	Steam Vol. Inj. ml (CWE)	Steam Vol. Inj. %PV (CWE)	Inst. Prod. Rate ml/s	Inst. Oil Prod. ml	Inst. WOR ml/ml	Cum. Oil Prod. ml	Cum. Oil Rec. %IOIP	Cum. OSR ml/ml (CWE)
1	252.7	14.3	0.145	42.9	0.93	42.9	2.6	0.17
2	305.9	17.3	0.760	38.2	1.39	81.1	4.9	0.27
3	385.7	21.8	0.543	56.2	0.74	137.3	8.3	0.36
4	425.6	24.1	0.996	52.5	0.71	189.8	11.5	0.45
5	478.8	27.1	0.737	49.1	0.80	238.9	14.5	0.50
6	532.0	30.1	0.663	39.6	1.01	278.5	16.9	0.52
7	598.5	33.9	0.597	45.9	0.95	324.4	19.7	0.54
8	665.0	37.6	0.551	38.1	1.17	362.5	22.0	0.55
9	731.5	41.4	0.613	38.9	1.36	401.4	24.4	0.55
10	798.0	45.2	0.751	47.2	1.39	448.6	27.2	0.56

Table E22: Run FS9 (Horizontal Steam Injector and Vertical Producer, Scaled Model).

Pore Volume of Sand Pack:	1765.0 ml	Porosity of Sand Pack:	41.5 %
Irreducible Water Saturation:	9.6 %PV	Absolute Permeability of Pack:	4.6 darcies
Initial Oil Saturation:	90.4 %PV	Steam Injection Rate:	0.006 ml/s (CWE)

Sample no.	Steam Vol. Inj. ml (CWE)	Steam Vol. Inj. %PV (CWE)	Inst. Prod. Rate ml/s	Inst. Oil Prod. ml	Inst. WOR ml/ml	Cum. Oil Prod. ml	Cum. Oil Rec. %IOIP	Cum. OSR ml/ml (CWE)
1	52.4	3.0	0.001	11.8	0.00	11.8	0.7	0.23
2	56.0	3.2	0.017	10.4	0.00	22.2	1.4	0.40
3	59.6	3.4	0.017	10.0	0.00	32.2	2.0	0.54
4	65.0	3.7	0.017	15.3	0.00	47.5	3.0	0.73